

# Solid oxide fuel cell (SOFC) integrated power plants System and kinetic studies

Thallam Thattai, Aditya

10.4233/uuid:2c54c1c6-3f5f-43cd-897c-78d59db28e04

**Publication date** 

**Document Version** Final published version

Citation (APA)

Thallam Thattai, A. (2017). Solid oxide fuel cell (SOFC) integrated power plants: System and kinetic studies. [Dissertation (TU Delft), Delft University of Technology]. https://doi.org/10.4233/uuid:2c54c1c6-3f5f-43cd-897c-78d59db28e04

Important note

To cite this publication, please use the final published version (if applicable). Please check the document version above.

Copyright

Other than for strictly personal use, it is not permitted to download, forward or distribute the text or part of it, without the consent of the author(s) and/or copyright holder(s), unless the work is under an open content license such as Creative Commons.

Please contact us and provide details if you believe this document breaches copyrights. We will remove access to the work immediately and investigate your claim.

This work is downloaded from Delft University of Technology. For technical reasons the number of authors shown on this cover page is limited to a maximum of 10.

# SOLID OXIDE FUEL CELL (SOFC) INTEGRATED POWER PLANTS

SYSTEM AND KINETIC STUDIES

Aditya Thallam Thattai

# SOLID OXIDE FUEL CELL (SOFC) INTEGRATED POWER PLANTS

System and kinetic studies

## **Proefschrift**

ter verkrijging van de graad van doctor aan de Technische Universiteit Delft, op gezag van de Rector Magnificus prof. ir. K. C. A. M. Luyben, voorzitter van het College voor Promoties, in het openbaar te verdedigen op maandag 26 juni 2017 om 12:30 uur

door

# **Aditya Thallam Thattai**

Master of Science in Mechanical Engineering Delft University of Technology, the Netherlands geboren te Nagpur Vidarbha MS, India. Dit proefschrift is goedgekeurd door de

Promotoren: Prof. dr. ir. B. J. Boersma en Prof. dr. J. J. C. Geerlings

Copromotor: Dr. P. V. Aravind

Samenstelling promotiecommissie:

Rector Magnificus voorzitter

Prof. dr. ir. B. J. Boersma

Technische Universiteit Delft, promotor

Prof. dr. J. J. C. Geerlings

Technische Universiteit Delft, promotor

Technische Universiteit Delft, copromotor

Technische Universiteit Delft, copromotor

Onafhankelijke leden:

Prof. dr. ir. C. A. Ramirez Ramirez Technische Universiteit Delft

Prof. dr. ir. G. Brem Universiteit Twente Prof. dr. E. Worrell Universiteit Utrecht

Dr. A. Moreno ENEA, Italy

Prof. dr. D. J. E. M. Roekaerts Technische Universiteit Delft, reservelid







Copyright  $\ @$  2017 by A. Thallam Thattai

ISBN 978-94-6186-823-7

An electronic version of this dissertation is available at http://repository.tudelft.nl/.

Thesis cover designed by Reshu Gupta

अभङगुर् कलादान स्थुल लक्षत्वमीयुषे। तुङगय महसे (महते) तस्मै तुरङगय मुखे नमः॥

Salutations to Lord Hayagreeva, the Supreme Effulgence, whose gifts of knowledge are as innumerable as they are imperishable.

# Summary

Increased climate change over past decades has resulted in an increase in the average temperature (also called global warming) of Earth's climate system. At the recent Paris climate conference (COP21) in 2015, 195 countries in the world have agreed upon a stringent plan to limit global warming below  $2^o$ C. This demands a significant reduction in the industrial emission of greenhouse gases, predominantly carbon dioxide (CO<sub>2</sub>). Existing fossil fuel (coal, natural gas) fired power plants account for the majority share in global carbon dioxide (CO<sub>2</sub>) and other harmful (SO<sub>x</sub>, NO<sub>x</sub>) emissions. Therefore clean, efficient and flexible power plant concepts need to be developed towards upgrading existing power plants and to meet the strict CO<sub>2</sub> emission targets. Combined cycle power plants like the integrated gasification combined cycle, IGCC (coal based) and integrated reforming combined cycle, IRCC (natural gas based) can be utilized to produce electricity using fossil fuels at relatively high efficiencies compared to conventional single cycle plants.

Possible approaches to make IGCC/IRCC power plants cleaner, efficient and more flexible include biomass utilization (renewable energy source), application of CO<sub>2</sub> capture technologies, retrofitting with highly efficient fuel conversion technologies like solid oxide fuel cells (SOFCs) and energy/fuel storage. This dissertation primarily aims to provide design concepts and thermodynamic system analysis for large scale IGCC and IRCC power plants with a focus on achieving high electrical efficiencies, low CO<sub>2</sub> emissions and high operational flexibility. SOFCs have been explored as an efficiency augmenting technology and metal hydride based hydrogen storage as a flexibility option. Furthermore, future development of safe and optimally operating hydrocarbon (like natural gas (methane)) fuelled SOFC units on the basis of system and numerical models, requires reliable experimental data and understanding in the underlying reaction kinetics. Thereupon, an extended experimental study has been carried out in this work on methane steam reforming (MSR) kinetics in single operating SOFCs.

The dissertation comprises of 4 main parts: a) an experimental model validation study on high percentage (upto 70%) biomass co-gasification in IGCC power plants (called bio-IGCC) based on an existing coal based power plant in the Netherlands. b) a thermodynamic system study towards retrofitting SOFCs and CO<sub>2</sub> capture in existing IGCC power plants with a focus on near future implementation. c) a thermodynamic system design study on flexible IRCC power plants with metal hydride based hydrogen storage and a preliminary study on integrating SOFCs in natural

gas (methane) based power plant systems. d) an experimental study on methane steam reforming (MSR) reaction kinetics in single operating SOFCs.

Co-gasification of biomass like wood pellets combined with carbon dioxide (CO<sub>2</sub>) capture in existing coal based IGCC power plants has a large potential to reduce CO<sub>2</sub> emissions in the near future. Woody biomass is largely considered a carbon neutral fuel based on a hypotheses that it removes as much CO2 from the environment during its growth as is emitted after its conversion in industrial plants. In order to assess biomass co-gasification as a clean energy technology, high percentage (upto 70% energy based) biomass co-gasification tests were carried out in the past by NUON/Vattenfall at the currently defunct 253 MW<sub>e</sub> coal based Willem-Alexander Centrale (WAC), Buggenum in The Netherlands utilizing steam exploded wood pellets. Chapter 2 of this dissertation presents the obtained experimental data with a detailed and validated steady state thermodynamic off-design model developed as an aid to assess future plant operations. The validation study shows a reasonably accurate model prediction for a net power output of 173 MW, and a net plant efficiency of about 37.2%. Furthermore, the need to carry out co-gasification with high lower heating value (LHV) torrefied wood pellets has also been pointed out. Confirming previous reports in literature, an exergy analysis of the complete system indicates largest exergy destruction in the gasifier and gas turbine combustor, suggesting an additional scope for process improvements. Despite unavoidable inconsistencies in the obtained plant data, it has been shown that off-design thermodynamic models can be effectively utilized to predict power plant performance with a relatively high accuracy (within 3% relative deviation).

Solid oxide fuel cells (SOFCs), operating at high temperatures (700-1000°C) are fuel flexible and highly efficient electrochemical devices for electricity production. Existing coal/biomass fired IGCC power plants could be retrofitted with SOFCs and novel CO<sub>2</sub> capture technologies to reduce CO<sub>2</sub> emissions and increase net electrical efficiencies in near future. Utilization of SOFCs also promotes lower SO<sub>x</sub> and NO<sub>x</sub> emissions. Chapter 3 presents a detailed thermodynamic analysis towards retrofitting SOFCs and CO2 capture in bio-IGCC power plants using off-design models developed based on validated models presented in Chapter 2. Two systems have been presented: i) a system based on WAC design with partial SOFC-CO<sub>2</sub> capture retrofit i,e only part of the syngas fuel is utilized in the SOFC and CO<sub>2</sub> capture unit ii) a newly designed integrated gasification fuel cell (IGFC) system with CO2 capture wherein syngas fuel is completely converted in the SOFC unit. The two systems together have been used to pinpoint that existing IGCC power plants could be operated with more than 40% net electrical efficiency without major process modifications when partially retrofitted with SOFCs (upto 40 MW<sub>e</sub>) and oxy-combustion CO<sub>2</sub> capture. The study further reveals that full scale CO<sub>2</sub> capture and SOFC integration requires major redesign of the gas turbine and heat recovery steam generator (HRSG). The reduction in thermodynamic losses in both systems compared to the base system (presented in Chapter 2) without SOFC and CO2 capture has also been clearly pointed out with an exergy  $(2^{nd} \text{ law})$  analysis.

Natural gas, a relatively cleaner fossil fuel compared to coal, is an additional primary fuel utilized for electrical power production. *Chapter 4* of this disserta-

tion with an aim to assess operational flexibility presents a thermodynamic system study on IRCC power plants with metal hydride based hydrogen (H<sub>2</sub>) storage and pre-combustion CO<sub>2</sub> capture. The central idea explored in this study to introduce operational flexibility is, the storage of H<sub>2</sub> in a metal hydride (Magnesium hydride (MgH<sub>2</sub>)) during low power demand and utility of the stored H<sub>2</sub> for power production during high power demand. Metal hydrides (MH) as a H<sub>2</sub> storage option in power plants offer multiple advantages in terms of relatively high storage capacities (%wt) and extensive possibilities for heat integration within the system. The comparative study using steady state IRCC system models with and without H2 storage shows that addition of MH based H<sub>2</sub> storage in IRCC power plants causes an insignificant penalty of the net system efficiency and that these system could be operated with a time based average efficiency above 45% with appropriate heat integration. The H<sub>2</sub> split fraction and choice of the metal hydride (reaction enthalpy) are identified as two important design parameters. Additional aspects regarding the temperature pinch in the HRSG and feed water preheaters (FWP) have also been addressed. The reformer and gas turbine combustor have been identified as sources for the largest thermodynamic irreversibilities. As a preliminary investigation, Appendix 4A of this dissertation presents a system study towards retrofitting such systems with SOFCs towards reducing these irreversibilities.

Fuel conversion in SOFCs cannot be completely understood based only on thermodynamic investigations. It is of vital importance to also investigate the underlying reaction kinetics to develop larger, safer SOFC units for power plant integration and to precisely predict undesirable temperature gradients in the cell. Furthermore, it is also important to obtain reliable experimental data for developing accurate system and numerical models. Chapter 5 of this dissertation presents an experimental study on MSR kinetics in an operating single SOFC with Ni-GDC (gadolinium doped ceria) anodes. The study has been carried out for relatively low inlet steam concentrations (steam to carbon (S/C) ratio around 1) and moderate current densities upto 3000 A/m<sup>2</sup>. Based on experimental methane conversion obtained at various operating temperatures, gas compositions and current densities, a kinetic model has been developed to calculate and compare relevant kinetic parameters using two approaches - power law (PL) and general Langmuir-Hinshelwood (LH) kinetics. Results using both approaches indicate that electrochemical hydrogen oxidation (current) marginally promotes methane conversion and the MSR reaction rate. However, the inlet methane partial pressure and the operating temperature have been identified as the most important factors affecting the rate. Although both approaches predict the same net MSR reaction rates, a significant difference is observed in the predicted rate and species partial pressure distribution along the channel length. Furthermore, experiments indicate that methane reforming on anode current collectors in always not negligible, particularly at higher temperatures.

In a nutshell, the work presented in this dissertation is an important step forward towards the conceptual design and development of clean, efficient and flexible SOFC integrated IGCC/IRCC power plants. The work additionally exposes the importance and thermodynamic advantages of employing solid oxide fuel cells and metal hydride based hydrogen storage in large scale (>150 MW<sub>e</sub>) power plants. As

one of the highlights, the study reports a first of its kind model development and experimental validation based on a large scale 70% biomass co-gasification test in an existing IGCC power plant. The study reveals the increased importance, relevance and effectiveness of detailed steady state, thermodynamic, off-design power plant modeling and validation. Additionally, it has been shown on the basis of thermodynamic calculations that no major process modifications are needed in existing IGCC power plants to partially retrofit with SOFCs and CO<sub>2</sub> capture for boosting the electrical efficiency and reduce CO<sub>2</sub> and other harmful (SO<sub>r</sub>, NO<sub>r</sub>) emissions. Thermodynamic assessment on natural gas fired IRCC power plants with metal hydride based hydrogen storage indicates a large potential in terms of flexibility, heat integration and efficient load management. As a step further to accurately predict temperature gradients in SOFCs in future, the study has gone some way towards enhancing our understanding on methane steam reforming (MSR) kinetics in single operating SOFCs with Ni-ceria anodes. The study indicates the importance of selecting appropriate kinetic approaches and rate expressions to predict reaction rate and species distribution across the operating cell.

# **List of Abbreviations**

AC Air compressor

**ASR** Area specific resistance

**ASU** Air Separation Unit

ATR Auto Thermal Reformer

**CAES** Compressed Air Energy Storage

**CCS** Carbon Capture and Storage

**CCR** Carbon Capture Ratio

**CEM** Controlled evaporator mixer

**CFD** Computational fluid dynamics

**CO**<sub>2</sub> Carbon Dioxide

COS Carbonyl sulphide

**COV** Coefficient of variation

**CHP** Combined heat and power

**EES** Electrical Energy Storage

**EBTF** European Benchmarking Task Force

**EDX** Energy dispersive X-ray spectroscopy

**ECN** Energy research center of the Netherlands

**ESC** Electrolyte supported cell

**EU** European Union

**FWP** Feed water preheater

GCU Gas cleaning unit

**GDC** Gadolinium doped ceria

**GHG** Green house gas

**GHR** Gas Heated Reformer

GHR-ATR Gas Heated Reformer - Auto Thermal Reformer

**GT** Gas Turbine

**HRSG** Heat Recovery Steam Generator

**HP** High pressure

**H**<sub>2</sub> Hydrogen

**HCN** Hydrogen cyanide

H/C Hydrogen to carbon ratio

**HTF** Heat Transfer Fluid

**HT** High Temperature

**HTS** High Temperature Shift

**IGCC** Integrated gasification combined cycle

**IGFC** Integrated gasification fuel cell cycle

**IRCC** Integrated reforming combined cycle

**IP** Intermediate pressure

**IPFR** Ideal plug flow reactor

**LC** Load Curve

LH Langmuir-Hinshelwood

**LHV** Lower heating value

**LP** Low pressure

**LSM** Lanthanum strontium manganite

LT Low Temperature

**MEA** Monoethanolamine

MDEA Methyl diethanolamine

MH Metal Hydride

**MP** Medium Pressure

MT Medium Temperature

MSR Methane steam reforming

NG Natural Gas

NGCC Natural Gas Combined Cycle

O/C Oxygen to carbon ratio

**OCV** Open circuit voltage

PHES Pumped Hydro Electrical Storage

PL Power law

**SCGP** Shell coal gasification process

**SEM** Scanning electron microscopy

**SOFC** Solid Oxide Fuel Cell

**SEWGS** Sorption Enhanced Water Gas Shift

S/C Steam to Carbon ratio

**ST** Steam Turbine

**SGC** Syngas cooler

**TOT** Turbine Outlet Temperature

**VIGV** Variable inlet guide vane

WGS Water gas shift

**WAC** William Alexander Centrale

YSZ Yttria stabilized zirconia

# **Contents**

Su	mma	ry	vii			
Lis	st of A	Abbreviations	хi			
1	Introduction 1.1 Background					
	1.3	power plants	4 5			
	1.4 1.5 1.6	1.3.2 Solid oxide fuel cells (SOFC)	11 12			
2	High percentage biomass co-gasification in IGCC power plants					
	2.1 2.2	Introduction	16			
	2.3 2.4	Motivation	18 20			
	2.5	Modeling approach and description	21 21			
	2.6	Results and discussion	25 26 31 32			
3		d oxide fuel cell (SOFC) integrated bio-IGCC power plants	37			
	3.1 3.2 3.3	Background	39 40			

	3.4 3.5 3.6	3.3.2 IGFC-CC STEX (with full $CO_2$ capture)42Modeling approach and description43Results & Discussion473.5.1 Carbon deposition523.5.2 Exergy Analysis543.5.3 $CO_2$ neutrality and emissions56Conclusions58
4	Flex	ble IRCC power plants with hydrogen storage 61
•	4.1	Background
	4.2	Motivation
	4.3	System description & Modeling approach 64
		4.3.1 Case description and modeling approach
		4.3.2 Exergy calculation approach
	4.4	Results & Discussion
		4.4.1 Energy analysis
		4.4.2 Exergy Analysis
	4.5	Conclusions
	4.A	Retrofitted NGCC power plant system with solid oxide fuel cells 84 $$
		4.A.1 Background
		4.A.2 Model development - Assumption and description 84
		4.A.3 Retrofitted DIR-SOFC-GT system
		4.A.4 Retrofitted DIR-SOFC-CC system
		4.A.5 Results & Discussion
		4.A.6 Concluding remarks
5	Met	ane steam reforming (MSR) kinetics in single operating SOFCs 93
	5.1	Background
	5.2	Motivation
	5.3	Experimental
		5.3.1 Equipment and planar cell description
		5.3.2 Experimental methodology and Current-Voltage (I-V) charac-
	г 1	teristics
	5.4	Kinetic model and parameter estimation
		5.4.1 Ideal plug flow reactor (IPFR) assumption
		5.4.3 Langmuir-Hinshelwood (LH) kinetic model
	5.5	Results & Discussion
	5.5	5.5.1 Methane reforming on Ni current collector (mesh) 107
		5.5.2 Power law (PL) kinetics
		5.5.3 Langmuir-Hinshewood kinetics
		5.5.4 Carbon deposition
	5.6	Conclusions

6	Conclusions			
	6.1	Contri	butions & main findings	123
		6.1.1	High percentage biomass co-gasification in existing IGCC power plants	
		6.1.2	Retrofitting bio-IGCC power plants with SOFCs and CO <sub>2</sub> capture	124
		6.1.3	Flexible IRCC power plants with hydrogen storage	124
		6.1.4	Methane steam reforming (MSR) kinetics in SOFCs with Ni-	
	6.2	Recom	ceria based anodes	
Bil	oliogi	raphy		129
Lis	t of I	Publica	tions	153
Ac	know	ledgen	nents	155
Ab	out t	he autl	nor	159

# Chapter 1

Introduction

# 1.1 Background

Increased human industrial activities over the past century is a major cause for climate change. This agreement is documented not just in a single study, but by a converging stream of evidence over the past decades from surveys of climate scientists, content analyses of peer-reviewed studies and public statements issued by virtually every involved organization of experts in this field. [1-5] There has been a general increase in the earth climate system's average temperature (termed as global warming) over the past few decades particularly due to the heat absorption by greenhouse gases (GHG) like CO<sub>2</sub> and methane (CH<sub>4</sub>). This must be avoided to prevent catostrophic natural events and to provide a safe living environment for mankind. Increased emission of these gases by fossil fuel (coal/natural gas/crude oil) based industrial manufacturing/processing plants, power plants into the atmosphere is postulated as a major cause for global warming. In order to limit drastic climate change over the next decades, clean and efficient processes must be designed, particularly in the power plant sector. The power plant sector is the single major cause for the release of GHG gases in the American and European regions. [6, 7].

Reduction on the use of fossil fuels and increase in the use of renewable sources for large scale (MW scale) power generation has been agreed upon by many countries. Multiple initiatives and targets have been set like Paris COP21, Roadmap 2050 [8], the 2030 framework for climate and energy [9] to mitigate climate change in near future. However the use of fossil fuels will continue to play an important role in the coming decades particularly due to lower costs, higher reliability and to large extent convenience. As per statistics from 2014, almost 48% net electricity production has been utilizing combustible fossil fuels in the European Union (EU)[10].

In order to make a transition towards a more clean and sustainable energy based economy, it is crucial to develop on one hand novel renewable energy technologies (bioenergy, solar, wind, geothermal etc.) and on the other hand improve/upgrade existing fossil fuel (coal and natural gas) based power plants. Gasification of solid fuels like coal and reforming of natural gas to produce syngas (a mixture of hydrogen and carbon monoxide (CO)) offers multiple advantages for clean, efficient and flexible utility of these fossil fuels in power plants. Combined cycle (consisting of 2 thermodynamic power cycles) systems like the integrated gasification combined cycle (IGCC) and integrated reforming combined cycle (IRCC) are considered key power plant technologies for solid fuels (coal/biomass) and natural gas respectively [11, 12]. This is particularly due to their relatively higher thermodynamic efficiencies, larger operating flexibility, lower water consumption and possibilities for cogeneration compared to conventional single cycle (Brayton/Rankine) power plants [13, 14]. There are multiple approaches one could take to upgrade existing IGCC/IRCC power plants for lower GHG emissions and lower fossil fuel reliance:

- 1. to integrate renewable sources into existing power plants for eg. biomass utilization
- 2. to increase power plant efficiencies thereby reducing fuel consumption for eg.

by integrating/retrofitting fuel cell technologies

- 3. to increase operational flexibility in power plants for eg. with energy storage
- 4. to introduce transition technologies to lower CO<sub>2</sub> emissions for eg, with carbon capture and storage (CCS)

Biomass (bioenergy) is one of the only renewable sources of energy which can be coprocessed in existing fossil fuel conversion systems [15]. Biomass can be coprocessed as a fuel in coal based IGCC power plants (bio-IGCC plants) to promote CO<sub>2</sub> neutral power production. Biomass can be considered as a CO<sub>2</sub> neutral fuel (on an assumption that biomass removes as much CO<sub>2</sub> from the environment during its growth as is released during its combustion) [16–18]. Furthermore, carbon (CO<sub>2</sub>) capture and storage (CCS) is an available transition technology to reduce CO<sub>2</sub> emissions from fossil fuel based power plants. In parallel, it is also important to investigate options towards boosting power plant efficiencies significantly to reduce (fossil) fuel consumption. Fuel cells are high efficiency electrochemical devices which can convert chemical energy in fuels to electrical energy. In particular solid oxide fuel cells (SOFC) are considered suitable for power plant integration as they are fuel flexible, operating at high temperature, intrinsically CCS ready and relatively high contaminant tolerant [19].

Presently, research on high efficiency combined cycle power plant systems largely focus towards development of new systems with distant future implementation. Limited studies have been performed towards integrating (retrofitting) novel technologies in existing installations with a focus on near future implementation. In order to invest and implement suitable retrofits, it is of utmost importance to assess power plant off-design performance, required process modifications and operational boundaries based on the existing equipment in the power plant.

Thermodynamic system modeling can be an effective tool to evaluate power plant performance with alternative and off-design operating conditions. System evaluation using detailed models/simulations is considered as a base towards optimal design, control and operation of power plants. In order to assess the aforementioned approaches towards upgrading existing IGCC/IRCC power plants to achieve higher efficiencies, flexibility and low CO<sub>2</sub> emissions, detailed and validated thermodynamic models need to be developed. Such models also help in assessing thermodynamic feasibility and process constraints. Experimental research efforts are also important, however due to cost, time constraints and limited experience, experiments in power plants on a large scale are often not feasible. The main purpose of carrying out a system model analysis is to check whether the same electrical power output can be maintained with change in process/operating conditions. In addition it is important to predict thermodynamic operating efficiencies for these new systems and identify areas for further improvements.

The next two sections describe the need for increased efficiency and flexibility in power production and an overview of key enabling technologies. The main research targets have then been described, following with the scope and outline of the dissertation.

# 1.2 Need for increased efficiency and flexibility in power plants

Energy efficiency plays an important role in quantifying fuel utilization in power plants and thereby directly affecting the GHG emissions. A general definition for energy efficiency would be the ratio of product(s) energy content and source (fuel) energy content. There can be many ways of defining efficiency of a power plant, depending on what we consider as products. However, if we consider only electricity as the product and the energy in the input fuel i,e the lower heating value (LHV) as the source, it becomes evident that by increasing energy efficiencies, there is lower fuel consumption. Increasing energy efficiency of IGCC/IRCC power plants also reduces energy costs and thus makes the whole power generation cycle much cheaper. In addition to the energy efficiency, that is based on the 1st law of thermodynamics, it if often very useful to assess energy conversion systems like IGCC/IRCC power plants from an exergy point of view. This helps in identifying thermodynamic losses in the system and to establish further system improvements. A detailed explanation on the concept of exergy and exergy efficiency is given in the following chapter.

Furthermore, flexibility in power production remains a major requirement. With large investments in renewable energy technologies underway, an increase in the share of renewable electrical power in the total electrical power production is predicted in the future [20, 21]. This could result in large fluctuations in future power supply and demand [20, 21]. Electrical energy storage (EES) is considered as a potential solution to this, resulting in more reliable electrical power supply and reduction in energy costs. The basic concept is to store the produced electrical energy during low demand (base load) period and utilize the stored energy during high demand (peak load) periods. Different storage options have been developed in the last decades like batteries (also redox-flow), flywheels, pumped hydro storage, compressed air storage, natural gas storage and hydrogen storage. These options differ in terms of discharge time, energy content and efficiency [22]. With hydrogen being a co-product from the energy conversion processes in IGCC/IRCC power plants, investigations need to be carried out to assess the effects of integrating hydrogen storage in stationary power plants. Co-produced carbon free hydrogen could be stored during low demand hours thereby providing increased flexibility.

# 1.3 Overview of enabling technologies

This section gives a brief overview on the various enabling power plant technologies towards developing large scale (>150 MW $_e$ ) clean, efficient and flexible IGCC /IRCC power plants. A short introduction is first presented on available CCS technologies followed with a basic introduction to high temperature solid oxide fuel cells. Thereafter, the role of SOFCs towards developing high efficiency and clean combined cycle power plant systems has been clarified including the importance and challenges of hydrocarbon (methane) utilization in SOFCs.

## 1.3.1 Carbon (CO<sub>2</sub>) capture & storage (CCS)

Carbon capture and storage (CCS), is a process technology of capturing/separating waste carbon dioxide ( $CO_2$ ) from large sources, such as fossil fuel based power plants, transporting it to a storage site, and storing it at a location to prevent its release into the atmosphere, normally an underground geological formation. The aim is to prevent the release of large quantities of  $CO_2$  into the atmosphere, from fossil fuel use in power generation and other industries. Fig. 1.1 summarizes the various  $CO_2$  capture technologies. The next subsections give an overview of the three major capture technologies applicable to power plants. Storage of captured  $CO_2$  has not been addressed in this work and is considered out of scope for this project.

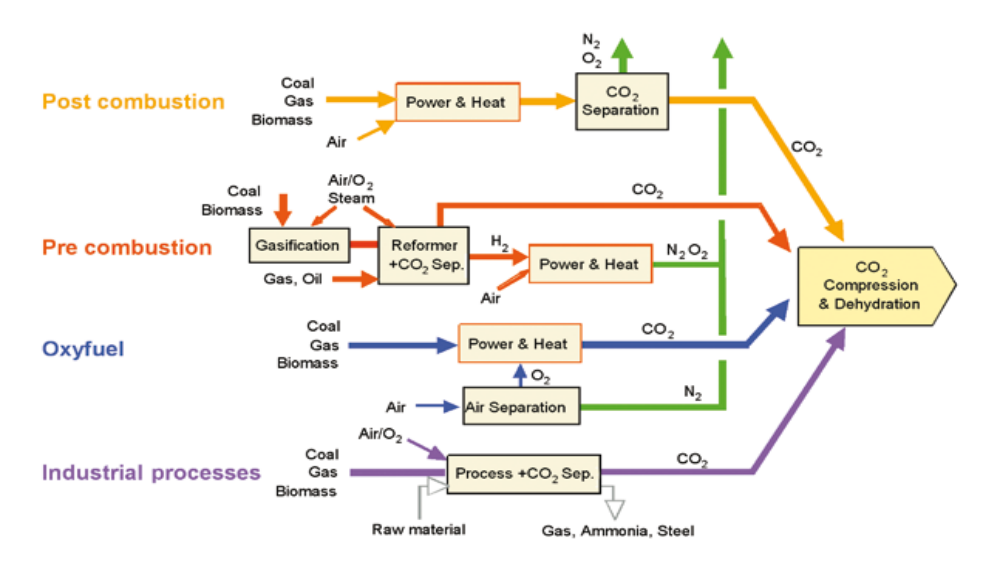


Figure 1.1: Overview of carbon capture technologies [23] - This thesis work investigates pre-combustion (Chapter 4) and oxy-fuel combustion (Chapter 3) technologies

## 1.3.1.1 Pre-combustion capture

Systems with pre-combustion capture consist of a process where CO<sub>2</sub> is separated before the fuel is combusted to produce power (for eg. with a gas turbine cycle). Fig.1.2 shows a simplified schematic for an IGCC power plant with pre-combustion CO<sub>2</sub> capture. In combined cycle power plants (IGCC/IRCC) with a hydrocarbon based fuel like coal/biomass/natural gas, syngas (mixtue of CO and H<sub>2</sub>) is first produced using a gasifier (IGCC) or reformer (IRCC). The resulting syngas then undergoes the water gas shift reaction (WGS) to convert CO to CO<sub>2</sub>. The CO<sub>2</sub> rich gas stream is then purified to obtain pure CO<sub>2</sub>, which can be compressed and stored. The high concentrations of CO<sub>2</sub> produced by the shift reactor (typically 15-60% by

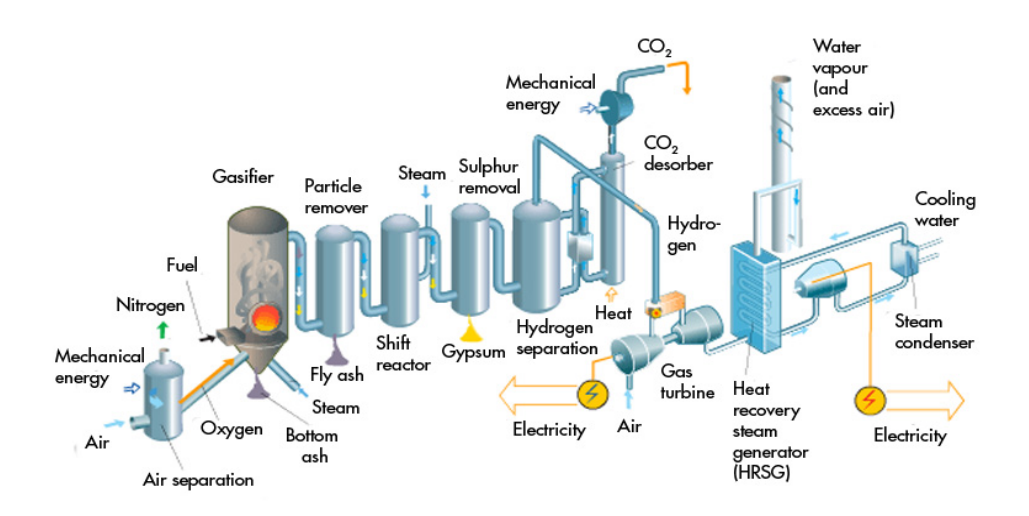


Figure 1.2: Process scheme of IGCC power plant with precombustion CO<sub>2</sub> capture [24]

volume on a dry basis) and the high pressures are favourable for  $CO_2$  separation by physical absorption.  $H_2$  rich fuel is utilized to produce power.

The sorption enhanced water gas shift (SEWGS) technology developed at the Energy Research Center of the Netherlands (ECN) is a powerful and efficient process for simultaneously carrying out the WGS reaction and in parallel capturing  $CO_2$ . The main advantage of the process include the high conversion of  $CO_2$  to  $CO_2$  by the shift reaction through the selective removal of the product  $CO_2$  [25]. Also the process is operated entirely at high temperature yielding hot streams of  $CO_2$  and  $CO_2$  and H<sub>2</sub>. Hydrogen obtained at high temperature with excess steam results in higher efficiency and reduced NOx emissions [25, 26]. The SEWGS unit produces two streams: a  $CO_2$  rich gas (>95% mol  $CO_2$ ) which is sent to the gas turbine combustor or stored and a  $CO_2$  rich gas (>95% mol  $CO_2$ ) which is sent to the  $CO_2$  storage unit.

In the SEWGS process, a  $K_2CO_3$  promoted hydrotalcite- based sorbent is used to adsorb  $CO_2$  and also as a catalyst for the shift reaction. The temperature of operation is typically  $400^oC$ . The SEWGS cycle is shown in Fig.1.3. The process utilizes 6 parallel reactors each consisting of 5 steps: feed (adsorption and shift takes place), rinse for clearing voids, depressurization, purge for sorbent regeneration and repressurization. The feed step involves feeding the reactor with syngas obtained from the pre-shift reactor to produce hydrogen. Next the reactor is rinsed with medium pressure steam to obtain syngas which is mixed with the feed. A pressure equalization step follows where the rinse gas expands through the reactor pushing the interstitial syngas to a reactor at lower pressure. In the blowdown (bd) and purge steps,  $CO_2$  is collected. With the repressurization of the reactor with part of the hydrogen, the reactor is ready for the next cycle.

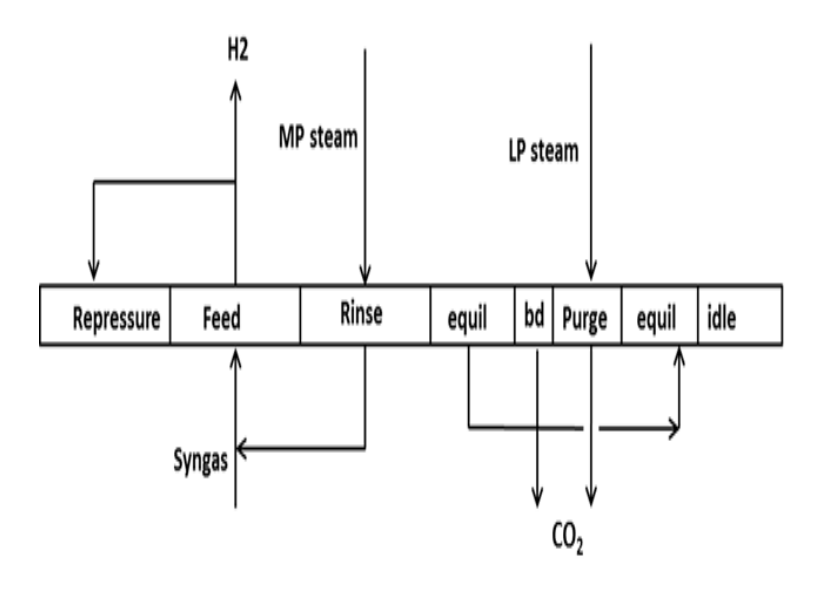


Figure 1.3: SEWGS process cycle [25]

## 1.3.1.2 Oxy-fuel combustion capture

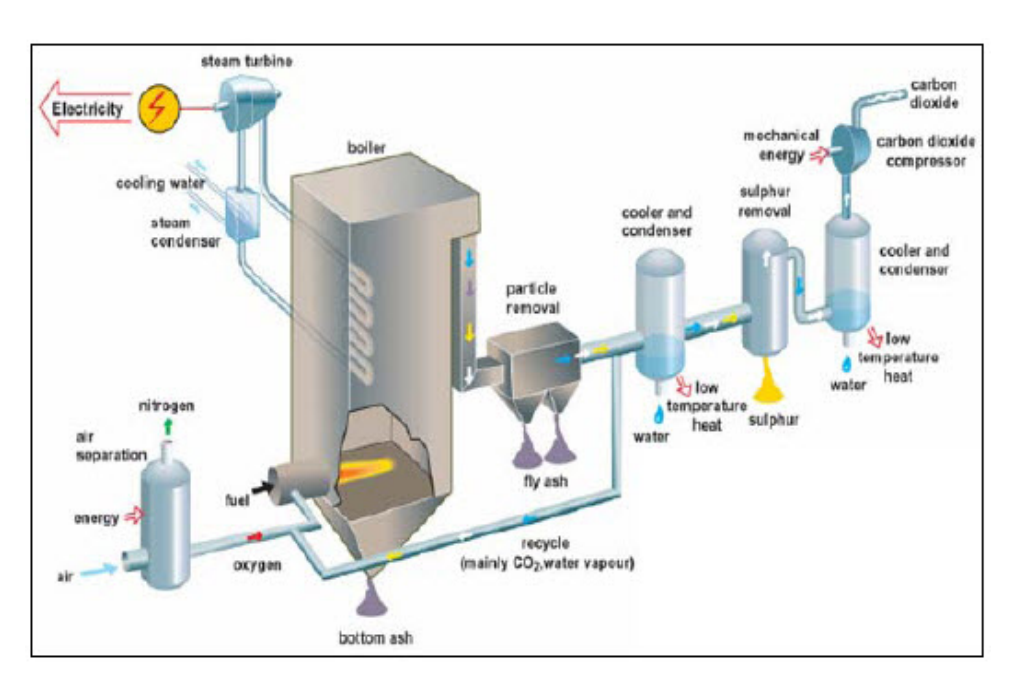


Figure 1.4: Process scheme of a power plant with oxyfuel combustion CO<sub>2</sub> capture [24]

Combusting fuel using pure oxygen (>95% vol purity) instead of air at near-stoichiometric conditions, results in a flue gas consisting mainly CO<sub>2</sub> (>80% on a dry basis), water vapor and small amounts of noble gases. Given that nitrogen is the main component in air used for combustion (79% volume), nitrogen dilution in flue gas can be avoided by switching from air combustion to pure oxygen combustion. If the fuel is clean, flue gas will mainly consist of CO<sub>2</sub> and water vapour. CO<sub>2</sub> can be easily separated by cooling and condensing out water [27]. Fig.1.4 shows a simplified schematic for an IGCC power plant with oxyfuel-combustion CO<sub>2</sub> capture. Oxyfuel combustion capture is particularly well suited for SOFC integrated IGCC/IRCC power plants as the unutilized fuel in the SOFC can be combusted with pure O<sub>2</sub> and followed with cooling and water condensation.

### 1.3.1.3 Post-combustion capture

Post-combustion systems separate  $CO_2$  from the flue gases produced by the combustion of the carbonaceous fuel with air. These systems normally use amine based solvents to capture the small fraction of carbon dioxide (typically <15% by volume) present in a flue gas stream in which the main constituent is nitrogen. Several chemical and physical absorption processes exist that can separate the  $CO_2$ . Common solvents used in chemical absorption processes are monoethanolamine (MEA), methyl diethanolamine (MDEA), Sulfinol while Rectisol, Purisol and Selexol are used in physical absorption processes [27].

The choice of the capture technology depends on many factors such as type of the power plant, operating conditions, scale of the capture unit, economic considerations and location. This dissertation focuses primarily on oxyfuel combustion and precombustion capture technology and their integration in bio-IGCC and IRCC power plant systems respectively. The next section provides a short introduction to SOFCs and their role as a key power plant technology to increase net plant efficiencies and flexibility.

# 1.3.2 Solid oxide fuel cells (SOFC)

SOFCs are highly efficient electrochemical devices that convert the chemical energy in a fuel into electricity without direct combustion. They are not subjected to the Carnot efficiency and the electrochemical conversion of fuel is thermodynamically more advantageous than combustion[28]. Solid oxide fuel cells(SOFC) operate at high temperatures between 700-1000°C, depending on the material. The performance and efficiency of SOFCs increase when operated under pressure. Because of their high temperature and operating pressure, SOFCs are considered ideal for integration in power generating systems. Their outlet gas streams can be expanded in a gas turbine (GT) to produce additional power or steam can be generated with the heat in the exhaust gas to power a steam Rankine Cycle. Furthermore the outlet gas streams can be easily integrated with CO<sub>2</sub> capture technologies to yield clean power. However, a major remaining challenge is the comparable sizing up of the SOFC unit for large scale power plants due to cost and material constraints.

The solid oxide fuel cell as shown in Fig.1.5 is constructed with two porous electrodes (anode and cathode) that sandwich a dense oxide ion-conducting ceramic material, the electrolyte. The thickness of each layer is generally of a few micrometers ( $\mu$ m) .Air is fed on the cathode side and gaseous fuel (H<sub>2</sub>, CO, CH<sub>4</sub>, syngas, ammonia, biogas etc.) is fed on the anode side. With a difference in the oxygen partial pressure between the electrodes, oxide ions (from cathode) diffuse through the electrolyte material and migrate to the other side of the cell where they come in contact with the anode. The oxygen ions encounter the fuel at the anode/electrolyte interface and react catalytically, producing water, carbon dioxide, heat, and electrons which are transported through an external circuit providing electrical energy.

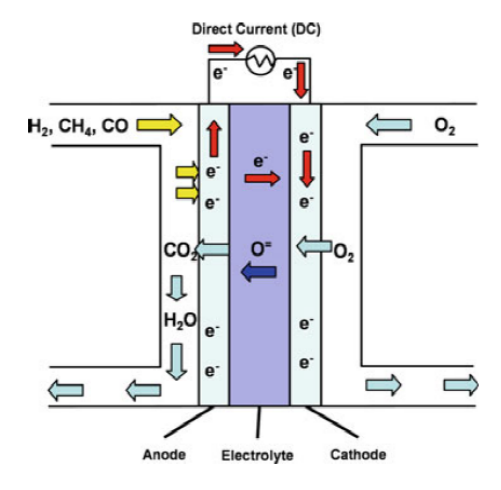


Figure 1.5: Schematic showing the working principle of SOFCs [29]

The porous anode in addition to the ceramic material (like YSZ (yttria stabilized zirconia), GDC (gadolina doped ceria)) also consists of metal catalysts like nickel (Ni) which help in promoting reaction rates. The ceramic-metallic (cermet) anode material thus becomes one of the most important aspect in designing SOFCs. The exothermic electrochemical oxidation reactions occuring in an SOFC are as shown in Eqn. 1.1 and Eqn. 1.2. Carbon monoxide (CO) oxidation (Eqn.1.3) is an additional electrochemical reaction to be considered in operating SOFCs, however it is generally reported that  $H_2$  oxidation is the predominant electrochemical reaction [30].

$$O_2 + 2e^- \to O^{2-}$$
 (1.1)

$$H_2 + O^{2-} \rightarrow H_2O + 2e^-$$
 (1.2)

$$CO + O^{2-} \rightarrow CO_2 + 2e^-$$
 (1.3)

SOFCs are fuel flexible [28, 31]. Hydrocarbon fuels like methane ( $CH_4$ ), CO, syngas, biogas etc. and other hydrogen containing fuels like ammonia can be utilized in

SOFCs. Fossil fuel based IGCC/IRCC power plants generally involve the conversion of the feedstock (fuel) to syngas (a mix of CO, H<sub>2</sub>, CO<sub>2</sub>) via an appropriate process (gasification/reforming) and the obtained syngas is utilized in a combined cycle to generate electric power. SOFCs could thus be integrated in such power plants partially replacing the less efficient combustion process [19, 32]. However there are many challenges towards SOFC integration in power plants, particularly due to the technology being relatively expensive, very high start-up and shut down times, limited demonstrations and operating challenges (like coking). With intensive global ongoing efforts [33, 34] on developing kW scale fuel flexible SOFC stacks, research needs to be carried out in understanding and assessing possibilities of integrating (or retrofitting) such SOFC stack modules in existing coal/biomass based IGCC/IRCC power plants.

In the case of IRCC power plants operating with natural gas as fuel, there exists also a possibility to directly utilize natural gas (consisting mainly CH<sub>4</sub>) as a fuel in SOFCs. Direct use of methane as fuel in SOFCs, called direct internal methane reforming can be considered as one of the most efficient methods of producing electricity [35]. Catalytic methane steam reforming (MSR) is also one of the most common methods for hydrogen production on an industrial scale. Thus direct CH<sub>4</sub> utilization in SOFCs offers additional prospects for hydrogen production and efficient power generation with natural gas. A better understanding on MSR reaction kinetics in operating SOFCs will aid in the development of optimal and safe SOFC modules for power plant integration. The next section gives a short introduction on internal MSR in SOFCs and the importance of experimental research efforts.

# 1.3.2.1 Methane steam refoming (MSR) in SOFCs - reaction kinetics and importance

The MSR reaction is shown in Eqn.1.4. The endothermic reaction produces syngas, a mix of CO and  $H_2$ . The produced CO could also react with steam at high temperature via the water gas shift (WGS) reaction (Eqn.1.5) to produce  $CO_2$  and  $H_2$ .

$$CH_4 + H_2O \rightarrow CO + 3H_2$$
  $\Delta H_{298K} = 206kJ/mol$  (1.4)

$$CO + H_2O \rightarrow CO_2 + H_2$$
  $\Delta H_{298K} = -41kJ/mol$  (1.5)

Due to the reaction rates and thermodynamics of the MSR and electrochemical reactions being different, undesirable temperature gradients arise in the anode leading to reduced performance. However the heat released by the electrochemical reactions (Eqn.1.2, Eqn.1.3) in the SOFC helps promote the MSR reaction. The main focus towards optimizing SOFC performance with internal MSR would be reduce these undesirable temperature gradients in the cell/stack. Inspite much progress in recent years towards developing novel anode materials, numerous challenges still remain to operate internal reforming SOFCs with minimal cell degradation and electrode poisoning. The nickel catalyst in the SOFC anode also promotes carbon deposition (coking) in the anode [31].

MSR reaction kinetics on Ni catalysts have been experimentally studied extensively in the past by numerous researchers particularly using test catalytic reactors

and catalyst beds [36–42]. However there is a shortage in experimental work using complete SOFC cermet anodes during operation (under the influence of current). Limited kinetic studies on MSR reaction kinetics are available which take into account the differing operating conditions like gas composition, temperature and current densities. Furthermore, multiple kinetic expressions (of various types like power law (PL), Langmuir-Hinshelwood (LH), first order (FO) kinetics) have been utilized by researchers [35] to quantify MSR reaction kinetic parameters. No consensus has yet been reached with these studies on reaction mechanisms, reaction rate expressions and proposed theories. Hence multiple experimental efforts are crucial in the coming future to further deepen our understanding on MSR reaction kinetics in operating SOFCs.

# 1.4 Energy storage

Ensuring reliable power supply to consumers is of prime importance for power utility companies. Electricity demand from various consumers can vary significantly depending on many factors like time, location, purpose and cost. Electricity prices also vary depending on time. The price of electricity is higher during high demand periods compared to low demand periods due to differences in cost of power generation. Hence, there needs to be a good balance between electricity supply and demand from power plants. Electrical energy storage (EES) options are suitable towards introducing operational flexibility in IGCC/IRCC power plants as aforementioned in section 1.2. Different EES options have been developed in the last decades towards introducing flexibility in power plants which have been listed below:

- **Mechanical storage**: This involves the storage of electricity using mechanical methods like Pumped hydro storage (PHS), Compressed air energy storage (CAES), Flywheels.
- Chemical storage: Chemical storage involves the storage of electricity with producing of secondary fuels like H<sub>2</sub> or synthetic natural gas (SNG). As an alternative, produced hydrogen in the system can also be stored directly prior to electricity production.
- Thermal storage: This option consists of storing electrical energy in the form of heat. Various options here consist of storage of sensible or latent heat and thermochemical adsorption or absorption storage methods.
- Electrochemical storage: Batteries are considered a suitable medium to store electrical energy. These can be either secondary batteries or redox-flow batteries.
- **Electrical storage**: These include supercapacitors and superconducting magnetic storage methods. However these have limited scope in application on large scale power plant systems

All the aforementioned EES options differ significantly in terms of discharge times, energy content and efficiency. Hydrogen is considered a potentially clean energy carrier for both mobile and stationary applications. Multiple options exist to store hydrogen like compressed storage, cryogenic storage and storage in metal hydrides. Storage in metal hydrides (MH) has the benefit that it requires lower pressures and reduced volumes [43] resulting in a safer system with reduced capital investments. An additional advantage is the possibility of integrating heat during the MH reaction resulting in a flexible system that is expected to maintain high efficiencies of the storage system and the plant during peak and off-peak demand periods. Nonetheless, there are major operating challenges with the usage of metal hydrides on large scale due to material stability issues, relatively fast degradation and high cost.

# 1.5 Research targets

Based on the broad motivation and concepts presented in the earlier sections, the main research targets for this work have been identified and are listed below:

- 1. Design, development and experimental validation of system concepts for bio-IGCC power plants based on high percentage (70%) biomas co-gasification tests carried out at the Willem-Alexander Centrale (WAC), a 253 MW<sub>e</sub> IGCC power plant in the Netherlands. The system study to be based on off-design steady state model development and subsequent validation with experimental data.
- A thermodynamic case study on retrofitting SOFCs and CO<sub>2</sub> capture in existing bio-IGCC power plants identifying process constraints and energy/exergy analysis, with a focus on enhancing operating efficiencies of existing bio-IGCC power plants in near future.
- 3. Design and thermodynamic assessment of a flexible natural gas fuelled IRCC (with CO<sub>2</sub> capture and hydrogen storage) power plant concept using steady state models.
- 4. A stepwise experimental investigation into internal methane steam reforming (MSR) kinetics in operating SOFCs to facilitate reliable numerical model development.

# 1.6 Scope & Outline

This dissertation carried out within the framework of the CATO-2B project (the Dutch national project on CCS), primarily comprises of multiple system conceptual studies and thermodynamic assessments towards developing high efficiency IGCC and flexible IRCC power plants with  ${\rm CO_2}$  capture. Process design and evaluation has been focused on achieving high net electrical and exergy efficiencies, minimize

 ${\rm CO_2}$  emissions and operational flexibility. Solid oxide fuel cells (SOFCs) have been chosen as an enabling technology to achieve high efficiency. As an extension, experimental investigations have also been carried to understand MSR reaction kinetics in SOFCs. The dissertation is divided in 6 chapters as outlined below:

*Chapter 1* is the introductory chapter giving technical background for the study and defining research targets.

Chapter 2 presents a detailed experimental validation and thermodynamic assessment on high percentage (70% on energy basis) biomass co-gasification in an existing coal based IGCC power plant (called bio-IGCC). An off-design steady state model has been developed and validated using experimental data from large scale tests carried out using steam exploded wood pellets at the Willem-Alexander Centrale, a 253 MW<sub>e</sub> IGCC power plant (now defunct) in the Netherlands.

Chapter 3 extends the system study presented in Chapter 2 towards integrating (retrofitting) SOFCs and oxy-combustion fuel  $\rm CO_2$  capture in existing bio-IGCC power plants. A case study is presented again based on the Willem-Alexander Centrale focussing on retrofitting and near future implementation.

Chapter 4 investigates flexibility aspects in natural gas based IRCC power plants with precombustion CO<sub>2</sub> capture and metal hydride based H<sub>2</sub> storage. Furthermore a preliminary system study has been presented in Appendix 4A on retrofitting natural gas combined cycle power plants with SOFCs.

Chapter 5 deals with experimental investigations on methane steam reforming (MSR) kinetics in operating single SOFCs (Ni-ceria based anodes). Experiments have been carried out using a planar electrolyte supported (ESC2) cell with a Ni-GDC anode under relatively low S/C ratios (around 1) and moderate current densities ( $I_c$ ) upto 3000 A/ $m^2$ . A comparative study between power law (PL) and Langmuir-Hinshelwood (LH) kinetics is presented.

*Chapter 6* reports the main conclusions of the dissertation with a section on recommendations for future work.

# Chapter 2

# High percentage biomass co-gasification in IGCC power plants

Biomass co-gasification in existing coal based IGCC power plants promotes renewable power production. Despite many recent efforts on a smaller scale, there still hasn't been any successful demonstration reported on high percentage (more than 50% on energy basis) biomass co-gasification at existing large scale IGCC power plants. This chapter reports experimental test data obtained from 70% biomass (steam exploded wood pellets) co-gasification tests carried out at the 253 MW<sub>e</sub> coal based Willem-Alexander Centrale (WAC), Buggenum in The Netherlands. A brief introduction on the WAC power plant has first been presented following with a thermodynamic analysis using a detailed and validated steady state system model. The validated model has been further utilized to predict plant performance involving 70% co-gasification with two fuel blends of torrefied wood pellets. The model predicts plant performance and process parameters with reasonable accuracy (less than 3% deviation). Exergy analysis indicates largest thermodynamic losses in the gasifier and during combustion, providing additional scope for efficiency enhancement. Furthermore, the presented test data serves as a reliable and prime data source for modeling studies. The validated models could serve as a strong platform to plan real plant operation with various biofuels and carry out studies involving novel technology integration, retrofitting (chapter 3) and plant optimization.

This chapter is published as: A. Thallam Thattai, V. Oldenbroek, L. Schoenmakers, T. Woudstra, P.V. Aravind, Experimental model validation and thermodynamic assessment on high percentage (up to 70%) biomass co-gasification at the 253 MW<sub>e</sub> integrated gasification combined cycle power plant in Buggenum, The Netherlands, Applied Energy, Volume 168, 15 April 2016, Pages 381-393, ISSN 0306-2619

## 2.1 Introduction

The role of biomass co-gasification in clean and sustainable power production has been of major global interest as biomass utilization could lead power plants to be carbon neutral and possibly carbon negative (if carbon capture and storage (CCS) is employed) [44–46]. With growing environmental concerns and stringent emission requirements, research and developement in high percentage biomass utilization in large scale power plants is highly important. One of the major priorities of the Dutch government has been to assess feasibility for biomass co-gasification to achieve high percentage renewable power production and carbon reduction [47]. Also, biomass co-gasification is a more suitable technology for solid fossil fuel power plants.

# 2.2 Plant overview and process description

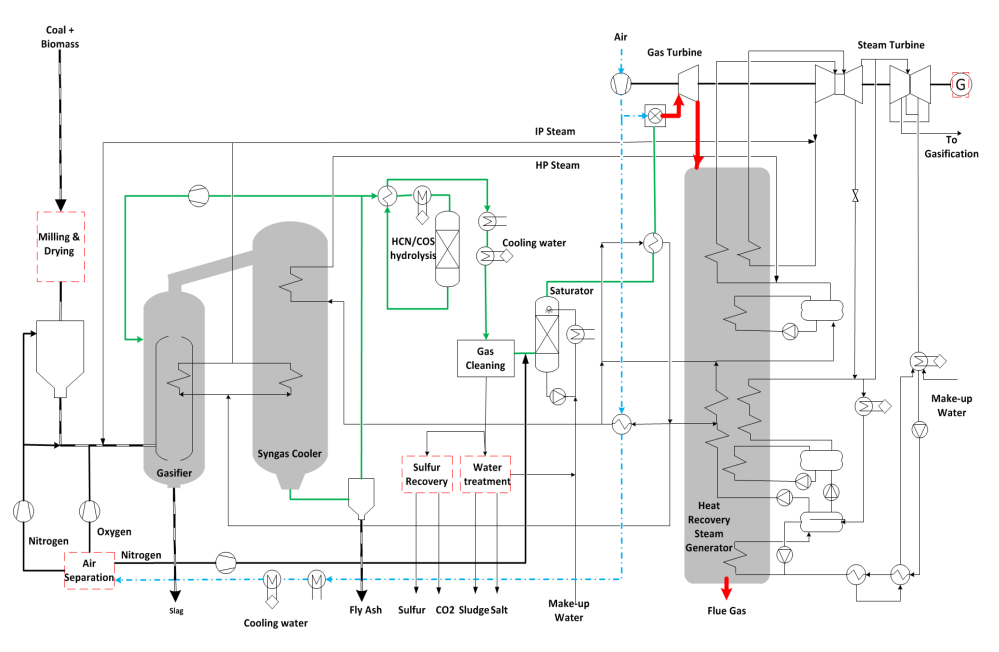


Figure 2.1: Process flow diagram for the Willem-Alexander Centrale (WAC)- Red dotted blocks have not been modelled in detail

The Willem-Alexander Centrale (acronymed in this dissertation as WAC) has been a key demonstration plant for coal based IGCC technology. The power plant was constructed in 1989 by Demkolec (defunct company now), a consortium of Dutch power producers [48]. It was originally a demonstration project (Demo KV-STEG) with the aim of proving the feasibility of the IGCC technology for power production on a large scale in The Netherlands. After the demonstration phase from 1993 through 1998 the plant was ready for commercial operation [48–50].

With the liberalization of the Dutch power market, N.V. Nuon Energy (subsidiary of the Swedish company Vattenfall since 2009) acquired the plant in 2001 with the main purpose of balancing the company's power supply and demand. In 2003, the company acquired Dutch power plants owned by the American power company Reliant Energy and this facilitated WAC to be operated as a base-load plant using coal and an increasing share of biomass [51].

Fig. 2.1 illustrates the primary components at WAC in a process flow diagram. The plant design is based on the Shell Coal Gasification Process (SCGP) to convert pulverized fuel mix to synthesis gas (syngas) under sub-stoichiometric conditions in a dry feed slagging entrained flow gasifier at high temperatures between 1500-1800°C. The gas is subsequently cooled to approximately 250°C to remove particulates, halogens, sulphur compounds and other contaminants. This is to avoid corrosive conditions in downstream process equipment and more importantly, avoiding harmful emissions through combustion of syngas. Prior, to combustion, syngas is diluted with N<sub>2</sub> and saturated with water vapour to lower combustion temperature and NO<sub>x</sub> emissions. Flue gas is then expanded in a gas turbine thereby generating power and the off-gas, which continues to exhibit a considerable amount of thermal energy, is directed through a heat recovery steam generator (HRSG). Subsequently a steam turbine unit is utilized at three different pressure levels for additional power generation. As shown in the the figure, the air cycle is 100% integrated i,e all air utilized in the plant is obtained. Detailed features of the various sub-systems in the plant can be found in previous work[52].

The increased need for flexible and efficient power plants also demands research into load flexibility and polygeneration aspects. IGCC power plants have also been studied by many researchers considering these aspects [53–58]. In order to develop such flexible systems with reduced emissions and high efficiencies it is important to understand and demonstrate real off-design operation of the plant with experimental tests and thermodynamic models. Based on these considerations a biomass scale-up project was carried out at WAC to assess high percentage (70% energy based) biomass co-gasification.

## 2.2.1 Biomass scale-up project at WAC

Biomass handling capabilities at WAC were extended with installation of a biomass silo and feed systems; continuous biomass co-gasification could thus be realized. Several types of biomass fuels like wood, chicken litter, paper sludge, sewage sludge and ground coffee beans were tested on a small and preliminary scale [59, 60]. Coal still could be used as a cheap and abundantly available back-up fuel in case of fluctuations in the biomass supply [47]. Based on small scale tests, milled wood pellets turned out to be the most suitable bio-fuel for scaling up biomass co-gasification at WAC [61]. Use of woody biomass in an entrained flow gasifier designed for coal leads to a drop in the gasifier cold gas efficiency (ratio of chemical energy in syngas to the chemical energy in the fuel) due to the higher hydrogen to carbon (H/C) and oxygen to carbon (O/C) ratios in biomass [15]. Further, biomass gasification under the same conditions yields less chemical energy in syngas and more sensible

heat [15]. The molar concentrations of carbon dioxide  $(CO_2)$  and water vapour  $(H_2O)$  also increase in the syngas at the expense of carbon monoxide (CO) and hydrogen  $(H_2)$  [15]. Increase in the sensible heat of syngas increases heat transfer requirements downstream and calculations showed that at maximum plant load the percentage of milled wood pellets (without pretreatment) in the fuel mix was limited to 15%.

The aim was to achieve a net electrical output of 230 MW while co-gasifying 70% biomass (target was set to 70% biomass in the fuel mix, energy based) [47, 61]. It was thus decided to utilize pre-treated biomass for the fuel blend to assess operational feasibility without major plant modifications. Pre-treatment of biomass enhances the quality of the biomass feedstock in terms of its mechanical, thermal and chemical properties [15]. Steam explosion and torrefaction are two of the available pre-treatment technologies that upgrade ligno-cellulosic biomass (like wood) to a higher quality fuel (increased LHV) [15, 62, 63]. Steam explosion is carried out typically at 160-260 °C; where biomass undergoes an explosive decompression thus yielding biomass with increased LHV [15, 63]. Torrefaction is an alternative pre-treatment method in which biomass is heated slowly to a temperature of 200-300 °C in a non-oxidizing atmosphere [15, 63]. This causes the biomass to become brittle and hydrophobic with a decrease in the O/C and H/C ratios. The changes in composition and lower heating value (LHV) have a beneficial effect on the gasifier cold gas efficiency. Torrefaction can yield a higher LHV end product than steam explosion in a relatively simpler process, also because with steam explosion, a drying operation must be performed before densification and use in co-gasification applications [63]. In addition, the existing coal mills at the plant can be utilized to co-grind biomass.

High percentage (70% on energy basis) co-gasification tests were carried out with steam exploded woodpellets as the first step in the biomass scale up project [61]. The large scale biomass co-gasification test carried out by NUON/Vattenfall at WAC utilized commercially obtained steam exploded woodpellets, called black pellets. The pellets are produced with a sequence of processes like drying, thermal conditioning, milling and pelletizing [64]. Wood chips are first dried to reduce moisture content to <10%. The chipped wood is sealed in a pressure vessel and pressurized with steam. A thermal conditioning step is followed then with a sudden release of pressure. This blows the biomass and leads to a tight, hard pellet bonded together. These pellets could be shipped, received, stored, conveyed and milled just like coal in the existing mills. Investigations were also required to understand the technical feasibility of co-gasifying torrefied woodpellets at WAC.

# 2.3 Motivation

Detailed and validated system models can be an effective tool to evaluate plant performance with alternative and safe operating conditions; hence it was decided to develop thermodynamic models based on the WAC plant design as an important aid to predict and verify off-design plant performance. In literature many studies can be found on IGCC modeling, mainly with coal [65–71] with a few studies on low percentage biomass co-gasification. Modeling results on IGCC systems have been reported for 20% co-gasification using sawdust [72, 73]. Additional results with 20% co-gasification of sewage sludge, meat and bone meal were reported [74]. Valero et al. [75] presents modeling evaluation of the oxy-co-gasification process for various types of biomass upto 10%. Various techno-economic and thermo-economic evaluation studies have been reported for various types of biomass on small to medium scale (upto 20  $MW_{th}$ ) [76–81] and economic studies of large scale biomass based IGCC systems have also been reported. [18, 82]

Majority of these modeling results rely on literature or small scale tests as a prime data source and reliability thus remains debatable. Also there exists an inadequacy in experiment based IGCC system assessments. Experimental studies have been reported on stand alone gasifier units, for e.g., by Fermoso et al. [83] where upto 10% co-gasification was studied with almond shells, olive stones and eucalyptus. A small scale (5.5 MW<sub>e</sub>) 100% biomass (rice husk and agricultural wastes) based IGCC demonstration project was carried out in China [84] and Sydkraft AB has demonstrated a small scale (6 MW<sub>e</sub>) biomass based IGCC power plant fuelled by wood in Vaernamo, Sweden [85]. Small percentage (2-4%) biomass co-gasification test data was reported by Sofia et al. [86] for the 300 MW Puertollano IGCC power plant in Spain with a techno-economic analysis for high percentage co-gasification.

Review on literature shows lack of availability in IGCC plant operating data for high percentage biomass co-gasification in large scale IGCC plants. This work, for the first time in scientific literature, strives to present the demonstration and actual plant data for high percentage (70% on energy basis) co-gasification carried out at a large scale IGCC power plant. The co-gasification test was carried out using steam exploded wood pellets. The experimental test data has also been utilized to develop a detailed and validated steady state thermodynamic model. The off-design model has been developed based on our previous work involving the development and validation of a design base case (100% coal gasification) model [52]. A well understood and well explained demonstration of high percentage biomass co-gasification in an existing large scale IGCC power plant is of crucial importance.

In this period of crisis for the power plant community where companies operating power plants are not able to justify their decisions to invest in new technologies and a growing environmental concern, it could help initiate a renewed interest in the development of carbon dioxide neutral (possibly negative if CCS is employed) power plants. A major engineering achievement as this could also be sufficient for effecting major changes in policies. The demonstration of the technology in such a large scale could help develop a renewed interest in biomass utilization amongst policy makers. This work in addition presents model predictions for co-gasification with torrefied woodpellets at WAC. The developed off-design models could be an important tool to plan real plant operation with various biofuels and to carry out further studies involving novel technology integration, retrofitting and plant optimization.

# 2.4 Case definition and fuel composition

Case	Feed fuel	LHV (MJ/kg)
BASE [52]	Australian Coal AUS-I	26.75
STEX	70% Steam exploded woodpellets + 30% Columbian coal	19.59
TORR-low	70% Torrefied woodpellets + 20% South African coal + 10% Columbian	22.87
	coal	
TORR-high	70% Torrefied woodpellets + 30% South African coal	23.82

Table 2.1: Case definition - STEX represents the validation case. TORR-low and TORR-high are defined based on the LHV of the fuel blend with torrefied pellets

Table 2.1 shows the definition for various cases considered in this study and the LHV of input fuel mix. The LHV for the coal powder in the BASE case was calculated based on design data and the Milne equation [52]. For the cases with biomass cogasification, the LHV was obtained directly from NUON/Vattenfall. STEX represents the validation case for the co-gasification test with steam exploded woodpellets. Fuel mix for the STEX co-gasification test was obtained by mixing coal and steam exploded woodpellets with simultaneous operation of two on-site stacker-reclaimers at different speeds over the coal and steam exploded woodpellet piles. The velocities were set in a ratio such that the estimated share of biomass in the fuel mix was 70% (on energy basis). Heating values and bulk densities were taken into account for determination of the speed ratio. Two cases: TORR-low and TORR-high have been defined with different fuel blends and LHV based on NUON/Vattenfall's requirements for predicting co-gasification with torrefied pellets.

# 2.4.1 Feedstock composition & heating values

The fuel mix composition for the different cases are shown in Table 2.2. This represents the composition of the fuel mix fed to the gasifier after the drying operation. The ultimate and proximate analysis of the various coal and biomass feedstock can be found in Table 2.3. The STEX case fuel powder (ultimate analysis) and ash analysis was carried out by NUON/Vattenfall at their laboratories [87]. Ash consists of various compounds but mainly quartz (SiO<sub>2</sub>), hematite (Fe<sub>2</sub>O<sub>3</sub>) and aluminium oxide (Al<sub>2</sub>O<sub>3</sub>). These three compounds with highest mole fraction are included in the fuel composition. Fuel mix for biomass co-gasification (both with steam exploded and torrefied pellets) contain negligible amout of limestone. Fuel composition for the BASE case is given only for reference.

(Wt%)	$Al_2O_3$	С	Cl	Fe <sub>2</sub> O <sub>3</sub>	Н	H <sub>2</sub> O	N	0	S	SiO <sub>2</sub>	SO <sub>3</sub>
BASE [52]	3.48	66.77	0.03	5.09	4.34	0.94	1.61	6.76	0.97	10.00	0.00
STEX	2.23	51.75	0.01	1.18	4.45	2.00	0.80	27.72	0.43	9.09	0.34
TORR-low	1.29	60.71	0.01	0.39	5.15	2.00	0.62	26.23	0.20	3.27	0.13
TORR-high	1.39	63.15	0.01	0.27	5.01	2.00	0.66	24.97	0.16	2.25	0.13

Table 2.2: Gasifier fuel mix composition for different cases - O/C and H/C ratios are highest for the STEX case and lower for TORR-low and TORR-high cases.

NUON/Vattenfall carried out laboratory tests to analyze the coal and biomass feedstocks. The ultimate and proximate analysis of the different feedstock has been shown in Table 2.3. Different types of coal (from different countries, different composition) and pellets were obtained from various suppliers to carry out these large scale tests. Fuel blends with the desired coal to biomass ratio were obtained by utilizing improvized processes on the old existing equipment (designed for coal) at the site. Inconsistencies do exist to a limited extent in the obtained final compositions due to this and also from multiple laboratory tests. This unquantifiable uncertainity is unavoidable for such a large scale test and seems acceptable.

	Ultimate Analysis										
	AUS-I coal	Columbian coal	Steam exploded pellets	Torrefied pellets	South African coal						
С	64.99	50.06	54.20	62.00	64.45						
H	5.28	3.36	5.97	5.56	3.56						
N	1.57	1.32	0.20	0.31	1.60						
0	15.02	8.98	39.11	31.61	16.70						
S	0.94	0.99	0.01	0.01	0.49						
Cl	0.00	0.015	0.004	0.004	0.004						
		Pro	oximate Analysis								
Ash (%)	12.20	35.27	0.50	0.50	13.19						
Moisture (%)	9.50	13.38	5.06	5.40	9.66						
Fixed Carbon (%)	47.80	25.70	19.17	31.91	53.45						
Volatile Matter (%)	30.50	25.65	75.27	62.19	23.70						
LHV (MJ/kg)	26.75	20.00	19.32	21.87	24.26						

Table 2.3: Raw fuel composition and lower heating values for the various coal and biomass types

# 2.5 Modeling approach and description

Cycle-Tempo, a Fortran based in-house modeling software package [88], is utilized for steady-state model development. The software has a system component library which can be assembled and modified by applying appropriate operating parameters to build a custom-made system configuration. Thermodynamic and required transport properties are computed using the in-house software library FluidProp [89].

# 2.5.1 Off-design model

Operation of the coal based WAC with 70% biomass co-gasification can be considered as an off-design situation in the context of modeling studies. An off-design analysis allows performance prediction due to change in the operating point of the system when compared to design case inputs and outputs. With an off-design model, the most important question to answer is whether the same electrical output can be maintained when co-gasifying biomass with coal. Also it is important to study several parameters like oxygen and fuel consumption, net plant efficiency, syngas flow and gas compositions. The BASE case IGCC model (design case) [52] is used to develop the off-design models for the cases with biomass co-gasification. Cycle Tempo offers possibility to model off-design behaviour of several components like turbines, heat exchangers, flash heaters, condensers and pipes.

• Turbines: Off-design calculations are possible for all types of turbines in Cycle Tempo. Traupel's formulae (a refinement of Stodola's cone law) are used to calculate off-design performance based on design case values. [88, 90, 91]. Design case values of pressures, flow rates and specific volumes are needed to compute the off-design turbine inlet pressure. Eqn.2.1 shows the Traupel's formulae considered in Cycle-Tempo to calculate the off-design inlet pressure  ${\bf p}$  from the specific volume  ${\bf v}$ , mass flow rate  ${\bf m}$  and the polytropic exponent  ${\bf n}$ . Subscript  ${\bf \alpha}$  represents the inlet and  ${\bf \omega}$  the outlet. Sub-subscript  ${\bf o}$  represents the design case value.

$$\frac{m}{m_o} = \frac{p_\alpha}{p_{\alpha_o}} \left\{ \frac{p_{\alpha_o} v_{\alpha_o}}{p_\alpha v_\alpha} \right\}^{1/2} \left[ \frac{1 - \left( \frac{p_\omega}{p_\alpha} \right)^{\frac{n+1}{n}}}{1 - \left( \frac{p_{\omega_o}}{p_{\alpha_o}} \right)^{\frac{n_o+1}{n_o}}} \right]^{1/2}$$
(2.1)

Applying Poisson's formula:

$$pv^n = \text{constant}$$
 (2.2)

$$p_{\alpha} = p_{\omega} \left\{ 1 + (k_{o}m)^{2} \frac{\nu_{\omega}}{p_{\omega}} \right\}^{\frac{n}{n+1}}$$
 (2.3)

$$k_o = \frac{1}{m_o} \left\{ \frac{p_{\omega_o}}{v_{\omega_o}} \right\}^{1/2} \left[ \left( \frac{p_{\alpha_o}}{p_{\omega_o}} \right)^{\frac{n_o + 1}{n_o}} - 1 \right]^{1/2}$$
 (2.4)

 $k_{\it o}$  is only dependent on the design case values and is therefore a constant. The polytropic constant is derived based on Eqn.2.2 for design and off-design conditions. The use of Eqn.2.3 to predict off-design pressure for steam turbines is well justified [91] but the equation is modified for the gas turbine employing the equation for subcritical nozzle flow as shown in Eqn.2.5.

$$\frac{m}{m_o} = \frac{p_{\alpha}}{p_{\alpha_o}} \left\{ \frac{p_{\alpha_o} v_{\alpha_o}}{p_{\alpha} v_{\alpha}} \right\}^{1/2} \left[ \frac{\left(\frac{p_{\omega}}{p_{\alpha}}\right)^{\frac{2}{n}} - \left(\frac{p_{\omega}}{p_{\alpha}}\right)^{\frac{n+1}{n}}}{\left(\frac{p_{\omega_o}}{p_{\alpha_o}}\right)^{\frac{2}{n}} - \left(\frac{p_{\omega_o}}{p_{\alpha_o}}\right)^{\frac{n+1}{n}}} \right]^{1/2}$$
(2.5)

• **Heat exchangers**: Cycle Tempo calculates the off-design heat transfer capacity UA (W/K) from the design case (UA)<sub>o</sub> value and mass flow rate (m<sub>o</sub>) which mostly influences the overall heat transfer coefficient. The off-design heat transfer rate is calculated as shown in Eqn.2.6. This formula should not be used for discontinuous temperature profiles.

$$UA = (UA)_o \cdot \left(\frac{m}{m_o}\right)^{0.8}$$
 (2.6)

- Flash heaters: Off-design calculations for flash heaters are not scaled with the UA-value since a reliable UA-value cannot be established for heat exchange between media showing phase changes. Depending on the ratio between the off-design mass-flow rate and the design mass-flow rate, temperature differences are adapted according to performance curves [92].
- **Condensers**:The heat exchanging area is an input to calculate the off-design behaviour in Cycle-Tempo. With a known heat transfer and cooling water temperatures, the overall heat transfer in the off-design case will be calculated according to instructions as stated in the VDI Heat Atlas [93].
- Other components: Other major components of the system include the gasifier and combustor. Off-design modeling of these components demands knowledge and an accurate model for heat release/heat transfer in these components and variation in the gasification/combustion chemistry. For example, the heat absorbed by the gasifier walls/the heat transferred to the gasifier cooling system etc. This heat depends on the thickness of the slag layer and models to predict this are very complex to develop and not readily available. Also due to high operating temperatures  $(T_{gasifier} > 1500^{o}C, T_{comb} = 1050^{o}C)$ , it is reasonable to assume a constant operating profile for these components.

Not all plant operating units/components have been included in the models; only those that are thermodynamically relevant. The auxilliary power consumption is however appropriately accounted for. The red dotted blocks shown in Fig.2.1 have not been included in the model.

- Coal/biomass milling and drying: The fuel preparation unit involving milling and drying has not been modeled, but the electrical power consumption has been included in the total auxiliary load. The fuel composition of dried and pulverized fuel mix is used as an input for the gasifier.
- **Fly ash removal**: Fly ash cyclone and ceramic filter after gasification and the syngas cooler are modeled as a single fly ash separator.
- Gas cleaning and sulphur removal: The wet scrubbing section (wash columns) consists of two scrubbers in series, with an air cooler in the water recycle loop (water supply to the first scrubber is condensed water at the outlet of the second scrubber). In the model this is simplified to a single scrubber with excess water supply and appropriate temperature specifications. Sulphur removal (as H<sub>2</sub>S/COS) is modeled with complete removal of H<sub>2</sub>S from syngas with appropriate pressure and temperature specifications and partial removal of CO<sub>2</sub>, taking into account the co-absorption of CO<sub>2</sub> (about 30%) during amine wash. The Claus-SCOT unit to produce elemental sulphur (S) from H<sub>2</sub>S has not been included in the model.
- Generator & waste water treatment: The generator unit and waste water treatment are seen as thermodynamically irrelevant and therefore not modeled in detail. The mechanical efficiency of the generator has been taken into

account and the power consumption in the waste water treatment has been accounted for in the total auxilliary load.

• Air separation unit (ASU): Majority of the auxiliary power consumption in the plant is by the air separation unit, particularly the oxygen and nitrogen compressors [52]. Power consumption by these compressors has been included in the analysis based on partial modeling and a scaling approach. A detailed explanation on this is given in section 2.5.2.

Since the design case (BASE) model was converted to an off-design model, input data for individual components are mostly unchanged. For components in off-design mode, the design case (BASE) model data is provided as additional input. Different fuel input mass flow rates, gasifier temperature and auxilliary load estimation are used for the off-design models, which are further elaborated in the following sections.

### 2.5.2 Auxiliary load estimation

Parameter	Value (MW)
Dilution N <sub>2</sub> Compressor	6.90
O <sub>2</sub> Compressor	5.50
Pure N <sub>2</sub> Compressor	2.00
Quench gas compressor	1.15
Cooling and Feed water system	3.96
Fuel Milling and circulation pumps	2.50
Tracing	0.70
Miscellaneous (GCU etc.)	8.50
<b>Total</b> (variable based on operating condition)	31-35

Table 2.4: Auxilliary power consumption - Major consumption is by to the  $N_2$  and  $O_2$  compressor in the ASU

Table 2.4 shows the auxilliary load as defined in the off-design models. The nitrogen and oxygen compressors in the ASU are major constituents of the auxilliary load. Off-design operation of the plant causes a variation in the  $O_2$  and  $N_2$  mass flow rate requirements. For off-design calculations, in order to estimate power consumption by the  $O_2$  and  $N_2$  compressors in a consistent manner, a scaling approach was used based on plant data with no co-gasification. The ASU utilizes as much air as the  $O_2$  requirement in the gasification process. A fixed  $O_2$  requirement (95% purity) by the gasifier leads to a fixed total  $N_2$  production. The ASU produces two  $N_2$  streams: impure  $N_2$  used for syngas dilution and pure  $N_2$  used mainly for pressurization, conveying of pulverized fuel and syngas purge systems. Production of pure  $N_2$  is only slightly load dependent, the production of dilution  $N_2$  is largely related to the  $O_2$  demand. Plant data for 3 operating points (part-load) indicated a linear dependancy of  $O_2$  flow on the dilution  $N_2$  flow. Data plots of ASU power

consumption versus  $O_2$  flow were also available and indicated a linear correlation between compressor power comsumption and the  $O_2$  flow as shown in Fig.2.2.

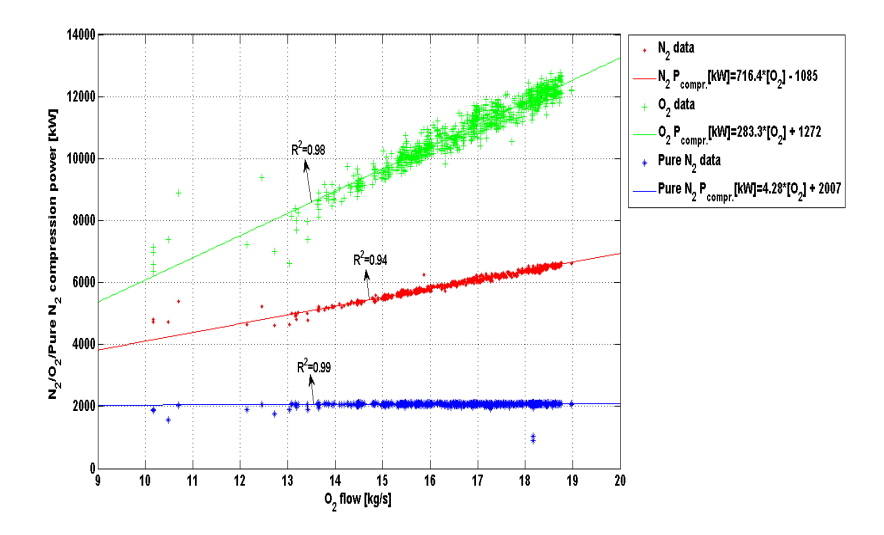


Figure 2.2: Plant data showing dependency of ASU compressor power consumptions on gasifier O2 flow

With these data plots a linear correlation was established between  $N_2/O_2$  compressor power consumption and dilution  $N_2/O_2$  flow  $(\dot{m}_{N_2}, \dot{m}_{O_2})$  respectively as shown in Eqn.2.7 and Eqn.2.8.

$$N_2$$
 compression power(kW) =  $a * \dot{m}_{N_2} + b$   $b = 590$  (2.7)

O<sub>2</sub> compression power(kW) = 
$$a * \dot{m}_{O_2} + b$$
  $b = 1252$  (2.8)

The variable part  $(a*\dot{m})$  is simulated with a compressor in the model (see Fig.2.3). A sweep in the N<sub>2</sub>/O<sub>2</sub> mass flow rates was performed to estimate the value of b. The difference in the compressor power consumption between plant data and model output represents the intercept b. The obtained values of b have been then manually inserted in Cycle-Tempo. Change in the power consumption of the pulverizers has also been taken into account. A large deviation in the power consumption by other utilities wasn't expected; hence a constant value has been used for the other constituents of the auxilliary load.

# 2.6 Results and discussion

As the first step, implementation of the off-design model was verified by comparing results between the BASE case model in design [52] and off-design mode. This comparison showed identical results ensuring correct implementation of the off-design model. STEX case model (off-design mode) validation was then performed

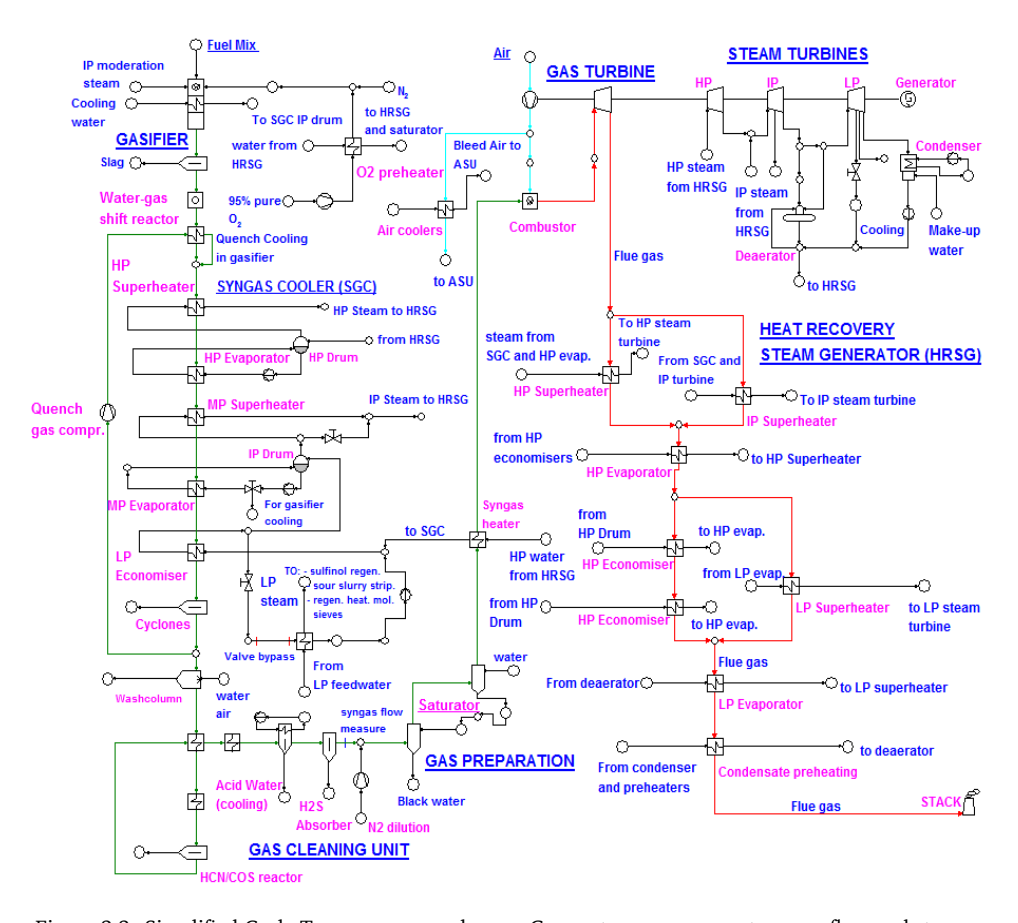


Figure 2.3: Simplified Cycle-Tempo process scheme - Green streams represent syngas flow, red streams represent flue gas and blue streams represent air flow. Streams indicating detailed process/heat integration have been excluded to maintain clarity.

with actual experimental data. The next section 2.6.1 gives the results and detailed explanation for the validation study. Model predictions obtained for TORR-low and TORR-high cases have been presented in section 2.6.2 and an exergy analysis for the STEX and TORR-high case is shown in section 2.6.3.

#### 2.6.1 STEX model validation

Table 2.5 presents the experimental test data and the model validation results for the STEX case. The test data includes measurement of thermodynamic parameters at key locations in the plant. A few parameters like the gasifier temperature and saturator syngas outlet temperature have been calculated based on heat transfer measurements. In addition to these parameters, syngas composition was also measured which has been presented in Table 2.6. Fig.2.3 shows the simplified Cycle-Tempo

	STEX - Test Data	STEX - Model Output		STEX - Test Data	STEX - Model Output
Fuel Input			Gas preparation		
Input pulverized Coal, kg/s	23.74	23.74	Nitrogen temperature, <sup>o</sup> C	58.10	59.00
LHV, MJ/kg	19.59	19.59	Nitrogen pressure, bar	13.01	13.01
Thermal input, MW	465.00	465.00	Nitrogen mass flow, kg/s	38.32	38.00
Gasifier			Saturator syngas outlet temperature, <sup>o</sup> C	119.54	119.62
Outlet presssure, bar	24.90	24.90	Preheater syngas outlet temperature, °C	277.00	292.41
Outlet temperature, °C	1515.00	1515.00	Powerblock		
Oxygen mass flow, kg/s	14.73	14.74	Air compressor discharge, bar	9.40	9.05
Moderation steam, kg/s	1.18	1.18	Air bleed, kg/s	61.90	61.90
Quench gas recycle, kg/s	58.70	52.42	Combustion chamber pressure, bar	9.15	8.78
Temperature quench gas, °C	272.00	243.40	HP Steam turbine inlet pressure, bar	85.80	92.93
Quench pressure after compres., bar	24.30	24.90	HP Steam turbine outlet pressure, bar	26.60	27.82
Syngas cooler			HP Turbine inlet temperature, °C	478.70	473.71
Syngas inlet temperature, °C	845.00	820.00	HP Turbine Outlet temperature, °C	318.20	311.92
Syngas outlet temperature, °C	267.00	229.40	HP Steam mass flow, kg/s	64.70	65.64
HP steam to HRSG, kg/s	37.40	36.82	IP Steam turbine inlet pressure, bar	25.70	23.82
HP steam to HRSG: Temperature, °C	346.20	363.90	IP Steam turbine outlet pressure, bar	3.53	3.59
IP steam to HRSG, kg/s	11.06	15.60	IP Turbine inlet temperature, °C	461.00	463.50
IP steam to HRSG: Temperature, °C	347.40	321.69	IP Turbine Outlet temperature, °C	207.80	227.34
LP steam: Pressure, bar	9.60	9.00	IP Steam mass flow, kg/s	73.40	80.13
LP steam: Temperature, °C	173.40	175.36	LP Steam turbine inlet pressure, bar	4.57	3.59
LP steam: Mass flow, kg/s	7.50	4.34	HRSG		
Cyclones			HP Steam raising mass flow, kg/s	27.20	28.80
Outlet temperature syngas, °C	261.00	229.39	HP Superheater outlet temperature, °C	484.30	476.34
Wash columns			HP Superheater outlet pressure, bar	88.60	97.93
Outlet mass flow syngas, kg/s	35.70	40.93	LP Steam raising mass flow, kg/s	6.10	4.15
Pressure syngas, bar	22.50	24.52	LP Superheater outlet temperature, °C	232.30	233.25
HCN/COS reactor			LP Superheater outlet pressure, bar	4.75	3.59
Outlet temperature syngas, °C	187.30	191.80	Power output		
Outlet pressure, bar	20.70	21.72	Gross Power output, MW	199.60	204.85
H <sub>2</sub> S absorber			Auxiliary load, MW	30.56	31.82
Outlet temperature syngas, <sup>o</sup> C	40.00	40.00	Net Power output, MW	169.10	173.02
Mass flow syngas, kg/s	33.50	33.14	Net efficiency, %	36.37	37.20

Table 2.5: STEX model validation - Process parameters compared with experimental test data. Power output and net efficiency are predicted with less than 3% deviation

model scheme as an aid to interpret results from Table 2.5. The full model scheme can be found in Appendix A.

Table 2.5 shows a fair comparison between the STEX test data and the model output. Power output and net efficiency are predicted with reasonable accuracy (about 3% relative deviation). The model overpredicts the net power output by about 4 MW. This deviation is not necessarily caused by model simplifications; it has been indicated that ageing of the plant and also an increased auxiliary load have caused a decrease in the net efficiency and power output over the years. In addition, during the test, the operation of a pilot CO<sub>2</sub> capture set-up (not included in the model) consumed roughly about 1% of the clean syngas, representing net power loss of about 1.8 MW.

Model output for the syngas cooler and the heat recovery steam generator (HRSG) show relatively high deviations compared to the test data. The model predicts a lower LP steam production from the syngas cooler (SGC) which can be attributed to

fouling in the HP evaporator. The fouling in the HP section caused a shift in the heat transfer to the LP section of the SGC. The LP economisers with the LP steam generator in the water circulation loop, were to a very large extent able to compensate for the lack of heat transfer in the HP section of the SGC. The shift in heat transfer to the LP section causes a higher LP steam production in the SGC during real operation. A relatively high deviation is also seen in the SGC syngas outlet temperature which is attributed to fouling and a lower SGC heat transfer during real operation.

The syngas flow rate at several stages downstream the SGC is predicted with a fair accuracy. The higher syngas flow rate in the model at the outlet of the washcolumns is due to the modeling approach with a single separator as stated in section 2.2. The outlet temperature of the second scrubber (in the water recycle loop) in the real plant was controlled around 110°C. In order to obtain a higher water slip to the desulphurization unit, the scrubber could have been operated at a slightly higher temperature which causes a difference in the syngas moisture content at the outlet. As the scrubbing unit was modeled as a single separator, this fluctuation in the water temperature of the second scrubber could not be taken into account. Prediction of mass flow rates, temperatures and pressures across the gas cleaning unit, N<sub>2</sub> dilution and saturator matches well with the test data. The air compressor outlet pressure as well as the combustor outlet pressure are marginally underpredicted by the model. A possible reason for this could be the position of the GT compressor inlet guide vanes. In the plant, this was determined based on the ASU pressure instead of the turbine outlet temperature. An important aspect to notice with the experimental test is also that the gas turbine was able to cope up with the changes in flow rates and gas compositions.

The model also predicts a lower LP steam flow rate from the HRSG. This again can be explained by the shift of heat transfer from the high temperature to the low temperature section of the HRSG. One reason may be fouling, another reason could be the way the inlet guide vanes of the GT compressor were controlled. During part load operation the guide vanes were often opened further to obtain a higher air flow and thus a higher pressure of the ASU feed. However the higher air flow caused a lower HRSG flue gas inlet temperature; thus a lower driving force for heat transfer in the high temperature sections.

Part load operation of the gas turbine has a large influence on the total plant performance. The installation at WAC is a single shaft Siemens V94.2 gas turbine as shown in Fig. 2.4. The gas turbine thermal efficiency( $\eta_{th,GT}$ ) is closely related with the pressure ratio (r) as shown in Eqn.2.9

$$\eta_{th,GT} = 1 - \left(\frac{1}{r}\right)^{\frac{\kappa-1}{\kappa}} \qquad r = \frac{p_3}{p_4}$$
(2.9)

 $\kappa$  is the specific heat ratio. When the gas turbine is operating under part load (off-design condition), the inlet mass flow rate and inlet pressure decreases when compared to operation at full load (design condition[52]). Thus the off-design pressure ratio is lower than the design case leading to a lower thermal efficiency of the gas turbine. Due to a reduction in the turbine inlet temperature ( $T_3$ ), the temperature of heat addition to the steam cycle is also lower compared to the design case. This

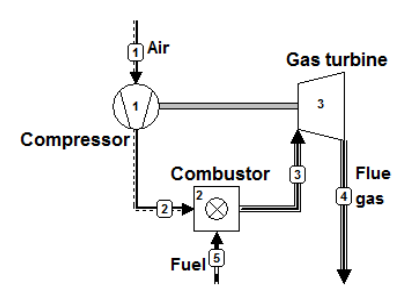


Figure 2.4: Schematic - single shaft gas turbine as installed at the Willem-Alexander Centrale

results in a lower thermal efficiency and reduced performance of the steam cycle. A lower thermal efficiency of the gas turbine and steam cycle ultimately leads to a reduced total plant performance in the considered off-design case. This trend is also predicted by Traupel's formula (Eqn.2.5) and can be clearly seen with the modeling results and test data.

Table 2.6 compares the syngas composition (on a dry basis) with test data at two specific points, after the wash column and after gas cleaning (H<sub>2</sub>S removal). The gas composition after gas cleaning has been estimated by NUON-Vattenfall based on the composition measured after the wash columns. The developed model predicts the gas composition reasonably well at both locations. Molar fractions of H2, N2 and Ar are slightly underpredicted by the model while CO and CO2 mole fractions are slightly higher compared to the measured values; CO<sub>2</sub> content though matches well with test data after gas cleaning. During real operation, more N<sub>2</sub> is added in the system which could not be taken into account in the model due to unavailability and uncertainity in the test data. Process engineers at the plant have also pointed out that the nitrogen transport gas measurement could be too low. Overall, the N<sub>2</sub> content does not have a major effect on plant performance. The higher (about 5%) CO content in the model could be due to a slightly different water gas shift (WGS) reaction temperature and fuel composition. This leads to a higher CO2 and H2 mole fraction in the syngas. Uncertainty exists in the fuel composition; particularly the oxygen content as this was calculated by difference. Also on a mole basis, the LHV for CO and H<sub>2</sub> are comparable, hence a change in the water gas shift reaction temperature would not have a drastic effect on the syngas LHV. The very small deviations could also be due to a slightly different gasifier temperature and different water gas shift effect or combinations of both during real operation, as both these temperatures were estimated.

The WAC IGCC power plant is based on the SHELL coal gasification process which is an entrained flow gasifier operating at high temperatures of about 1500°C. The coal and biomass feed is pulverized to fine particles. With a sufficient residence time and high temperatures the tar yield was negligible[94]. Process engineers at WAC have not observed the presence of tar components and problems relating to tar deposition were also not encountered in the gas cleaning/cooling units.

Validation of the model in both design [52] and off-design mode makes it well

	After v	vashcolumn	After gas cleaning			
%	Test data	Model Output	Test data	Model Output		
$\overline{H_2}$	27.53	26.13	28.40	26.97		
$N_2$	7.34	6.22	7.58	6.42		
AR	0.98	0.82	1.01	0.84		
$\mathrm{CH}_4$	0.01	0.00	0.00	0.00		
CO	54.72	57.13	56.22	58.96		
$CO_2$	9.29	9.41	6.79	6.80		
COS	0.01	0.02	0.00	0.00		
$H_2S$	0.12	0.25	0.00	0.00		
Total	100.00	100.00	100.00	100.00		

Table 2.6: STEX model validation - comparison of syngas composition (dry basis) after washcolumns and after gas cleaning with experimental test data

suited for plant performance prediction with fuel blends containing 70% torrefied woodpellets. The model calculations and independent calculations by Nuon/Vattenfall show that a net output of 230 MW is not achievable with co-gasification of steam exploded woodpellets. Due the lower LHV of steam exploded woodpellets compared to coal, the fuel mass flow to the gasifier had to be increased in order to maintain the same electrical output.

There were three main constraints which had to be considered: the capacity of the powder coal feed system, the ASU oxygen production capacity and the heat input to the syngas cooler. The capacity of the powder coal feeding system was certainly insufficient to operate the plant at 230 MW electrical output using a fuel mixture with 70% steam exploded woodpellets. But there was a hardware modification foreseen which could have solved this bottleneck. The oxygen production capacity was not of major concern as the oxygen requirement was more or less proportional to the thermal input to the gasifier. Even at maximum plant load using a fuel mixture with 70% steam exploded wood pellets, the oxygen requirements would stay within the maximum production capacity of the ASU. The real bottleneck was the maximum cooling capacity of the syngas cooler. In practice this was limited to appr. 92 MW. Because of the lower cold gas efficiency and thus a higher heat load to the syngas cooler, the maximum cooling capacity of the syngas cooler was already exceeded at a plant load well below 230 MW. Increase of the cooling capacity was impossible without major plant modifications.

On this basis, NUON-Vattenfall decided to investigate possibilities to co-gasify torrefied woodpellets. Due to lower H/C and O/C ratios compared to steam exploded wood pellets, the cold gas efficiency would not reduce significantly and it was expected that the heat input to the syngas cooler would stay below 92 MW at the desired plant load. The validated model was thus used to predict the plant output and performance for two fuel blends containing torrefied woodpellets (TORR-low and TORR-high cases). The next section describes the prediction results for the TORR-low and TORR-high cases.

	TORR-low	TORR-high		TORR-low	TORR-high
Fuel Input			Gas preparation		
Input pulverized Coal, kg/s	24.21	24.21	Nitrogen temperature, <sup>o</sup> C	59.00	59.00
LHV, MJ/kg	22.87	23.82	Nitrogen pressure, bar	12.01	13.50
Thermal input, MW	553.68	576.68	Nitrogen mass flow, kg/s	48.00	51.50
Gasifier			Saturator syngas outlet temperature, °C	120.00	120.00
Outlet presssure, bar	23.90	23.90	Preheater syngas outlet temperature, °C	298.40	300.60
Outlet temperature, °C	1500.00	1500.00	Powerblock		
Oxygen mass flow, kg/s	18.20	18.45	Air compressor discharge, bar	10.44	10.80
Moderation steam, kg/s	0.50	0.50	Air bleed, kg/s	76.43	77.50
Quench gas recycle, kg/s	58.37	58.92	Combustion chamber pressure, bar	10.17	10.53
Temperature quench gas, °C	248.26	248.67	Gas Turbine inlet temperature, °C	994.90	1018.00
Quench pressure after compres., bar	23.90	23.90	HP Steam turbine inlet pressure, bar	111.10	115.80
Syngas cooler			HP Steam turbine outlet pressure, bar	32.36	33.45
Syngas inlet temperature, °C	820.00	820.00	HP Turbine inlet temperature, °C	489.99	495.59
Syngas outlet temperature, <sup>o</sup> C	233.26	233.52	HP Turbine Outlet temperature, °C	320.71	324.06
HP steam to HRSG, kg/s	43.62	44.67	HP Steam mass flow, kg/s	78.30	81.40
HP steam to HRSG: Temperature, °C	362.69	362.75	IP Steam turbine inlet pressure, bar	28.36	29.45
IP steam to HRSG, kg/s	16.58	16.59	IP Steam turbine outlet pressure, bar	4.13	4.36
IP steam to HRSG: Temperature, °C	331.90	333.50	IP Turbine inlet temperature, °C	484.10	491.70
LP steam: Pressure, bar	9.00	9.00	IP Turbine Outlet temperature, °C	238.40	245.70
LP steam: Temperature, °C	175.36	175.36	IP Steam mass flow, kg/s	94.27	97.36
LP steam: Mass flow, kg/s	5.19	5.28	LP Steam turbine inlet pressure, bar	4.13	4.32
Cyclones			HRSG		
Outlet temperature syngas, <sup>o</sup> C	233.25	233.50	HP Steam raising mass flow, kg/s	34.67	36.75
Wash columns			HP Superheater outlet temperature, °C	492.40	497.90
Outlet mass flow syngas, kg/s	46.90	47.50	HP Superheater outlet pressure, bar	116.10	120.80
Pressure syngas, bar	23.52	23.52	LP Steam raising mass flow, kg/s	4.34	4.39
Outlet temperature syngas, <sup>o</sup> C	139.80	136.10	LP Superheater outlet temperature, °C	246.30	249.30
HCN/COS reactor			LP Superheater outlet pressure, bar	4.13	4.36
Outlet temperature syngas, <sup>o</sup> C	192.00	192.00	Power output		
Outlet pressure, bar	23.52	20.72	Gross Power output, MW	261.40	277.50
H <sub>2</sub> S absorber			Auxiliary load, MW	34.93	37.10
Outlet temperature syngas, <sup>o</sup> C	40.00	40.00	Net Power output, MW	226.50	240.40
Mass flow syngas, kg/s	39.43	40.81	Net efficiency, %	40.90	41.69

Table 2.7: Comparison of model process parameters for TORR-low and TORR-high cases. Operation with a high LHV fuel blend is essential to achieve the desired power output

# 2.6.2 Performance prediction with torrefied woodpellets

Model calculations with steam exploded pellets show that it is not possible to achieve a net output of 230 MW with a constraint of the maximum SGC heat transfer. Based on NUON-Vattenfall requirements, prediction results were obtained using the validated model for higher LHV fuel blends consisting of torrefied pellets. Table 2.7 shows the output parameters for the TORR-low and TORR-high cases.

A net output of 226.5 MW is achieved for the TORR-low case with maximum SGC heat transfer. It is immediatly seen that in order to achieve the target of 230 MW, a higher LHV fuel mix is required. The TORR-high case gives a net output of about 240 MW with a net efficiency of 41.60%. Plant performance during real operation is expected to be lower than the predicted performance as explained in the previous section. For both cases, the total SGC heat transfer was within a safe

limit of 91 MW. Parametric evaluation from Table 2.7 shows that less steam is added during gasification than the STEX case. This steam was added primarily because it had a beneficial effect on fines concentration and stability in the slag bath circulation flow. The gas turbine inlet temperature also increases to  $1018^{o}$ C approaching a value close to the design case model [52]. A higher auxiliary load is also calculated for the cases with torrefied pellets. This is due to additional power requirements by the  $N_2$  and  $O_2$  compressors in the ASU. Since quantitative data was not readily available, a constant value (as shown in Table 2.4) has been used for the fuel milling, tracing and miscellaneous power consumption. Milling of torrefied pellets in practice would require lower power than steam exploded pellets. Table 2.8 shows the syngas composition for both the cases after the washcolumn and gas cleaning unit. A higher  $H_2$  and CO content is observed in the syngas in comparison with the STEX case. The  $CO_2$  content is lower, accordingly. With a lower H/C and O/C ratio compared to the STEX case, the fuel mix composition in the TORR-high and TORR-low cases are more similar to the design case fuel composition.

Based on this analysis, it is concluded that a net output of 230 MW could be achieved at the Willem-Alexander Centrale utilizing 70(%) high LHV fuel blend with torrefied pellets, fulfilling the aforementioned plant constraints. As ageing and fouling aspects have not been taken into account in the model, in practice with a higher auxilliary load, a slightly lower net power output is expected.

	After wa	After gas	After gas cleaning			
Mole (%)	TORR-low	TORR-high	TORR-low	TORR-high		
$\overline{H_2}$	26.60	26.54	27.18	27.01		
$N_2$	5.97	5.80	6.10	5.90		
Ar	0.85	0.83	0.86	0.84		
$\mathrm{CH}_4$	0.00	0.00	0.00	0.00		
CO	59.73	61.27	61.03	62.36		
$CO_2$	6.74	5.46	4.82	3.88		
COS	0.01	0.01	0.00	0.00		
$H_2S$	0.09	0.08	0.00	0.00		
Total	100.00	100.00	100.00	100.00		

Table 2.8: Syngas composition (dry basis) after washcolumns and after gas cleaning for TORR-low and TORR-high cases as predicted by the developed off-design model

# 2.6.3 Exergy Analysis

Exergy analysis is an important tool in thermodynamic evaluation of systems to identify thermodynamic losses [32]. Identification of these losses help in process diagnosis and to devise novel solutions towards reducing these losses. Cycle-Tempo offers a possibility to calculate exergy flows, exergy losses and exergy efficiencies as an aid to carry out second law analyses. The exergy of matter is calculated as the reversible (maximum) work derived by bringing matter in thermomechanical and chemical equilibrium with the reference environment. Thus the exergy of matter is

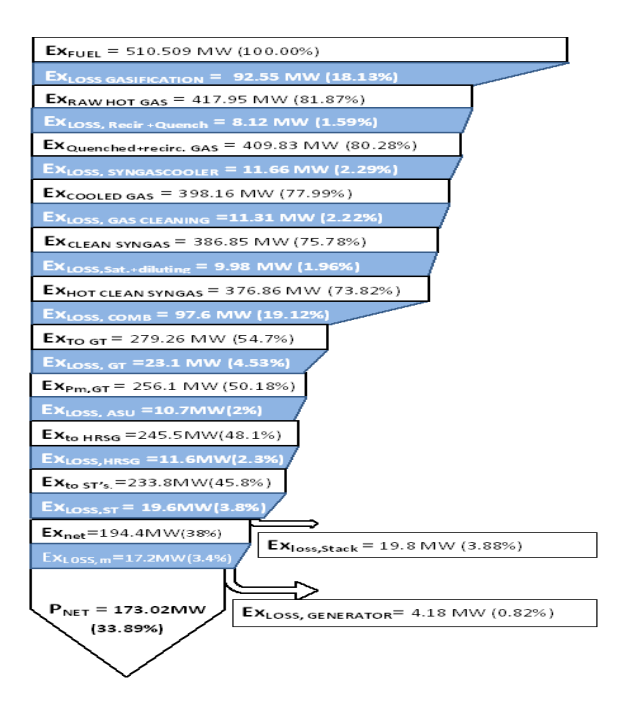


Figure 2.5: Exergy flow diagram for STEX case - Losses during gasification and combustion are the highest

calculated as a sum of the thermomechanical and chemical exergies. In principle, the kinetic and potential exergies are also included but since they do not usually change significantly, this is neglected in the calculation. In order to quantify the exergy loss; the exergy of matter, exergy of heat (in case of heat transfer to/from the environment) and exergy of work (in case of work generation/consumption) is calculated for all streams/components [32]. The exergy loss is then calculated as the difference between the incoming and outgoing exergy. The functional exergy efficiency is calculated according to Eqn.2.10, where  $\rm Ex_{source}$ ,  $\rm Ex_{product}$  and  $\rm Ex_{loss}$  represent the exergy source, product exergy and exergy losses respectively:

$$\eta_{\text{ex}} = \frac{\text{Ex}_{\text{product}}}{\text{Ex}_{\text{source}}} = \frac{\text{Ex}_{\text{source}} - \text{Ex}_{\text{loss}}}{\text{Ex}_{\text{source}}}$$
(2.10)

Table 2.9 shows the exergy efficiencies for the three cases considered in this study. Operation with high LHV torrefied pellets gives the highest exergy efficiency, comparable to the base case exergy efficiency [52]. Fig.2.5 and Fig.2.6 show the exergy flow diagram for the STEX and TORR-high cases respectively illustrating the exergy losses due to various operations in the plant.

With both cases, exergy losses during gasification and combustion contribute largely to the irreversibilities in the system (about 37-38% of the total exergy loss). Exergy losses due to syngas cooling, cleaning and saturation are relatively small while losses in the combined cycle and ASU are approximately 12-13%. The per-

Parameter	BASE[52]	STEX	TORR-low	TORR-high
Exergy Input (MW)	638.80	510.50	598.22	620.72
Exergy Gross Output (MW)	288.70	204.84	261.44	277.57
Exergy net output (MW)	254.09	173.02	226.51	240.46
Exergy efficiency (%)	39.77	33.89	37.86	38.73

Table 2.9: Exergy output and exergy efficiency for various cases - TORR-high gives the highest exergy efficiency

centage exergy loss due to gasification is slightly higher with co-gasification when compared to the design case. This is attributed to the higher H/C , O/C ratios in the fuel mix and the lower cold gas efficiency. A slight reduction is observed in the percentage of exergy loss (relative) in the GT combustor; mostly due to the lower syngas LHV compared to the design case. Comparison of results from the the exergy flow diagrams between STEX and TORR-high also indicates the thermodynamic advantage of using torrefied biomass. Fraction of exergy losses due to the various operations are lower with the TORR-high case. A lower O/C and H/C ratio in the fuel mix helps in reducing irreversities due to gasification. The results obtained in this study also show similar trends obtained with the theoretical modeling study carried out by Prins et al. [95].

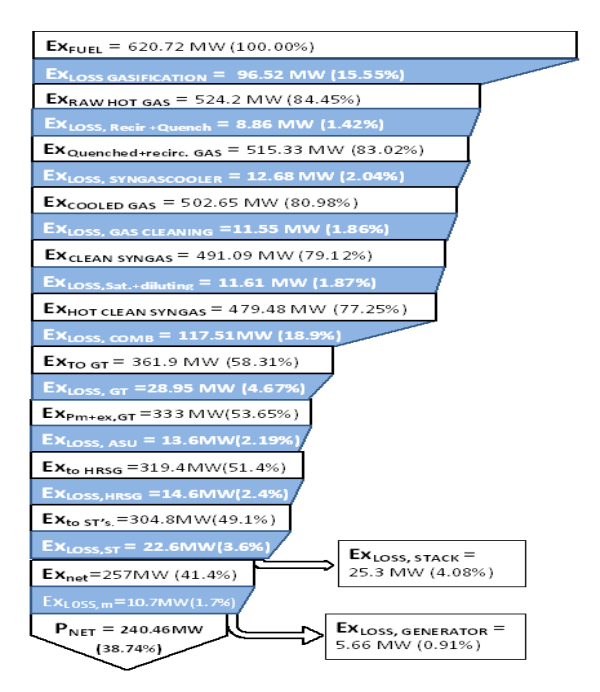


Figure 2.6: Exergy flow diagram for TORR-high case - Exergy losses are lower compared to the STEX case

### 2.7 Conclusions

Demonstration tests on high percentage biomass co-gasification at a large scale power plant have shown that existing coal based IGCC plants can be operated with an increasing percentage of biomass in the fuel mix without extensive plant modifications. Such demonstrations are also of vital significance for the further development of low emission/carbon neutral plants. A detailed thermodynamic analysis has been carried out with first of its kind experimental data from high percentage (70%) biomass (steam exploded wood pellets ) co-gasification tests carried out at the 253 MW<sub>e</sub> Willem-Alexander Centrale IGCC plant in Buggenum, the Netherlands. Presented test data serves as a comprehensive, reliable and first of its kind literature data source for large scale-high percentage biomass co-gasification in IGCC plants. The steady state model validation study reveals that inspite inescapable sources of inconsistencies, such models can be effectively utilized to predict the plant performance with a relatively high accuracy (within 3% relative deviation). Fouling in the HP section of the SGC has been identified as the main reason for the deviations in the prediction of IP/LP steam flows. From the model calculations, it is also concluded that in order to achieve a net output of 230 MW without extensive plant modifications, a high LHV fuel blend with a relatively high quality coal and torrefied pellets is essential. A net electrical efficiency of 41.5% is predicted for this case. Gasification and combustion have been identified as the processes with the highest exergy destruction indicating a potential for further optimization of the system.

The developed off-design models could serve as a strong platform and play an instrumental role to plan real plant operation with various biofuels and to carry out studies involving novel carbon capture technology integration, retrofitting with advanced technologies (for eg. with high temperature fuel cells) and IGCC plant optimization. Irreversibilities occurring during combustion can be significantly reduced by the (partial) replacement with solid oxide fuel cells (SOFC) due to the direct electrochemical conversion of syngas. The next chapter presents a thermodynamic approach and assessment of retrofitting bio-IGCC power plants with SOFCs and CO<sub>2</sub> capture towards developing carbon neutral/negative power plants.

# Chapter 3

# Solid oxide fuel cell (SOFC) integrated bio-IGCC power plants

Energy efficiency is one of the most important factors that has a direct influence on fuel consumption and GHG emissions from fossil fuel power plants. Operating power plants with the highest possible efficiency is key towards reducing fossil fuel consumption and increasing clean power production. In this regard, it is important to understand the effects of integrating novel and highly efficient technologies like solid oxide fuel cells (SOFC) to upgrade existing power plants in the near future. This chapter presents a detailed thermodynamic case study (including exergy analysis) on the Willem-Alexander Centrale (WAC) power plant in the Netherlands towards integrating SOFCs in existing bio-IGCC power plants (with 70% biomass cogasification). Two systems have been presented: I) a SOFC retrofitted IGCC system with partial oxy-fuel combustion CO<sub>2</sub> capture with a focus on near future implementation II) a new redesigned integrated gasification fuel cell (IGFC) system with full oxy-fuel CO<sub>2</sub> capture. It is concluded that existing IGCC power plant fuel cell retrofits could be operated without major plant modifications and relatively high electrical efficiencies of more than 40%(LHV). In order to apply full scale CO<sub>2</sub> capture, major process modification and redesign needs to be carried out. Additional discussions have also been presented on carbon deposition in SOFCs and biomass CO<sub>2</sub> neutrality.

This chapter is published as: A. Thallam Thattai, V. Oldenbroek, L. Schoenmakers, T. Woudstra, P.V. Aravind, Towards retrofitting integrated gasification combined cycle (IGCC) power plants with solid oxide fuel cells (SOFC) and CO<sub>2</sub> capture - A thermodynamic case study, Applied Thermal Engineering, Volume 114, 5 March 2017, Pages 170-185, ISSN 1359-4311

# 3.1 Background

Utilization of biomass as feedstock to produce electrical power offers a large potential to develop CO<sub>2</sub> neutral power plants [16–18]. Biomass based IGCC power plants (bio-IGCC) with CO<sub>2</sub> capture (CC) could be a potential solution for developing CO<sub>2</sub> negative power plants since the stored CO<sub>2</sub> originates from biomass while biomass absorbs CO<sub>2</sub> for its growth. With high CO<sub>2</sub> capture rates such plants can significantly contribute to mitigation of the energy system emissions [79]. However the utilization of CO<sub>2</sub> capture leads to a reduction in the net electrical/exergy efficiencies [96, 97]. In order to boost electrical/exergy efficiencies the system could be improved by partially replacing highly irreversible processes like combustion with highly efficient electrochemical conversion [98]. The amount of biomass co-gasification is key to the CO<sub>2</sub>-negative capabilities of power plants. With successful large scale experimental demonstrations (Chapter 2 of this thesis) on high percentage (70%) biomass co-gasification like at the 253 MW<sub>e</sub> Willem-Alexander Centrale (WAC) in the Netherlands, it is very important to assess possibilities of developing high efficiency and CO<sub>2</sub> neutral power plants based on this demonstration.

Electrochemical conversion of syngas derived from coal/biomass gasification to produce power has been postulated as a more efficient route as compared to conventional combustion based gas turbine systems[99]. Solid oxide fuel cells (SOFC) are high efficiency (upto 70%) electrochemical devices which can be utilized to produce electrical power and heat. A significant number of modeling investigations have been carried out in the past by multiple research groups on the prospects of integrating SOFCs in coal based IGCC power plant systems. Park et al. [100, 101] reported a comparative system study for pre-combustion and oxy-fuel combustion CO<sub>2</sub> capture in SOFC integrated IGCC plants concluding a better performance with oxy-fuel combustion CO<sub>2</sub> capture. Braun et al. [102] investigated the performance of a SOFC integrated coal based gasification power plant concept with a organic Rankine cycle power generator as the bottoming cycle. A quasi-2D finite volume SOFC model has been presented by Li et al. [103, 104] as an aid for IGFC system analysis. Spallina et al. [105] have reported a novel coal based IGFC plant system design with CO<sub>2</sub> capture giving a net plant efficiency of about 47.5%. A zero-emmision power plant concept was reported by Adams et al. [106] by combining coal gasification with solid oxide fuel cells. They conclude that the use of SOFCs with unmixed anode and cathode exhausts makes the process inherently CO<sub>2</sub> capture friendly. A number of system and economic investigations have also been reported by the Department of Energy (DoE), USA assessing various configurations for coal based IGFC power plant designs [107–112]. Additional IGFC system concepts and designs have been presented by Ghezel-Ayagh et al. [113], Li et al. [114], Rudra et al. [115]. A comprehensive exergy and economic analysis on advanced coal based IGCC-CCS and IGFC-CCS was carried out by Siefert et al. [116]. It can be seen that much research work on integrating SOFCs has been focussed on coal based IGCC power plant systems and all these studies present the design/performance of new systems focussed on long term implementation.

In the recent past, a few system investigations have also been reported on SOFC

integration in IGCC power plants with biomass co-gasification. Jin et al. [117] conducted investigations on comparing the thermodynamic and economic performance of biomass based IGCC with and without SOFC integration. CO2 capture was not considered in this study. They reported a net electrical efficiency of 47.1% for the bioIGCC-SOFC system. Paengjuntuek et al.[118] presented simulation results for an integrated biomass gasification fuel cell plant with a net energy efficiency of 69.38% (combined heat and power). Naraharisetti et al.[119] have reported a comparative study for a biomass based IGCC and IGFC with biomass and natural gas as fuel using multi-objective optimization (MOO). A detailed and comprehensive study has been reported by Sadhukhan et al. [120] with process simulation and methodology for the integrated design of biomass gasification fuel cell systems and comparison of these biomass gasification combined cycle systems. They identify process constraints and extreme operating conditions for the SOFC unit and the steam cycle. Literature review thus reveals that research on SOFC and CO<sub>2</sub> capture integration in coal/biomass based IGCC power plant systems has only been focussed on the design of new systems. There exists an absence in information available on the thermodynamic effects of retrofitting solid oxide fuel cells in existing IGCC power plants with CO<sub>2</sub> capture with a focus on near future implementation. Despite information available on retrofitting CO<sub>2</sub> capture in IGCC power plants [121, 122], nothing has yet been reported concerning SOFC integration.

### 3.2 Motivation

Retrofitting existing power plants marks a major step in evaluating novel technologies in terms of application in near future. With intensive global ongoing efforts [33, 34] on developing kW scale fuel flexible SOFC stacks, research needs to be carried out in understanding and assessing challenges in retrofitting such SOFC stack modules in existing coal/biomass based IGCC power plants. In order to make choices to retrofit, it is of utmost importance to assess power plant off-design performance, required process modifications and operational boundaries based on the existing equipment in the power plant. Multiple challenges exist to retrofit syngas fed SOFCs in existing power plants like cost, process design, material availability, contaminant tolerance, carbon deposition [123]. However apart from challenges to be overcome in the SOFC module itself, it is also important to assess system/process constraints based on the existing equipment in the power plant.

Detailed system models can be effective tools to evaluate off-design plant performance with alternative and safe operating conditions. Operation of the coal based WAC with 70% biomass co-gasification, SOFC and  $\mathrm{CO}_2$  capture can be considered as an off-design situation in the context of modeling studies. Based on the validated model presented in Chapter 2, thermodynamic off-design models could be developed to predict performance and identify process constraints in the WAC plant when retrofitted with solid oxide fuel cells and oxy-fuel combustion  $\mathrm{CO}_2$  capture technology.

This chapter presents a thermodynamic system study towards integrating SOFCs

Case	Description
STEX (no CC)	IGCC system based on WAC plant design with a fuel consisting of 70% steam exploded woodpellets and 30% Columbian coal (Refer to Chapter 2)
SOFC-CC Retrofit STEX (partial CC)	STEX case based on WAC plant design with retrofitted SOFC stack and partial oxy-combustion ${\rm CO_2}$ capture. The SOFC stack is not the main power producing unit.
IGFC-CC STEX (full CC)	STEX case in a redesigned IGFC configuration with full oxy-combustion $\rm CO_2$ capture based on WAC gasifier and gas cleaning unit (GCU) design. The SOFC stack is the main power producing unit. The original GT is replaced with an air expander

Table 3.1: Case definition

and CO<sub>2</sub> capture in IGCC power plants in near future, by suggesting a step wise scale up strategy. For the first time, a reliable steady state model based study is presented towards retrofitting SOFCs and partial oxy-fuel combustion CO<sub>2</sub> capture in existing IGCC power plants (with upto 70% biomass co-gasification). Focus has been given to identify bottleneck thermodynamic situations and process modifications. Detailed thermodynamic models are discussed for two systems: i) a SOFC- partial oxyfuel combustion CO<sub>2</sub> capture retrofitted IGCC system based on WAC plant design. The system involves the use of a split stream of syngas after gas cleaning in an SOFC stack unit to develop additional power. ii) a redesigned highly efficient and fully integrated gasification fuel cell (IGFC) system with full oxy-fuel combustion CO<sub>2</sub> capture (see Chapter 1 section1.3.1.2) based on the existing WAC gasifier and gas cleaning unit (GCU); wherein all syngas produced in the gasifier is fed to the SOFC unit and consequently to the HRSG and CO<sub>2</sub> capture unit.

# 3.3 Case and process description

A detailed overview on IGCC process at the the coal based Willem-Alexander Centrale (WAC) has been given in Chapter 2 (section 2.2). In this section, the various cases considered in this study and the corresponding processes are described.

Table 3.1 shows the definition for various cases considered in this study. The approach is to first investigate the system when retrofitted with a smaller SOFC stack module; the combined cycle still being the largest power producer. This represents the SOFC-CC Retrofit STEX case. The second case with a large SOFC stack module and full  $\rm CO_2$  capture i,e the IGFC-CC STEX case has been selected to identify the major process constraints and redesign necessary to scale up towards a full integrated IGFC power plant with  $\rm CO_2$  capture. STEX represents the previously experimentally validated case (Chapter 2 of this thesis) for the co-gasification test at WAC with 70% steam exploded woodpellets. This reference case is presented to compare the performance of the SOFC-CC Retrofit STEX and IGFC-CC STEX cases.

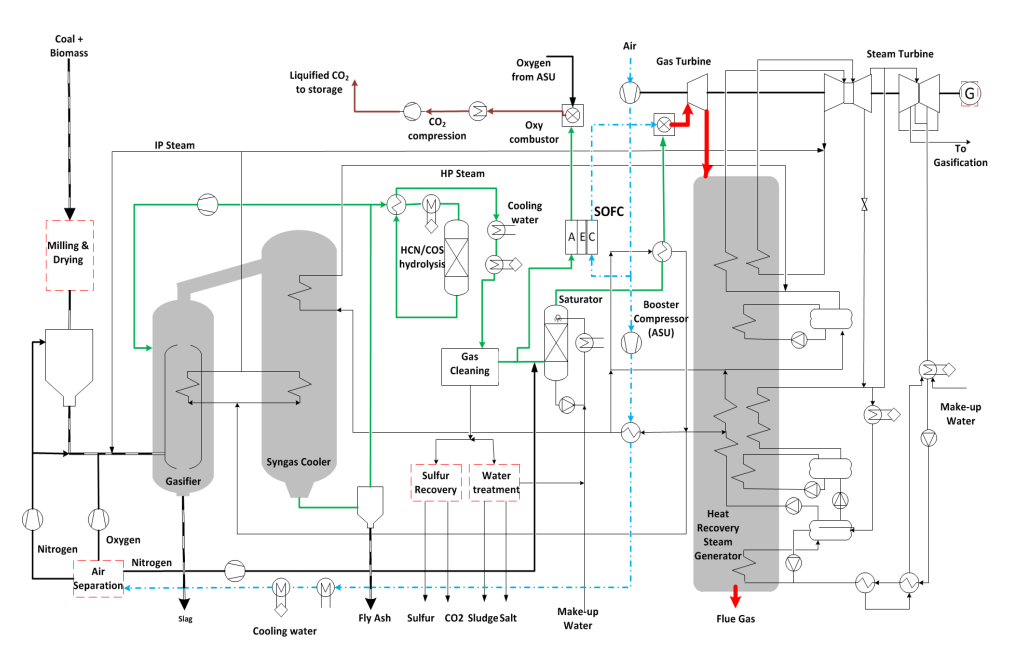


Figure 3.1: Process flow diagram for SOFC-CC Retrofit STEX system - Red dotted blocks have not been modelled, brown streams represent CO<sub>2</sub> flow

### 3.3.1 SOFC-CC Retrofit STEX (with partial CO<sub>2</sub> capture)

Fig. 3.1 illustrates the primary components of the proposed retrofitted WAC system in a process flow diagram. Coal and biomass mixture is pulverized and blown into the gasifier and the produced syngas is cooled and cleaned to remove HCN/COS and sulphur based compounds (H<sub>2</sub>S). A part of the clean syngas is then extracted, preheated and fed to the SOFC stack. The remaining syngas is diluted with N<sub>2</sub>, saturated with water vapour and fed to the gas turbine combustor. Cathode air for the SOFC stack is extracted also from the air compressor. Partial CO<sub>2</sub> capture is then employed. The unconverted syngas at the SOFC stack anode outlet is combusted with an oxy-fuel combustor with pure O<sub>2</sub> (95% vol from ASU) to produce a gas mixture primarily consisting of CO<sub>2</sub> and H<sub>2</sub>O. This gas mixture is then cooled to condense out moisture to obtain pure CO<sub>2</sub>. A multistage compressor with intercooling is then employed to compress CO<sub>2</sub> to the desired storage pressure. Depleted cathode outlet air from the SOFC stack is fed to the gas turbine (GT) combustor. The flue gas from the GT combustor is guided through a gas turbine expander generating power and further through a heat recovery steam generator (HRSG). The generated steam in the HRSG is then expanded in steam turbines for additional power generation.

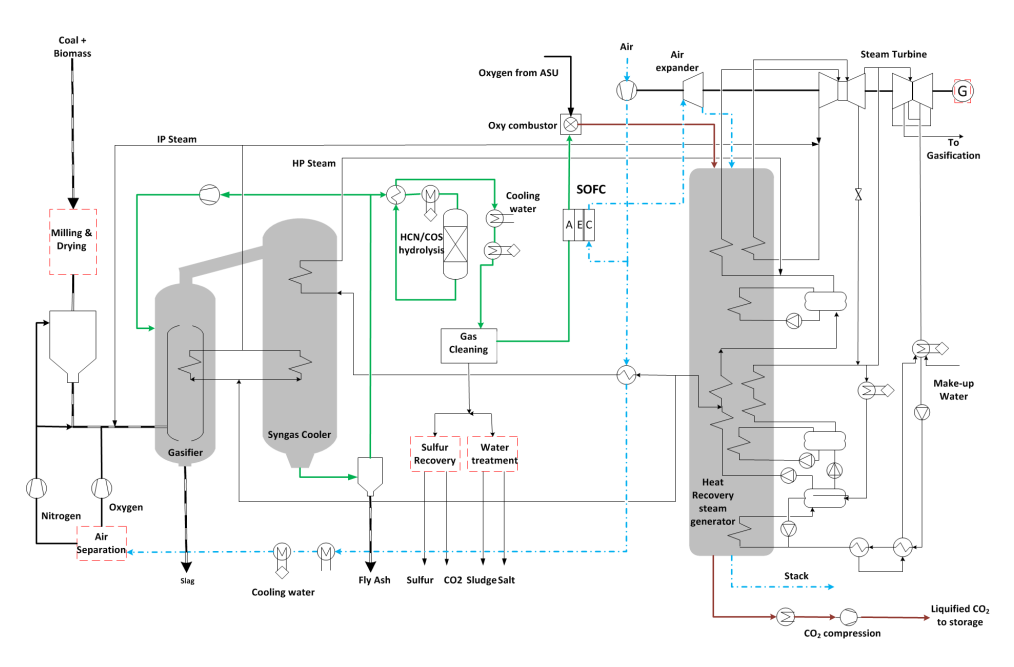


Figure 3.2: Process flow diagram for IGFC-CC STEX system - Red dotted blocks have not been modelled

### 3.3.2 IGFC-CC STEX (with full CO<sub>2</sub> capture)

The second system consists of a redesigned (but based on WAC gasifier and GCU design) IGFC power plant system with full oxy-combustion CO<sub>2</sub> capture. Fig.3.2 shows the process flow diagram for this system. The system consists of an identical gasifier, syngas cooler and gas cleaning unit as the retrofitted system described in the previous subsection. All the clean syngas obtained after gas cleaning is fed as fuel to the SOFC stack unit. As bulk of the clean syngas is converted through electrochemical oxidation in the SOFC stack module instead of the GT combustor, this system does not require the N<sub>2</sub> dilution and saturation unit after the gas cleaning unit (GCU). N2 dilution and water vapour saturation is utilized mostly to limit high combustion temperatures and NO<sub>x</sub> emissions [99]. Hence the co-produced N<sub>2</sub> in the ASU is vented to the atmosphere or can be considered as a co-product. The SOFC stack replaces the combustion chamber of the gas turbine. A pressurized SOFC stack is considered for maximizing efficiency. To carry out full CO<sub>2</sub> capture, the anode outlet gas is then directed to an oxy-fuel combustor where the remaining fuel is combusted with pure oxygen (95%) at near stoichiometric conditions. The oxygen required for the oxy-fuel combustor is obtained from the existing ASU. The outlet gas from the oxy-combustor mainly consisting of CO<sub>2</sub> and H<sub>2</sub>O is cooled to condense out moisture to obtain pure CO<sub>2</sub>. The thermal energy in the outlet gas is recovered partly in a newly designed pressurized HRSG. An identical CO2 cooling and compression process is then utilized as in the retrofitted system. The cathode outlet air stream from the SOFC stack, depleted in O2 content, cannot be utilized in the combustor as this will lead to undesirable nitrogen in the captured  $CO_2$  stream. Hence the original WAC flue gas GT expander is replaced with an air expander. This expanded air stream is cooled in the HRSG to generate additional steam and subsequently vented into the atmosphere via the stack.

# 3.4 Modeling approach and description

The validated Cycle-Tempo system model presented in Chapter 2 has been used as the base for developing models with SOFC and  ${\rm CO_2}$  capture integration. The STEX case fuel mix as described in Chapter 2 section 2.1 has been used as feedstock in the models. This fuel mix composition is shown in Table 3.2. The ultimate and proximate analysis of the coal and biomass feedstock can be found in the previous chapter (Table 2.3).

Component	$Al_2O_3$	С	Cl	$Fe_2O_3$	Н	$H_2O$	N	О	S	$SiO_2$	$SO_3$
(Wt%)	2.23	51.75	0.01	1.18	4.45	2.00	0.80	27.72	0.43	9.09	0.34

Table 3.2: Gasifier input fuel mix composition (STEX)

Input data for the gasifier, gas cleaning and saturation, gas turbine and steam turbine units remain unchanged. The gas turbine combustor has been modelled with air-fuel equivalence ratio ( $\lambda$ ) of 2.0 and a combustor outlet temperature of 1575°C, assuming no NO<sub>x</sub> formation at these conditions. The main input parameters only for the SOFC unit and oxy-fuel combustion CO<sub>2</sub> capture unit are presented in this section. Table.3.3 shows the main input parameters (assumed) used in the

Assumed design conditions			
Operating cell temperature, <sup>o</sup> C	900.00		
Current density, A/m <sup>2</sup>	2500.00		
Fuel utilization, %	0.85		
Equivalent resistance ( $R_{eq}$ ), $\Omega$ -m <sup>2</sup>	5.00e-5		
Anode & Cathode inlet gas temperature, °C	850.00		
Pressure loss (anode and cathode), bar	0.05		
DC to AC conversion efficiency, %	95.00		
Recirculation compressor isentropic efficiency, %	0.85		
Geometry assumptions			
Design	Planar		
Operating mode	Direct internal reforming (DIR)		
Anode material	Ni/GDC		
Cathode material	LSM-YSZ		
Electrolyte material	YSZ		
Support	Electrolyte		

Table 3.3: Cycle-Tempo SOFC model - Assumed design parameters, gemometry and materials

Cycle-Tempo SOFC model. The SOFC operating conditions, geometry and materials have been chosen on a generic basis for standard performance. Cycle-Tempo

Parameter	Value
CO <sub>2</sub> final discharge pressure, bar	150.00
CO <sub>2</sub> discharge temperature, <sup>o</sup> C	30.00
CO <sub>2</sub> compressor isentropic efficiency, %	80.00
Oxy-combustor reaction pressure, bar	10.75
Oxy-combustor reaction temperature, <sup>o</sup> C	1050.00
Oxy-combustor pressure drop, bar	0.27
Cooling water pump isentropic efficiency, %	65.00
Cooling water temperature difference, <sup>o</sup> C	5.00

Table 3.4: Input parameters - Oxy-combustion CO2 capture

offers an in-built SOFC model based on thermodynamic and electrochemical considerations. The model calculates the active area, voltage, current and the electrical power [92]. As the first step, an equilibrium calculation is carried out based on the inlet fuel (anode) composition, specified reaction temperature and pressure. A calculation procedure is then carried out to calculate other electrochemical parameters. The reversible voltage is calculated with the Nernst equation(Eqn.3.1) assuming that only H<sub>2</sub> is electrochemically oxidized:

$$E_x = E^0 + \frac{R.T}{2.F} ln \left\{ \frac{y_{O_2,c}^{1/2} \cdot y_{H_2,a}}{y_{H_2O,a}} \cdot p_{cell}^{1/2} \right\}$$
(3.1)

 $E^0$  is the standard reversible voltage for hydrogen, that only depends on the temperature, and is calculated from the change in the Gibbs energy  $\Delta G$ . F is the Faraday constant, R is the universal gas constant and T is the operating cell/stack temperature.  $y_{O_2,c}$  represents the mole fraction of oxygen on the cathode side,  $y_{H_2,a}$  is the mole fraction of hydrogen in the anode fuel stream and  $y_{H_2O,a}$  represents the mole fraction of water vapour on the anode side.  $p_{cell}$  is the cell/stack operating pressure. The actual operating voltage  $V_{cell}$  and the current  $I_{cell}$  is calculated as in Eqn.3.2 and Eqn.3.3 respectively:

$$V_{cell} = E_x - \Delta V_x \qquad i_x = \frac{\Delta V_x}{R_{eq}}$$
 (3.2)

$$I_{cell} = \frac{U_f.\phi_{m,a,in}}{M_{mol,a}}.(y^0_{H_2} + y^0_{CO} + y^0_{CH_4}).2F$$
(3.3)

 $\Delta V_x$  represents the overpotentials/losses in the SOFC. The current density  $(i_x)$  is proportional to the voltage loss by analogy with Ohm's law.  $R_{eq}$  is the equivalent cell/stack resistance.  $U_f$  is the fuel utilization of the SOFC stack, $\phi_{m,a,in}$  is the mass flow rate of inlet fuel to the anode and  $M_{mol,a}$  is the molar mass of the anode inlet fuel. Mass transport of  $O_2$  from the cathode side is also calculated based on the current. Use of numerical subroutines is made to calculate these quantities over the cell. More detailed information on the calculation procedure can be found in the Cycle-Tempo technical manual[92].

The oxy-combustion  $CO_2$  capture process has been modeled considering maximum heat integration in the system and high  $CO_2$  purity. The main input parameters for the  $CO_2$  capture model have been tabulated in Table.3.4. A 2 stage compression process with intercooling is utilized to compress the pure  $CO_2$  stream. Cooling water available at around  $12^{\circ}C$  is used for intercooling. In order to minimize the use of cooling water, heat from the capture unit is utilized to generate low pressure steam, which is subsequently used for condensate preheating. A total pressure drop of 2.5 bar is assumed for the cooling water system.

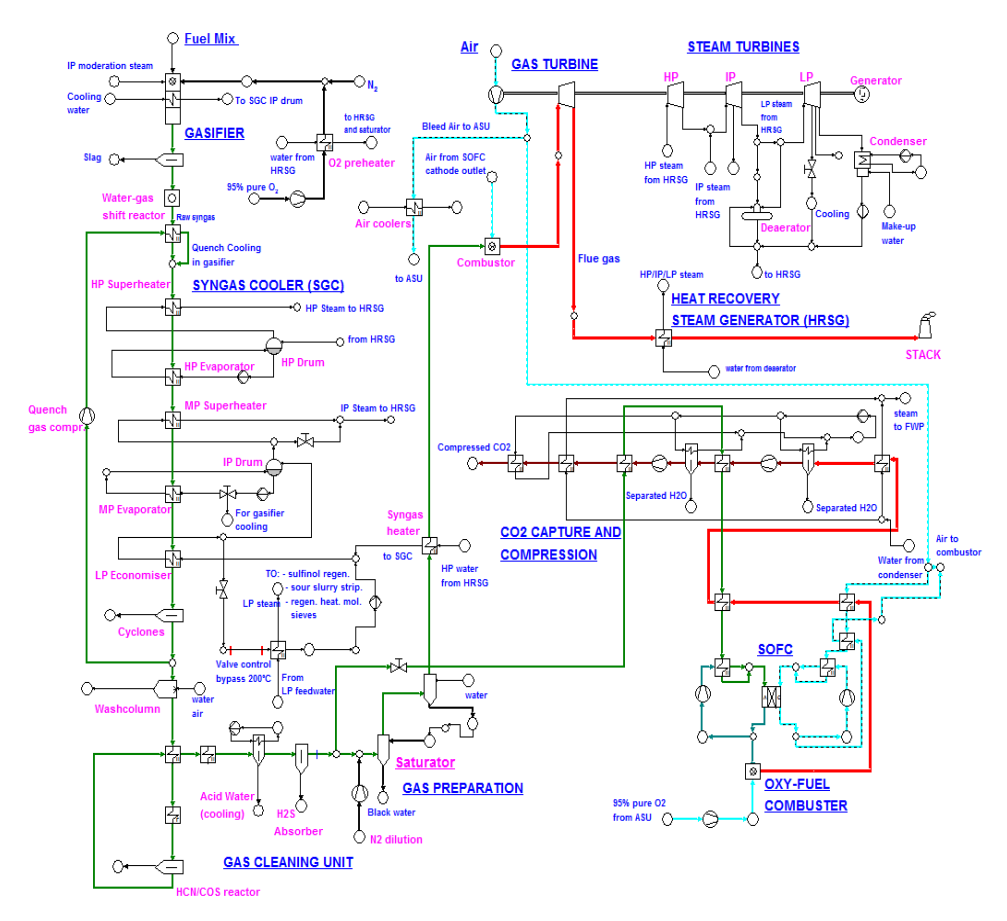


Figure 3.3: Simplified process scheme for SOFC-CC Retrofit STEX (partial CO<sub>2</sub> capture) case- Green streams represent syngas flow, red streams represent flue gas and blue streams represent air flow. Streams indicating detailed process/heat integration have been excluded to maintain clarity.

Fig.3.3 shows the simplified Cycle-Tempo model scheme for the SOFC-CC Retrofit STEX case. The SOFC unit and the partial oxy-combustion CO<sub>2</sub> capture unit have not been modelled in off-design mode as these are newly sized equipment added to the WAC system. In the SOFC unit, anode and cathode off-gas recirculation is utilized to maximize stack performance. Previous studies have indicated that utiliza-

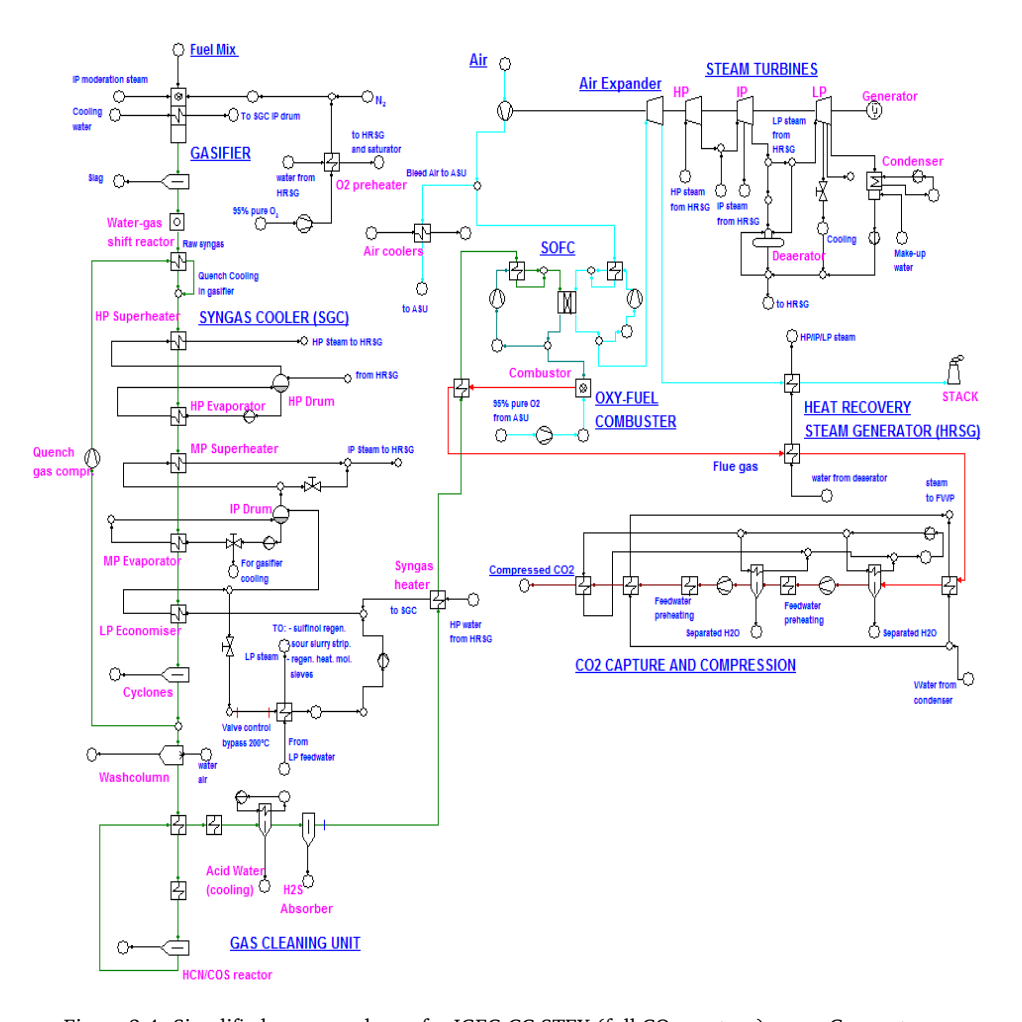


Figure 3.4: Simplified process scheme for IGFC-CC STEX (full  $CO_2$  capture) case - Green streams represent syngas flow, red streams represent flue gas and blue streams represent air flow. Streams indicating detailed process/heat integration have been excluded to maintain clarity.

tion of anode/cathode off-gas recirculation facilitates improved stack performance also considering syngas internal reforming within the stack[124]. The hot flue gas from the oxy-fuel combustor is cooled down to 780°C and preheat air fed into the cathode. Subsequent cooling of the flue gas is achieved by preheating the clean syngas stream to 750°C. The flue gas is then passed through the CO<sub>2</sub> capture and compression unit. The cathode outlet gas is partially cooled down to preheat air before being sent to the gas turbine combustor. Two dummy heat exchangers are used to calculate the anode and cathode recycle flows. The HRSG design is largely based on the original WAC HRSG design as described in Chapter 2. This has just been shown in the scheme with a single heat exchanger to maintain clarity.

Fig.3.4 shows the simplified Cycle-Tempo model scheme for the IGFC-CC STEX case. In this case, all equipment downstream the gas cleaning unit i,e SOFC,  $CO_2$  capture unit, HRSG, air expander and steam turbine cycle are not modeled in off-design mode as they are newly designed. The inlet syngas fuel to the SOFC anode is preheated to  $750^{\circ}$ C with flue gas from the oxy-fuel combustor. The HRSG involves the use of expanded air and flue gas (from oxy-fuel combustor) to generate HP, IP and LP steam. An integrated process is utilized where flue gas is utilized in the HP economizer, HP evaporator and IP superheater; while the expanded air is used in the LP evaporator and LP superheater. The cooled air is then used to preheat syngas and finally discharged to the atmosphere. Auxilliary load for both cases mainly comprises of power required for  $N_2$  and  $O_2$  compression in the ASU, fuel milling, power required in pumps, tracing and other miscellaneous power requirements. In addition, in both the cases, power is required for  $CO_2$  compression in the  $CO_2$  capture unit. This has also been included in the calculation of the total auxilliary load.

# 3.5 Results & Discussion

The off-design performance of the SOFC-CC Retrofit STEX system and the IGFC-CC STEX system has been evaluated by analyzing operating parameters and gas compositions at various locations. Table 3.5 shows the model results for the SOFC-CC Retrofit STEX case with a comparison to the modelled STEX case. As it can be seen the thermal input to the gasifier has been kept constant in order to make the comparison. The off-design system performance of the existing equipment (gasifier, SGC and syngas cleaning unit) remains almost unchanged as seen from the table. A slightly higher temperature is used in the saturator. The syngas flow to the N<sub>2</sub> dilution and saturator is smaller in comparison to the STEX case due to a split stream of syngas fed to the SOFC. Consequently, the N<sub>2</sub> flow for dilution is decreased to 33 kg/s (A minimum flow rate of 33.0 kg/s N<sub>2</sub> dilution flow is obligatory for the ASU molecular sieves regeneration). Due to the syngas split stream to the SOFC, there is 28% reduction in the flue gas mass flow rate to the HRSG. This results in a lower steam production (HP/IP/LP) in the HRSG compared to the STEX case as a result of lower heat available in the HRSG.

The air mass flow rate is calculated in the model based on the requirements in the GT combustor and ASU. The discharge pressure from the air compressor is also calculated based on the integrated gas turbine cycle. An important observation from the results is the 18% lower air compressor discharge pressure in the SOFC-CC Retrofit STEX compared to the STEX case. The oxygen demand in the retrofitted plant is even higher than the STEX case, due to additional O<sub>2</sub> requirement in the oxy-combustor. Hence the ASU will require high pressure air flow to cater to the higher oxygen demand. The low air compressor discharge pressure as indicated in Table.3.5 will be insufficient to feed air to the ASU. A booster air compressor (as shown in Fig.3.1) would thus be required to provide high pressure (10.5 bar in the design (BASE) case[125]) air to the ASU.

The gas turbine will be in part load operation in the retrofitted system. The thermal input to the GT combustor in the WAC design IGCC case with coal gasification[11] was 480.3 MW $_{th}$ . Thermal inputs in the STEX case and SOFC-CC Retrofit STEX case are 347.2 MW $_{th}$  and 267.9 MW $_{th}$  respectively. It can thus be seen that the thermal input in these cases are about 73% and 56% of the design case respectively. With a 9% (on mass basis) syngas split stream fed to the SOFC, the mass flow rate at the gas turbine expander inlet reduces by 28% compared to the STEX case. The GT produces a power output of about 174 MW $_e$ ; a 27% reduction compared to the STEX case. Thus, the part load condition of the gas turbine when retrofitted with SOFCs and partial CO $_2$  capture is significant when compared with the STEX and design (BASE) IGCC case.

The GT part load condition and outlet temperature could be controlled to some extent using the variable inlet guide vanes (VIGV)[126]. It has been pointed out that until about 55-60% part load condition (based on GT thermal input/coupling power), the outlet temperature of the GT could be kept constant. In practice, this is challenging because it is also necessary to maintain sufficient discharge pressure from the integrated air compressor for the ASU due to aforementioned reasons. The gas turbine will thus operate at a part load just within the range of the VIGVs. An important aspect to note is that with a small reduction in the GT outlet temperature, the inlet pressure will increase (Stodola's cone law) and consequently the SOFC pressure, voltage and power production will increase. Furthermore, the isentropic efficiency for the GT expander, air compressor and steam turbines has been assumed constant in this study. In reality, the isentropic efficiency of the GT will decrease when operating under part load [126]. However estimation of the isentropic efficiency under part load condition requires additional turbine data (performance maps) which is generally not readily available (often confidential information). For the steam turbines (particularly HP and IP turbine), a significant change in the isentropic efficiencies is not expected despite part load operation. The isentropic efficiency of these turbines (without governing stage) largely depend of the pressure ratio, volume flow and inlet temperature [127].

A syngas LHV range of about 4.3-5.5 MJ/kg is preferred for stable GT combustor operation at WAC. An important consideration with the SOFC-CC Retrofit STEX case is the 13% lower LHV of the syngas fuel to the combustor (see Table 4.12) compared to the STEX case. The difference in the clean syngas composition and LHV at the combustor inlet between both the cases arises due to the difference in  $N_2$  dilution as aforementioned. In practice, a low (or high) LHV (< 4.2 MJ/kg) lead to combustion/flame stability problems in the combustor as indicated by process engineers from the plant. This could lead to the need of a different combustor and/or fuel injectors[126, 128]. This can be a major challenge as the GT burner might have to be suitably modified/replaced. Alternative methods of achieving a higher syngas LHV could be by adjusting syngas dilution and lower water vapour saturation, lower SOFC fuel utilization and lower syngas flow to SOFC (smaller SOFC stack). However all these measures would decrease the GT cycle and SOFC performance. Operation of the system with 70% torrefied woodpellets instead of 70% steam exploded woodpellets could also be a solution to increase LHV of the

	STEX (no CC)	SOFC-CC Retrofit STEX (partial CC)		STEX (no CC)	SOFC-CC Retrofit STEX (partial CC)
Fuel Input		(partial CC)	HP Turbine inlet temperature, <sup>o</sup> C	473.71	516.04
Input pulverized fuel, kg/s	23.74	23.74	HP Turbine Outlet temperature, °C	311.92	346.22
LHV, MJ/kg	19.59	19.59	HP Steam mass flow, kg/s	65.64	62.04
Thermal input, $MW_{th}$	465.00	465.00	IP Steam turbine inlet pressure, bar	23.82	23.25
Gasifier	100.00	100.00	IP Steam turbine outlet pressure, bar	3.59	3.37
Outlet presssure, bar	24.90	24.90	IP Turbine inlet temperature, °C	463.50	499.65
Outlet temperature, <sup>o</sup> C	1515.00	1515.00	IP Turbine Outlet temperature, °C	227.34	250.00
Oxygen mass flow, kg/s	14.74	14.74	IP Steam mass flow, kg/s	80.13	76.55
Moderation steam, kg/s	1.18	1.18	LP Steam turbine inlet pressure, bar	3.59	3.34
Quench gas recycle, kg/s	52.42	52.42	SOFC unit	0.07	0.0 1
Temperature quench gas, <sup>o</sup> C	243.40	243.17	Fuel LHV, MJ/kg	_	10.42
Quench pressure after compres.,bar	24.90	24.90	Anode flow (in), kg/s	_	18.45
Syngas cooler			Anode flow (out), kg/s		23.17
Syngas inlet temperature, <sup>o</sup> C	820.00	820.00	Anode recirculation flow, kg/s		9.44
Syngas outlet temperature, <sup>o</sup> C	229.40	229.17	Cathode flow (in), kg/s		252.69
HP steam to HRSG, kg/s	36.82	35.02	Cathode flow (out), kg/s		247.97
HP steam to HRSG: Temperature, <sup>o</sup> C	363.90	367.09	Cathode recirculation flow, kg/s		81.60
IP steam to HRSG, kg/s	15.60	16.15	Voltage, V		0.83
IP steam to HRSG: Temperature, °C	321.69	318.14	Active Area, m <sup>2</sup>		22785.97
LP steam: Pressure, bar	9.00	9.00	Anode recir. compressor consumption, $kW_e$		39.70
LP steam: Temperature, <sup>o</sup> C	175.36	175.36	Cathode recir.compressor consumption, $kW_e$	-	372.53
LP steam: Mass flow, kg/s Cyclone	4.34	4.31	Power, MW <sub>e</sub> Oxy-fuel CC	-	47.55
Outlet temperature syngas, <sup>o</sup> C	229.39	229.17	CO <sub>2</sub> purity, mol %		89.09
Wash column		,,	Captured CO <sub>2</sub> flow , kg/s		11.69
Outlet mass flow syngas, kg/s	40.93	40.94	Oxygen flow to oxy-combustor, kg/s	-	0.93
Pressure syngas, bar	24.52	24.52	Oxy-combustor temperature, <sup>o</sup> C		1567.28
Outlet temperature syngas, <sup>o</sup> C	145.10	146.36	Oxy-combustor pressure, bar	-	7.00
HCN/COS reactor			CO <sub>2</sub> compressor 1 outlet pressure,bar	-	32.25
Outlet temperature syngas, °C	191.80	192.00	CO <sub>2</sub> compressor 2 outlet pressure, bar	-	152.26
Outlet pressure, bar	21.72	21.72	Cooling water flow, kg/s		193.15
H <sub>2</sub> S absorber			CO <sub>2</sub> compressor 1 consumption,MW <sub>e</sub>		1.83
Outlet temperature syngas, °C	40.00	40.00	$CO_2$ compressor 2 consumption, $MW_e$	-	1.48
Mass flow syngas, kg/s	33.14	33.14	Condensed water flow, kg/s	-	1.98
Gas preparation			Generated steam flow, kg/s	-	3.05
Nitrogen temperature, <sup>o</sup> C	59.00	59.00	HRSG		
Nitrogen pressure, bar	12.01	12.01	HP Steam raising mass flow, kg/s	28.80	27.02
Nitrogen mass flow, kg/s	38.00	33.00	HP Superheater outlet temperature, <sup>o</sup> C	476.34	516.04
Saturator syngas outlet temperature, °C	119.62	125.00	HP Superheater outlet pressure, bar	97.93	96.06
Preheater syngas outlet temperature, °C  Powerblock	292.41	283.56	LP Steam raising mass flow, kg/s LP Superheater outlet temperature, °C	4.15 233.25	1.71 269.99
Air compressor discharge, bar	9.05	7.42	LP Superheater outlet pressure, bar	3.59	2.77
Air bleed, kg/s	61.90	72.63	Power output	0.07	<b>□.</b> //
Combustion chamber pressure, bar	8.78	7.24	Gross Power output, $MW_e$	204.85	223.64
Gas Turbine inlet temperature, °C	919.20	950.00	Auxiliary load, $MW_e$	31.82	34.04
HP Steam turbine inlet pressure, bar	92.93	96.06	Net Power output, MW <sub>e</sub>	173.02	189.59
HP Steam turbine outlet pressure, bar	92.93 27.82	27.25	Net efficiency, %	37.20	40.77

Table 3.5: Model results SOFC-CC Retrofit STEX - A comparison is presented with the STEX case

syngas fuel to the GT combustor. As the case presented here is a limiting case with maximum syngas split to the SOFC, the aforementioned alternative methods in principle should help achieve a higher syngas LHV when a smaller SOFC stack is

Case	$H_2$	$N_2$	AR	$CH_4$	CO	$CO_2$	$H_2O$	$H_2S$	LHV (MJ/kg)
STEX	11.89	43.00	0.37	0.00	25.99	3.00	15.75	0.00	4.28
SOFC-CC Retrofit STEX	10.32	44.07	0.32	0.00	22.58	2.61	20.10	0.00	3.73

Table 3.6: Clean syngas composition(% mol), input to GT combustor

used for retrofitting.

The SOFC stack operates at a pressure of about 7.32 bar in the retrofitted system and produces a net power output of about 47.5 MW<sub>e</sub>. An important thing to keep in mind is that this is for a thermodynamically limiting case; where we try to show the real thermodynamic/process constraints with existing plant equipment. The study clearly indicates that smaller stacks (with power levels from kW<sub>e</sub> to 40 MW<sub>e</sub>) can be integrated in existing IGCC power plants without major thermodynamic/process implications. Most power utility companies and organizations are currently focussing towards large scale newly designed IGFC power plants. The authors believe that an alternative and more logical approach towards introducing SOFCs in IGCC power plants is to carry out a step wise integration (retrofitting). The size of the SOFC stack should be incremented gradually, synchronous with latest technology development. Commercial syngas fed pressurized (in the same range as considered in this work) SOFC modules are currently available [33, 34, 129, 130] in the kW<sub>e</sub> to 1 MW<sub>e</sub> range and such units should be considered to retrofit in existing IGCC plants. Step wise scaling up in the size of the SOFC stack module will also promote technology development to some extent, as operating/practical challenges with real syngas can be identified even while operating with smaller SOFC stacks.

Table 3.7 shows the model results for the IGFC-CC STEX case with a comparison to the STEX case. The net electrical efficiency of 47.9% is comparable with values reported in literature for coal based IGFC-CC systems[100, 105, 108]. Absence of  $N_2$  dilution leads to the absence of ASU  $N_2$  compression, which is a major contributor in the auxilliary load (refer to Chapter 2). Process parameters upstream gas preparation are very comparable between both the cases. Notable differences are a higher IP, LP steam flow in the SGC and a lower syngas temperature after preheating. The increase in the IP/LP steam production in the SGC is particularly due to a marginally higher (0.3%) syngas flow (the temperatures are very similar).

Considering that the SOFC is the main power producing unit in the IGFC-CC STEX case, significant differences can be observed between both systems in the power block and HRSG. Despite the same amount of clean syngas used to generate power in the SOFC stack, there is a considerable reduction (about 55% on mass basis) in the HRSG HP steam production. The LP steam production is however about 3 times higher.

The SOFC unit in this case operates at a pressure of 10.5 bar and produces a net power of about 168 MW which is about 75% of the net power plant output. The anode and cathode recirculation compressor power consumptions are much higher compared to the SOFC-CC Retrofit STEX case due to higher gas flow rates resulting from the design of SOFC module (anode/cathode recirculation) and HRSG, where two heat sources, namely the expanded air and CO<sub>2</sub> rich flue gas are utilized. However the net power produced by the steam turbines (HP/IP/LP) is only about 9%

	STEX (no CC)	IGFC-CC STEX (full CC)		STEX (no CC)	IGFC-CC STEX (full CC)
Fuel Input		(run 00)	HP Turbine inlet temperature, <sup>o</sup> C	473.71	507.72
Input pulverized Coal, kg/s	23.74	23.74	HP Turbine Outlet temperature, <sup>o</sup> C	311.92	322.29
LHV, MJ/kg	19.59	19.59	HP Steam mass flow, kg/s	65.64	46.64
Thermal input, $MW_{th}$	465.00	465.00	IP Steam turbine inlet pressure, bar	23.82	29.00
Gasifier	100100	100100	IP Steam turbine outlet pressure, bar	3.59	4.25
Outlet presssure, bar	24.90	24.90	IP Turbine inlet temperature, °C	463.50	510.00
Outlet temperature, <sup>o</sup> C	1515.00	1515.00	IP Turbine Outlet temperature, <sup>o</sup> C	227.34	256.76
Oxygen mass flow, kg/s	14.74	14.73	IP Steam mass flow, kg/s	80.13	61.23
Moderation steam, kg/s	1.18	1.18	LP Steam turbine inlet pressure, bar	3.59	4.25
Quench gas recycle, kg/s	52.42	52.70	SOFC unit	0.07	1.20
Temperature quench gas, <sup>o</sup> C	243.40	246.95	Fuel LHV, MJ/kg	_	10.43
Quench pressure after compres.,bar	24.90	24.90	Anode flow (in), kg/s	_	68.19
Syngas cooler	21.70	21.70	Anode flow (out), kg/s		85.60
Syngas inlet temperature, <sup>o</sup> C	820.00	820.00	Anode recirculation flow, kg/s		35.05
Syngas outlet temperature, °C	229.40	232.85	Cathode flow (in), kg/s	-	917.13
HP steam to HRSG, kg/s	36.82	33.77	Cathode flow (out), kg/s		899.71
HP steam to HRSG: Temperature, <sup>o</sup> C	363.90	373.17	Cathode recirculation flow, kg/s		760.90
IP steam to HRSG, kg/s	15.60	16.23	Voltage, V		0.83
IP steam to HRSG: Temperature, °C	321.69	326.97	Active Area, m <sup>2</sup>		84015.1
LP steam: Pressure, bar	9.00	9.00	Anode recir. compressor consumption, $kW_e$	-	96.82
LP steam: Temperature, <sup>o</sup> C	175.36	175.36	Cathode recir. compressor consumption, kW <sub>e</sub>	-	2408.60
LP steam: Mass flow, kg/s	4.34	5.02	Power, MW <sub>e</sub>	-	167.61
Cyclones	4.34	3.02	Oxy-fuel CC	-	10/.01
Outlet temperature syngas, °C	229.39	232.85	CO <sub>2</sub> purity, mol %		89.12
Wash column	447.37	232.03	Captured CO <sub>2</sub> flow , kg/s	-	43.09
Outlet mass flow syngas, kg/s	40.93	40.99	Oxygen flow to oxy-combustor, kg/s	-	3.41
Pressure syngas, bar	24.52	24.52	Oxy-combustor temperature, <sup>o</sup> C	-	1567.62
Outlet temperature syngas, <sup>o</sup> C	145.10	146.69	Oxy-combustor pressure, bar		10.15
HCN/COS reactor	143.10	140.09	CO <sub>2</sub> compressor 1 outlet pressure,bar	-	41.08
Outlet temperature syngas, <sup>o</sup> C	191.80	192.00	CO <sub>2</sub> compressor 1 outlet pressure, bar	-	150.80
Outlet pressure, bar	21.72	21.72	Cooling water flow, kg/s	-	1299.13
H <sub>2</sub> S absorber	21./2	21./2	CO <sub>2</sub> compressor 1 consumption,MW		6.10
Outlet temperature syngas, <sup>o</sup> C	40.00	40.00	CO <sub>2</sub> compressor 1 consumption, MW	-	4.14
1 , ,			- 1	-	7.32
Mass flow syngas, kg/s Gas preparation	33.14	33.14	Condensed water flow, kg/s	-	6.89
Nitrogen temperature, <sup>o</sup> C	59.00	_	Generated steam flow, kg/s  HRSG	-	0.69
Nitrogen temperature, °C Nitrogen pressure, bar	13.01	-		28.80	12.87
0 1		-	HP Steam raising mass flow, kg/s		
Nitrogen mass flow, kg/s	38.00 119.62	-	HP Superheater outlet temperature, <sup>o</sup> C	476.34 97.93	507.72
Saturator syngas outlet temperature, °C		270.00	HP Superheater outlet pressure, bar		119.80
Preheater syngas outlet temperature, °C	292.41	270.00	LP Steam raising mass flow, kg/s	4.15	12.87
Powerblock	0.05	10.50	LP Superheater outlet temperature, <sup>o</sup> C	233.25	255.00
Air compressor discharge, bar	9.05	10.50	LP Superheater outlet pressure, bar	3.59	4.25
Air bleed, kg/s	61.90	86.43	Power output	004.05	060.40
Combustion chamber pressure, bar	8.78	-	Gross Power output, MW <sub>e</sub>	204.85	260.49
Gas Turbine/Air expander inlet temperature , <sup>o</sup> C	919.20	950.00	Auxiliary load, MW <sub>e</sub>	31.82	37.44
HP Steam turbine inlet pressure, bar	92.93	119.80	Net Power output, $MW_e$	173.02	223.05
HP Steam turbine outlet pressure, bar	27.82	32.70	Net efficiency, %	37.20	47.96

Table 3.7: Model results IGFC-CC STEX - A comparison is presented with the STEX case

lower than the STEX case. The important point to note is that oxy-combustion  $CO_2$  capture has a relatively large negative effect on the net plant efficiency. The auxiliary load in the IGFC-CC STEX case is about 5.6 MW (19%) higher than the STEX

case mainly due to the 2 stage  $CO_2$  compression in the  $CO_2$  capture unit. Air bleed for the ASU from the air compressor is also increased due to additional oxygen requirements in the oxy-fuel combustor which leads to an increase in the auxilliary load due to additional  $O_2$  compression. However due to the absence of the dilution  $N_2$  compressor and reduced power consumption in the HP water pump , the increase in auxilliary load is not drastic. As seen from Table 3.7, the stored  $CO_2$  stream is about 89% pure. The gas mixture consists of about 9%  $N_2$ , 1.5% of Ar and trace quantities of  $O_2$  and  $O_2$ 0. Presence of  $O_2$ 1 is due to the slight oxygen excess in the oxy-fuel combustor ( $O_2$ 1 and a part of  $O_2$ 2 originate from the 95% pure  $O_2$ 2 mixture from the ASU used in the gasifier and oxy-fuel combustor. The remaining  $O_2$ 2 comes from the fuel and the fuel transport gas to the gasifier.

Case	$H_2$	$N_2$	AR	$CH_4$	CO	$CO_2$	$H_2O$	$H_2S$	LHV (MJ/kg)
SOFC-CC Retrofit STEX	3.25	6.40	0.84	0.00	9.58	55.94	23.98	0.00	1.03
IGFC-CC STEX	3.26	6.39	0.84	0.00	9.59	57.91	24.01	0.00	1.03

Table 3.8: Anode outlet gas composition(% mol), input to oxy-fuel combustor

Table 3.8 shows the anode outlet gas compositions and LHV from the SOFC unit for both the cases. The LHV of the outlet gas is considerably low and it is assumed that the oxy-fuel combustor (newly designed) can cope with this. In case of unstable operation, however pure syngas could be partly utilized. In the IGFC-CC STEX case, it is important to note that the low LHV fuel to the oxy-fuel combustor leads to low thermal input to the air expander. This leads to a lower thermal energy in the HRSG and consequently lower power production from the steam turbines.

# 3.5.1 Carbon deposition

Operating SOFCs with syngas as fuel certainly offers advantages in terms of boosting efficiencies and flexibility. However, an important operating challenge is to prevent carbon deposition/coking. Under certain operating conditions, syngas and CO decompose to create solid carbon formations in Ni-based anodes or anode inlet/outlet pipes [131, 132]. The electrochemical performance of the anode then drastically reduces due to a decrease in the active area, which also results in a large polarization resistance. The SOFC model in this study has been developed under the assumption of an Ni-GDC anode (Table 3.3) and hence it is important to assess the possibility of carbon deposition. Ternary phase diagrams based on thermochemical equilibrium calculations (free energy minimization) are useful to predict the theoretical boundary limits for carbon deposition depending on the operating condition [133].

Point	Location	Pressure (bar) (SOFC-CC Retrofit STEX/IGFC-CC STEX)	Temperature (°C)
Α	Anode inlet (pipe) before recirculation	7.35/10.50	750.00
В	Anode inlet (pipe) after recirculation	7.32/10.48	850.00
C	Anode outlet (pipe)	7.27/10.43	950.00

Table 3.9: Operating points/locations considered to evaluate the systems for carbon deposition

In order to assess the possibilities of carbon deposition in both the cases, operating conditions have been considered at three locations within the system as listed in Table 3.9. Based on these conditions, equilibrium calculations have been performed using the software Factsage [134] to obtain the C-H-O ternary phase diagram (Fig.3.5). Fig.3.5a and Fig.3.5b are the ternary phase diagrams for the SOFC-CC Retrofit STEX and IGFC-CC STEX case respectively. The red curve represents the boundary limits for the gas conditions at the anode inlet before recirculation and point A represents the actual operating point. The green curve represents the boundary limits for the gas conditions at the anode inlet after recirculation and point B represents the actual operating point. The blue curve represents the boundary limits for the gas conditions at the anode outlet after recirculation and point C represents the actual operating point.

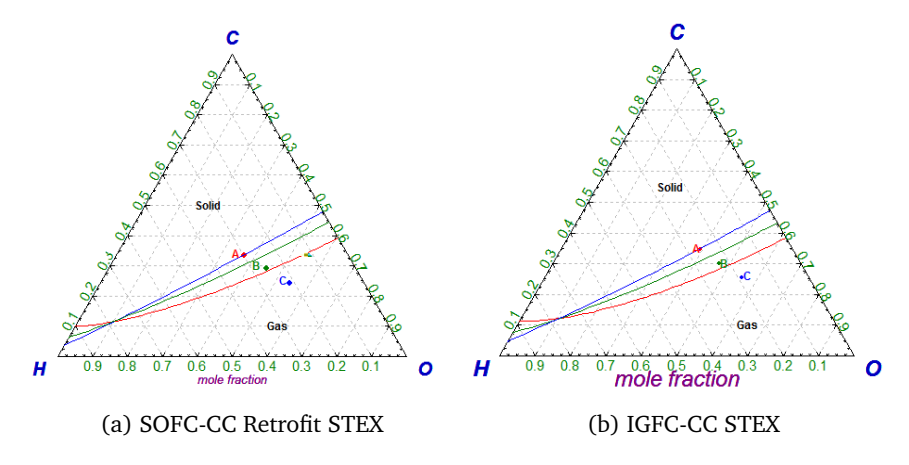


Figure 3.5: Ternary phase diagram showing equilibrium lines and operating points to indicate possibilities of carbon deposition

As seen from both the figures, point A lies above the corresponding equlibrium curve indicating a possibility of coking. The conditions at the actual inlet to the SOFC anode (point B) and the anode outlet (point C) are below the corresponding equilibrium curves thus indicating theoretically safe operating conditions. Addition of steam to the extracted syngas is a possible option to reduce the possibility of coking at point A [132]. However it is important to note that steam should then be extracted from the system and this will lead to drop in the net electrical efficiency. Preliminary calculations for the SOFC-CC Retrofit STEX case indicate that the drop in net electrical efficiency could be about 0.2-0.5% points with IP steam extraction from the syngas cooler. Considering the scope of this work, a detailed analysis on this has yet not been carried out. Carbon deposition also depends on other factors like residence time, reaction/surface conditions in pipes etc. Despite possibilities of carbon deposition in the SOFC upstream sections (pipes) of the system i,e from the GCU to the SOFC unit or after the syngas cooler, process engineers at WAC have not observed any significant coking in the past in these lines during normal operation with coal or biomass. Hence it is assumed that the operating conditions upstream the syngas preheaters and SOFC unit are safe to prevent carbon deposition. This work indicates the risks of carbon deposition (particularly in the SOFC inlet), however additional investigations regarding carbon deposition in SOFC retrofitted IGCC systems is highly encouraged.

#### 3.5.2 Exergy Analysis

Exergy analysis for both the systems have been carried out using Cycle-Tempo as described in the previous chapter in section 2.6.3. In principle, exergy efficiency is calculated for each component by the program with appropriate product and source(s) consideration. Detailed information on this can be found in the program manual [32, 135]. The total exergy efficiency ( $\eta_{\rm ex}$ ) for the system is calculated according to Eqn.2.10,

	STEX		SOFC-CC	Retrofit STEX	IGFC-CC STEX		
	Energy	Exergy	Energy	Exergy	Energy	Exergy	
Input (MW)	465.06	510.50	465.06	510.50	465.06	510.50	
Gross Power (MW)	204.85	204.85	223.64	223.64	260.50	260.50	
Auxilliary load (MW)	31.82	31.82	34.04	34.04	37.44	37.44	
Net Power (MW)	173.02	173.02	189.59 189.59		223.05	223.05	
Net efficiency (%)	37.20	33.89	40.77 37.13		47.96	43.68	

Table 3.10: Exergy output and exergy efficiency for various cases

The exergy of the solid fuel mix (Exergy input) is estimated by Cycle Tempo using a method described by Baehr[136]. Table 3.10 gives an overview of energy (1st law) and exergy (2nd law) analysis for the 2 cases in comparison with the STEX case. An exergy efficiency of about 37% is obtained with the retroffited system indicating that existing IGCC plants can still be operated with higher electrical/exergy efficiencies (about 12% higher) with retrofitting direct internal reforming solid oxide fuel cells and oxy-fuel CO<sub>2</sub> capture technologies. This efficiency boost with a relatively low carbon footprint can be considered as a possible solution to operate existing power plants with reduced emissions and high efficiency in near future. With a newly designed IGFC power plant with oxy-combustion CO<sub>2</sub> capture, a much higher exergy efficiency of about 44% is obtained. The increase in the exergy efficiency due to electrochemical fuel conversion is compensated with exergy losses and exergy destruction in the CO<sub>2</sub> capture unit. However, there is an increase of about 10 percentage points (25% increase) in the exergy efficiency.

Fig. 3.6 shows the exergy flow diagram for the SOFC-CC Retrofit STEX case illustrating the exergy loss/destruction due to various operations in the plant. Exergy loss and destruction due to the partial  $CO_2$  capture account for about 1.2% of the total exergy losses. In comparison with the STEX case (refer to chapter 2, Fig. 2.5), the stack losses are also lower due to the lower concentrations of  $CO_2$  and  $CO_2$  and  $CO_3$  and  $CO_3$  in the total exergy losses. Exergy destruction during gasification and combustion still contribute largely to the irreversibilities in the system, however an important

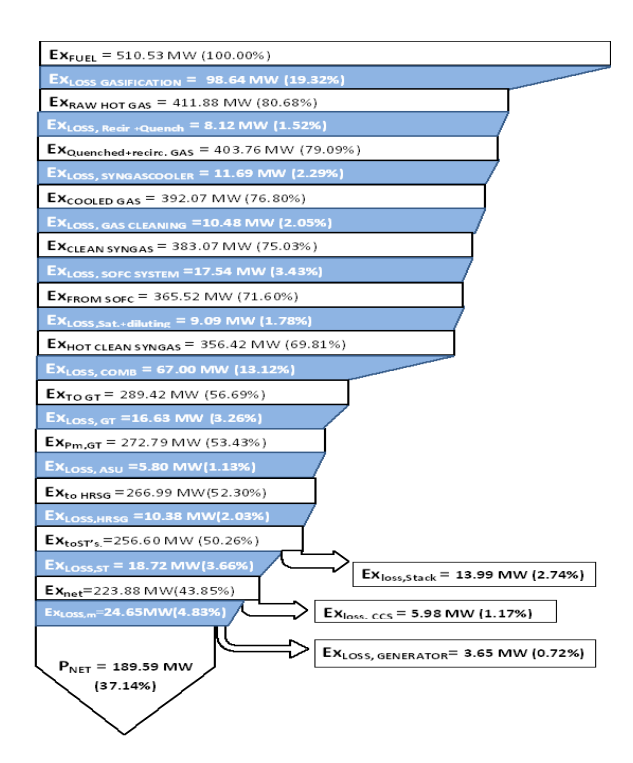


Figure 3.6: Exergy flow diagram for SOFC-CC Retrofit STEX (with partial CC) case - Exergy destruction during GT combustion are lower than the STEX case with the partial replacement of combustion with electrochemical oxidation in the SOFC

observation to be noted is the reduced exergy destruction in the GT combustor. The exergy destruction in the GT combustor in the STEX case is about 97.6 MW; about 19% of the total exergy losses (refer to chapter 2, Fig.2.5). The partial replacement of fuel combustion with electrochemical conversion leads to a 30% reduction in the exergy destruction in the GT combustor. Hence despite the utilization of oxycombustion  $CO_2$  capture, it is seen that retrofitting SOFCs in existing IGCC power plants is beneficial from the exergy/electrical efficiency point of view.

Fig.3.7 shows the exergy flow diagram for the IGFC-CC STEX case. The CO<sub>2</sub> capture unit contributes with about 8% to the total exergy losses. As it can be seen, gasification is the largest source of exergy destruction. Complete replacement of combustion with electrochemical oxidation in the SOFC unit leads to a reduction in total exergy losses with exergy destruction in the SOFC unit being relatively low (<5%). Exergy loss through the exhaust stack (air) is largely negligible. The figure shows a combined loss/destruction of about 3.5% in the gas cleaning unit and due to syngas preheating.

From the exergy analysis of both systems it can be seen that retrofitting IGCC plants with SOFC-CO<sub>2</sub> capture offers significant thermodynamic advantages in terms of boosting electrical and exergy efficiencies. Despite concerns regarding material, cost and scaling up; further research (particularly market based and thermo-

economic evaluations) of solid oxide fuel cell integration in existing large scale bio-IGCC power plants is highly encouraged.

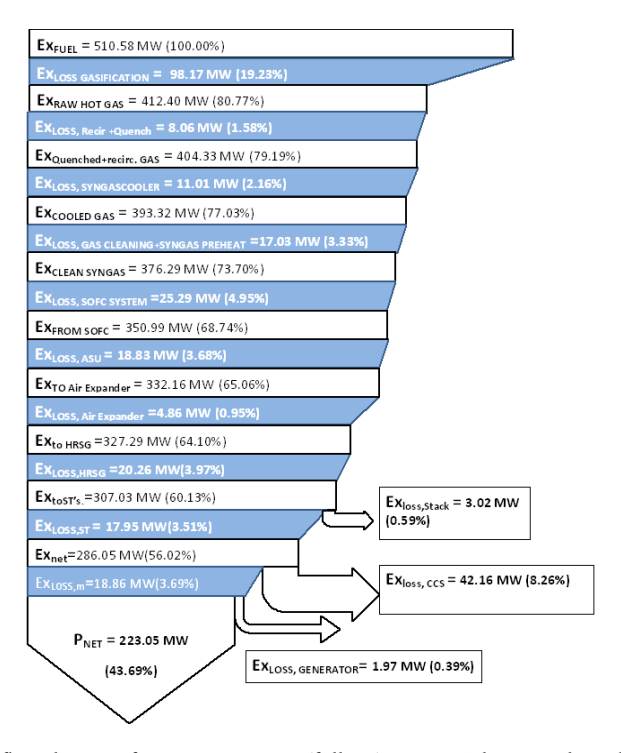


Figure 3.7: Exergy flow diagram for IGFC-CC STEX (full CC) case - High exergy loss/destruction due to  $CO_2$  capture is compensated by the high efficiency SOFC system rendering a relatively high net exergy efficiency

#### 3.5.3 CO<sub>2</sub> neutrality and emissions

Power production with high percentage of biomass in the fuel blend offers a possibility to design a  $CO_2$  neutral/negative system. Bio-energy with carbon capture and storage (BECCS) promotes negative  $CO_2$  emissions. The concept of biomass  $CO_2$  neutrality is generally based on an assumption that biomass removes as much  $CO_2$  from the environment during its growth as is released during its combustion. The wood pellet biomass is considered as a  $CO_2$  neutral fuel in this study. Table.3.11 shows a parametric comparison between the various cases considering  $CO_2$  neutrality and emissions. The fuel input in all the three cases is a blend of 70% biomass and 30% coal (energy based). Based on our assumption, this means that even without  $CO_2$  capture (STEX case), the system is highly  $CO_2$  neutral. The remaining undesired  $CO_2$  non-neutrality originates from the 30% coal in the fuel blend.

The total CO<sub>2</sub> flow in the system has first been calculated as the sum of CO<sub>2</sub> coabsorbed in the H<sub>2</sub>S absorber [137], CO<sub>2</sub> released through the stack and the pure captured  $CO_2$  in the  $CO_2$  capture unit. The  $CO_2$  co-absorbed in the  $H_2S$  absorber is part of emissions as this is just vented out from the plant. The  $CO_2$  emitted from the system is a sum of the vented  $CO_2$  from the  $H_2S$  absorber and the  $CO_2$  released through the stack. The captured  $CO_2$  has been calculated based on the purity of the  $CO_2$  stream (Table 3.5 and Table 3.7). With a fixed fuel input mass flow, the amount of  $CO_2$  produced per unit mass of fuel (fuel specific  $CO_2$ ,  $\gamma$ ) is calculated. The fuel specific  $CO_2$  from pure coal ( $\gamma_{coal}$ ) has been calculated to be 2.45 based on the BASE (with no biomass co-gasification) case (The BASE case has been described in detail in our previous article [11]). As the STEX blend contains less carbon and more oxygen than coal (Table 2.2), the fuel specific  $CO_2$  is much lower than with pure coal. The coal based  $CO_2$  flow is then calculated using  $\gamma_{coal}$  as shown in Eqn.3.4:

Coal based 
$$CO_2$$
 flow = 0.3. Fuel input.  $\gamma_{coal}$  (3.4)

The coal based CO<sub>2</sub> capture fraction is then calculated with Eqn.3.5:

Coal based 
$$CO_2$$
 capture fraction =  $\frac{\text{Captured } CO_2 \text{ flow}}{\text{Coal based } CO_2 \text{ flow}}$  (3.5)

The  $CO_2$  neutrality factor then has been calculated using Eqn.3.6, taking into account the captured  $CO_2$  from the 30% non-neutral coal in the fuel blend.  $\gamma_{coal}$  plays a central role in determining the neutrality factor as it can be seen from Eqn.3.5 and Eqn.3.4. Since Coal based  $CO_2$  is directly calculated as a scaled parameter using  $\gamma_{coal}$ , the neutrality factor cannot be directly utilized to estimate the coal/biomass based  $CO_2$  emissions. The factor is an indicator showing the scale of biomass utilization and  $CO_2$  capture in the system.

$$CO_2$$
 neutrality factor = 0.7 + 0.3.(Coal based  $CO_2$  capture fraction) (3.6)

Parameter	STEX	SOFC-CC Retrofit STEX	IGFC-CC STEX
Parameter	(no CC)	(partial CC)	(full CC)
Input Fuel flow , kg/s	23.74	23.74	23.74
Co-absorbed CO <sub>2</sub> flow in H <sub>2</sub> S absorber, kg/s	1.89	1.91	1.90
CO <sub>2</sub> flow through stack (exhaust), kg/s	43.25	31.53	0.06
Captured CO <sub>2</sub> flow, kg/s	0	11.70	43.12
Net Power Output, MW <sub>e</sub>	173.02	189.59	223.05
<b>Total CO</b> <sub>2</sub> , kg/kWh <sub>e</sub>	0.94	0.86	0.73
Coal based $CO_2$ , kg/kWh <sub>e</sub>	0.36	0.33	0.28
Biomass based CO <sub>2</sub> , kg/kWh <sub>e</sub>	0.58	0.53	0.45
Captured CO <sub>2</sub> , kg/kWh <sub>e</sub>	0	0.22	0.69
$CO_2$ emitted, kg/kWh <sub>e</sub>	0.94	0.64	0.03
CO <sub>2</sub> neutrality factor	0.7	0.9	1.44
Net CO <sub>2</sub> emitted, kg/kWh <sub>e</sub>	0.36	0.11	-0.41

Table 3.11: System evaluation for CO<sub>2</sub> neutrality and emissions

The biomass based  $CO_2$  as shown in the table can be considered as negative  $CO_2$  emissions based on the assumption that this  $CO_2$  originates from the atmosphere

and is also released in equal amounts from the system. The Net  $CO_2$  emitted is then calculated by subtracting the biomass based  $CO_2$  and the captured  $CO_2$  from the total amount of  $CO_2$ . As it can be seen from Table.3.11 the SOFC-CC Retrofit STEX system results in a  $CO_2$  neutrality factor of 0.9 while the IGFC-CC system results in a higher than unity  $CO_2$  neutrality factor of 1.44. The net  $CO_2$  emissions are much lower in the SOFC-CC Retrofit STEX and negative in case of the IGFC-CC system. The  $CO_2$  emitted for the STEX case are comparable to values cited in literature for biomass co-gasification[138, 139]. Retrofitting with  $CO_2$  capture (SOFC-CC Retrofit STEX case) reduces the  $CO_2$  emitted by almost 45% and application of full scale  $CO_2$  capture (IGFC-CC STEX case) leads to a very low  $CO_2$  emission.

Feasibility and sensitivity studies towards sizing the SOFC stack module and CO<sub>2</sub> capture unit for retrofitting is highly recommended. It has been indicated in this work that coking/carbon deposition is a major risk (particularly at the SOFC anode inlet pipes) in the retrofitted system. Detailed investigations on this aspect giving possible solutions are highly recommended as future work. SOFC operation with real syngas also needs experimental and system investigation. In addition, the gas turbine part load operation and ways to minimize its effect on the plant performance should be further researched upon.

#### 3.6 Conclusions

A thermodynamic case study has been presented towards integrating (retrofitting) solid oxide fuel cells (SOFCs) and CO<sub>2</sub> capture in existing IGCC power plants utilizing high percentage (upto 70%) biomass co-gasification with a focus on near future implementation. The study is helpful to further evaluate design/sizing challenges in SOFC-CO<sub>2</sub> capture retrofitted IGCC power plant systems for near future implementation, gas turbine part load behaviour and techno-economic aspects. Various thermodynamic aspects have been addressed and process modifications have been identified to retrofit SOFCs in IGCC systems.

It is concluded that existing integrated gasification combined cycle power plants (coal/biomass based) could be operated without major plant modifications and relatively high electrical efficiencies of more than 40% (LHV) by retrofitting with solid oxide fuel cells (SOFC) (producing upto  $40~\text{MW}_e$  electric power) and partial oxycombustion  $\text{CO}_2$  capture. Exergy (2nd law) analysis indicates that exergy destruction due to GT combustion reduce significantly (about 30%) in the retrofitted system due to partial replacement with electrochemical conversion. Total exergy efficiency increases to about 37% (increase by 9%) when retrofitted with SOFC and partial oxy-combustion  $\text{CO}_2$  capture.

Control of the the gas turbine (GT) expander outlet temperature with variable inlet guide vanes (VIGV) to minimize part load effects is crucial when retrofitted with SOFCs. Furthermore, the discharge pressure from the main air compressor is much lower (about 18%) in the retrofitted system. In order to meet the oxygen demand and to feed bleed air to the ASU at design pressure, a booster air compressor would be required. Resizing the SOFC stack and/or modifications in the N<sub>2</sub> dilution and

water saturation unit might be required to obtain an acceptable LHV for clean syngas; thus enduring flame stability in the GT combustor. Retrofitting with SOFC and partial oxy-combustion CO<sub>2</sub> capture also leads to a considerable (about 12% in our limiting case) reduction in the IP/LP steam production due to the lower syngas flow (and hence heat transfer) in the combined cycle. Based on these process constraints presented in this work, appropriate engineering solutions should be developed by the industry. Retrofitting with partial CO<sub>2</sub> capture reduces the specific emissions by almost 45%. To apply full scale integration of SOFC and oxy-combustion CO<sub>2</sub> capture (IGFC-CC STEX case), the flue gas GT expander should be replaced by an air expander and the WAC design based HRSG has to be significantly redesigned. CO<sub>2</sub> negative IGFC power plants can be developed by utilizing 70% biomass in the fuel feed and full oxy-combustion CO<sub>2</sub> capture with a very low specific CO<sub>2</sub> emission.

### Chapter 4

# Flexible IRCC power plants with hydrogen storage

Operational flexibility in power plants is essential to cater to large variations in power supply and demand. Energy storage technologies can be utilized in large scale natural gas combined cycle (NGCC) power plants to introduce operational flexibility. This chapter presents a thermodynamic study (including exergy analysis) on flexible NGCC power plants with pre-combustion CO<sub>2</sub> capture, called integrated reforming combined cycle (IRCC) power plants. Hydrogen storage using metal hydrides (MH) has been explored as a flexibility option in large scale IRCC power plants. A comparative analysis has been presented using steady state ASPEN Plus models for a reference NGCC system, an IRCC system and a Flexible IRCC system with MH (MgH<sub>2</sub>) based hydrogen storage. The study indicates that such Flexible IRCC systems could be operated with a time based average (considering charging and discharging) electrical efficiency above 45% depending on the amount of hydrogen stored, appropriate heat integration and choice of the metal hydride. Furthermore, it is concluded that addition of MH based H<sub>2</sub> storage in an IRCC system does not lead to significant electrical/exergy efficiency penalty. The system concept presented in this work can be further utilized to explore the applicability of metal hydride based hydrogen storage in large scale combined cycle power plants.

**This chapter is published as:** A. Thallam Thattai, T. Woudstra, B. J. Wittebrood, W. G. Haije, J. J. C. Geerlings, P.V. Aravind, *System design and exergetic evaluation of a flexible integrated reforming combined cycle (IRCC) power plant system with carbon dioxide (CO<sub>2</sub>) capture and metal hydride based hydrogen storage, International Journal of Greenhouse Gas Control, Volume 52, September 2016, Pages 96-109, ISSN 1750-5836* 

#### 4.1 Background

Increasing worldwide carbon emissions and its role in climate change has convinced policymakers to set restrictions on the emission of Green house gas (GHG). Conventional power plants have a large share in the emission of GHG, predominantly CO<sub>2</sub> and therefore current research focuses on renewable power producing technologies and reducing CO<sub>2</sub> emissions in conventional power plants. Carbon capture and storage (CCS) has the potential to reduce overall mitigation costs and increase flexibility in achieving greenhouse gas emission reductions [140].

Natural gas is an abundantly available fuel for power production in the Netherlands, owing to its large reserves and production. The Netherlands is the second largest producer and exporter of natural gas in Europe [141] and producing clean electrical power from gas could be a viable and economical option. The installed power capacity of the current electricity network can be divided in a base load (nuclear, hydro and coal), intermediate load (combined cycles) and peak load (hydro, simple cycles) [20]. Modern natural gas combined cycle plants (NGCC) plants typically operate with a fast start-up, shut-down, load cycling and high part load efficiency. Therefore they are very suitable for operating in the intermediate load range [142]. NGCC power plants with pre-combustion carbon dioxide (CO<sub>2</sub>) capture (see Chapter 1 section1.3.1.1); called integrated reforming combined cycle (IRCC) [143] could be attractive technology for near future power/fuel production owing to their relatively high efficiency, reduced GHG emissions and high reliability [144, 145].

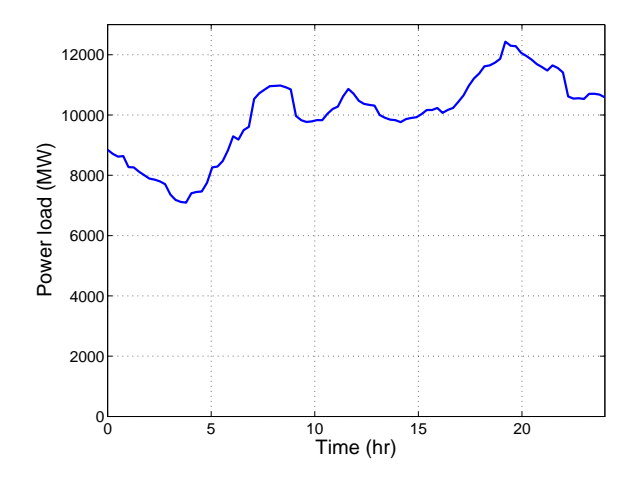


Figure 4.1: A typical daily network load curve for a summer day in the Netherlands [146].

Increase in the share of renewable power in meeting future energy demands is mandatory. However due to large intermittency in renewable energy sources like wind, solar, relatively large fluctuations are expected in future power supply. In order to deliver electricity with high reliability and minimal interruption, flexible power plants have to be designed to handle fluctuations in the daily/seasonal power demand [142]. Fig.4.1 shows a typical daily network load curve in the Netherlands

[146]. This typical summer load curve shows that peak power demand is in the evening ( $19^{th}$  hour) while the lowest (off-peak) power demand is in the morning ( $4^{th}$  hour) with the power demand varying approximately between 50% and 100% of the total peak power demand. Such large variations in daily electrical power demand require fast load-following plant operations to ensure a reliable and efficient electricity network.

With an IRCC plant, hydrogen co-production and storage during off-peak hours and utilization of the stored hydrogen for peak power production could introduce operational flexibility. Part of the hydrogen rich gas after pre-combustion CO<sub>2</sub> capture (see Chapter 1 section 1.3.1.1) can be stored during low power demand and this stored hydrogen can eventually be used for peak power production. Electrical Energy Storage (EES) options can cope with the variations in net power resulting in more reliable electrical power supply and reduction in energy costs. Different EES options have been developed in the last decades like batteries, flywheels, Pumped Hydro Electrical Storage (PHES), Compressed Air Energy Storage (CAES) and natural gas or hydrogen storage mainly differing in discharge time, energy content and efficiency [22] (See Chapter 1 section 1.4)). The cost of storing energy in a hydrogen storage system is much lower than the cost of storing the same amount of energy in batteries [147]. Hydrogen is considered a potentially clean energy carrier for both mobile and stationary applications. By employing IRCC power plants, carbon free hydrogen could be co-produced and stored during off-peak load hours thereby providing increased flexibility.

Multiple options exist to store hydrogen like compressed hydrogen storage, cryogenic storage and storage in Metal Hydride (MH). Since the volumetric energy density of hydrogen at standard conditions is low, hydrogen should be packed as close as possible. Compressed hydrogen storage tanks can contain pressures upto 700 bar (6.7 wt%) [148]. Pressures up to 800-900 bar can be achieved by use of high strength tanks. However, high-pressure vessels present a considerable risk and the energy required for the compression of hydrogen to 800 bar can increase to about 12-16% of its calorific value [148]. The density of liquefied cryogenic gases is considerably higher as compared to compressed gases. However, the tank system is complex and liquefaction of hydrogen requires about 20%-30% energy of the calorific value of hydrogen [149]. Hydrogen storage in metal hydrides has the benefit that it requires lower pressures and reduced volumes [43] resulting in a safer system with reduced capital investments. An additional advantage of using MH in such a system is the possibility of integrating heat during the MH reaction resulting in a flexible system that is expected to maintain high efficiencies of the storage system and the plant during peak and off-peak hours.

Extensive application based research has been performed in recent years on metal hydride based hydrogen storage for applications in the transport sector [150–153]. Research efforts though have been rather limited for stationary applications and much is focussed on small scale systems. Hoffman et al.[150] have discussed various mobile and stationary applications for metal hydride based hydrogen storage and indicate that magnesium and iron-titanium alloys are promising materials. Other metal hydride based stationary system studies focus mainly on trigeneration systems

[154], combined electrolysis/power generation combined system [155], small scale residential application [156], stationary systems utilizing proton exchange membrane (PEM) fuel cells[157, 158] and solar/wind energy based systems [159, 160].

#### 4.2 Motivation

Literature review shows a lack in system level investigations on metal hydride based hydrogen storage in stationary large scale combined cycle power plant systems. Many companies now are investing in developing metal hydride based storage tanks and pumps in the low/intermediate power level range [161–163]. 2G Cenergy have already delivered hydrogen fueled CHP cogeneration systems with metal hydride storage [164]. With more intensive and dedicated research efforts in developing novel MH materials it could be possible to develop large scale storage modules applicable in stationary power plant systems.

Despite major concerns on the economic impacts and scaling up issues, it is very important to evaluate the thermodynamic implications and opportunities of utilizing metal hydride based storage in combined cycle power plants. A system modeling study showing the steady state model performance of the flexible power plant is a first and necessary step towards understanding feasibility and implementation of such systems. From a thermodynamic point of view, multiple challenges exist in developing such systems which include process design, metal hydride selection, heat integration and heat management due to the different nature of the metal hydride charging (exothermic) and discharging (endothermic) reactions.

The main aim of this chapter is to address flexibility aspects in power production by presenting a novel system design and detailed thermodynamic analysis of a large scale IRCC power plant with MH based  $H_2$  storage. Sorption enhanced water gas shift (SEWGS) technology [25] has been utilized for pre-combustion  $CO_2$  capture (section 1.3.1.1). The main objective of this work is a detailed thermodynamic assessment of the complete system showing the operating thermodynamic limits, associated bottlenecks and important thermodynamic parameters for system optimization. Furthermore, an exergy (2nd law) analysis is depicted with additional discussions on hydrogen purification (moisture removal), part load behaviour and heat exchanger sizing.

#### 4.3 System description & Modeling approach

A simple schematic for the flexible IRCC power plant system is shown in Fig.4.2. Natural gas (fuel) and oxygen (from the Air Separation Unit (ASU)) is preheated and fed to the gas heated reformer - auto thermal reformer (GHR-ATR). The GHR-ATR is a heat exchanger type reactor where the heat from the outlet of the ATR is used to carry out some pre-reforming in the GHR [165]. Pure oxygen is used in the reformer instead of air to prevent  $N_2$  dilution. The ASU has not been modelled in detail in this study; only the power consumption has been appropriately accounted

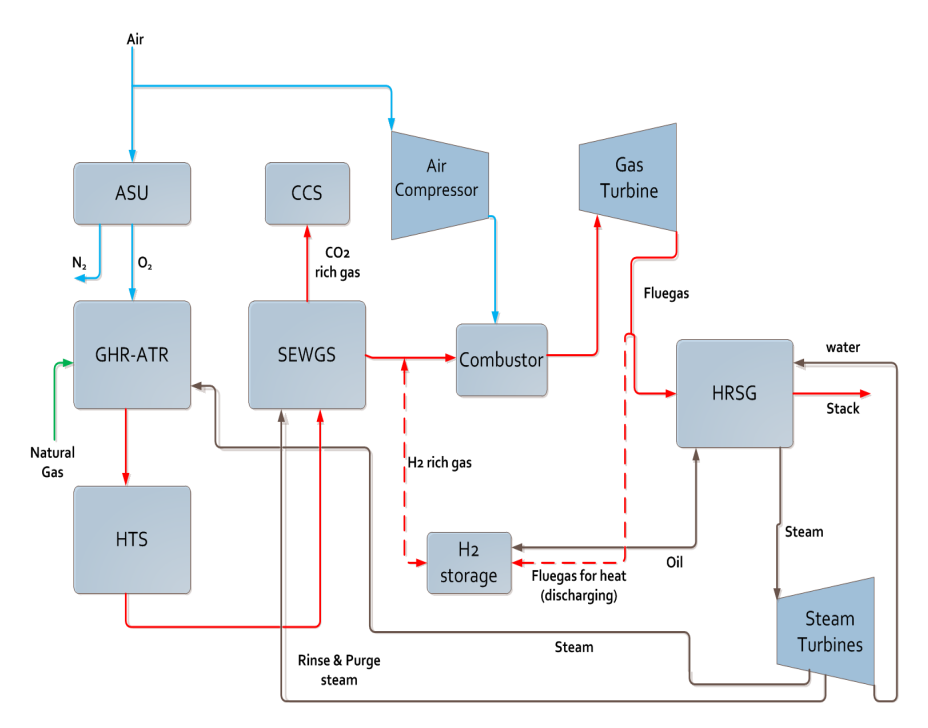


Figure 4.2: Process flow schematic diagram for the Flexible IRCC power plant system with MH based hydrogen storage - red lines indicate syngas/ $H_2$  flow, blue line indicates air/ $O_2/N_2$  flow and green line is the NG flow

for in the calculations. Air for the ASU is not obtained from the gas turbine compressor. Steam required for reforming is extracted from the outlet of the HP steam turbine. The obtained syngas at the outlet of the reformer is fed to the HTS reactor where part of the CO is converted to CO<sub>2</sub>. The obtained gas at the HTS outlet is then sent to the sorption enhanced water gas shift (SEWGS) reactors for complete conversion of CO to CO<sub>2</sub>. SEWGS technology developed at the Energy Research Center of the Netherlands (ECN) is a powerful and efficient process for simultaneously carrying out the WGS reaction and in parallel capturing CO<sub>2</sub>. The main advantage of the process include the high conversion of CO to H<sub>2</sub> by the shift reaction through the selective removal of the product CO<sub>2</sub> [25]. The CO<sub>2</sub> rich stream also contains moisture which can be easily removed by condensation. The pure CO<sub>2</sub> stream is then compressed to the desired pressure and is available for storage.

The hydrogen rich stream is dehumidified and fed into the metal hydride (MH) reactor unit for storage. The heat integration between the MH storage reactor and a thermal fluid (oil) DOWTHERM-A[166] as the heat transfer medium allows flexible switching between charging and discharging. Heat transfer from the thermal fluid is used to generate additional steam during charging mode (exothermic) while heat is provided to the oil from the flue gases during the discharging mode (endothermic). The fluid has been reported to be stable at high operating temperatures [166] and

is thus used for the heat transfer in this study only in its liquid phase to ensure isothermal behavior.

#### 4.3.1 Case description and modeling approach

In order to compare performance of the flexible system, steady state models were developed for a reference NGCC (without CCS and hydrogen storage) system and an IRCC system (with pre-combustion  $CO_2$  capture). Table.4.1 gives a summary of the various cases considered in this study. Based on the typical load curve (Fig.4.1)

Case	Description
Reference NGCC	Conventional NGCC system with triple pressure (HP/MP/IP) steam cycle
IRCC	Reference NGCC with pre-combustion CCS using GHR-ATR and SEWGS technology
Flexible IRCC	IRCC with a MH based H <sub>2</sub> storage unit

Table 4.1: Case definition - A reference NGCC model and the IRCC model have been developed to compare the performance of the Flexible IRCC system

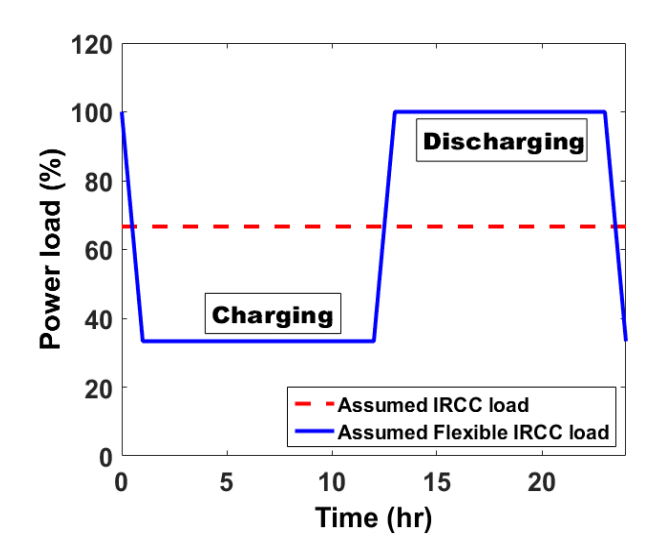


Figure 4.3: Assumed load curve (simplified) for the Flexible IRCC power plant system

a simplified load curve has been assumed in this work to assess flexibility through hydrogen storage in IRCC plants. Fig.4.3 shows this simplified load curve. Full load is chosen as the net power output from the Flexible IRCC system during peak demand with the minimum (base) load being 33.33% of the peak load (much lower than the curve shown in Fig.4.1). In practice the power plant operation and the load dynamics will depend on other external factors, however as the starting step a simplified load curve as shown in Fig.4.3 has been assumed. The IRCC load is then about 50% of the peak load. In order to achieve a 50% lower off-peak load and a 50% higher peak load, it is postulated that approximately 50% (on mol basis) of

the hydrogen available after pre-combustion CO<sub>2</sub> capture be stored during off-peak hours and the stored hydrogen is utilized for peak power production. Based on this postulation, this work also tries to identify the deviation in the load curve from the assumed load curve since additional power (due to additional steam production) is produced during off-peak hours (charging) while heat is extracted from GT flue gases during peak hours (discharging).

General modeling inputs for all models have been obtained from a common European reference framework as defined by the European Benchmark Task Force (EBTF) document [167]. ASPEN Plus process modelling package has been used to realize the model using the Soave-Redlich-Kwong (SRK) equation of state as the thermodynamic model for gas mixtures and ASME 1967 steam table correlations (STEAM-TA) for the water/steam cycle. The EBTF document [167] natural gas feed composition is shown in Table 4.2.

CH	$C_2H_6$	C <sub>3</sub> H <sub>8</sub>	n-C <sub>4</sub> H <sub>10</sub>	iso-C <sub>4</sub> H <sub>10</sub>	n-C <sub>5</sub> H <sub>12</sub>	iso-C <sub>5</sub> H <sub>12</sub>	$CO_2$	$N_2$	LHV(MJ/kg)
% vol 89.0	00 7.000	1.000	0.051	0.050	0.005	0.004	2.000	0.890	46.502

Table 4.2: Feed natural gas composition (% vol) and LHV[167]

Process data for the SEWGS unit has been obtained from literature[168]. Data for the sorbent Beta has been used in this modeling work. Modeling input parameters for the GHR-ATR unit and the CCS unit have also been obtained from literature and have been tabulated in Table 4.3.

GT Air Compressor		Condenser	
Pressure ratio	18.10	Pressure (bar)	0.048
Isentropic efficiency (%)	89.50	Exit Temperature (°C)	26.00
Mechanical efficiency (%)	99.60	Pumps	
GT Combustor		Discharge pressure HP/MP/LP (bar)	120/32/5
Pressure drop (bar)	0.50	Pump efficiency (%)	70.00
Heat loss (MW $_{th}$ )	2.00		
Gas Turbine expander		Steam Turbines	
Outlet pressure (bar)	1.01	HP inlet pressure (bar)	120.00
Turbine outlet temperature (°C)	603.00	MP inlet pressure (bar)	32.00
Isentropic efficiency (%)	87.20	LP inlet pressure (bar)	5.00
		Isentropic efficiency (%)	90.00
GHR-ATR		CCS unit	
ATR equilibrium temperature (°C)	1050.00	CO <sub>2</sub> flashing temperature (°C)	50.00
S/C ratio	2.50	Final delivery pressure (bar)	110.00
Pressure (bar)	25.00	Final delivery temperature (°C)	25.00
SEWGS unit		CO <sub>2</sub> pump efficiency (%)	75.00
Inlet Temperature (°C)	400.00	CO <sub>2</sub> pump driver efficiency (%)	95.00
S/C ratio - Rinse	0.23	Compressor intercooling temperature (°C)	28.00
S/C ratio - Purge	0.85	Carbon capture ratio (%)	95.00
Purge steam pressure (bar)	1.10	CO <sub>2</sub> stream purity (% vol)	99.60
Purge steam temperature (°C)	400.00	Discharge pressure final stage (bar)	80.00
Rinse steam temperature (°C)	400.00		

Table 4.3: Model input parameters for the various blocks

Numerous options exist for chosing a metal hydride for hydrogen storage. Fig.4.4 shows the Van't Hoff diagram for various metal hydrides. Magnesium hydride

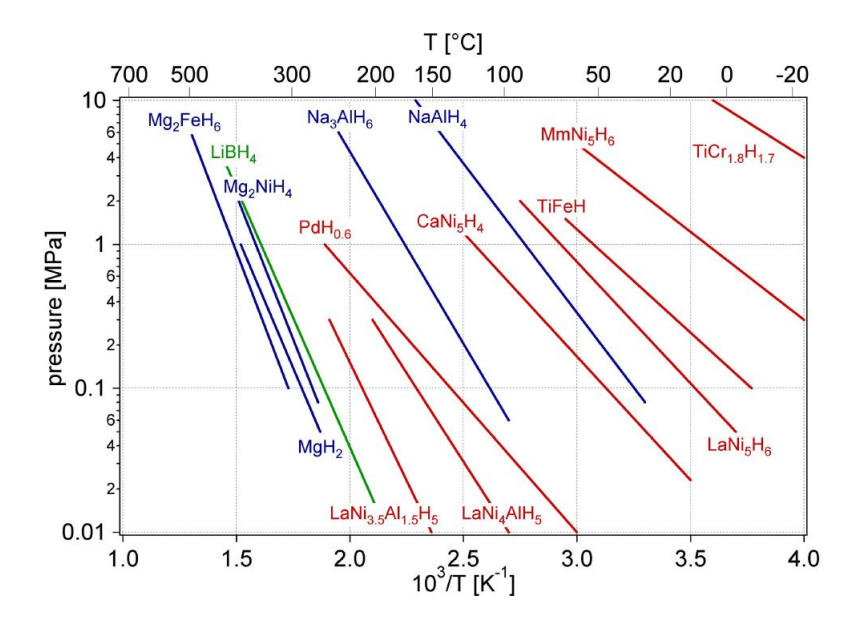


Figure 4.4: Van 't Hoff diagram of various metal hydrides [148] - MgH<sub>2</sub> has been selected in this study based on its high operating temperature and storage capacity

(MgH<sub>2</sub>) has been chosen as the hydrogen storage medium due to its relatively high storage capacity, stability and relatively high operating temperature of about  $400^{o}$ C, matching the H<sub>2</sub> rich gas temperature at the SEWGS outlet.

The charging and discharging reactions for the MgH<sub>2</sub> system [169] are:

$$Mg + H_2 \stackrel{charging}{\rightleftharpoons} \underset{discharging}{eherging} MgH_2 \quad \Delta H = -76000 \text{J/mol H}_2 \quad \Delta S = -135.6 \text{J/K/mol H}_2 \quad (4.1)$$

$$ln(P) = \frac{\Delta H}{RT} - \frac{\Delta S}{R} \tag{4.2}$$

A daily cycle of 12 hours charging and 12 hours discharging has been assumed (Fig.4.3). Also to simplify the analysis, system dynamics of switching between charging and discharging have not been considered i,e an immediate switch between charging and discharging has been assumed. The MH storage unit has been modeled with a purely thermodynamic approach. The net heat release/requirement is calculated by adding the heat of reaction ( $\Delta$ H) to the sensible heat required to heat the MH bed to the operating temperature [170]. A full conversion is assumed for the MH reaction 4.1 to simplify the analysis. A pressure loss of 3 bar at the H<sub>2</sub> feed side has also been assumed to calculate the equilibrium temperature from the Van't Hoff equation (Eqn.4.2). Table 4.4 lists the thermodynamic properties, equilibrium pressure and temperature for the metal hydride during charging and discharging.

The triple pressure (120 bar, 32 bar and 5 bar) Heat Recovery Steam Generator (HRSG) has been modeled in detail with a network of pumps, economizers,

Parameter	Value
Heat of reaction ΔH (J/mol H <sub>2</sub> )	76000.00
Change in entropy $\Delta S$ (J/K/mol H <sub>2</sub> )	135.60
Charging Plateau pressure (bar)	22.00
Charging Equilibrium temperature (°C)	418.00
Discharging Plateau pressure (bar)	28.00
Discharging Equilibrium temperature (°C)	431.00

Table 4.4: Properties, pressure and temperature for the selected metal hydride

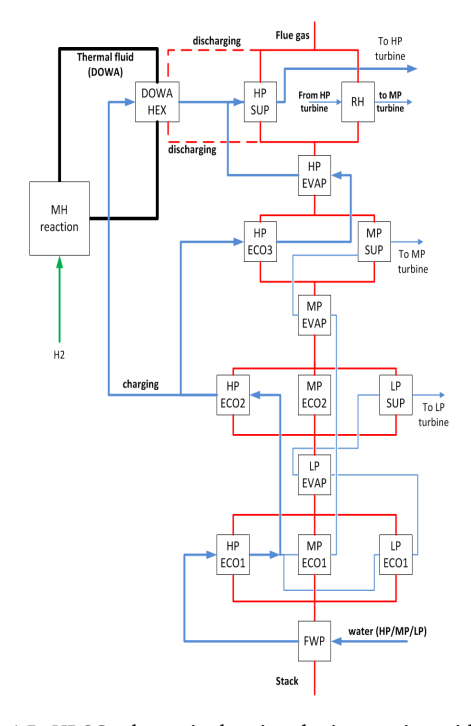


Figure 4.5: HRSG schematic showing the integration with the MH unit

evaporators and superheaters. A schematic of the HRSG showing the integration with the MH unit is shown in Fig.4.5. The minimum approach temperature (pinch point  $\Delta T$  or minimum  $\Delta T$ ) for the evaporators has been chosen as  $10^{o}$ C. Two separate steady state models have been developed for the charging and discharging mode.

The GT turbomachinery (gas turbine expander, air compressor) will be under part load operation during charging mode. The isentropic efficiencies of the expander and compressor have been assumed constant as reliable data (performance maps) are not readily (often confidential information) available in open literature.

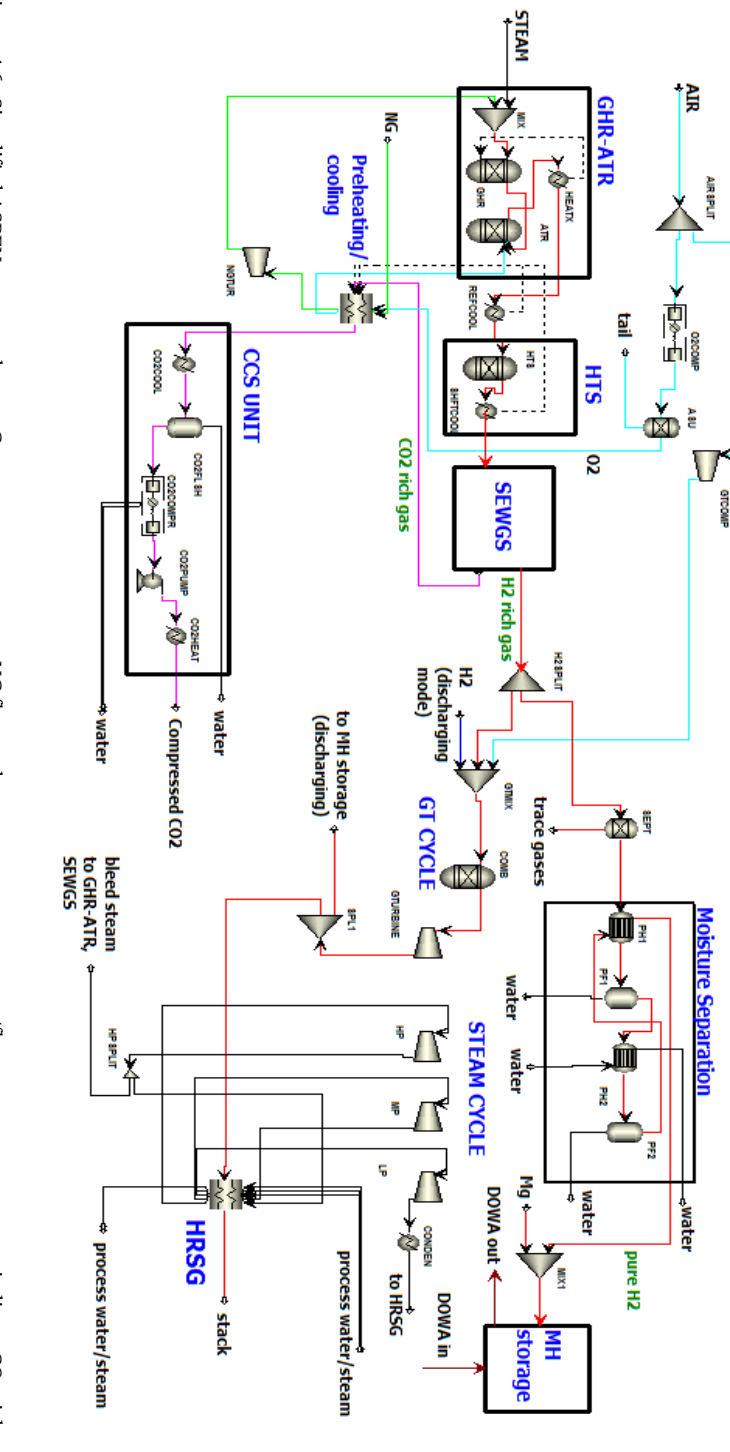


Figure 4.6: Simplified ASPEN process scheme - Green streams represent NG flow, red streams represent syngas/flue gas, magenta streams indicate CO2 rich gas and blue streams represent air flow. Streams indicating detailed process/heat integration have been excluded to maintain clarity.

However a sensitivity study has been presented in section 4.4 describing the part load behaviour of the system with varying expander and compressor isentropic efficiencies. Despite part load operation for the steam turbines (particularly HP and MP turbine), a significant change in the isentropic efficiencies is not expected. The isentropic efficiency of these turbines (assuming without governing stage) largely depend of the pressure ratio, volume flow and inlet temperature [127]. These parameters remain largely unchanged in the charging and discharging case.

Fig. 4.6 shows the simplified ASPEN Plus flowsheet for the Flexible IRCC system. As it can be seen in the figure, the thermal fluid (DOWA) is used to transfer heat to the HRSG to generate additional steam in charging mode. In the discharging mode, part of the hot flue gas at the outlet of the gas turbine is used to provide heat to the MH storage unit. The released hydrogen is then mixed (GTMIX) with compressed air and sent to the GT combustor. Steam required for the GHR-ATR and SEWGS is obtained by bleeding from the HP turbine and using additional expansion to reach the desired pressures. Natural Gas (NG), oxygen preheating and  $CO_2$  cooling is carried out by heat integrating the reforming and HTS processes as shown in Fig. 4.6 by the dotted lines (heat streams). The cooled  $CO_2$  is compressed with a 3 stage compressor and pumped up to the desired pressure of 110 bar. Input parameters for the main unit operations have been obtained from the EBTF document[167].

The hydrogen rich gas at the outlet of the SEWGS unit comprises of a significant amount of water vapour as shown in Table 4.5. In order to store hydrogen in the metal hydride unit, this moisture must be separated out from the gas mixture to yield pure hydrogen. Presence of moisture and other impurities can inhibit the

	$CH_4$	$H_2$	H <sub>2</sub> O	CO	$CO_2$	N <sub>2</sub>
% vol	0.10	81.50	16.70	0.05	1.27	0.38

Table 4.5: H2 rich gas composition at SEWGS outlet (% vol)

performance of the MgH<sub>2</sub> metal hydride bed [171]. Table. 4.5 shows that other gases like CH<sub>4</sub>, CO<sub>2</sub>, CO are present in the H<sub>2</sub> rich gas mixture in very minute quanties (<0.1% vol). The current study assumes moisture as the major impurity. Furthermore, the gas concentrations of other gases could in practice be reduced by adjusting the process parameters of the GHR-ATR/SEWGS unit. Discussions on this is however out of scope of this work. In order to seperate out moisture from the H<sub>2</sub> rich gas, a combination of heat exchangers and flash vessels have been used as shown in Fig. 4.6. A pinch of 10°C has been assumed in both heat exchangers (PH1, PH2). Two flash vessels operating at 145°C and 40°C are used to carry out the moisture seperation. The H<sub>2</sub> gas stream obtained at the outlet is 99.7 % (mol) pure. The pure H<sub>2</sub> gas stream is heated back to a temperature of about 410°C and is then fed to the MH storage unit. Additional options to carry out moisture separation/gas purification include the use of dessicants (zeolites, silica gel etc.) These options can be used to attain very high purity gas streams, although costs could be a major constraint. Regeneration of these sorbents is energy intensive and generally expensive. The practicality of utilizing such materials is out of scope of this work, the presented calculations could however be utilized to develop novel dessicant materials if required.

Research on reducing moisture content in the  $H_2$  rich gas from the SEWGS unit has also been carried out in the recent past. The optimization yields a SEWGS cycle that consumes significantly less steam than the designs earlier presented in literature [172, 173]. The steam to carbon (S/C) ratio in the rinse and purge steps were lowered to as low as 0.03 and 0.08 respectively. This ultimately leads to a reduced moisture content in the outlet  $H_2$  rich gas and hence this may avoid the need of a dessicant system for hydrogen purification. Also a boost in the net efficiency of the system is expected with a reduced steam demand from the power island for the rinse and purge steps [173]. Studies and optimization of the model with this new process data will be part of future work.

#### 4.3.2 Exergy calculation approach

Results obtained from the ASPEN Plus models have been utilized to compute exergy flows for all streams. The exergy of matter is calculated as the reversible (maximum) work derived by bringing the system in thermomechanical and chemical equilibrium with the reference environment. Thus, the net exergy of every steam has been accounted for by adding the thermomechanical exergy and chemical exergy as shown in Eqn.4.3 [174], [175].

$$\dot{E}x = \dot{E}x_{tm} + \dot{E}x_{ch} \tag{4.3}$$

The thermomechanical and chemical exergy of a stream are defined as shown in Eqn.4.4 and Eqn.4.5:

$$\dot{E}x_{tm} = \Sigma \phi_i \cdot \left\{ (h_i - h_{i,0}) - T_0(s_i - s_{i,0}) \right\}$$
(4.4)

$$\dot{E}x_{ch} = \Sigma\phi_i \cdot \left[\Delta g_i + R \cdot T_0 \left\{ ln\left(\frac{P_0}{P_i}\right) - \nu_{o_2,i} \cdot ln\left(\frac{P_0}{P_{o_2,i}}\right) \right\} \right] \tag{4.5}$$

where  $\phi_i$ ,  $h_i$  and  $s_i$  are the mole flow, enthalpy and entropy of component i in the stream at the temperature and pressure of the mixture;  $h_{i,0}$  and  $s_{i,0}$  are the molar enthalpy and entropy at standard conditions.  $\Delta g_i$  is the Gibbs free energy of the  $i^{th}$  component which represents the reversible work generated due to conversion of the component, if required, into an existing environmental component. The second term in Eqn.4.5 represents the reversible work due to expansion of the component to its environment partial pressure  $(p_i)$  and the last term is the reversible work of compressing oxygen to its partial pressure in the environment  $(P_{o_2,i})$  in stoichiometric amount  $(v_{o_2,i})$  required for the conversion of the component. R is the molar gas constant.

As the  $H_2$  storage unit has been modelled with a purely thermodynamic approach, the exergy loss in the storage unit has been calculated based on the reversible work (change in Gibbs free energy) produced due to reaction 4.1. During charging, the reversible work  $W_{rev}$  has been calculated as shown in Eqn. 4.6:

$$W_{rev,tot} = W_{rev,1} + W_{rev,reac} + W_{rev,3}$$
 (4.6)

$$\begin{split} W_{rev,1} &= \dot{n}_{H_2}.(c_{p,H_2}.(T_0 - T) - T_0.c_{p,H_2}.ln\{\frac{T_0}{T}\}) + \dot{n}_{Mg}.(c_{p,Mg}.(T_0 - T) - T_0.c_{p,Mg}.ln\{\frac{T_0}{T}\}) \\ &+ \dot{n}_{H_2}.R.T_0.ln\{\frac{P_0}{P}\} \end{split} \tag{4.7}$$

$$W_{rev,reac} = \dot{n}_{Mg}.\{(h_{0,MgH_2} - h_{0,Mg} - h_{0,H_2}) - T_0.(s_{0,MgH_2} - s_{0,Mg} - s_{0,H_2})\}$$
(4.8)

$$W_{rev,3} = \dot{n}_{Mg}.(c_{p,MgH_2}.(T - T_0) - T_0.c_{p,MgH_2}.ln\{\frac{T}{T_0}\})$$
 (4.9)

 $W_{rev,1}$  (Eqn.4.7) represents the reversible work obtained to expand and cool reactants Mg, H<sub>2</sub> to the reference pressure P<sub>0</sub> (1.013 bar) and temperature T<sub>0</sub> (298.15K) from the system pressure P and temperature T.  $W_{rev,reac}$  (Eqn.4.8) is the reversible work due to the MH reaction 4.1 to form MgH<sub>2</sub>.  $W_{rev,3}$  (Eqn.4.9) represents the reversible work obtained to compress and heat the product MgH<sub>2</sub> from the reference state to the discharging conditions. The specific heat  $c_p$  has been assumed constant in the calculations; the operating temperature not varying significantly.  $h_0$  and  $s_0$  are the standard state enthalpy and entropy, values for which have been obtained from thermodynamic tables. A similar calculation procedure has been followed for the discharging case, initially expanding and cooling reactant MgH<sub>2</sub> to reference state, compressing and heating products Mg and H<sub>2</sub> to the charging conditions.

#### 4.4 Results & Discussion

#### 4.4.1 Energy analysis

Table 4.6 shows the modeling results of the thermodynamic analysis for the different cases including the total fuel input, power consumption, power production, Carbon Capture Ratio (CCR) and the calculated net electrical efficiencies of the system. The net GT output and the net power output have been calculated as shown in Eqn.4.10 and Eqn.4.11 respectively.

The net process output includes the additional power generated by a natural gas expander which is used to expand the inlet NG flow from 70 to 25 bar, a steam turbine to expand from the HP ST outlet pressure to 1.1 bar for the purge stream (SEWGS) and a steam turbine to expand from the HP ST outlet pressure to 25 bar for the GHR-ATR steam inlet. The process input involves the power input required by the HP/MP/LP pumps, the oxygen compressor (ASU) and for CO<sub>2</sub> compression (CCS unit).

The net GT power output in the IRCC case is slightly higher than the Reference NGCC case inspite the same fuel input. Since  $CO_2$  is separated out pre-combustion in the IRCC case, the fuel to the combustor is predominantly  $H_2$  and water vapour.

			Flexible IRCC						
Parameter	Reference NGCC	IRCC		min ΔT ev	$ap = 10^{o}C$		min $\Delta T$ evap = $15^{\circ}C$		
	Reference NGCC	INCC	H <sub>2</sub> s <sub>1</sub>	olit 50%	H <sub>2</sub> sp	olit 30%	H <sub>2</sub> s <sub>1</sub>	plit 50%	
			charging	discharging	charging	discharging	charging	discharging	
Input (MW <sub>th</sub> )	719.47	719.47	719.47	719.47	719.47	719.47	719.47	719.47	
Net GT output $(MW_e)$	272.79	279.38	138.00	411.14	193.51	357.39	136.00	411.14	
Consumption AC (MW $_e$ )	278.01	250.01	126.81	384.63	177.87	332.56	126.81	384.63	
ST Output HP ( $MW_e$ )	30.70	35.08	30.88	32.51	32.32	33.29	30.95	32.73	
ST Output MP (MW <sub>e</sub> )	49.39	24.78	23.54	34.38	25.47	31.95	23.17	33.22	
ST Output LP (MW <sub>e</sub> )	72.83	40.47	31.30	59.93	36.85	54.02	30.91	58.72	
Net ST Output (MW <sub>e</sub> )	152.92	100.33	85.72	126.82	94.64	119.26	85.03	124.67	
Process Input (MW <sub>e</sub> )	1.52	45.66	45.87	46.13	45.72	45.87	45.87	46.13	
Process Output (MW <sub>e</sub> )	0.00	14.77	14.28	14.28	14.28	14.28	14.28	14.28	
Net Plant Output (MW <sub>e</sub> )	424.19	348.82	192.13	506.11	256.71	445.06	189.44	503.96	
Carbon Capture Ratio	-	0.95	0.95	0.95	0.95	0.95	0.95	0.95	
Stack Temperature (°C)	81.08	111.93	80.35	120.22	97.55	117.59	85.89	125.86	
Energy content H <sub>2</sub> (MW <sub>th</sub> )	-	-	335.23	335.23	201.14	201.14	335.23	335.23	
Net Elec. Efficiency (%)	58.96	48.48	50.00	47.99	49.53	48.34	49.30	47.78	
Average Efficiency (%)	58.96	48.48	4	8.52	4	8.77	48.19		

Table 4.6: Simulation results of the difference cases.

The LHV of the fuel is lower when compared to the Reference NGCC case leading to a lower gross GT power output. Also the air flow requirement in the combustor reduces leading to a lower Consumption AC in the IRCC case. But since the drop in Consumption AC is larger than the drop in the gross GT power output, the net GT power output is slightly higher in the IRCC case. Analyzing the electrical efficiency of the Flexible IRCC system with only the natural gas as fuel input is not appropriate since additional hydrogen is produced during charging and consumed during discharging. The effective fuel input is compensated for by this additional hydrogen consumption/production and therefore the electrical efficiency is defined as in Eqn. 4.12 and Eqn. 4.13,  $Q_{in}$  is the input NG energy content and  $Q_{H_2}$  is the energy content of the stored  $H_2$ :

$$\eta_{netelec,charging} = \frac{P_{net}}{Q_{in} - Q_{H_2}} \tag{4.12}$$

$$\eta_{netelec,discharging} = \frac{P_{net}}{Q_{in} + Q_{H_2}} \tag{4.13}$$

In order to make a valid comparison between the different systems, the total performance of the flexible system has also been analyzed with a time based (12 hours of charging and 12 hours of discharging) average net electrical efficiency as shown in Eqn. 4.14. The carbon capture ratio(CCR) [168] is evaluated across the Sorption Enhanced Water Gas Shift (SEWGS) unit with Eqn. 4.15. A CCR value of 0.95 has been used for all the cases.

$$\eta_{elec,average} = \frac{P_{net,charging} + P_{net,discharging}}{2 * Q_{in}} \tag{4.14}$$

$$CCR = \frac{(CO + CO_2)_{in} - (CO + CO_2)_{out}}{(CO + CO_2)_{in}}$$
(4.15)

With introduction of H<sub>2</sub> storage using a high temperature metal hydride (MgH<sub>2</sub>) it is seen that the net electrical efficiency is about 50% during charging and 48% during discharging. The difference in the efficiency values during charging and discharging can be attributed to the heat/power demand in the Gas Heated Reformer - Auto Thermal Reformer (GHR-ATR), SEWGS and the CO<sub>2</sub> unit. The heat/power demand in the GHR-ATR, SEWGS and Carbon Dioxide (CO<sub>2</sub>) unit remains the same during charging and discharging due to a constant fuel input. In order to fulfill this heat/power demand, a lower net power output is achieved in the charging case due to the H<sub>2</sub> split in spite the additional steam generation by the thermal fluid cooler. During discharging, additional hydrogen is fed in to the gas turbine cycle which leads to higher power output. The flexible system shows an average electrical efficiency (Eqn. 4.14) of about 48.5%.

Fig. 4.7a and Fig. 4.7b show the variation in the net electrical efficiency of the IRCC system with different HP, MP and LP steam turbine pressure levels. The figures show a reduction in system electrical efficiency with a higher Low pressure (LP) steam pressure level (constant MP pressure of 32 bar and HP pressure of 120 bar). Fig. 4.7b shows a better system performance for an increase in the HP steam pressure level and a reduction in MP pressure steam level (constant LP steam pressure of 5 bar). The trends in system performance are as expected [176] verifying the system model formulation and calculations. The results of this steam pressure level

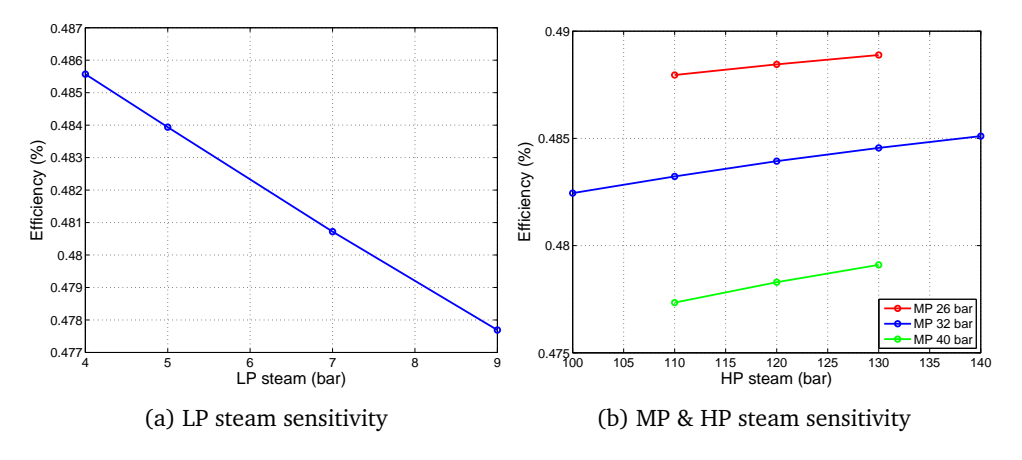


Figure 4.7: Sensitivity in the LP, MP, HP steam pressure levels with electrical efficiency for the IRCC system - system electrical efficiency increases for a lower LP and MP steam pressure level and higher HP steam pressure level.

sensitivity analyses confirm that a better performance can be reached for selecting a lower LP and MP steam pressure level and a higher HP steam pressure level. The selection of the optimum pressure level also depends on economic considerations ,this being out of scope for this work.

Heat integration in the system plays a crucial role in determining the net electrical efficiency of the system. Figure 4.8a shows the Q-T diagram with composite curves for the HRSG and the thermal fluid cooler during the charging mode in the

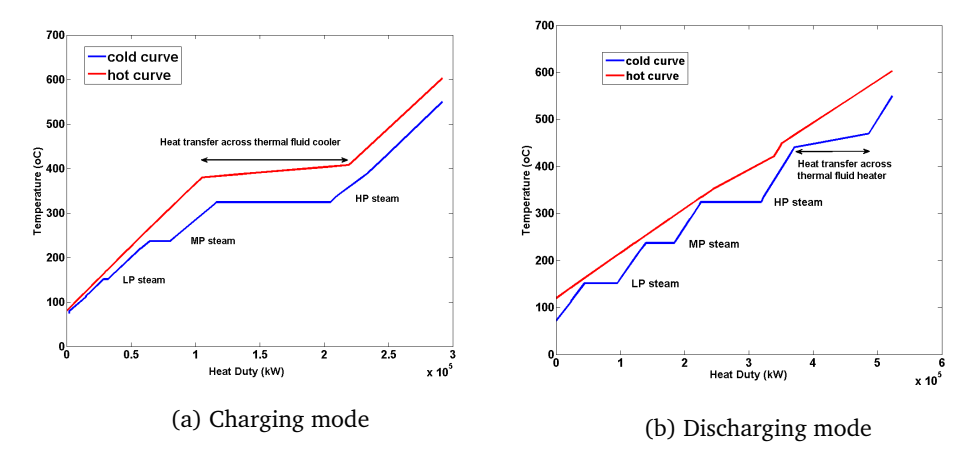


Figure 4.8: Composite curve for the Flexible IRCC system

high temperature MgH $_2$  system . As aforementioned the heat released during charging mode is utilized to generate HP steam in the HP evaporator. The curve shows that in order to achieve the desired pinch of  $10^{\circ}$ C in the HP, MP and LP evaporators of the HRSG, there is reduction in the amount of MP and almost no production of LP steam. Also, a low temperature difference (about  $10^{\circ}$ C) is observed between the hot and cold side in the low temperature economizer section. This will in practice result in a larger and more expensive heat exchanger. The simulation results also indicate that a pinch  $\Delta T$  of about  $5^{\circ}$ C is achieved in the FWP. In order to achieve this low temperature approach, in practice a large surface area of the heat exchanger is required.

An indication of the variation in the heat exchanger area is shown in Table 4.7. The table shows the effective heat capacity values (UA) in the HRSG including for an additional case with a pinch  $\Delta T$  of 15°C in the evaporators instead of 10°C. A smaller pinch  $\Delta T$  of 10°C in the evaporators leads to the need for a large FWP (UA value indicated in bold). In order to limit this area and the  $5^{\circ}$ C pinch  $\Delta$ T in the FWP, the pinch  $\Delta T$  in the evaporators can be increased leading to a higher flue gas inlet temperature in the FWP. The table clearly shows that with a higher pinch  $\Delta T$  in the evaporators, the heat exchanging area in the FWP reduces. In the discharging case, it can be seen that the maximum UA values are obtained for the HP evaporators. As this is the maximum area considering all the cases, the HRSG should be designed for this value. Table 4.6 shows the simulation results in terms of the power output and net electrical efficiencies for the case with a higher pinch  $\Delta T$  in the evaporators. A slight decrease of about 0.33% points is observed in the average electrical efficiency. A higher pinch ΔT in the evaporators causes a lower steam turbine power output leading to a drop in the net efficiency. Figure 4.8b shows the composite curves for the discharging mode in the MgH<sub>2</sub> system. The diagram gives a clear indication of the different pinch points achieved in the evaporators and the thermal fluid heater as the flue gases have been utilized to provide the required MH reaction heat.

	Reference NGCC	IRCC	Flexible IRCC H <sub>2</sub> split 50% (UA)					
Heat exchanger	Reference NGCC	IKCC	min ΔT e	$evap = 10^{o}C$	min ΔT e	$vap = 15^{o}C$		
	UA (kW/K)	UA (kW/K)	Charging	Discharging	Charging	Discharging		
FWP	985.00	575.64	1744.35	589.05	1049.80	508.14		
HP LT Economizer	732.49	769.24	1040.08	636.94	713.31	500.89		
HP MT Economizer	649.68	679.34	940.08	578.47	771.88	513.94		
HP HT Economizer	2077.80	2267.37	468.18	1576.74	470.27	1582.14		
Reheater	518.96	250.17	326.79	451.82	320.49	435.46		
HP Evaporator	1999.90	1964.02	790.75	2456.03	793.26	2460.69		
HP Superheater	612.37	678.45	729.16	1211.12	728.07	1172.42		
MP MT Economizer	86.72	69.90	120.98	204.18	75.83	142.18		
MP LT Economizer	147.99	120.34	240.10	351.74	155.84	253.32		
MP Evaporator	888.09	762.51	596.51	1731.00	458.79	1311.57		
MP Superheater	92.33	78.43	64.66	187.79	57.89	165.15		
LP Economizer	149.58	140.97	24.88	226.91	18.56	177.67		
LP Evaporator	1209.65	1141.69	235.23	1845.60	185.54	1525.17		
LP Superheater	48.74	45.84	8.56	156.99	7.69	130.76		
Oil Cooler (charging)	-	-	1479.93	-	1480.37	-		
Oil heater (discharging)	-	-	-	2231.23	-	2231.34		

Table 4.7: HRSG heat exchanger sizing - values of UA (kW/K) for various cases

Table.4.6 also presents the model results for a  $H_2$  split of 30% instead of 50%. A slight increase is observed in the average efficiency of the system, almost matching the efficiency of the IRCC case. Additionally the issue of a small pinch  $\Delta T$  in the FWP and a large heat exchanging area is avoided in this case as more heat is available from the flue gas in the HRSG. The analysis presented in this section indicate that such steady state models can be effectively used to indicate thermodynamic constraints in the system and as a design tool for the new system. The next section presents an exergy analysis of the Flexible IRCC system indicating the major thermodynamic losses within the system.

A comparison is shown in Fig.4.9 between the assumed load curve (Fig.4.3) and the actual load curve (calculated). With a 50% H<sub>2</sub> split, there is a small deviation between both the curves. The calculated peak load is about 45% of the base load while the minimum load is 55% of the base load. Thus, there is a small shortage in H<sub>2</sub> storage during the off-peak and peak hours. During charging, this imbalance arises due to the additional HP steam generation and power production in the steam cycle. The H<sub>2</sub> split fraction after the SEWGS unit specified in the model is based on the total molar flow of the H<sub>2</sub> rich gas. After gas purification (block SEPT in Fig. 4.6) and moisture separation, the molar flow rate of pure  $H_2$  (which is stored) is thus lower. During discharging, as the GT combustor is fed with this stored H<sub>2</sub>, a lower gas turbine power output than the desired power output is obtained. Also since part of the flue gas is utilized to provide heat for H<sub>2</sub> release in the MH unit, there is a reduction is the total steam turbine power output. These factors lead to a deviation in the load curve during discharging. The comparison shows that flexible operation of the system with the assumed load curve could be achieved with a slightly higher H2 split after the SEWGS unit. However increasing the H2 split to more than 50% might need modifications in the HRSG operation with no LP steam production (Fig.4.8a).

Part load operation of the gas turbine expander and air compressor also influ-

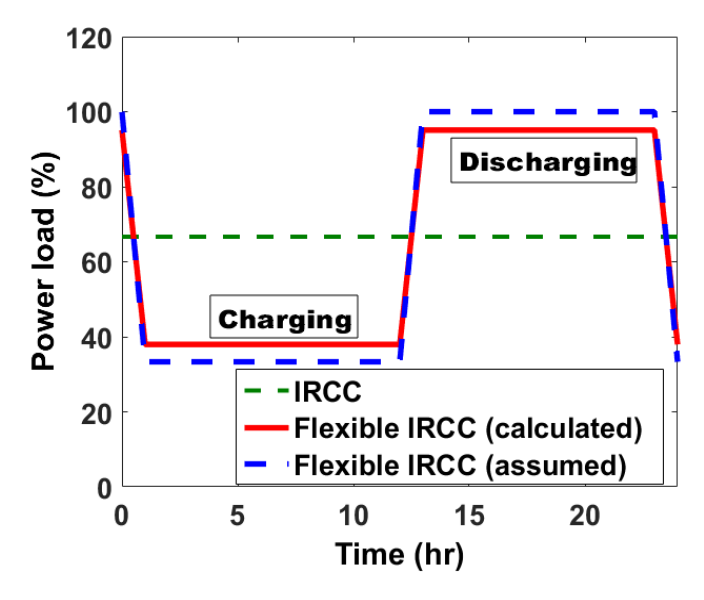


Figure 4.9: Comparison of load curve for the Flexible IRCC system

ences the total system performance. During charging, the expander and compressor operate under significant part load which leads to a drop in the isentropic efficiencies [177]. As the isentropic efficiency is an input in the models, reliable data (performance maps) is required showing the variation of isentropic efficiency with the operating load. Due to the confidential nature and unavailability of this data, a sensitivity analysis has been performed (Fig.4.10) showing the system performance for varying isentropic efficiencies of the expander and air compressor.

The red curve shows the variation of average electrical efficiency with the air compressor isentropic efficiency ( $\eta_{is,comp}$ ) and the blue curve shows the variation with the GT expander isentropic efficiency ( $\eta_{is,expander}$ ). It can be clearly seen that the effect of  $\eta_{is,expander}$  on system performance is more stronger than  $\eta_{is,comp}$ . With a 10% reduction in  $\eta_{is,expander}$ , a drop of about 3% is observed in the average electrical efficiency; while with a 10% reduction in  $\eta_{is.comp}$ , a drop of about 1% is observed in the average electrical efficiency. In order to investigate the combined sensitivity of  $\eta_{\rm is,expander}$  and  $\eta_{\rm is,comp}$  a range of values were considered between 100% and about 77% of the full load value. Table.4.8 lists the input values for  $\eta_{is,expander}$  and  $\eta_{is,comp}$ used for the combined sensitivity study and the results are also shown in Fig.4.10. A combined drop in  $\eta_{is,expander}$  and  $\eta_{is,comp}$  has considerable effect of the system performance. A drop of 10% in  $\eta_{is.expander}$  and  $\eta_{is.comp}$  leads to a drop of about 4% in the average electrical efficiency. With a significant drop of 23% in  $\eta_{is,expander}$  and  $\eta_{\rm is,comp}$ , the average electrical efficiency drops by almost 13%. The actual drop in the isentropic efficiencies is largely turbomachinery specific and hence speculating on it without having reliable data (operating maps) is not appropriate in view of the authors. Further research towards part load behaviour of such systems is required

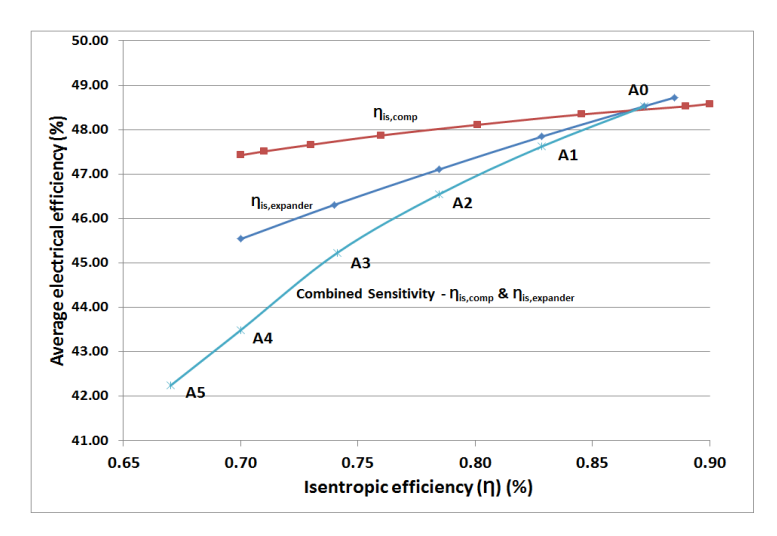


Figure 4.10: Sensitivity of part load isentropic efficiencies - results are shown for varying gas turbine, air compressor and combined isentropic efficiencies

	GT expander isentropic efficiency	Air compressor isentropic efficiency
	$(\eta_{is,expander})$ (%)	$(\eta_{is,comp})(\%)$
A0(full load)	87.20	89.00
A1	82.84	84.55
A2	78.48	80.10
A3	74.12	75.65
A4	70.00	70.00
A5	67.00	68.00

Table 4.8: Input GT expander and air compressor isentropic efficiencies to assess GT part load behaviour - values range from 100% full load values to 77% full load value

and highly encouraged. However it can be concluded from the sensitivity study that despite part-load operation during charging, average electrical efficiencies of about 44-45% could be achieved with the Flexible IRCC system.

In order to minimize the undesirable low Gas Turbine (GT) efficiency during part load, an alternative GT cycle configuration could be used, for eg. installation of differently sized gas turbines for operation during charging mode and discharging mode or a twin gas turbine in a parallel configuration. The choice of this configuration depends also on costs and practical constraints. This is out of scope for this work. However, the simulation results from this study can be used to design and assess various configurations.

The flexible system design developed in this work is based on a standard metal hydride (MgH<sub>2</sub>). MgH<sub>2</sub> has been chosen considering the relatively high storage capacity and high operating temperatures (matching the upstream process conditions). The reaction enthalpy ( $\Delta$ H) and the H<sub>2</sub> split fraction are two important parameters for the system design and performance. A lower  $\Delta$ H results in lower equilibrium temperature based on the Van't Hoff relation Eqn.4.2 (for a constant

Parameter	Reference NGCC	IRCC		Flexible IRCC					
				min ΔT ev	$ap = 10^{o}C$		min ΔT e	$vap = 15^{o}C$	
			H <sub>2</sub> s <sub>1</sub>	olit 50%	H <sub>2</sub> split 30%		H <sub>2</sub> split 50%		
			charging	discharging	charging	discharging	charging	discharging	
$Ex_{NG}$ (MW)	753.92	753.92	753.92	753.92	753.92	753.92	753.92	753.92	
$Ex_{storedH_2}$ (MW)	0.00	0.00	335.39	335.39	201.23	201.23	335.39	335.39	
Ex, reaction $W_{rev}$ (MW)	0.00	0.00	62.02	31.44	37.21	29.72	62.02	31.44	
Ex <sub>source</sub> (MW)	753.92	753.92	480.55	1057.92	589.90	925.43	480.55	1057.92	
Exproduct (MW)	424.14	348.84	192.15	506.12	256.72	445.08	191.47	503.98	
Ex <sub>loss</sub> (MW)	329.75	405.08	288.65	553.12	333.64	481.46	289.35	553.12	
Exergy efficiency (%)	56.26	46.27	39.93	47.71	43.44	47.97	39.79	47.71	
Avg. Exergy efficiency (%)	56.26	46.27	4	6.30	4	6.54	4	6.12	

Table 4.9: Exergy output and functional exergy efficiency for various cases

pressure and  $\Delta S$ ). This then demands a lower operating temperature of the thermal fluid (oil) which also influences then the choice of the thermal fluid. Also the heat transfer from the MH unit to the steam cycle reduces having implications of the HP steam production. A considerably low temperature of the thermal fluid would also mean that HP steam may not be possible to generate from the heat released due to the MH reaction. The system then should be redesigned to generate MP/LP steam. A higher  $\Delta H$  will result in a higher equilibrium temperature and a larger heat transfer from the MH unit to the steam cycle. With a  $H_2$  split of 50% this can have a bottleneck situation in the FWP/economizers (large pinch region). A slightly higher  $\Delta H$  and a slightly lower  $H_2$  split fraction is thus recommended for a more practical HRSG design. The choice of a suitable  $H_2$  split fraction and thermodynamic parameters of the MH can thus be further optimized based on the actual peak and minimum loads. This choice must also be supported with an economic evaluation.

#### 4.4.2 Exergy Analysis

The importance of carrying out an exergy analysis has been described in Chapter 2 section 2.6.3. The functional exergy efficiency in this study has been defined separately for charging and discharging. Analogous to the electrical efficiency defined in Eqn.4.12 and Eqn.4.13, the exergy efficiency is defined as:

$$\eta_{ex,charging} = \frac{P_{\text{net}}}{Ex_{\text{source}}}$$
(4.16)

$$\eta_{ex,discharging} = \frac{P_{\text{net}}}{Ex_{\text{source}}}$$
(4.17)

Table 4.9 shows the exergy efficiency for the various cases considered in this study.  $\text{Ex}_{storedH_2}$  represents the exergy of the stored hydrogen. Ex, reaction  $\text{W}_{rev}$  calculated with Eqn.4.6 is the reversible work which is available due to the MH reaction. For the Flexible IRCC system the source exergy is then calculated as shown in Eqn.4.18 and Eqn.4.19.

$$Ex_{source}$$
 (charging) =  $Ex_{NG}$  - ( $Ex_{storedH_2}$  -  $Ex$ , reaction  $W_{rev}$ ) (4.18)

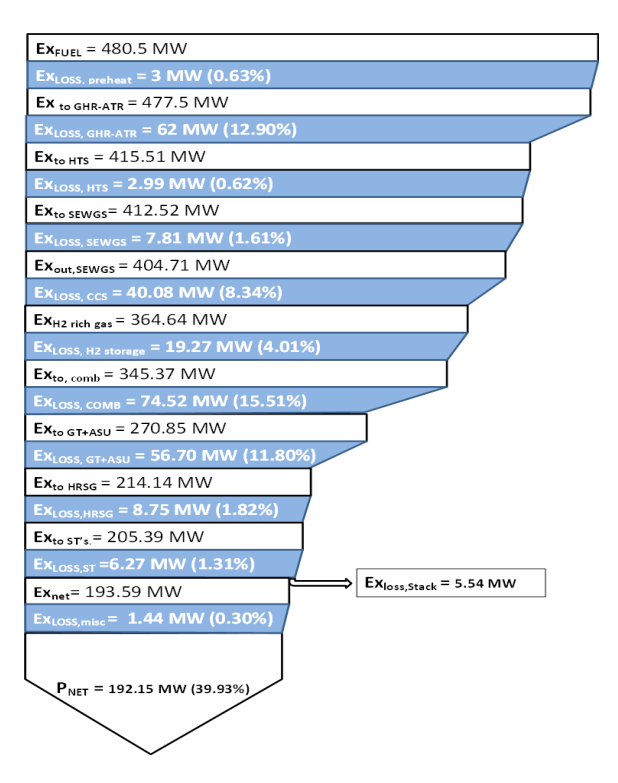


Figure 4.11: Exergy flow diagram - Flexible IRCC charging mode

$$Ex_{source}$$
 (discharging) =  $Ex_{NG}$  + ( $Ex_{storedH_2}$  -  $Ex$ , reaction  $W_{rev}$ ) (4.19)

The IRCC system gives a net exergy efficiency of about 46.3%, a significant reduction from the reference case of 56.3%. The implementation of CCS includes the additional conversion steps in the Gas Heated Reformer (GHR), Auto Thermal Reformer (ATR), SEWGS and compressing  $CO_2$  resulting in additional exergy losses. This results in a larger total exergy loss in the system and reduction in the exergy efficiency. The exergy efficiency for the Flexible IRCC system in charging and discharging mode for  $H_2$  split of 50% and HRSG evaporator pinch  $\Delta T$  of  $10^{\circ}C$  is about 40% and 48% respectively as shown in Table.4.9. A time based average exergy efficiency can then be defined as in Eqn.4.20:

$$\eta_{\text{ex,avg}} = \frac{\text{Ex}_{\text{product,charging}} + \text{Ex}_{\text{product,discharging}}}{2 * \text{Ex}_{\text{source}}}$$
(4.20)

Calculations indicate that the Flexible IRCC power plant could still be operated with a relatively high average exergy efficiencies of about 46.3%, very comparable to the IRCC case. Table 4.9 also shows the exergy efficiencies for cases with a  $\rm H_2$  split of 30% and HRSG evaporator pinch  $\Delta T$  of 15°C. With a higher pinch in the HRSG evaporators there is a marginal change in the average exergy efficiency.

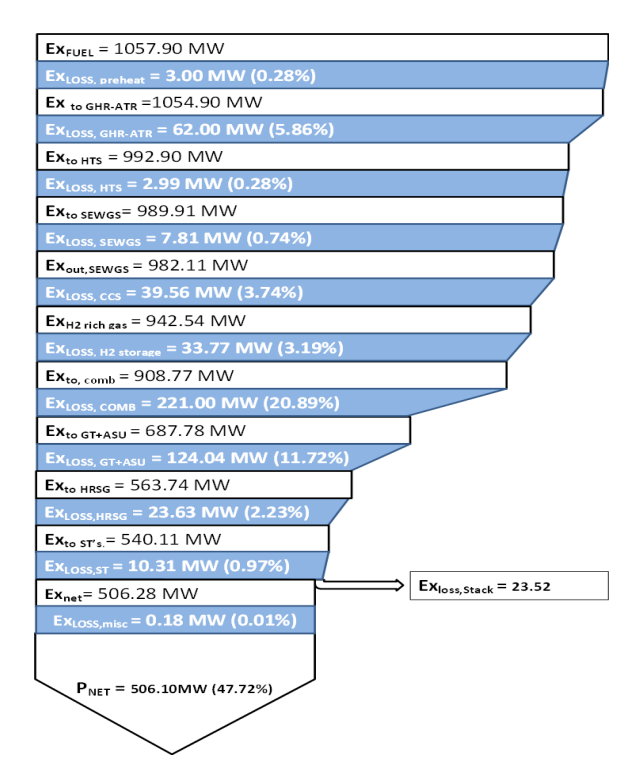


Figure 4.12: Exergy flow diagram - Flexible IRCC discharging mode

The results of the  $2^{nd}$  law analysis for the Flexible IRCC system in charging and discharging mode are also shown in the form of exergy flow diagrams in Fig.4.11 and Fig.4.12 respectively. The figure illustrates the major exergy losses due to various operations in the plant. The largest exergy losses in both modes take place in the GT combustor, the ATR, the gas turbine-ASU unit and the CCS unit[178]. The conversion of fuel in the combustor leads to a high conversion of chemical exergy enabling a large increase in physical exergy due to a high temperature of more than 1250°C reached in the outlet of the combustor, however the combustor is still the main contributor to irreversibilities in the plant. An ATR includes the combustion of pre-reformed NG feed burned to heat the reactants in the reforming reactions and is therefore also one of the major contributors to irreversibilities. The gas turbine and the ASU show a large exergy loss due to mixing, expansion in the turbine and oxygen compression and seperation in the ASU. The CCS unit also contributes significantly (about 8%) to the total exergy destruction. This is particularly due to the large compression process and the exergy lost due to the stored CO<sub>2</sub> stream. An important point to note is the relatively low exergy destruction (3-4%) due to the MH based hydrogen storage unit. Hence implementation of the MgH<sub>2</sub> based hydrogen storage does not lead to large irreversibilities in the system.

Large exergy losses due to combustion and reforming can be reduced by par-

tial/full replacement with electrochemical conversion processes (for eg. solid oxide fuel cells (SOFCs)) [19]. A preliminary system investigation on SOFC integration in NGCC power plant systems has been presented in Appendix 4A.

#### 4.5 Conclusions

A thermodynamic system evaluation has been presented for a Flexible IRCC power plant system with pre-combustion CCS and metal hydride based H<sub>2</sub> storage. Heat released during charging is utilized to generate HP steam for the MgH<sub>2</sub> based system while flue gases from the gas turbine outlet is utilized to provide heat in the discharging mode. The study as a theoretical approach tries to assess the thermodynamic performance of a Flexible IRCC power plant system. As the first step, a simplistic approach has been chosen with several assumptions, particularly the MH reactor unit. However some important conclusions have been drawn from the study.

- Flexible IRCC power plants could still be operated with a time based average electrical efficiency above 45% depending on the H<sub>2</sub> split fraction, choice of the metal hydride and appropriate heat integration in the system.
- Addition of MH based H<sub>2</sub> storage in an IRCC system does not lead to significant penalty in the total plant energy/exergy efficiency, indicating that such systems could be designed to operate and manage load fluctuations with relatively high average electrical/exergy efficiencies.
- Heat integration reveals that a higher temperature pinch in the HRSG evaporators is more beneficial particularly for the FWP in the HRSG. Additionally it is shown that with a 50% storage of hydrogen, the low pressure section in the HRSG becomes almost redundant.
- Inspite additional steam generation during storage, a reasonably good operating load curve is obtained based on the simulation results and hence such systems could be of potential use to manage load fluctuations in NGCC power plants.
- Exergy (second law) analysis for the Flexible IRCC system reveals that the combustor and the GHR-ATR are the largest contributors to the irreversibilities in the system. System improvements of these units will yield the largest effect on the total system performance. The hydrogen storage system contributes about 3-4% to the system irreversibilities.
- The MH reaction enthalpy ( $\Delta H$ ) and the  $H_2$  split fraction are two important parameters for the system design.

## 4.A Retrofitted NGCC power plant system with solid oxide fuel cells

#### 4.A.1 Background

Chapter 4 of this dissertation depicts the advantages of utilizing metal hydride based H<sub>2</sub> storage as a flexibility option in natural gas based IRCC power plants. A second law analysis (see section 4.4.2) shows that large irrreversibilities exist in the processes of autothermal reforming and GT combustion. Analogous to the study presented in Chapter 3 on retrofitting SOFCs in bio-IGCC power plant systems, studies also need to be carried out to understand the effects of retrofitting natural gas based systems like IRCC and natural gas combined cycle (NGCC) power plants. Retrofitting existing natural gas fired power plants with high efficiency solid oxide fuel cells (SOFC) could be one of the promising options for high efficiency power generation with flexible hydrogen production. This section presents a preliminary system study on retrofitting NGCC power plant systems with SOFCs. SOFC-gas turbine (GT) systems can offer high efficiency power production with methane as fuel[19, 98, 179]. Replacing part of fuel combustion with electrochemical oxidation helps in reducing exergy losses and hence an increase in the net efficiency of the system. These high temperature fuel cells are also capable of internal reforming of carbonaceous fuels like natural gas (mainly methane) thereby offering possibilities for the co-production of hydrogen[35, 36] and clean power. The main advantage of using SOFCs as direct internal reforming (DIR) devices is the efficient use of the excess heat generated in the fuel cell for the endothermic methane steam reforming (MSR) reaction (Eq. 1.4) as described in more detail in Chapter 1 section 1.3.2.1:

#### 4.A.2 Model development - Assumption and description

In order to assess the thermodynamic effects of retrofitting SOFC stacks in NGCC power plants, two ASPEN Plus steady state models have been developed based on the Reference NGCC model described in Chapter 4. A 2 step approach is presented with ASPEN Plus system models to show the thermodynamic effects of retrofitting a NGCC power plant with a DIR-SOFC stack. The first model (DIR-SOFC-GT) demonstrates the effect of retrofitting only the gas turbine cycle with an DIR-SOFC stack while in the second model (DIR-SOFC-CC), a steam cycle is added to the SOFC-GT system to show the influence of retrofitting DIR-SOFCs in combined cycle power plant systems.

#### 4.A.3 Retrofitted DIR-SOFC-GT system

The DIR-SOFC-GT model (as shown in Fig.4.13) has been developed in ASPEN Plus using existing unit operation modules and functions. High pressure natural gas is expanded (NGTURB) to the SOFC operating pressure (about 18 bar). A splitter (NGSPLIT) is then used to split fuel required for the SOFC stack and the remaining is sent to the combustor (COMB). Anode gas recycling is used where the split fraction

for the splitter (ANODSPLI) is fixed based on the desired steam to carbon (S/C) ratio. Anode gas is recycled based on a fixed pressure ratio (=3) between the recycled gas and the fresh fuel.

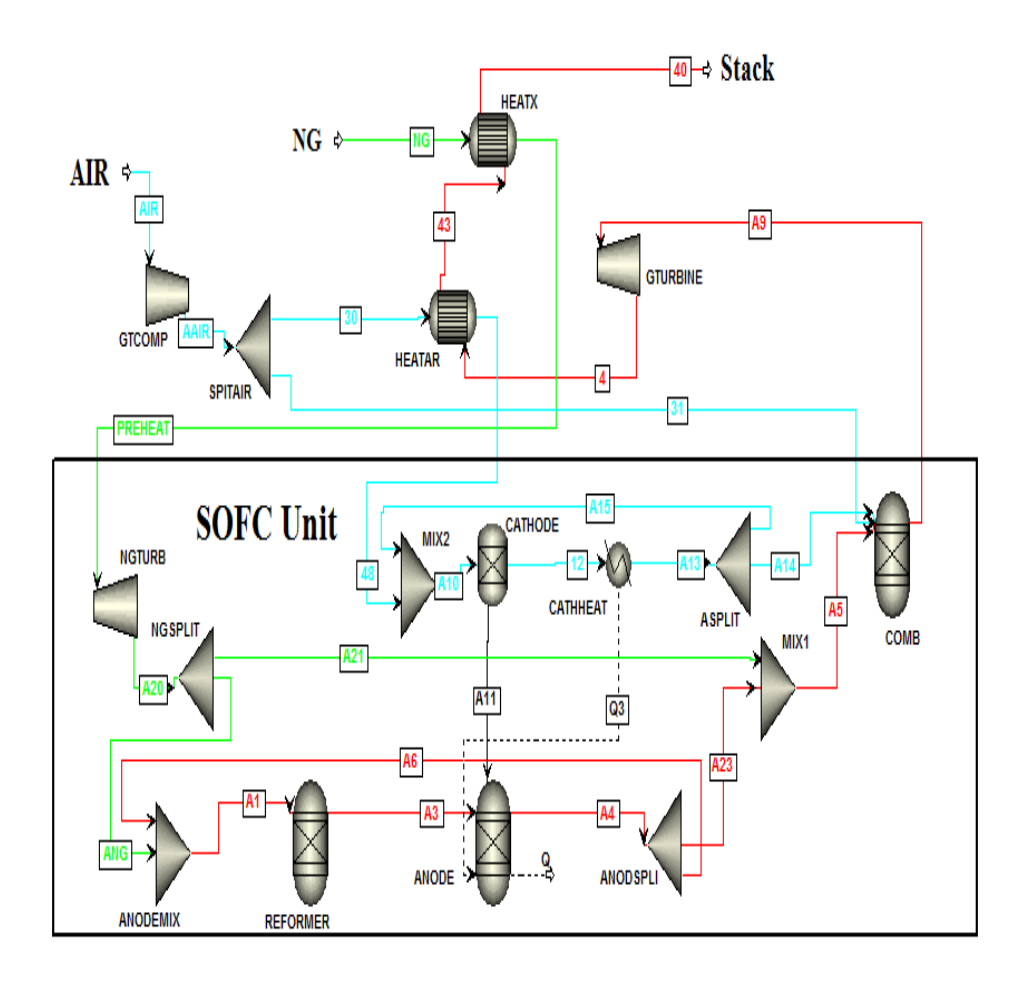


Figure 4.13: ASPEN Plus scheme for the DIR-SOFC system - Green streams represent NG flow, red streams represent syngas/flue gas and blue streams represent air flow

A pre-reformer (REFORMER) is used to convert higher hydrocarbons and reduce carbon formation at the anode. The pre-reformer process in this block has been designed as an adiabatic process. The model is designed on the assumption that only  $H_2$  is electrochemically oxidized and that CO is converted through the shift reaction considered to be at equilibrium.

Also it is assumed that  $CH_4$  in the fuel channel only undergoes reforming (Eq.1.4), subsequently water gas shift (Eq.1.5) but is not electrochemically oxidized. Air for the cathode side is preheated with the exhaust from the gas turbine and further

heated with cathode air recycling (ASPLIT). A separator (CATHODE) is used to provide the required oxygen for the electrochemical reaction (R3). The amount of O2 required is calculated using a calculator block based on the fuel utilization and the equivalent hydrogen flow rate. Heat stream Q3 gives the amount of heat provided to the air by the electrochemical reaction. A combustor (COMB) is used to combust fuel and the remaining H2, CO the fuel (stream 5) with oxygen in the depleted air stream (stream 13). The combustion reactions are specified in the AFTERBRN block. The hot flue gases are then expanded through the gas turbine (GTURBINE).

SOFC parameters including the cell voltage and current have been calculated using a Design-Spec in ASPEN Plus. An iterative procedure is used where the fresh input fuel flow is calculated based on the fixed output power and current density. This determines the split fraction for the splitter (NGSPLIT). The cell voltage is calculated using Eqn.4.21:

$$E = E_{\text{Nernst}} - E_{\text{ohm}} - E_{\text{act}} - E_{\text{conc}}$$
 (4.21)

where E is the actual voltage and  $E_{Nernst}$  is the Nernst potential.  $E_{ohm}$ ,  $E_{act}$  and  $E_{conc}$  are the ohmic, activation and concentration losses respectively.  $E_{ohm}$  has been calculated using equations for the ohmic losses in the anode, cathode, electrolyte and the interconnects[180].  $E_{act}$  includes activation losses both in the anode and cathode[181].  $E_{conc}$  has been obtained based on calculations performed by Campanari et al.[182]. Current output (I) from the stack can then be calculated based on the fixed output power. The equivalent  $H_2$  flow (kmol/hr) is calculated as in Eqn.4.22:

$$n_{H_2,eq} = \frac{I.3600}{2.F.U_f.1000} \tag{4.22}$$

where F is the Faraday constant (C/mol) and  $U_f$  is the fuel utilization factor. The fresh fuel flow is then calculated (Eqn.4.23) by dividing  $n_{H_2,eq}$  with the equivalent carbon composition of the fuel.

$$n_{\text{fuel}} = \frac{n_{H_2,eq}}{(y_{H_2} + y_{CO} + 4.y_{CH_4})} \tag{4.23}$$

y being the molar fraction. The net efficiency is calculated as in Eqn.4.24:

$$\eta_{net} = \frac{P_{out}.\eta_{inv}}{m_{\text{fuel}}.\text{LHV}_{\text{fuel}}} \tag{4.24}$$

 $\eta_{inv}$  is the DC to AC inverter efficiency,  $m_{fuel}$  is the inlet fuel flow rate (kg/hr) and LHV<sub>fuel</sub> is the lower heating value (KJ/kg) of the inlet fuel. Table 4.10 shows the main input parameters for the DIR-SOFC model.

#### 4.A.4 Retrofitted DIR-SOFC-CC system

Integration of a DIR-SOFC stack in an NGCC plant offers an alternative option to replace conventional reforming processes for H2 production. Fig.4.14 shows the ASPEN Plus flowsheet of the DIR-SOFC integrated NGCC system. A steam cycle is

Parameter	Value
Power output (MW)	200
SOFC Temperature (°C)	1000
Pressure (bar)	18.3
DC-AC inverter effic.(%)	92
Fuel utilization factor $(U_f)$	0.7
Current Density (A/m²)	3500
S/C ratio	1.2
Pressure ratio (recycling)	3
Pressure loss	0

Table 4.10: Assumed input parameters for the SOFC model

added to the retrofitted SOFC-GT system described in the previous section. Operating parameters (equipment efficiencies/condensing temperature/pressure) for the cycle have been obtained from the EBTF document[167]. Design-specs have been used to set the mass flow rate of steam and the pump outlet pressure.

#### 4.A.5 Results & Discussion

The results obtained from the simulations for the three system models have been tabulated in Table 4.11. As seen the air flow rate, the GT output power, TIT and TOT are kept same in all the cases. The reference NGCC model gives a net plant efficiency (LHV) of 57.8%. This value seems to be very reasonable in comparison to value reported in literature that range from 55.9% to 58.3%[183, 184]. Power output from the gas turbine is almost twice that from the steam cycle. The net power output from the system is about 413 MW. Process power consumption amounts to 0.68 MW due to the BFW pump. The efficiency reduction is due to the consumption in the GT air compressor which amounts to 276.5 MW.

The retrofitted DIR-SOFC-GT model gives a net efficiency (LHV) of 65.8% with a slightly lower input than the reference case. Addition of steam cycle to the retrofitted GT adds another efficiency point, with a net efficiency of 66.8%. As seen from the table the power output from the steam cycle in the retrofitted case is only about 6 MW. Thus the size of the steam cycle reduces considerably under the set of conditions for retrofitting. This is particularly due to the lower stack temperatures from the SOFC-GT system.

Fuel utilization factor, SOFC power output and current density are important parameters which influence the performance of system. A balance of these input parameters has to be found for a reasonable retrofit. A lower fuel utilization is advantageous as it reduces the fuel flow for combustion and thus an increase in exergetic efficiency. But on the other hand it causes a reduction in the S/C ratio and thus an invalid pre-reformer. Also for a fixed power output, with a lower fuel utilization it becomes a challenge to obtain the heat produced in the cell required for the reforming reaction. The S/C ratio could be maintained with additional steam injection, but the sensitivity of this to the plant will be further investigated in future.

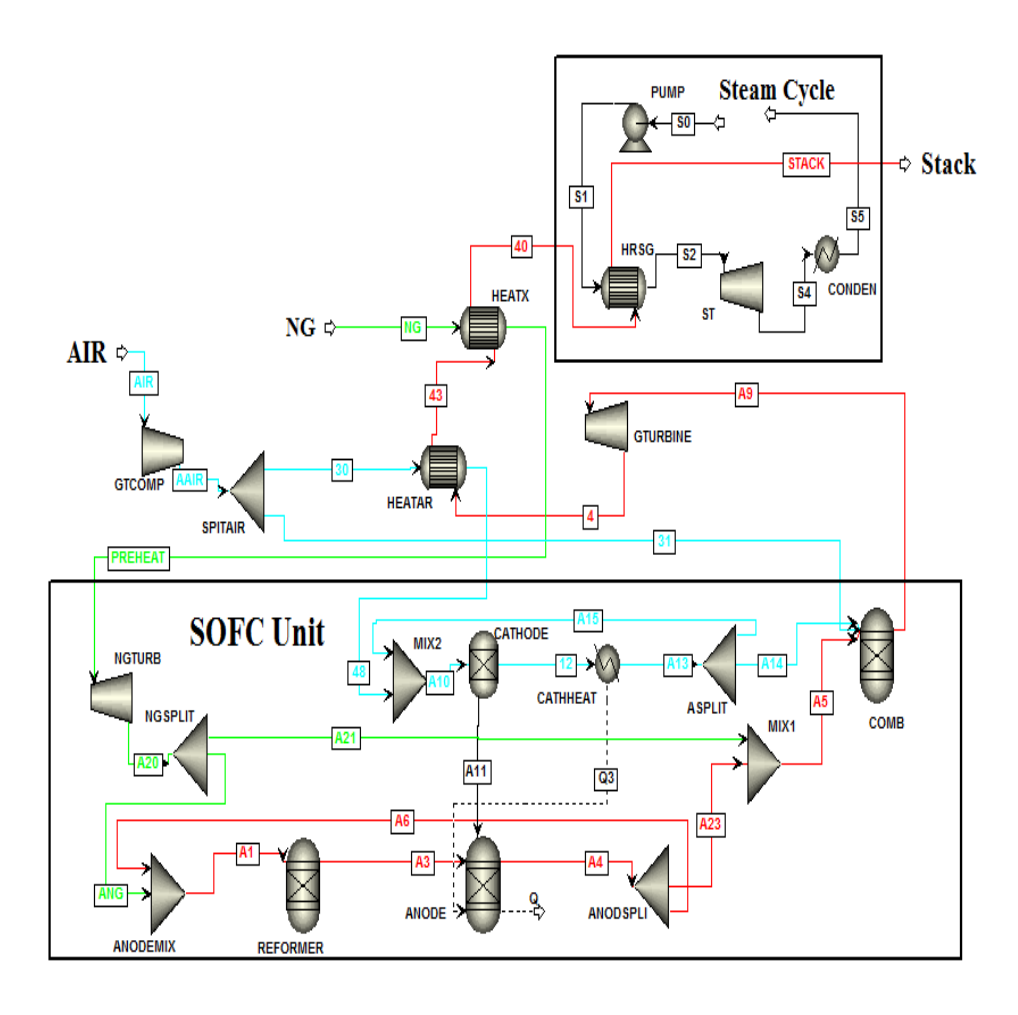


Figure 4.14: ASPEN Plus scheme for the DIR-SOFC-NGCC system - Green streams represent NG flow, red streams represent syngas/flue gas and blue streams represent air flow

A high current density leads to a higher heat generation in the cell and thus affects the fuel and air flow rates (split fraction) to the stack. Based on a number of trial cases, one set of operating conditions were obtained for the fuel utilization, the SOFC power output and current density. The authors do not claim this to be the most optimum set of conditions. Further optimization studies will be carried out in future. The Nernst voltage obtained for the DIR-SOFC was about 0.97 V. Ohmic and activation losses of about 0.29 V and 0.032 V represent most of the voltage losses. Since the current density and fuel utilization factor are high enough, the concentration losses are low. The anode and stack outlet gas composition is shown in Table 4.12. It is seen that bulk of the stack outlet flow is composed of nitrogen. Anode outlet gas composition shows that there is no methane present, ensuring that

Parameter	Reference NGCC	DIR-SOFC-GT	DIR-SOFC-CC
Input (MW)	714	711	711
Net GT Power (MW)	283.5	283.5	283.5
GT Air Compr. (MW)	276.5	276.5	276.5
ST Power (MW)	130	-	6.5
Process Consumption (MW)	0.68	-	0.01
Net Process Power output (MW)	=	1.2	1.2
Turbine Inlet Temperature (°C)	1274.5	1274.5	1274.5
Turbine Outlet temperature (°C)	603	603	603
Voltage (V)	-	0.65	0.65
Current (MA)	-	308	308
Cathode inlet temperature (°C)	-	950	950
Natural gas fraction to SOFC(%)	-	64.5	64.5
Air fraction to SOFC (%)	-	73	73
Net Power Output (MW)	413	468	475
Net Efficiency (%)	57.8	65.8	66.8

Table 4.11: Results - System output parameters

almost all methane is reformed.

%mol	CO	H2	N2	O2	CO2	H2O	AR
Anode Outlet	16.60	23.20	0.20	-	18.00	42.00	-
Stack Outlet	-	-	74.40	12.40	3.90	8.30	0.88

Table 4.12: Composition of outlet gas streams

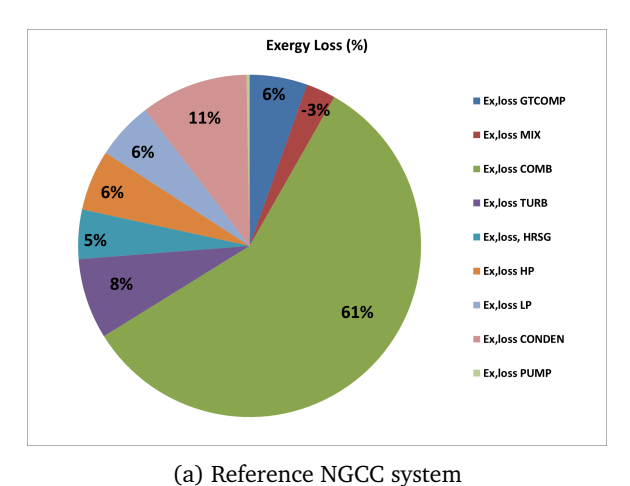
Parameter	Reference NGCC	DIR-SOFC-GT	DIR-SOFC-CC
Exergy Input (MW)	755.50	747.00	747.00
Exergy net output (MW)	326.00	279.00	62.70
Exergy loss (MW)	326.00	279.00	62.70
Exergy efficiency (%)	56.80	62.70	61.00

Table 4.13: Exergy output and exergy efficiency

The DIR-SOFC stack gives a net efficiency (LHV) of about 43.5% as calculated from Eqn 4. Thus it is understood that for retrofitting a SOFC stack with a gas turbine, a compromise needs to made with the SOFC efficiency. A higher fuel utilization will increase the efficiency but as aforementioned, it reduces the exergy efficiency due to a higher loss in the combustor.

#### 4.A.5.1 Exergy analysis

Fig.4.15a and Fig.4.15b show the exergy losses (%) in the reference NGCC and the DIR-SOFC-GT system respectively. A major percentage of exergy is lost in the gas turbine combustor. The SOFC represents a much lower fraction of the exergy



0.3% Exergy Loss (%) 2% \_0.4% ■ ANODE ■ ANODEMIX 0.8% ■ ANODSPLI 11.5% 2% ■ ASPLIT ■ CATHHEAT ■ CATHODE ■ СОМВ ■ GTCOMP ■ GTURBINE ■ HEATAR ■ HEATX MIX1 59% ■ MIX2 ■ NGSPLIT ■ NGTURB ■ REFORMER

(b) DIR-SOFC-GT system

Figure 4.15: Exergy losses in percentage

losses within the system. Table 4.13 shows the exergy efficiency of the three systems considered in this study. It is seen that when the gas turbine is retrofitted with a SOFC stack, the irreversibilities decrease and the exergy efficiency increases. Thus electrochemical conversion is more beneficial than combustion considering exergy losses.

# 4.A.6 Concluding remarks

A preliminary thermodynamic system study is presented on the effect of retrofitting NGCC power plants with DIR-SOFCs. Three models have been presented: a reference case natural gas combined cycle (NGCC) without a SOFC stack, a gas turbine cycle (GT) retrofitted with a direct internal reforming (DIR)-SOFC stack and a third model with an addition of a steam cycle to the DIR-SOFC-GT system. The retrofitted DIR-SOFC-GT model gives a high net efficiency (LHV) of about 66% with the SOFC

stack output of about 200 MW, giving an indication that retrofitting gas turbines is highly advantageous. With a bottoming steam cycle, it is seen that the steam cycle size (power output) reduces considerably with a slight improvement in the net thermal efficiency. It is concluded that retrofitting GT with DIR-SOFCs is more advantageous than retrofitting combined cycle plants. Gas turbine combustion represents the major irreversibility in the system but the exergy efficiency increases (efficiency higher than 60%) with a DIR-SOFC retrofitted system. Thus partial replacement of combustion with electrochemical oxidation using SOFCs helps in reducing exergy losses in the system. Hydrogen co-production and storage from such systems could also be possible, however this needs further investigation.

# Chapter 5

# Methane steam reforming (MSR) kinetics in single operating SOFCs

Solid oxide fuel cells (SOFC) offer multiple advantages in terms of high efficiency and fuel flexibility. However major operating challenges remain due to undesirable temperature gradients and carbon deposition when operated with hydrocarbon fuels. In order to design efficient natural gas (methane) fuelled SOFC units and reliable numerical models, it is crucial to investigate underlying internal reforming kinetics. This chapter presents an experimental study on methane steam reforming (MSR) kinetics on single operating SOFCs with Ni-GDC (Gadolinium doped ceria) anodes with relatively low steam to carbon (S/C) ratios (around 1) and current densities upto 3000 A/m<sup>2</sup>. A first of its kind comparative study has been performed between two kinetic approaches - Power law (PL) and Langmuir-Hinshelwood (LH). Firstly it has been shown that methane reforming on metallic (Ni) current collectors may not be always negligible, contrary to literature reports. The study further confirms previous findings that electrochemical oxidation (current) promotes the MSR reaction rate. Furthermore, steam is seen to have an adverse effect on the reaction rate. The PL and LH kinetic models predict the same net reaction rate, however both approaches predict significantly different rate and species partial pressure distributions along the reactor length. No significant carbon deposition has been observed during the experimental study which has been further confirmed using a SEM-EDX analysis.

**This chapter is submitted for publication**: A. Thallam Thattai, L. van Biert, P. V. Aravind, *On direct internal methane steam reforming kinetics in operating solid oxide fuel cells with nickel-ceria anodes*, **submitted to Journal of Power Sources** 

# 5.1 Background

Among conventional fossil fuels, natural gas is considered a relatively cleaner fuel (lower carbon footprint and emissions)[123] and thus research into the development of novel gas based technologies is important. Furthermore, significant changes in global energy markets make it necessary to develop decentralised, novel, efficient and flexible energy technologies. Fuel cells offer many advantages compared to conventional gas/steam turbine based electricity production in terms of efficiency and flexibility [185]. As aforementioned in Chapter 1 (section 1.3.2), fuel flexible solid oxide fuel cells (SOFCs) are capable of internally converting the chemical energy in hydrocarbon fuels like natural gas, syngas into electricity (and heat) with high efficiencies (upto 60%)[186].

Previous chapters in this dissertation collectively outline the important role pressurized SOFCs can play for highly efficient power production with combined cycle power plant systems. It has also been shown in Appendix 4A that retrofitting natural gas based systems with SOFCs can facilitate highly efficient power production. Such systems can be only developed further with detailed knowledge on intrinsic reactions in the SOFC unit and the associated chemical kinetics. As the first step, it is crucial to study reaction kinetics on operating SOFCs at atmospheric pressure to establish reliable trends. Further kinetic studies should then be carried out with pressurized SOFCs.

The possibility of direct internal methane reforming in SOFCs offers many advantages as it allows us to overcome the need of an external reformer, thereby reducing cost and complexity. A fully integrated SOFC unit also helps to avoid extensive fuel preparation facilities. Internal methane reforming in SOFCs can be carried out either using mainly steam (methane steam reforming or MSR (Eqn. 1.4) and/or CO<sub>2</sub> (dry reforming) as a reforming agent. Steam is still the most commonly used reforming agent, although the use of CO<sub>2</sub> is also being much researched upon in the recent past focussing on biogas as a fuel [37, 187, 188].

Nickel (Ni) based anodes (see Chapter 1 section 1.3.2) have been used very widely in SOFCs as Ni is a well known methane reforming catalyst[189]. However the presence of Ni in the SOFC anode also promotes carbon deposition, which causes rapid cell degradation. The endothermic MSR reaction produces syngas, a mix of CO and H<sub>2</sub>. The produced CO could also react with steam at high temperature via the water gas shift (WGS) reaction (Eqn.1.5) to produce CO<sub>2</sub> and H<sub>2</sub>. The WGS reaction is generally assumed at/near equilibrium; the reaction being much faster than the MSR reaction[30, 190, 191]. The interaction between the slower MSR reaction and exothermic H<sub>2</sub> electrochemical oxidation (Eqn.1.2) is complex and not well understood. The electrochemical reaction(s) is responsible for the flow of electrons thereby producing current, steam, power and heat. One of the major issues with internal steam reforming in SOFCs is the different reaction rate between the MSR reaction and the electrochemical reactions.

Due to the large number of catalytic (Ni) sites available in the porous anode, the MSR reaction is relatively fast [192]. There can be electrochemical  $H_2/CO/CH_4$  oxidation in SOFCs, but  $H_2$  oxidation is seen to be more preferential, particularly on Ni

and ceria based anodes [193]. The MSR reaction is an endothermic reaction, while the WGS reaction is slightly exothermic. Due to the reaction rates and thermodynamics of the MSR and the H<sub>2</sub> electrochemical reaction being different, undesirable temperature gradients arise in the anode leading to cell degradation and reduced performance. However the heat released by the electrochemical reactions in the SOFC helps promote the MSR reaction. The main focus towards optimizing SOFC performance with internal MSR would be reduce these undesirable temperature gradients in the cell/stack.

An important step to reduce these temperature gradients within methane(or natural gas) fuelled SOFC anodes is to improve our understanding on MSR reaction kinetics in operating mode i.e under the influence of current. MSR reaction kinetics on Ni catalysts have been extensively studied experimentally in the past decades by numerous researchers, particularly using test catalytic reactors and catalyst beds [36-42]. Since the last decade, experimental research has also been carried out on MSR kinetics in Ni based SOFC anodes. A comprehensive review on these studies can be found in multiple review articles [41, 123, 194]. There are often large overlaps in the use of MSR reaction rate expressions among industrial catalyst studies and cermet SOFC anode studies. However an important aspect to keep in mind is that, with a cermet anode, the ceramic is generally an oxygen-ion conductor while with industrial catalysts the support material (e.g, alumina) is not. Additionally the porous structure in a cermet anode is not the same as in a catalyst bed. Hence in order to improve and fully understand SOFC performance with internal MSR, researchers have to carry out extensive experimentation with complete SOFC cermets/cells/stacks under operation.

MSR kinetic studies in literature can be broadly differentiated in 3 ways based on the type of reaction rate expression used: power law (PL) expressions, first order (FO) in methane and Langmuir-Hinshelwood (LH) type expressions. The three approaches differ significantly with respect to the their assumptions making the choice for a rate expression quite challenging. The PL approach simplifies the analysis a lot by ignoring the reaction mechanism and elementary steps, the FO approach assumes only a strong dependance of the methane partial pressure while with LH expressions, care has to be taken in formulating the rate expression using appropriate adsorption/desorption parameters.

Table.5.1 shows a summary of the relevant internal MSR kinetic studies (experimental) in literature using Ni based SOFC cermet anodes. The assumed reaction rate expression and its type has been listed with important operating parameters like the cell temperature, steam to carbon ratio and current density. The table clearly shows that the reported kinetic parameters (activation energy  $E_a$ , pre-exponential factor (k), reaction orders) differ significantly and thus it is very challenging to attain consensus. An important aspect to keep in mind is also that it is not appropriate to compare results on a quantitative basis from these studies, as they have been carried out in a varied set of operating conditions, test benches and cell geometries.

Timmermann et al.[204] Achenbach et al.[196] Nakagawa et al.[195] Souentie et al.[199] Belyaev et al.[201] Parsons et al.[197] Ahmed et al.[203] Bebelis et al.[202] Dicks et al.[200] Lee et al.[198] Fan et al.[190] Reference Ni-GDC and Au-Ni-GDC anode Ni-CGO and Ni-YSZ anodes Ni-ZrO2-CeO2 electrode Material/configuration Ni-YSZ-CeO2 anode Ni-YSZ cermet film Ni-ZrO2 cermet Ni-GDC anode Ni-YSZ cermet Ni-YSZ anode Ni-YSZ anode Ni cermet Type of kinetic rate expression Ξ Ξ H FO H FO PL Ы 뇓 FO  $r_{CH_4} = k_0.\exp(-E_a/RT)\left(1 - \frac{p_{CO}p_{H_2}^c}{p_{CH_4}.p_{H_2}o.K_p}\right).p_{CH_4}$  $r_{CH_4} = k_{ad} \cdot p_{CH_4} \cdot \left(1 - \frac{k_{ad}}{k_r \cdot K_{H_2O}}, \frac{p_{H_2} \cdot p_{CH_4}}{p_{H_2O}}\right)$  $r_{CH_4} = k_0 \cdot \exp(-E_a/RT) \cdot p_{CH_4}(p_{H_2O})^{\alpha}$  $r_{CH_4} = k_0 \cdot \exp(-E_a/RT) \cdot p_{CH_4}^{\alpha_{CH_4}} \cdot p_{H_2O}^{\alpha_{H_2O}}$  $r_{CH_4} = k_0 \cdot \exp(-E_a/RT) \cdot p_{CH_4}^n \cdot p_{H_2O}^m$  $r_{CH_4} = k_0 \cdot \exp(-E_a/RT) \cdot p_{CH_4}^{\alpha} \cdot p_{H_2O}^{\beta}$  $r_{CH_4} = \frac{1}{(1+K2.p_{CH_4}+K3.p_{H_2}o)^2}$  $r_{CH_4} =$  $r_{CH_4} = \frac{k_a \cdot p_{CH_4}}{1 + k \cdot (\frac{p_{CH_4}}{P_{H_2O}})}$  $r_{CH_4} = k.(p_{CH_4})^{1.25}$ Rate expression  $r_{CH_4} = k.p_{CH_4}$  $\left(1+K_{H}\cdot p_{H_{2}}^{0.5}+K_{S}\cdot \frac{p_{H_{2}O}}{p_{H_{2}}}\right)$  $K1.K2.K3.p_{CH_4}.p_{H_2}$ range  $^{o}$ C Temperature 800-1000 700-1000 800,950 854-907 700-100C 800-900 800-850 800-900 700-940 700-750 960 S/C ratio 1.5 - 2.450.25,11.4 - 3.00.2 - 102.6-8 2-7.4 0-3 2-4 2-8 1-7 ω density (A/m<sup>2</sup>)Curren 2500 147  $E_a = 26.3 \text{ KJ/mol}, m = 0, n = 1.19$  $k_0 = 4.05e-05 \text{ mol/(s-m}^2-Pa^{1.19})$  $k=2.4 e-3 mol.s^{-1}.atm^{-1.25}$  $E_a = 82 \text{ KJ/mol}$  $k_0 = 4274 \text{ mol/(s-m}^2\text{-bar)}$  $E_a = 96-117 \text{ KJ/mol}$  $\alpha_{CH_4}$ =0.7,  $\alpha_{H_2O}$ =-0.08  $E_a = 63-88 \text{ KJ/mol}$  $k_0 = 21 \text{ mol/(s-cm}^2\text{-bar)}$  $E_a = 135 \text{ KJ/mol}$  $k_a = 15-45e-06$ , k = 0.23Kinetic parameters  $\alpha = -1.25$  $E_a = 98.23 \text{ KJ/mol}$  $\alpha = 0.85, \beta = -0.35$  $E_a = 95 \text{ KJ/mol}$  $E_a$ =230 KJ/mol  $E_a = 163 \text{ KJ/mol}$  $E_a = 18 \text{ KJ/mol}$ 

Table 5.1: Literature summary on MSR reaction kinetics with Ni based cermet anodes

Additionally the approach for experimental data management and analysis (for eg, fitting of parameters, error estimation etc.) varies widely. The table also shows the lack in experimental efforts on MSR kinetics with operating SOFCs i,e under the influence of current. Despite the additional complexity introduced due to current, it is important to obtain experimental data and establish kinetic trends for the MSR reaction in operating SOFCs. Moreover, majority experimental investigations on MSR have been carried out with high steam to carbon (S/C) ratios (>1.5), mostly to prevent carbon deposition. In order to reduce steam consumption while operating SOFCs with methane as fuel, it is important to conduct experiments with lower S/C ratios. Only a few research groups have conducted tests with relatively low S/C ratios (<1.5) as seen from the table.

## 5.2 Motivation

The lack in experimental investigations on internal MSR in operating SOFCs also adversely affects modeling research. SOFC models are helpful tools as they allow us to predict temperature profiles/gradients within the cell/stack and thereby develop optimal operating conditions. Since the last few years extensive modeling efforts have been taken by multiple research groups towards modeling SOFCs with internal MSR. Many types of models (CFD, steady state sytems, cell/stack design concepts, micromodels) have been developed and reported in literature, an elaborate review on which can be found in many articles [41, 123, 192]. Development of reliable SOFC models requires reliable experimental data in terms of kinetic parameters like activation energy, pre-exponential factor and reaction orders. Reaction rate expressions using one of the 3 aforementioned approaches (PL/FO/LH) are fitted for the experimentally obtained methane conversion data with appropriate optimization scripts/subroutines to obtain various kinetic parameters. Despite significant progress in the conceptual formulation of MSR reaction rate expressions using these approaches, there exists a shortage in experimental data on MSR reaction kinetics with operating SOFCs. Additionally a comparison between the kinetic approaches is never reported.

Ceria has been of much interest as an anode material due to its high electrocatalytic activity without additives and its higher resistance to carbon deposition compared with YSZ[31, 179, 193, 205, 206]. The polarisation resistance for  $H_2$  oxidation on ceria is also shown to be lower than Ni based anodes[207]. Furthermore, MSR activation energies with ceria doped anodes are also reported to be lower than Ni-YSZ anodes [196, 202]. Gadolinium doped ceria (GDC) has been of much interest as a SOFC anode material due to its improved performance with direct utilization of methane [31, 205, 208–210]. Ni-GDC cermet anodes have been used to investigate reforming kinetics in the past [190, 199, 211] particularly due to their high electrocatalytic activity, resistance to carbon deposition and relatively higher contaminant (like  $H_2$ S/HCl) tolerance. However, experimental research on MSR kinetics using complete Ni-GDC cermet anodes in operating SOFCs has been rather limited.

This chapter presents an experimental study on internal MSR kinetics in operating SOFCs (Ni-ceria based anodes) with a focus on relatively low S/C ratios (around 1) and moderate current densities (I<sub>c</sub>) upto 3000 A/m<sup>2</sup>. Experiments have been carrried out using a planar electrolyte supported (ESC2) cell with a Ni-GDC anode under varying operating conditions of gas composition, temperatures and current densities. A step by step experimental approach and analysis is presented including equilibrium calculations and reaction metrics. A preliminary experimental investigation on MSR kinetics in operating SOFCs was carried out within our research group [190] in the past using power law rate expression for high S/C ratios (>2) and low current densities (upto 1000 A/m<sup>2</sup>). The focus of this study is to obtain kinetic trends using both power law (PL) and Langmuir-Hinshelwood (LH) rate formulations on much lower inlet steam concentrations (S/C around 1) and higher current densities. For the first time in literature, a comparison has been presented between both approaches for operating SOFCs to assess the effect of using different kinetic approaches. The results presented in this work are helpful towards the development of more detailed kinetic models and to design future experiments.

# 5.3 Experimental

## 5.3.1 Equipment and planar cell description

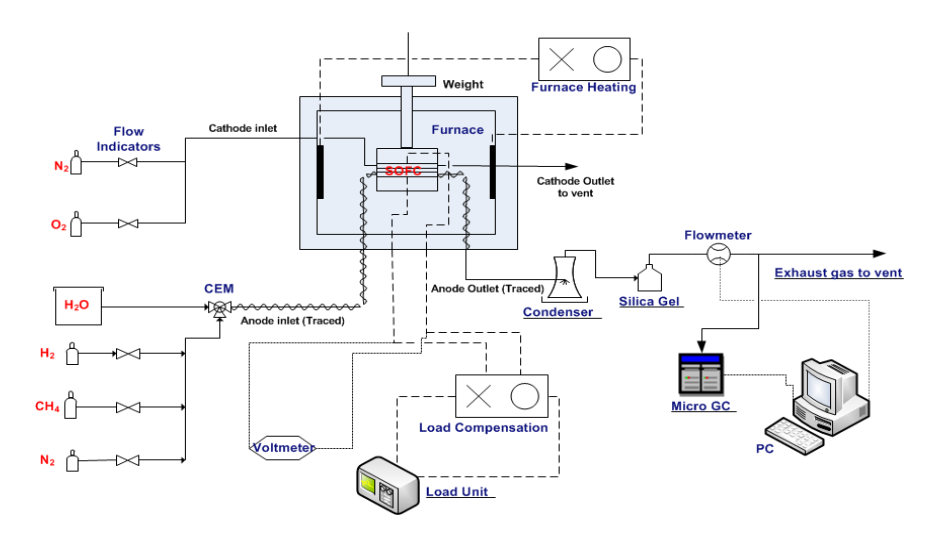


Figure 5.1: Schematic of the experimental test bench

Fig.5.1 shows a schematic of the experimental test bench used in the study. Dry gases ( $CH_4$ ,  $H_2$ ,  $O_2$  and  $N_2$ ) are fed to the SOFC from gas bottles using calibrated mass flow controllers (Bronkhorst EL-Flow Series) and pressure reducers. Steam is added to the dry inlet gas mix using a Bronkhorst controlled evaporator mixer (CEM) where the dry gases are mixed with controlled amount of water vapour. The

anode inlet pipe is heat traced to maintain an inlet gas temperature of 120°C. Hence all calculations including volume flow rates and S/C ratios have been carried out at this temperature. Simulated air (1200 mln/min N<sub>2</sub>, 300 mln/min O<sub>2</sub>) is used at the cathode inlet. The cathode off-gas is directly vented out. In order to calculate methane conversion (x) in the SOFC anode, the anode outlet gas was analyzed using a Agilent 490 micro GC. The micro GC consists of a Molsieve 5A column to measure the flow fraction of H<sub>2</sub>, CH<sub>4</sub>, CO and a Pora Plot U column to measure the concentration of CO<sub>2</sub>. The micro GC output concentrations were normalized to calculate the mole fractions of the various gases. To cool the anode outlet gas and prevent moisture entering the micro GC columns, a water filled bubbling condenser and a dessicant bottle (filled with silica gel) is used before the micro GC. A mass flow meter is then used to measure the total dry anode outlet flow. The system is operated at ambient (atmospheric) pressure. An electronic load unit (Kikusui, PLZ603W), supported with a compensation voltage unit (as power supply) is used for applying current to the cell. The load unit is operated in a constant current mode.

Commercial electrolyte supported cells (ESC2, manufactured by H.C Starck) were used to carry out the experimental investigation. The planar sqaure cell (9x9cm active area) is placed on a square ceramic (alumina) block in a quadratic electrically heated (in presence of nitrogen) furnace which consists of a platinum current collector (or mesh) on the cathode side and a nickel mesh on the anode side. The cell consists of a 35  $\mu m$  thick NiO-GDC (Ni-Gd $_{0.1}$ Ce $_{0.9}$ O $_{1.95}$ ) anode, 100  $\mu m$  YSZ electrolyte and a 40  $\mu m$  LSM (La $_{1-x}$ Sr $_x$ MnO $_{3-\delta}$ ) cathode. The anode consists of about 57% wt NiO. The planar cell is sealed gas tight in the ceramic block using Thermiculite (mica) seals both on the anode (0.3mm thickness) and cathode (0.7mm thickness) sides. Additional weight was added using a ceramic column on top of the block to ensure gas sealing.

# 5.3.2 Experimental methodology and Current-Voltage (I-V) characteristics

The NiO-GDC cell was reduced with a standard procedure at a temperature of 950°C. A high reduction temperature has been used for an improved cell performance in consultation with SOFC manufacturers. The reduction procedure involved a gradual increase in the  $H_2$  feed from a low  $H_2$  concentration of about 2% (vol) to 100% over a period of 4 hours. The cell was first tested for its performance with pure  $H_2$ . The obtained current-voltage (I-V) characteristics are shown in Fig.5.2. The area specific resistance (ASR) on pure  $H_2$  at  $T_{cell} = 950^{\circ}C$  was about 0.79  $\Omega$ -cm². The central aim of this study is to investigate MSR kinetics in operating Ni based SOFCs with lower steam concentrations (S/C around 1.0) at the anode inlet. In order to asses the effect of gas composition, 7 gas mixtures have been defined as shown in Table 5.2. The table gives the inlet gas composition in vol % and also the steam to carbon (S/C) ratio. A, B, C and D represent gas compositions with increasing steam partial pressure while D, E, F and G represent gas compositions with increasing methane partial pressure. The  $N_2$  flow is calculated to add up to a total

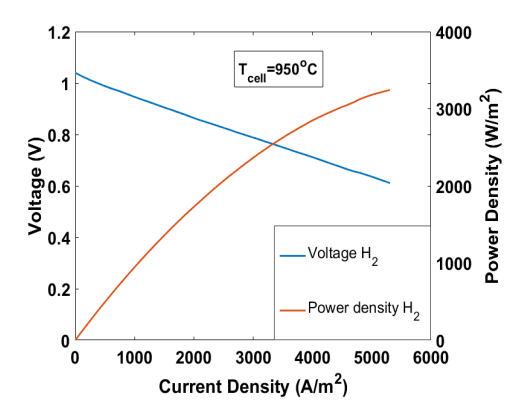


Figure 5.2: I-V characteristics for operation with pure H<sub>2</sub> at  $T_{cell} = 950^{\circ}C$ 

inlet gas flow rate of 1200 mln/min (at  $T=120^{o}C$ ). The high total volumetric flow ensures flooded conditions and hence also results in low fuel utilizations. Minimal amount of  $H_2$  was added to ensure a reducing environment in the anode. The experiments have been carried out at 3 different cell temperatures:  $830^{o}C$ ,  $800^{o}C$  and  $770^{o}C$ . Current imposed on the cell has been varied to obtain methane conversion data for current densities from 0 (open circuit conditions) to  $3000 \text{ A/m}^2$ . Fig.5.3 shows the I-V characteristics obtained using composition A at  $T_{cell} = 830^{o}C$ . The calculated ASR is  $1.61 \Omega$ -cm<sup>2</sup>.

vol %	$\mathbf{CH}_4$	$H_2O$	$\mathbf{H}_2$	$N_2$	S/C
Α	33.00	36.90	3.30	26.80	1.13
В	33.00	39.30	3.30	24.40	1.20
C	33.00	41.80	3.30	21.90	1.28
D	33.00	44.30	3.30	19.40	1.35
E	36.00	44.30	3.30	16.40	1.24
F	38.90	44.30	3.30	13.50	1.15
G	41.80	44.30	3.30	10.60	1.07

Table 5.2: Anode inlet gas compositions for a total flow of 1200 mln/min at 120°C

Starting with the highest temperature, the anode inlet gas compositions were varied sequentially as listed in Table.5.2. For each inlet gas composition, the I-V characteristics and anode outlet gas composition have been obtained. The methane conversion (x) has been calculated based on the outlet gas composition (measured using Agilent 490 micro GC) and a carbon balance [37, 212] using Eqn.5.1:

$$x = \frac{y_{CO} + y_{CO_2}}{y_{CH4} + y_{CO} + y_{CO_2}}$$
 (5.1)

where  $y_i$  denotes the mole fraction of gas species i. An important aspect to keep in mind before measuring the outlet gas composition is to ensure steady state operating conditions. Fig. 5.4 shows the variation in the methane conversion (x) over

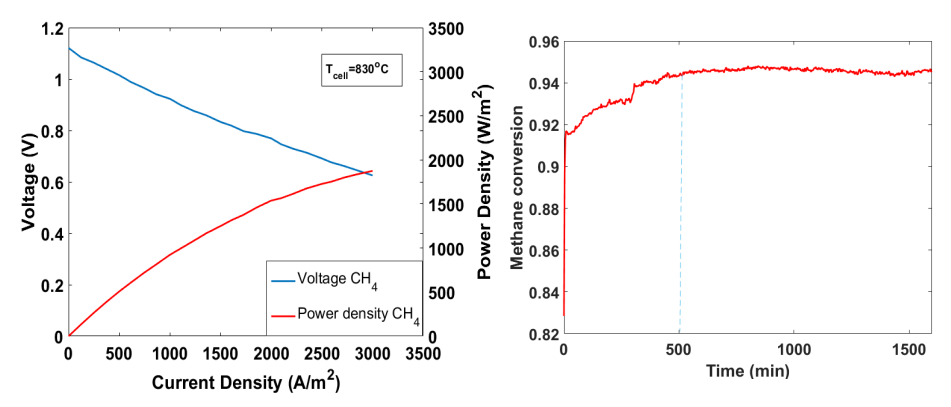


Figure 5.3: I-V characteristics for operation with Composition A at  $T_{cell} = 830^{o}C$ 

Figure 5.4: Variation in methane conversion over time

time (in mins) for composition A at  $T_{cell} = 830^{o}C$ . As it can be seen a steady conversion is obtained only after 8-9 hours. Experimental measurements with all 7 gas compositions have been carried out ensuring steady flow.

# 5.4 Kinetic model and parameter estimation

A kinetic model which calculates kinetic parameters based on the experimental methane conversion (x) is essential to establish trends and further understand the reaction kinetics. This section describes the kinetic model developed in this study using the power law (PL) and Langmuir-Hinshelwood (LH) rate formulation.

# 5.4.1 Ideal plug flow reactor (IPFR) assumption

The MSR reaction rate can be mathematically expressed based on an ideal plug flow reactor (IPFR) assumption. This assumption can be justified due to the relatively small fuel channel dimensions, low gas velocities and low Reyolds number. Such a mathematical formulation is also based on an assumption that there is no pressure drop across the reactor and no catalyst decay. In reality, this is not true particularly with pressurized reactors; however in this experimental work, a significant deviation is not expected due to operation at ambient conditions. The MSR reaction rate ( $r_{CH_4}$ ) across an elemental volume dV can be expressed as in Eqn.5.2:

$$-r_{CH_4} = \frac{dF_{CH_4}}{dV} = \frac{d(F_{CH_4,0}(1-x))}{dV} = -F_{CH_4,0} \cdot \frac{dx}{dV}$$
 (5.2)

where x is the methane conversion,  $F_{CH_4}$  is the methane molar flow rate (mol/s) and  $F_{CH_4,0}$  is the methane molar flow rate (mol/s) at the anode inlet. Integrating over the entire reactor volume V gives the rate equation as shown in Eqn.5.3:

$$\frac{V}{F_{CH_{A},0}} = \int_{0}^{x_{out}} \frac{dx}{-r_{CH_{A}}}$$
 (5.3)

 $x_{out}$  represents the methane conversion at the anode outlet. The MSR reaction rate can also be expressed in terms of the species partial pressures thereby linking important kinetic parameters such as rate constant (k), reaction orders ( $\alpha$ ) and activation energy ( $E_a$ ). The following sections describe the reaction rate equations using the Power law (PL) and Langmuir-Hinshelwood (LH) formulations.

#### 5.4.2 Power law kinetic model

A simplistic approach to quantify MSR reaction kinetics is to formulate the rate equation assuming a single step reaction. With the law of mass action, this essentially leads to a power rate law type rate equation [213] as shown in Eqn.5.4. k is the rate constant which is independent of species concentration, but dependent on other variables that influence the rate. It can be calculated using the Arrhenius equation (Eqn.5.5).  $k_0$  is the pre-exponential factor, R is the universal gas constant and T is the operating temperature in K.

$$-r_{CH_4} = k \cdot p_{CH_4}^{\alpha_{CH_4}} \cdot p_{H_2O}^{\alpha_{H_2O}}$$
 (5.4)

where

$$k = k_0 \cdot exp(\frac{-E_a}{RT}) \tag{5.5}$$

Using Eqn.5.3 and Eqn.5.4, the rate constant k can be calculated per unit volume by evaluating the integral as shown in Eqn.5.6:

$$k = F_{CH_4,0} \cdot \int_0^{x_{out}} \frac{dx}{p_{CH_4}^{\alpha_{CH_4}} \cdot p_{H_2O}^{\alpha_{H_2O}}}$$
 (5.6)

The activation energy  $E_a$  can be obtained from the slope of the Arrhenius plot using Eqn.5.7(based on Eqn.5.5).

$$ln(k) = \frac{-E_a}{R} \cdot \frac{1}{T} + ln(k_0)$$
 (5.7)

In order to estimate kinetic parameters, the species partial pressures  $(p_i)$  need to be expressed as a function of the methane conversion (x). The methane partial pressure can be calculated as shown in Eqn.5.8:

$$p_{CH_4} = f(1-x).P (5.8)$$

f is a factor correlating various gas flows to the methane molar flow  $F_{CH_4,0}$  at anode inlet as defined by Eqn.5.9.

$$f = (\frac{F_{total,0}}{F_{CH_4,0}} + 2x)^{-1}$$
 (5.9)

Here  $F_{total,0}$  is the total molar flow rate at anode inlet and P is the system pressure (atmospheric).

The hydrogen electrochemical reaction (Eqn.1.2 and Eqn.1.1) produces steam and this has to be considered while determining the partial pressure for steam and

hydrogen. For this reason a current to carbon ratio (CC) is defined as shown in Eqn.5.10:

$$CC = \frac{I}{2F \cdot F_{CH_4,0} \cdot x_{out}} \tag{5.10}$$

where I the current in Amperes (A) and F=96485 C/mol is the Faraday constant. The simultaneous occurrence of the WGS reaction (Eqn.1.5) has also to be taken into account to calculate  $p_{CO}$  and  $p_{CO_2}$ . The progress of the WGS reaction can be expressed as  $y = x \cdot x_{CO}$ . y represents the amount of methane that is converted to carbon dioxide. The value of y can be calculated using the equilibrium constant ( $K_{eg,wgs}$ ) for the reaction as shown in Eqn.5.11:

$$K_{eq,wgs} = e^{-\frac{\Delta G_{wgs}^0}{RT}} = \frac{p_{CO_2} \cdot p_{H_2}}{p_{CO} \cdot p_{H_2O}} = \frac{y(HC + x(3 - CC) + y)}{(x - y)(SC - x(1 - CC) - y)}$$
(5.11)

In order to reduce computation time,  $K_{eq,wgs}$  has been calculated based on a temperature fitted equation[214] as shown in Eqn.5.12:

$$K_{eq,wgs} = e^{((4202.5/T) - 3.928)}$$
 (5.12)

The steam and hydrogen partial pressures can then be calculated as shown in Eqn.5.13 and Eqn.5.14:

$$p_{H_2O} = f(SC - x(1 - CC) - y).P (5.13)$$

$$p_{H_2} = f(HC + x(3 - CC) + y).P (5.14)$$

SC and HC represent the steam to carbon and hydrogen to carbon ratio at anode inlet respectively.  $p_{CO}$  and  $p_{CO_2}$  can then be calculated as shown in Eqn.5.15 and Eqn.5.16:

$$p_{CO} = f(x - y).P (5.15)$$

$$p_{CO_2} = f y.P \tag{5.16}$$

# 5.4.3 Langmuir-Hinshelwood (LH) kinetic model

Catalytic reactions like the MSR reaction in reality consist of a sequence of elementary steps. These multiple reaction steps involve the adsorption and desorption of reactants, products and intermediate species on the surface of the catalyst [215]. The classical theory of Langmuir helps in formulating a rate equation (called the Langmuir-Hinshelwood rate equation) taking into account adsorption/desorption on catalyst surfaces. The rate formulation is based on an assumption that all species are chemisorbed and accomodated on the surface before any reaction. Furthermore, a monolayer coverage is assumed. A general rate equation for reactions catalyzed by solids accounting for chemisorption can be written as a combination of 3 groups as shown in Eqn5.17 [213, 216]:

$$r = \frac{\text{(kinetic factor)(driving force)}}{\text{(adsorption term)}}$$
 (5.17)

The driving force (df) gives information on the reaction equilibrium. For the MSR reaction, the driving force term (df) has been calculated for the various gas compositions and temperatures using Eqn. 5.18 assuming a surface reaction [213]:

$$df = 1 - \frac{p_{CO} \cdot p_{H_2}^3}{K_{eq,msr} \cdot p_{CH_4} \cdot p_{H_2O}}$$
 (5.18)

 $K_{eq,msr} = e^{-\frac{\Delta G_{msr}^0}{RT}}$  represents the equilibrium constant for the MSR reaction. In order to reduce computation time,  $K_{eq,msr}$  has been calculated based on a temperature fitted equation[214] as shown in Eqn.5.19:

$$K_{eq,msr} = e^{((-27070/T) + 30.032)}$$
 (5.19)

The Langmuir-Hinshelwood rate equation including the kinetic factor(k) and the adsorption term (denominator) can be written as shown in Eqn.5.20[213, 217]:

$$r_{CH_4} = k.p_{CH_4}.\frac{p_{H_2O}^a}{p_{H_2}^b}.\frac{\mathrm{df}}{(1 + K_{H_2O}\frac{p_{H_2O}}{p_{H_2}} + K_{CH_4}.p_{CH_4})^2}$$
(5.20)

Xu et al.[36] have carried out comprehensive work on intrinsic MSR reaction kinetics with Ni/MgAl<sub>2</sub>O<sub>4</sub> catalyst using LH rate expressions derived on the basis of a reaction scheme and rate determining step. They have formulated the rate expression on the hypothesis of dominant methane adsorption in line with many other literature studies [36, 198, 201]. The same presumption is also applied in this work in formulating Eqn.5.20. Furthermore, since a detailed reaction mechanism and rate determining step has not been determined in this work, a general rate equation has been formulated with respect to the steam and hydrogen partial pressure. Hence exponents a and b for the steam and hydrogen partial pressures respectively. are optimally calculated in the kinetic model. A similar rate formulation has been previously utilized in the past to investigate MSR kinetics on a Ni-alumina catalyst [39]. The LH rate equation used in this work thus differs from that postulated in the work of Xu et al.[36] particularly with respect to the variable effect of steam and hydrogen partial pressure  $(p_{H_2O}, p_{H_2})$  on the reaction rate.  $K_{CH_4}$  and  $K_{H_2O}$  are the adsorption rate constants for methane and steam respectively. These adsorption rate constants can be estimated using an Arrhenius type equation as shown in Eqn.5.21 and Eqn.5.22:

$$K_{CH_4} = A_{CH_4} \cdot exp(\frac{-\Delta H_{CH_4}}{RT})$$
 (5.21)

$$K_{H_2O} = A_{H_2O} \cdot exp(\frac{-\Delta H_{H_2O}}{RT})$$
 (5.22)

where  $A_{CH_4}$  and  $A_{H_2O}$  are the pre-exponential factors,  $\Delta H_{CH_4}$  and  $\Delta H_{H_2O}$  are the adsorption enthalpies for methane and steam respectively. The adsorption enthalpies obtained by Xu et al.[36] ( $\Delta H_{CH_4}$  = -38.28 kJ/mol,  $\Delta H_{H_2O}$  = 88.68 kJ/mol) have

Temperature(°C)	$K_{CH_4}$	$K_{H_2O}$	$A_{CH_4}$
830	0.4355	0.6415	0.0067
800	0.2173	0.2000	0.0003
770	0.3217	0.1301	0.0039

Table 5.3: Adsorption parameters for the LH kinetic model

been utilized to calculate the adsorption rate constants. Table.5.3 shows the calculated adsorption parameters for the LH kinetic model. The validity of the methane adsorption constants has been evaluated on the basis of a few thermodynamic criteria/guideline[36, 38, 218] that are helpful to evaluate if the adsorption parameters are consistent and thermodynamically meaningful.

- 1. Adsorption is exothermic i,e  $-\Delta H_{CH_4} > 0$ . A negative methane adsorption enthalpy means that this rule is satisfied.
- 2. Decrease in entropy after adsorption. i,e  $0 < -\Delta S_{CH_4} < S_{g,CH_4}^0$  or  $\exp((-S_{g,CH_4}^0)/R) < A_{CH_4} < 1$ .  $S_{g,CH_4}^0$  represents the standard methane entropy which has a value of 186.1 J/(mol.K). Evaluation of  $\exp((-S_{g,CH_4}^0)/R)$  and Table.5.3 show that this rule is satisfied.
- 3.  $ln(A_{CH_4}) \le (12.2 0.0014.\Delta H_{CH_4})/R$ . Table.5.4 shows that this rule is also satisfied.

Temperature(°C)	$ln(A_{CH_4})$	$(12.2 - 0.0014.\Delta H_{CH_4})/R$
830	-5.00	1.47
800	-5.81	1.47
770	-5.54	1.47

Table 5.4: Table showing that the calculated methane adsorption constants satisfy thermodynamic criteria 3

4. The absolute values of entropy change( $\Delta S_{CH_4} = -ln(A_{CH_4}).R$ ) in this case are 41.61 J/mol.K, 48.29 J/mol.K, 46.11 J/mol.k for the three temperatures (830°C, 800°C, 770°C) respectively. Usually this value should be higher than 42 J/mol.K and thus this rule is also satisfied (except for the higher temperature).

Using Eqn.5.3 and Eqn.5.20, the rate constant k can be calculated per unit volume by evaluating the integral as shown in Eqn.5.23:

$$k = F_{CH_4,0} \cdot \int_0^{x_{out}} \frac{dx}{p_{CH_4} \cdot \frac{p_{H_2O}^a}{p_{H_2}^b} \cdot \frac{df}{\left(1 + K_{CH_4} \cdot p_{CH_4} + K_{H_2O} \cdot \frac{p_{H_2O}}{p_{H_2}}\right)^2}}$$
(5.23)

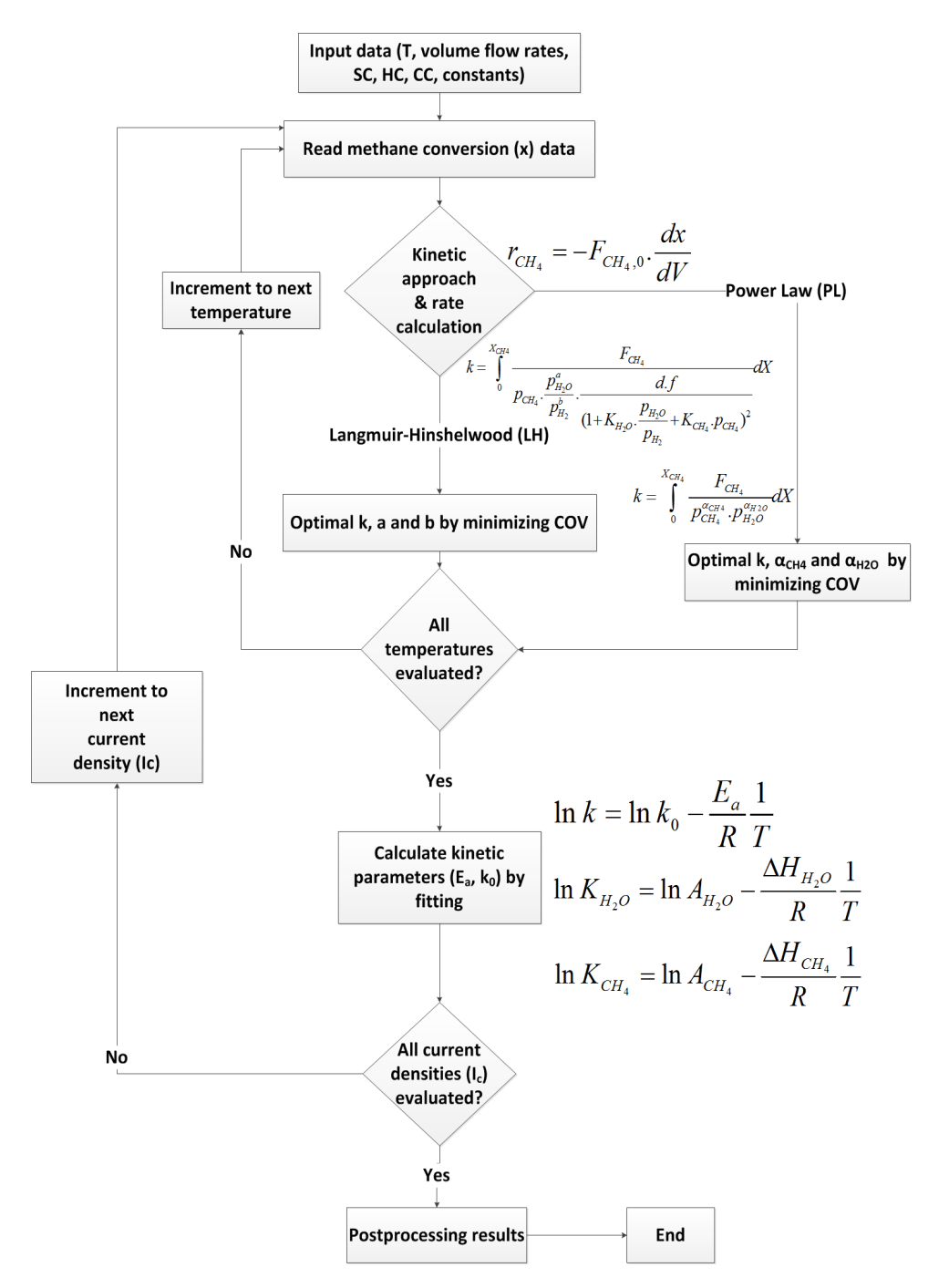


Figure 5.5: Flowsheet indicating the approach for data fitting to obtain kinetic parameters

Whether the rate formulation is of PL or LH type, calculation of the rate constant/kinetic factor k requires optimization, since k should be independant of the composition (as stated in section 5.4.2). For the power law case, the reaction orders  $\alpha_{CH_4}$  and  $\alpha_{H_2O}$  are calculated for the minimum deviation in the value of k. The coefficient of variation (COV) (defined as the ratio of standard deviation to the mean) has been used as the parameter to be minimized. For the LH case, the exponents a and b for steam and hydrogen respectively are determined for the minimum COV in the value of k defined by Eqn.5.23. Activation energy for the LH rate expression is calculated using the Arrhenius plot (Eqn.5.7). A MATLAB script (Appendix) has been developed to estimate the MSR reaction rate and kinetic parameters for both PL and LH rate formulations. Fig.5.5 shows a flowsheet indicating the main logic of this script.

## 5.5 Results & Discussion

A step-by-step investigation on intrinsic MSR kinetics has been carried out in this work to obtain reliable kinetic trends. As the first investigation, preliminary results have been presented for methane reforming on the Ni current collector. The following subsections describe the main results obtained using the PL and LH kinetic models and a comparison between MSR kinetics using both approaches. As the last subsection, results based on equilibrium calculations have been presented to investigate carbon deposition.

## 5.5.1 Methane reforming on Ni current collector (mesh)

Experimental studies on MSR kinetics using SOFC cermet anodes (Table.5.1) in literature often do not report the effects of methane reforming on the current collector (mesh) itself. The mesh used is usually metallic (like Ni/Pt) which also is a good reforming catalyst. No study has been found in literature which tries to adequately quantify the extent of reforming on the Ni/Pt mesh. In the investigation reported by Souentie et al.[199], the authors have mentioned an insignificant catalytic rate, however no clear quantification was reported. In order to check the extent of the MSR reaction on the Ni-mesh and in the ceramic (alumina) block (in the absence of catalyst), a preliminary experimental test was carried out in this work. The test was carried out using an anode inlet gas composition of 33% vol  $CH_4$ , 37%  $H_2O$  and 30%  $N_2$  and a total volumetric flow rate of 1200 mln/min for two cell temperatures of  $900^{\circ}C$  and  $800^{\circ}C$ . Table.5.5 shows methane conversion obtained with

	Cell Temperature				
	900.00 800.00				
Ni-Mesh	0.20	0.10			
Ceramic block	0.02	0.01			

Table 5.5: Methane conversion(x) on Ni current collector and ceramic block/pipes at 800°C and 900°C

and without (ceramic block and pipes) the Ni mesh. As shown, methane conversion with only the ceramic block (without a Ni-mesh) is rather low and negligible. For the case with the Ni-mesh, it is seen that methane conversion is still relatively high (10%) and not completely negligible, particularly at higher temperatures. The results reported in this work therefore indicate MSR kinetics on the combined SOFC anode and Ni-current collector (mesh).

The test carried out in this work was with a high (flooded condition) inlet volumetric flow rate. The total volumetric flow rate is an important parameter for this investigation as it directly affects the gas residence time (defined as the ratio of reactor volume and the total volumteric flow rate). For lower volumetric flow rates i,e higher residence time it is expected that methane conversion will be higher. This is an important consideration particularly for kinetic studies at high SOFC fuel utilizations. Additional experiments need to be carried out to verify this and establish more quantitatively the extent of methane conversion on the Ni-mesh; however this study clearly indicates that methane steam reforming on the metallic current collector may not be always negligible (except for low operating temperatures) and must be considered in SOFC kinetic studies. The following sections describe the results obtained using PL and LH formulations following with a brief section on carbon deposition.

#### 5.5.2 Power law (PL) kinetics

Table.5.6 lists the experimental methane conversion (Eqn.5.1) at 3 different cell temperatures and 7 inlet gas compositions(see Table.5.2). The kinetic study using the PL formulation has been performed by analyzing various paramters like MSR reaction rate (at various operating temperatures, inlet gas compositions and current densities), reaction orders and the activation energy. Fig.5.6 shows the MSR reaction rate distribution using the PL rate equation (Eqn.5.4) along the normalized channel length at various operating temperatures under open circuit (IcO) conditions for composition D. The rate constant normalized reactor length has been calculated on the basis of methane conversion (x) and the maximum rate constant k. The MSR reaction rate increases with increasing operating temperatures, verifying previous studies in literature[39, 190, 199]. The plot further indicates a decreasing reaction rate along the fuel channel with  $p_{CH_4}$  highest at the inlet and decreasing along the channel (See Fig.5.9).

Fig.5.9. shows a sharp increase in the hydrogen partial pressure ( $p_{H_2}$ ) and a gradual increase in CO partial pressure ( $p_{CO}$ ) along the reactor length, despite a decrease in the MSR reaction rate. Under open circuit conditions, bulk of the produced hydrogen (also produced with the WGS reaction) remains unconverted and furthermore the WGS reaction is assumed to reach equilibrium relatively fast. This results in an sharp increase in hydrogen concentration and a gradual increase in CO concentration along the reactor length. Fig.5.7 shows the variation in the MSR reaction rate at  $T_{cell} = 800^{\circ}C$  with varying inlet gas compositions ( $p_{CH_4}$ ,  $p_{H_2O}$ ) as listed in Table.5.2. The plot indicates a relatively strong positive influence of the methane partial pressure  $p_{CH_4}$  on the reaction rate (compositions D, E, F and G). This ob-

Temperature (°C)	$I_c$ (A/m <sup>2</sup> )	Anode inlet composition						
		Α	В	С	D	Е	F	G
	0	0.947	0.946	0.958	0.952	0.969	0.942	0.892
	500	0.977	0.955	0.956	0.955	0.980	0.965	0.934
	1000	0.986	0.961	0.961	0.959	0.985	0.975	0.969
830	1500	0.990	0.964	0.963	0.961	0.988	0.980	0.978
	2000	0.992	0.967	0.966	0.963	0.990	0.983	0.985
	2500	0.994	0.969	0.967	0.965	0.991	0.985	0.987
	3000	0.995	0.972	0.970	0.968	0.992	0.987	0.990
	0	0.903	0.930	0.937	0.929	0.895	0.887	0.825
	500	0.945	0.948	0.945	0.934	0.902	0.903	0.877
	1000	0.960	0.957	0.951	0.938	0.910	0.915	0.913
800	1500	0.968	0.963	0.955	0.941	0.915	0.923	0.930
	2000	0.973	0.967	0.959	0.943	0.920	0.929	0.942
	2500	0.977	0.971	0.961	0.945	0.907	0.935	0.951
	3000	0.980	0.974	0.964	0.949	0.925	0.940	0.956
	0	0.797	0.843	0.856	0.851	0.806	0.647	0.619
	500	0.856	0.869	0.863	0.861	0.814	0.655	0.636
	1000	0.902	0.887	0.871	0.868	0.824	0.658	0.658
770	1500	0.914	0.897	0.877	0.873	0.833	0.678	0.684
	2000	0.928	0.905	0.884	0.878	0.840	0.687	0.708
	2500	0.937	0.914	0.891	0.886	0.850	0.700	0.725
	3000	0.943	0.920	0.900	0.893	0.859	0.707	0.743

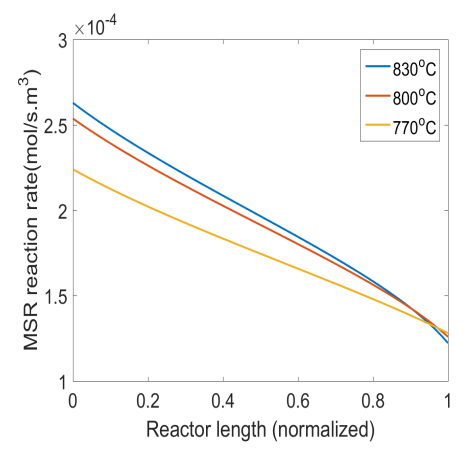
Table 5.6: Experimental methane conversion (x)

servation additionally verifies the similar trend reported in literature [39, 190, 195, 196, 200]. Furthermore it is also seen that the reaction rate is more strongly dependent on variation in  $p_{CH_4}$  (D, E, F, G) than the variation in  $p_{H_2O}$  (A, B, C, D). Under open circuit conditions, steam has a mixed effect (positive influence when A and B are compared, negative influence when B, C and D are compared) on the MSR reaction rate. However it can be seen that the rate is fairly independant of the steam partial pressure ( $p_{H_2O}$ ) under the investigated range of operating conditions, confirming previous reports [195, 196].

#### 5.5.2.1 Role of electrochemical oxidation

Under the influence of current, part of hydrogen produced via the MSR and WGS reaction is electrochemically oxidized to produce  $H_2O$  (see Eqn.1.1 and Eqn.1.2). Fig.5.8 shows the variation in the MSR reaction rate along the channel length at open circuit (IcO) and varying current densities of 500 A/m², 2000 A/m² and 3000 A/m². The plot indicates an increase in the MSR rate, although the increase is relatively marginal. The reaction rate is seen to increase slightly (<2%) with increasing current densities. A slight increase in the outlet methane conversion (x) with increasing current densities as shown in Table.5.6 additionally verifies this trend.

Comparison between the species partial pressure at open circuit (Ic0) conditions and under load (at 3000  $A/m^2$ ) is also shown in Fig.5.9. The marginal increase

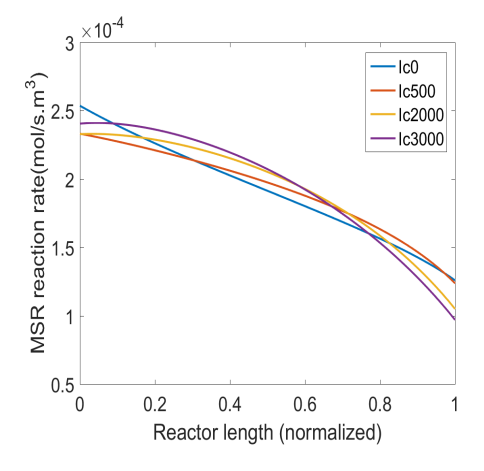


3 ×10<sup>-4</sup>

Reactor length (normalized)

Figure 5.6: PL MSR reaction rate at various operating temperatures for open circuit (Ic0) condition and composition D

Figure 5.7: PL MSR reaction rate at various anode inlet gas compositions for open circuit (Ic0) condition and  $T_{cell} = 800^{o}C$ 



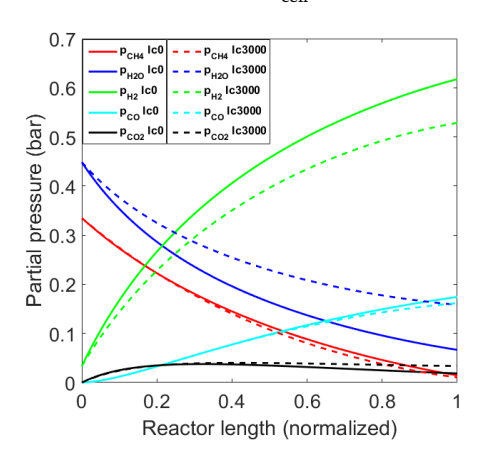
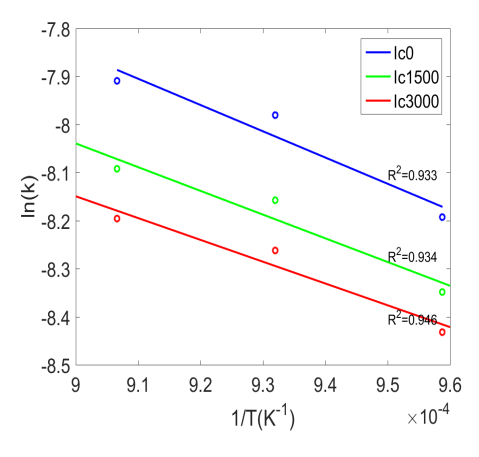


Figure 5.8: PL MSR reaction rate at various current densities for  $T_{\rm cell} = 800^{o} C$  and composition D

Figure 5.9: PL species partial pressure (bar) for open circuit (Ic0) and Ic=3000 A/m² and  $T_{cell} = 800^{o}C$  and composition D

in the MSR reaction rate is also reflected in the methane partial pressure distribution. A slight reduction in  $p_{CH_4}$  is observed with current. The plot also shows a significant decrease in  $p_{H_2}$  and a significant increase in  $p_{H_2O}$  under load due to electrochemical oxidation. Fig.5.10 shows the Arrhenius plots for various current densities and the linear fit (see Eqn.5.7) used to calculate the activation energy ( $E_a$ ) and pre-exponential factor ( $E_a$ ). The plot indicates a decreasing rate constant  $E_a$  with increasing current densities in agreement with previous studies [190].

Fig.5.11 shows the variation in the methane and steam reaction orders ( $\alpha_{CH_4}$  and  $\alpha_{H_2O}$ ) with varying current density. Under the influence of current,  $\alpha_{CH_4}$  is positive and  $\alpha_{H_2O}$  is negative. A positive methane reaction order and a negative steam



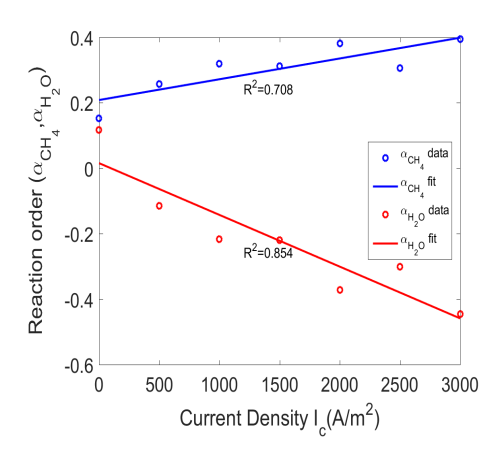


Figure 5.10: Arrhenius plots with PL rate formulation at various current densities and  $T_{cell} = 830^{\circ}C$ 

Figure 5.11: Variation in  $\alpha_{CH_4}$  and  $\alpha_{H_2O}$  with current density

reaction order is also in agreement with previous findings in literature[190, 203]. With increasing current density, it is also seen that  $\alpha_{CH_4}$  increases while  $\alpha_{H_2O}$  decreases. The strong decrease in  $\alpha_{H_2O}$  at higher current densities is thought to be due to the higher steam concentration in the anode due to electrochemical oxidation. A more rapid decrease in the steam reaction order compared to the methane reaction order with increasing current densities also indicates the significant difference in the reaction rate between MSR (Eqn.1.4) and  $H_2$  electrochemical oxidation (Eqn.1.1 and Eqn.1.2). The next subsection describes the results obtained with the Langmuir-Hinshelwood (LH) kinetic model.

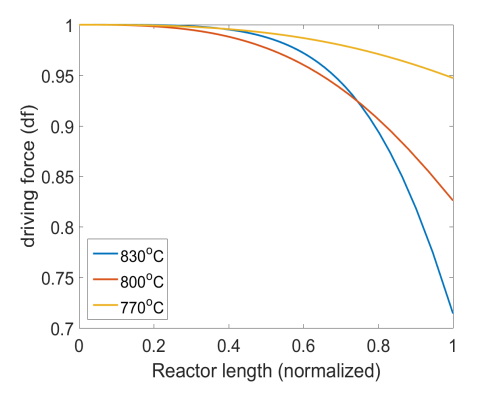
# 5.5.3 Langmuir-Hinshewood kinetics

In order to assess MSR kinetics with operating SOFCs, it is of utmost importance to first assess equilibrium conditions using the inlet gas compositions (Table.5.2). As aforementioned in section 5.4.3, the driving force (df) term (see Eqn.5.18) gives an indication of the reaction equilibrium. df should in principle be zero at conditions of equilibrium ensuring a zero reaction rate.

#### 5.5.3.1 MSR reaction equilibrium

$T_{cell}$ (°C)	$K_{eq,msr}$	$K_{eq,wgs}$
830	242.21	0.89
800	121.95	0.99
770	59.02	1.10

Table 5.7: Equilibrium constants for the MSR and WGS reaction



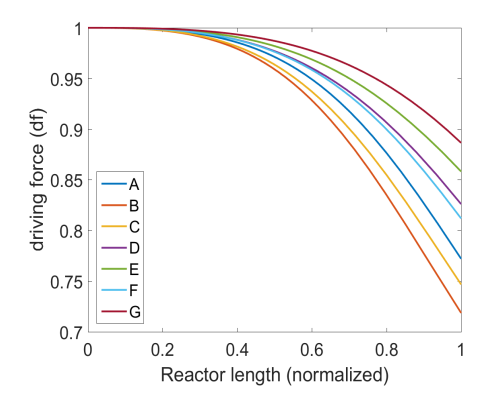


Figure 5.12: Driving force (df) at various cell temperatures for composition D and open circuit (Ic0) condition - df increases with decreasing cell temperature

Figure 5.13: Driving force at T<sub>cell</sub>=800°C for various gas compositions and open circuit (Ic0) condition

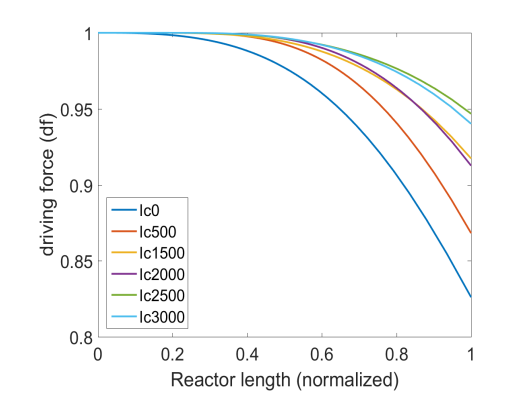


Figure 5.14: Driving force at various current densities for composition D and  $T_{cell}$  =800°C

Table.5.7 lists the values for the equilibrium constant for the MSR ( $K_{eq,msr}$ ) and WGS reaction ( $K_{eq,wgs}$ ) which have been used to calculate df. Fig.5.12, Fig.5.13 and Fig.5.14 show the driving force distribution along the normalized reactor (channel) length for varying operating temperatures (at open circuit (IcO) conditions and composition D), varying gas compositions(at  $T_{cell}=800^{\circ}C$  and open circuit (IcO) condition) and varying current densities (at  $T_{cell}=800^{\circ}C$  and composition D) respectively. The plots indicate a high driving force near the inlet as the methane and steam partial pressure is highest near the inlet. The driving force decreases along the channel length due to the difference in species partial pressures ( $p_{CH_4}$ ,  $p_{H_2O}$ ,  $p_{CO}$ ,  $p_{H_2}$ ), indicating that conditions near the anode outlet are closer to equilibrium. With a reduction in the cell temperature, df increases principally due to a lower  $K_{eq,msr}$  and differences in the species partial pressures. Under the influence

of current (Fig.5.14), it is seen that df increases along the channel when compared to open circuit (Ic0) conditions. This can be explained based on the fact that part of the produced hydrogen with the MSR reaction is consumed under the influence of current facilitating a higher driving force for the forward MSR reaction to occur.

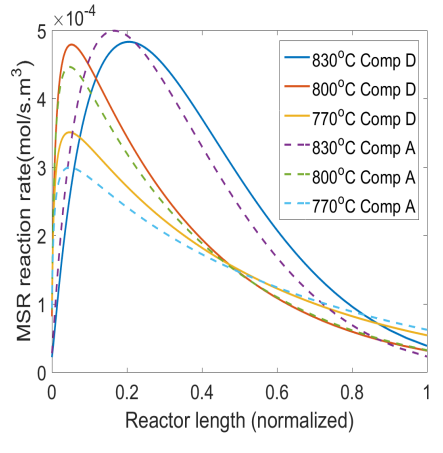
# 5.5.3.2 Influence of temperature and inlet gas composition on MSR reaction rate

Fig. 5.15 shows the MSR reaction rate distribution along the normalized channel length at various operating temperatures for open circuit (Ic0) conditions and composition D. In addition, rate distributions are also shown for open circuit (Ic0) conditions and composition A (dashed curves). The plot indicates that MSR reaction rate increases with increasing operating temperatures. The reaction rate is maximum near the fuel inlet which is also in agreement with the PL prediction (see Fig. 5.6). Fig. 5.18 indicates a subsequently decreasing methane partial pressure  $p_{CH_4}$  distribution along the reactor length. Fig. 5.16 shows the variation in the MSR reaction rate at  $T_{cell} = 800^{o}C$  and open circuit (Ic0) condition with varying inlet gas compositions. The plot clearly reconfirms the dominant role of inlet methane partial pressure  $p_{CH_4}$  (composition D, E, F and G) compared to the steam partial pressure.

#### 5.5.3.3 Role of electrochemical oxidation

Fig. 5.17 shows the LH MSR reaction rate distribution along the normalized channel length at open circuit (Ic0) and current densities of 500 Å/m² and 3000 Å/m². The MSR reaction rate is seen to increase rapidly near the anode inlet (higher methane partial pressure) and reach a maximum near the inlet. Thereupon, the reaction rate decreases along the reactor length. When the cell is operated on current, multiple processes occur within the anode which lead to a shift in the reaction rate maxima and a more gradual increase in the MSR reaction rate compared to open circuit (IcO) conditions. Due to electrochemical hydrogen oxidation (Eqn. 1.2), additional steam is produced increasing the partial pressure of steam, thereby lowering the MSR reaction rate[39, 190]. Additionally there exists an effect of the cell temperature. Considering the combined interaction and different rates between the endothermic MSR reaction (Eqn.1.4) and exothermic H<sub>2</sub> oxidation reaction (Eqn.1.2), the cell temperature is expected to vary under the influence of current. This temperature change has a direct influence on the MSR reaction rate. Thus, despite a net increase in MSR reaction rate under the influence of current, the local reaction rate is seen to increase more gradually under the influence of current. The effect of this is also visible in the species partial pressure distribution in Fig.5.18 wherein the partial pressure of each specie varies more rapidly near the inlet under open circuit (IcO) conditions.

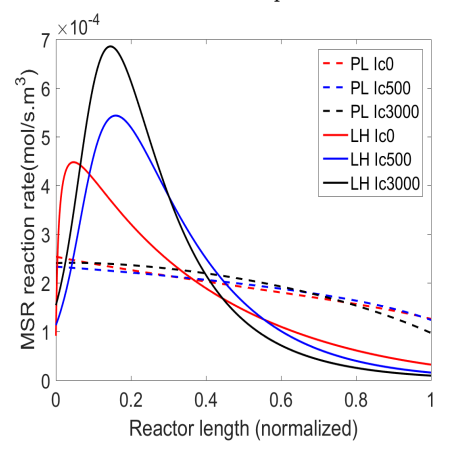
Fig.5.17 also shows a comparison between the MSR reaction rates between PL and LH approaches. The plot clearly indicates a significant difference in the reaction rate distribution with both approaches. The LH rate expression predicts a much higher reaction rate, particularly near the channel inlet and a lower rate near



×10<sup>-4</sup> 6 ٠Δ MSR reaction rate(mol/s.m<sup>3</sup>) В C D Ε G 2 0 0 0.2 0.6 0.8 Reactor length (normalized)

Figure 5.15: LH MSR reaction rate at various operating temperatures for open circuit (Ic0) condition and composition D

Figure 5.16: LH MSR reaction rate at various anode inlet gas compositions for open circuit (Ic0) condition and  $T_{\rm cell}$  = 800°C



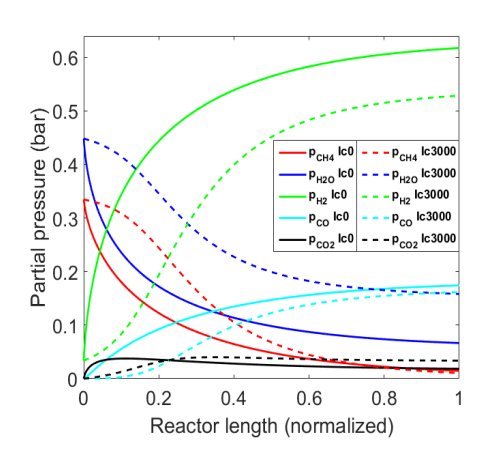


Figure 5.17: LH MSR reaction rate at various current densities for  $T_{\rm cell}$  =  $800^o$ C and composition D. For comparison, the PL MSR reaction rate is also shown.

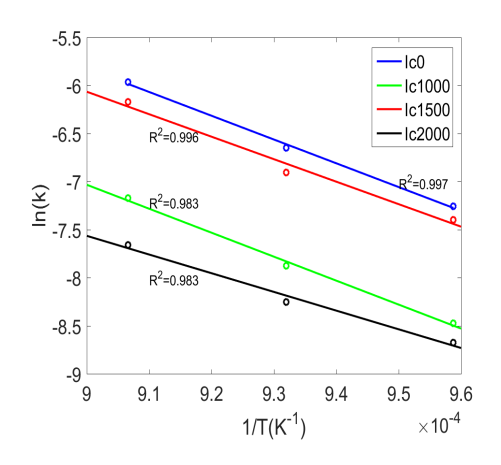
Figure 5.18: LH species partial pressure (bar) for open circuit (IcO) and Ic=3000 A/m² and T<sub>cell</sub>=800°C and composition D

the outlet. The net reaction rate (obtained by calculating the area under the rate curve) for the PL and LH case at open circuit (IcO), T<sub>cell</sub>=800°C and composition D is 1.91e-04 mol/s.m³ and 1.90e-04 mol/s.m³ respectively. This means that both the approches predict the same net reaction rate but different rate distributions. Comparison between Fig.5.9 and Fig.5.18 also clearly shows that the species partial pressure change more rapidly in the LH case near the inlet compared to the PL case. The rate and species distribution are important considerations while predicting temperature gradients along the anode both with experiments and modelling. The fact that different kinetic approaches result in different rate and species dis-

tribution along the channel length is an important aspect to be kept in mind to accurately predict temperature gradients in SOFC anodes.

Ic (A/m <sup>2</sup> )	a	b
0	0.007	1.210
500	-0.373	-0.033
1000	-0.610	1.339
1500	-0.555	0.271
2000	-1.117	0.583
2500	-0.596	0.014
3000	-0.843	-0.022

Table 5.8: Calculated values of exponents a and b for varying current densities



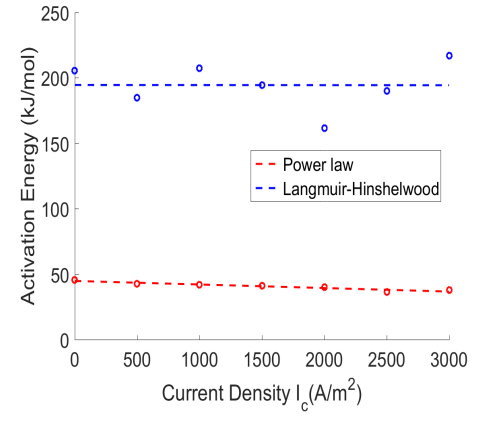


Figure 5.19: LH Arrhenius plots at various current densities

Figure 5.20: Comparison between the calculated activation energy (E<sub>a</sub>)(kJ/mol) using PL and LH kinetic model for varying current densities

Table.5.8 shows the calculated exponents a (for steam) and b (for hydrogen) for varying current densities. Negative values of a indicate a negative effect of steam partial pressure on the reaction rate. A similar observation was made also using the PL formulation (section 5.5.2.1) under the influence of current. However a highly non linear dependancy is observed in the steam and hydrogen partial pressures on the current density. This suggests a complex reaction mechanism and additionally a need for further mechanistic investigations on the basis of elementary reactions. Fig.5.19 shows the Arrhenius plots for various current densities and the linear fit (see Eqn.5.7) used to calculate the activation energy ( $E_a$ ) and pre-exponential factor ( $k_0$ ). The plots reconfirm the trend of a decreasing rate constant k with increasing current densities as shown in the PL case (see section 5.5.2.1).

Fig.5.20 shows the variation in the activation energy (kJ/mol) with varying current densities both with the PL and LH rate expressions. The PL rate expression

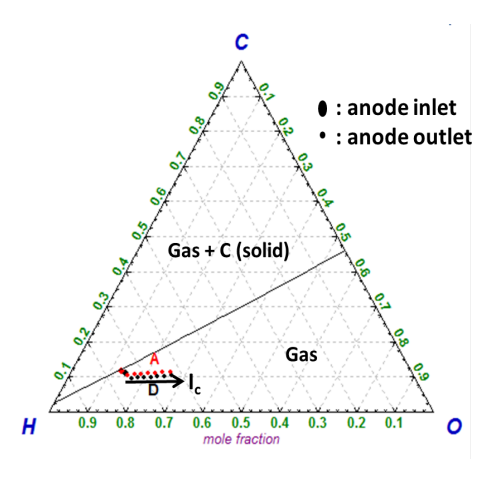
yields a lower activation energy compared to the LH rate expression. As the LH rate formulation also takes into account the adsorption/desorption enthalpies, the activation energy predicted with the LH rate is expected to be higher than the PL rate expression[215]. The values of activation energy predicted by both approaches are in agreement with previously reported values in literature [36, 39, 190, 204]. Furthermore, it is seen that PL activation energy seems to be fairly constant with varying current densities. Results with the LH kinetic model indicate a larger difference in the activation energy compared to the PL, however this deviation is not very significant. A comparison between both approaches indicates that electrochemical oxidation (current) may not be causing a significant change in the activation energy. A detailed explanation on this can be obtained only on the basis of a more detailed investigation into the elementary MSR reaction chemistry.

This investigation hasn't been focussed to address in detail the reaction mechanism on Ni-GDC anodes. However the qualitative kinetic trends obtained in this work are helpful to deduce mechanistic details by comparison with elementary MSR kinetics on Ni-GDC anodes. A positive reaction order with respect to methane with both approaches is consistent with literature indicating methane adsorption as one of the rate controlling steps. It is well known that ceria plays an important role in the intrinsic MSR kinetics. Elementary MSR kinetics have been studied for Ni/YSZ anode supports by Hecht et al [219]. They have proposed an extensive reaction mechanism with 42 elementary reactions involving 6 gas phase and 12 surface adsorbed species. However, there hasn't been any research efforts yet to study elementary MSR kinetics on ceria based SOFC catalysts/anodes. In order to develop a more detailed kinetic model with a mechanistic outlook, additional experimental studies focussing on elementary reaction chemistry have to be carried out. Furthermore, based on elementary steps, energetics have to be evaluated using methods like UBI-QEP[220] and reactor network models. Based on fitting results obtained using experimental methane conversion and a comparison to the energetics obtained from elementary kinetics, indications could be obtained regarding the reaction mechanism and the rate determining step(s). This is out of scope for this work, however it is highly encouraged as a future research activity to improve our understanding on MSR intrinsic kinetics in Ni-ceria based operating SOFCs.

# 5.5.4 Carbon deposition

Carbon deposition is one of the most important operating challenge for SOFCs operated with hydrocarbon fuels. Presence of carbon containing species like CO, CO<sub>2</sub> and CH<sub>4</sub> on the anode side can lead to carbon formation. To check effects of the relatively low inlet S/C ratios used in this work, a brief analysis was carried using equilibrium calculations in Factsage (a commercial program to carry out multiphase equilibrium calculations) [134] and scanning electron microscopy with energy dispersive X-ray spectroscopy (SEM-EDX).

Thermodynamic equilibrium calculations are helful to indicate theoretical limits for the operating paramters like temperature and S/C ratio. Fig.5.21 shows a ternary diagram indicating the carbon (C), hydrogen (H) and oxygen(O) mole frac-



1.7 of the control o

Figure 5.21: Ternary diagram showing anode inlet and outlet conditions for composition A (red) and composition D (black) at  $T_{cell} = 770^{o}C$  with increasing current density ( $I_{c}$ )

Figure 5.22: Oxygen to Carbon (O/C) ratio along the reactor length at various current densities ( $I_c$ )

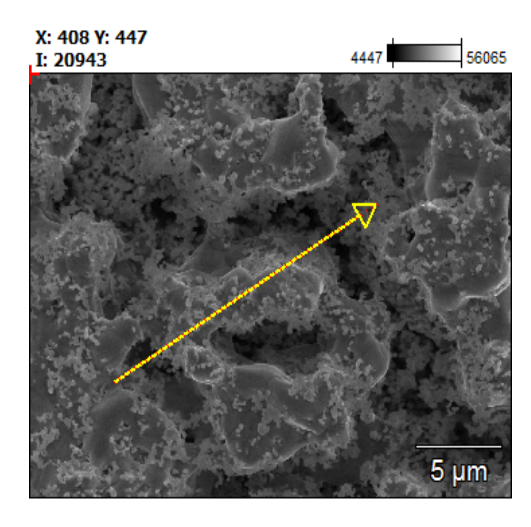


Figure 5.23: SEM image of the anode cross section after experimentation

tions at the anode inlet and anode outlet for two gas compositions (A and D) at  $T_{\rm cell}=770^{o}$ C. As it can be seen conditions at the anode inlet are closer to the gassolid equilibrium line. Another important aspect to note is the right shift in the outlet conditions under the influence of current. As current is drawn more steam is produced due to the electrochemical hydrogen oxidation (Eqn.1.2 and Eqn.1.1) and this causes the O/C ratio to increase. Fig.5.22 shows the oxygen to carbon ratio along the channel length at various current densities. Operating the cell at higher current densities causes the steam and oxygen concentration to increase along the

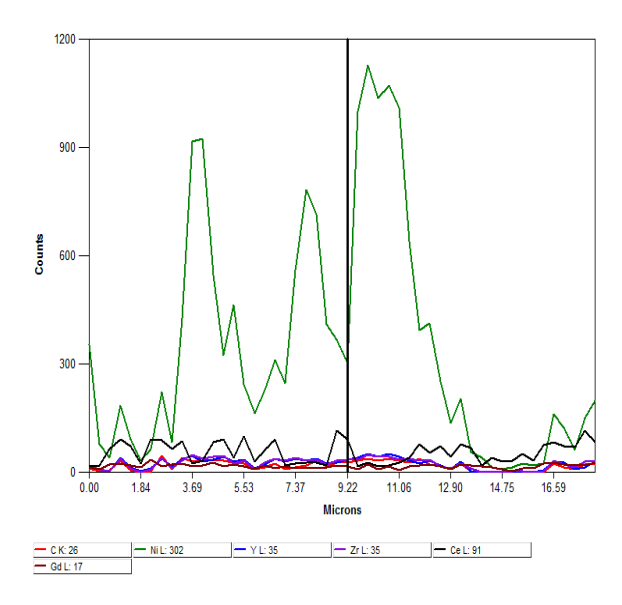


Figure 5.24: Line scan EDX analysis for the Ni-GDC cell after experimentation

channel. Furthermore, the O/C ratio decreases more rapidly under open circuit conditions compared to when operated under load.

Fig.5.23 and Fig.5.24 show the SEM image and the line plot from the EDX analysis respectively. Fig.5.24 indicates the presence of a relatively low amount of carbon in the anode. This insignificant carbon count is attributed to cell manufacturing and deposited carbon species (intermediate) on the catalyst surface. No carbon deposition was observed visually on the anode surface after experimentation.

## 5.6 Conclusions

An experimental investigation on methane steam reforming (MSR) kinetics has been presented for Ni-GDC anode based operating SOFCs with relatively low S/C ratios (~1), moderate current densities (upto 3000 A/m²) and low fuel utilization. As one of the main focus, a comparative study has been performed using power law (PL) and Langmuir-Hinshelwood (LH) reaction rate expressions to asssess the effects of using different kinetic formulations. The study further reports a trend analysis for various kinetic parameters like reaction rate, reaction orders, activation energy and rate constants. Some important conclusions could be drawn from the work which are listed below:

Methane steam reforming on metallic (Ni/Pt) anode current collectors (mesh) may not always be negligible (particularly for operating temperatures above 800°C) contrary to reports in literature.

- Both PL and LH kinetic approaches show that electrochemical oxidation (current) promotes methane conversion and the MSR reaction rate, however the effect of temperature is seen to be more dominant.
- The MSR reaction rate is a stronger function of the methane partial pressure compared to the partial pressure of steam.
- Both the PL and LH kinetic models predict exactly the same net MSR reaction rate, however there is a significant difference in the rate and species distribution along the channel length with both approaches. Despite both the approaches predicting a higher rate near the fuel inlet and lowest near the outlet, the LH approach predicts a much higher (peak) MSR reaction rate near the anode inlet compared to the PL approach leading to a different rate and species distribution. A simplified kinetic approach like PL may thus not be sufficient towards accurately predicting temperature gradients in SOFC anodes.
- Electrochemical oxidation (current) seems to cause an insignificant change in the MSR activation energy. However, further investigations on elementary reaction chemistry are required to verify this observation.
- A negative dependancy of steam on the MSR reaction rate is obtained using both PL and LH rate formulation, in agreeement with studies in literature. Under the influence of current, both the PL and LH rate expressions yield a highly non linear dependancy (reaction orders/exponents) on steam and hydrogen partial pressures suggesting a complex mechanism.
- No significant carbon deposition has been observed after the Ni-GDC cell was operated on methane with relatively low steam to carbon ratios of around 1.0-1.5.
- The interaction between electrochemical oxidation (current) and the MSR reaction is highly complex suggesting the possibility of multiple rate determining steps depending of the operating condition; acurately predicting the intrinsic kinetics using a kinetic model requires the development of elementary reaction chemistry on Ni-ceria based anodes and further experimental investigations.

The obtained results in this study provide a better insight on the influence of electrochemical reactions on MSR and also show the sensitivity in results due to different kinetic formulations. The used approach is helpful in formulating future experimental work and towards developing a more robust and complete kinetic model including elementary MSR kinetics. Furthermore, data presented in this work can be used towards numerical (CFD) and system model development and validation.

# Chapter 6

# Conclusions

This project was undertaken to develop clean, high efficiency and flexible bio-IGCC (Integrated gasification combined cycle) and IRCC (Integrated reforming combined cycle) power plant concepts and carry out detailed thermodynamic evaluations. Solid oxide fuel cells (SOFC) have been chosen as the enabling technology to achieve high efficiency and metal hydride based hydrogen storage to achieve operational flexibility. In order to design and develop optimal hydrocarbon fuelled SOFC units for power plant integration, it is also of prime importance to investigate underlying reaction kinetics. Hence, an extended experimental study has been carried out on methane steam reforming(MSR) kinetics in single operating SOFCs with nickel(Ni)-ceria based anodes to highlight the importance of using appropriate kinetic approaches. The following section summarizes chapterwise the contributions and main findings of this dissertation. Recommendations for continuing the research work in future are then presented in Section.6.2

# 6.1 Contributions & main findings

# 6.1.1 High percentage biomass co-gasification in existing IGCC power plants

The dissertation (Chapter 2) reports a first of its kind experimental demonstration and data for a high percentage (70%) and large scale biomass co-gasification test carried out at an existing coal based IGCC power plant. With this work it has been shown that IGCC power plants can be operated with very high percentage (upto 70% on energy basis) of biomass in the fuel blend without extensive power plant modifications.

A validated off-design thermodynamic model has been developed in this work based on design drawings of the 253 MW $_e$  Willem-Alexander Centrale IGCC plant in Buggenum, the Netherlands. The detailed model is a valuable asset towards planning, executing and/or verifying IGCC power plant operations with a different fuel than what it is designed for and with a relatively high accuracy (<3%). The deviations in model predictions are particularly in the syngas cooler (SGC); the main reason being fouling in the HP section. It has been shown that co-gasification with high LHV pretreated biomass (torrefied) is essential to achieve the design case electrical output. Furthermore, the presented exergy(2nd law) analysis indicates gasification and combustion as sources of highest exergy destruction.

The reported demonstration test and modeling work presented in this dissertation is of high importance particularly to the power plant and bioenergy industry, where companies are currently unable to justify decisions making large investments on biomass co-gasification at existing coal fired IGCC power plants. Furthermore, such major demonstration achievements and detailed themodynamic evaluations could help develop a renewed interest amongst environmental agencies and policy makers towards development of low emission/carbon neutral power plants.

# 6.1.2 Retrofitting bio-IGCC power plants with SOFCs and CO<sub>2</sub> capture

Based on successful large scale biomass co-gasification tests at existing IGCC power plants (as reported in Chapter 2), there also exists an urgent need to develop clean and highly energy efficient power plant concepts with a focus on near future implementation. Chapter 3 of this dissertation presents a thermodynamic evaluation and approach towards retrofitting solid oxide fuel cells (SOFC) and CO<sub>2</sub> capture in large scale bio-IGCC power plants using experimentally validated models (presented in Chapter 2). The case study based on the Willem-Alexander Centrale (WAC) IGCC power plant in the Netherlands points out that net electrical efficiencies (LHV) of more than 40% could be obtained by partially retrofitting SOFCs (producing upto 40 MW<sub>e</sub>) and oxy-fuel combustion CO<sub>2</sub> capture in large scale bio-IGCC power plants in near term future. Retrofitting an existing IGCC power plant with SOFCs and CO<sub>2</sub> capture causes a significant part load condition for the gas turbine (GT). It has been concluded from this work that controlling the GT expander outlet temperature using the variable inlet guide vanes (VIGV) is crucial to reduce part load effects. Furthermore the original WAC system needs to be modified by including a booster air compressor in the air separation unit (ASU) and modifying the N<sub>2</sub> dilution/water saturation unit to avoid instabilities in the GT combustor. Exergy destruction is shown to be reduced by about 30% in the retrofitted system due to partial replacement of GT combustion with electrochemical conversion in SOFCs.

Using two system models employing partial and full SOFC-CO<sub>2</sub> capture, it has also concluded that for full scale SOFC integration and CO<sub>2</sub> capture, the original WAC design needs to be significantly modified to include a newly designed CO<sub>2</sub> capture unit, SOFC unit and heat recovery steam generator (HRSG). A newly designed integrated gasification fuel cell (IGFC) system is proposed wherein the existing WAC flue gas expander is replaced with an air expander and furthermore the HRSG is redesigned significantly. The fully integrated IGFC system gives a net electrical efficiency of about 47%.

The study demonstrates the large potential towards developing carbon neutral/carbon negative IGCC power plants in near future. Model based calculations show that applying full-scale  $CO_2$  capture in an IGFC system with 70% biomass (steam exploded woodpellets) co-gasification results in a carbon negative (about 40%) footprint. The essential process modifications identified in this work to partially retrofit SOFCs and  $CO_2$  capture is highly crucial information for the industry to develop appropriate engineering solutions. The developed models are also helpful to further investigate IGCC systems relating to the scaling up of the SOFC unit, minimizing GT part load effects and techno-economic evaluations.

## 6.1.3 Flexible IRCC power plants with hydrogen storage

Coal and natural gas are the two main fossil fuels which are utilized globally in power plants to produce electricity. Research efforts to reduce reliance on these fossil fuels and increase electrical efficiencies need to be thus focussed equally on coal based and natural gas based power plants. The integrated reforming combined cycle (IRCC) system is a natural gas based combined cycle system employing precombustion  $\rm CO_2$  capture. With a focus to investigate flexibility aspects and achieving high electrical efficiencies, Chapter 4 of this dissertation presents a thermodynamic system study on flexible IRCC power plants with metal hydride based hydrogen storage.

Metal hydride based hydrogen storage as a flexibility option in large scale power plants has hitherto never been investigated upon. This work for the first time brings forward the importance of investigating this option, considering the large scope for heat integration in the system. Heat released during charging is utilized to generate high pressure (HP) steam for the magnesium hydride (MgH $_2$ ) based system while flue gases from the gas turbine outlet is utilized to provide heat in the discharging mode. Based on the comparative system analysis using steady state models, it has been concluded that clean and flexible IRCC power plants could be operated with relatively high time based average electrical efficiencies above 45%. The hydrogen split fraction, choice of the metal hydride (reaction enthalpy) and the heat integration strategy have been identified as the main influencing factors on system design and net electrical efficiency. Furthermore, the study offers some insights into the effect of pinch and  $H_2$  split fraction on the HRSG design and operation.

Despite a simplistic approach and several assumptions particularly in the MH unit, this work provides a framework for further exploring metal hydride based hydrogen storage as a flexibility option in stationary systems. Exergy analysis indicates a large scope for process improvements. In this regard a preliminary investigation has been carried out in this work (Appendix 4A) towards retrofitting natural gas combined cycle (NGCC) systems (without pre-combustion CO<sub>2</sub> capture and hydrogen storage) with high temperature solid oxide fuel cells (SOFCs). The study indicates that high net electrical efficiencies (LHV) of more than 65% could be achieved by retrofitting SOFCs in NGCC power plant systems.

# 6.1.4 Methane steam reforming (MSR) kinetics in SOFCs with Ni-ceria based anodes

This dissertation set out to explore solid oxide fuel cells (SOFCs) as a core technology to enhance combined cycle power plant efficiencies. The advantages of SOFC integration in natural gas based power plants has been depicted in Appendix 4A. In order to design and develop optimal and safely operating SOFC units for integration in such power plants, it is crucial to attain a good understanding in the underlying chemical reaction kinetics. Chapter 5 presents an experimental study on MSR kinetics in operating single SOFCs with Ni-ceria based anodes with relatively low S/C ratios and moderate current densities. Experiments have been carried out using a single square cell with a Ni-GDC (gadolinium doped ceria) anode by varying gas compositions, cell temperatures and current densities. A kinetic model has been developed to calculate relavant kinetic parameters using the experimentally obtained methane conversion data. As a primary focus, the study has been carried out by comparing two kinetic approaches namely power law (PL) kinetics and

general Langmuir-Hinshelwood (LH) kinetics. This is the first study in literature reporting a comparison between PL and LH MSR kinetics for operating SOFCs with Ni-ceria based anodes.

As the first important finding, it has been shown that methane reforming on metallic (Ni/Pt) anode current collectors (mesh) may not be always negligible (particularly for operating temperatures above 800°C) in contrast to reports in literature. The research also confirms previous studies and contributes additional evidence suggesting that electrochemical oxidation (current) promotes methane conversion and the MSR reaction rate. The effect of temperature on the MSR reaction rate is however seen to be more dominant. For a given cell temperature and current density, the methane partial pressure is identified as the most dominant parameter influencing the MSR reaction rate. A second important finding from this work is the relatively low impact of electrochemical oxidation on the MSR activation energy. Furthermore, comparison between the PL and LH kinetic approaches reveals that despite both approaches predicting the same net reaction rate, there is a significant difference in the prediction of the rate and species distribution along the reactor length. This is an important aspect to be taken into account in kinetic studies towards accurately predicting temperature gradients and for further development of methane (natural gas) fuelled SOFC units.

Experimental investigations on MSR intrinsic kinetics in operating SOFCs i,e under the influence of current are limited in academic literature. A key strength of this study is the focus on investigating MSR kinetics with relatively low S/C ratios (around 1) and moderate current densities ( $I_c$ ) upto 3000 A/ $m^2$ . Such investigations are vital towards reducing steam consumption to safely operate internal reforming SOFCs and also to develop reliable numerical(CFD) models. The scope of this study was limited in terms of providing a deeper mechanistic outlook, however the importance of carrying out further experimentation and the need to develop elementary reaction chemistry on Ni-ceria based anodes has been pinpointed.

Despite its exploratory nature, this dissertation brings forward the increased importance and relevance of detailed power plant thermodynamic off-design modeling and validation. In addition, the importance of retrofitting existing IGCC power plants in near future to enhance performance and reduce CO<sub>2</sub> emissions has been adequately depicted in this work. The study brings to attention for the first time the role of solid oxide fuel cells (SOFCs) and metal hydride based hydrogen storage as effective applied technologies in the large scale power plant industry. Towards further development of SOFC units for power plant integration, this work brings out the drawbacks of using simplified rate kinetics in methane fuelled single operating SOFCs, based on a comparison between the two most widely used kinetic approaches. The study has revealed the increased need for further experimentation and development of MSR elementary reaction chemistry for ceria based SOFC anodes.

#### 6.2 Recommendations for future work

The research work carried out in this project provides a strong framework towards designing and thermodynamically evaluating large scale power plant systems using detailed steady state models and experimentally investigating MSR kinetics in operating solid oxide fuel cells (SOFCs). However the research has also thrown up several questions in need for further investigations.

- Process modifications towards implementing high percentage (70%) biomass co-gasification in existing IGCC power plants have been proposed in this work (Chapter 2). Using the presented thermodynamic analysis, techno-economic evaluations must be carried out to assess financial implications. In addition, a detailed part load evaluation is recommended to more accurately quantify the off-design system performance.
- The validated bio-IGCC model presented in Chapter 2 has been utilized to develop process concepts (Chapter 3) towards retrofitting bio-IGCC power plants with solid oxide fuel cells and oxy-combustion CO<sub>2</sub> capture. Using the developed models as a foundation, further research is required towards developing scaling up strategies for the SOFC and CO<sub>2</sub> capture unit based on market analysis. Furthermore, the retrofitted system should be evaluated on an economic basis to obtain investment and other financial estimates. Additional activities include the development of a more detailed model for the air separation unit (ASU) and a detailed turbomachinery (gas and steam turbines) part load assessment.
- This dissertation (Chapter 4) provides a basis to evaluate flexibility aspects (using metal hydride based hydrogen storage) in large scale natural gas based IRCC power plants. Additional investigations are required towards optimizing the metal hydride thermodynamic parameters, detailed design for the system capable of operating in both modes of operation and economic assessments based on the heat and mass balances developed in this study. Based on the preliminary analysis presented in this work (Appendix 4A) further modeling efforts should be carried out to develop flexible and integrated IRCC power plant system concepts with solid oxide fuel cells.
- A number of possible future kinetic studies on methane steam reforming are recommended using the step-by-step experimental approach presented in Chapter 5. As one of the primary activity, the influence of the metallic (Ni/Pt) anode current collector on the methane reforming rate should be further investigated. Additional experiments should also be carried out over a wider range of operating temperatures, gas compositions (influence of inlet H<sub>2</sub> partial pressure) and fuel utilizations. Another important activity is to further optimize the kinetic model presented in this work to include a more accurate depiction of adsorption/desorption parameters. As a long term research target, experimental and modeling efforts are encouraged towards develop-

ing elementary MSR reaction chemistry on Ni-ceria based anodes to carry out detailed mechanistic studies.

# Bibliography

- [1] Marcia Rocha Nadine Braun Marie Lindberg et al. Hanna Fekete, Marion Vieweg. Analysis of current greenhouse gas emission trends. Technical report, Ecofys, Climate Analytics and PIK, 2013.
- [2] Mike Hulme. 1.5 [deg]c and climate research after the paris agreement. *Nature Clim. Change*, 6(3):222–224, March 2016. ISSN 1758-678X. URL http://dx.doi.org/10.1038/nclimate2939.
- [3] Hoesung Lee. Turning the focus to solutions. *Science*, 350(6264):1007–1007, 2015. ISSN 0036-8075. doi: 10.1126/science.aad8954. URL http://science.sciencemag.org/content/350/6264/1007.
- [4] IPCC. Summary for policymakers. Technical report, Working Group I to the Fourth Assessment Report of the Intergovernmental Panel on Climate Change, 2007.
- [5] IPCC. Summary for policymakers. In: Climate Change 2014: Impacts, Adaptation, and Vulnerability. Part A: Global and Sectoral Aspects. Technical report, Working Group II to the Fifth Assessment Report of the Intergovernmental Panel on Climate Change, 2014.
- [6] United States Environmental Protection Agency. Inventory of u.s. greenhouse gas emissions and sinks: 1990-2013. Technical report, United States Environmental Protection Agency, 2015.
- [7] Vivien Foster and Daron Bedrosyan. Understanding co2 emissions from the global energy sector. Technical report, The World Bank, 2014.
- [8] European Climate Foundation. ROADMAP 2050 A practical guide to a properous low-carbon Europe Technical Analysis. Technical report, European Commission, 2010. URL http://www.roadmap2050.eu/attachments/files/Volume1\_fullreport\_PressPack.pdf.
- [9] European Commission. A policy framework for climate and energy in the period from 2020 to 2030. Technical report, European Commission, 2014. URL http://eur-lex.europa.eu/legal-content/EN/TXT/PDF/?uri=CELEX:52014DC0015&from=EN.

- [10] EUROSTAT. Electricity production, consumption and market overview. Online. URL http://ec.europa.eu/eurostat/statistics-explained/index.php/Electricity\_production,\_consumption\_and\_market\_overview.
- [11] E.J.O. Promes, T. Woudstra, L. Schoenmakers, V. Oldenbroek, A. Thallam Thattai, and P. V. Aravind. Thermodynamic evaluation and experimental validation of 253 MW Integrated Coal Gasification Combined Cycle power plant in Buggenum, Netherlands. *Applied Energy*, 155(0):181 194, 2015. ISSN 0306-2619.
- [12] Lars O. Nord, R. Anantharaman, M. Rausand, and O. Bolland. A qualitative reliability and operability analysis of an integrated reforming combined cycle plant with co<sub>2</sub> capture. *Int. J. of Greenhouse Gas Control*, 3:411–421, 2009.
- [13] Michael J. Moran and Howard N. Shapiro. *Fundamentals of Engineering Ther-modynamics 5th Edition*. John Wiley & Sons, Inc., 2006.
- [14] P.K. Nag. *Power Plant Engineering*, 4e:. McGraw Hill Education (India) Private Limited, 2014. URL https://books.google.nl/books?id=gs8\_CwAAQBAJ.
- [15] Wiebren de Jong and J. Ruud van Ommen. *Biomass as a Sustainable Energy Source for the Future: Fundamentals of Conversion Processes*, pages 36–68. John Wiley & Sons, Inc, 2014. ISBN 9781118916643.
- [16] Daniel L. Sanchez, James H. Nelson, Josiah Johnston, Ana Mileva, and Daniel M. Kammen. Biomass enables the transition to a carbon-negative power system across western north america. *Nature Clim. Change*, 5(3):230–234, March 2015. ISSN 1758-678X. URL http://dx.doi.org/10.1038/nclimate2488.
- [17] Daniel L. Sanchez and Daniel M. Kammen. A commercialization strategy for carbon-negative energy. *Nature Energy*, 1:15002–, January 2016. URL http://dx.doi.org/10.1038/nenergy.2015.2.
- [18] James S. Rhodes and David W. Keith. Engineering economic analysis of biomass IGCC with carbon capture and storage. *Biomass and Bioenergy*, 29 (6):440 450, 2005. ISSN 0961-9534.
- [19] Pa Ve Aravind, T. Woudstra, N. Woudstra, and H. Spliethoff. Thermodynamic evaluation of small-scale systems with biomass gasifiers, solid oxide fuel cells with Ni/GDC anodes and gas turbines. *Journal of Power Sources*, 190(2):461 475, 2009. ISSN 0378-7753.
- [20] L. Balling. Flexible future for combined cycle. Technical report, Siemens, December 2010.
- [21] Rosa Domenichini, Luca Mancuso, Noemi Ferrari, and John Davison. Operating flexibility of power plants with carbon capture and storage (CCS).

- Energy Procedia, 37:2727 2737, 2013. ISSN 1876-6102. doi: http://dx.doi.org/10.1016/j.egypro.2013.06.157. URL http://www.sciencedirect.com/science/article/pii/S1876610213004001. GHGT-11 Proceedings of the 11th International Conference on Greenhouse Gas Control Technologies, 18-22 November 2012, Kyoto, Japan.
- [22] D. Rastler. Electricity energy storage technology options. Technical report, Electric Power Research Institute (EPRI), December 2010.
- [23] Working Group III of the Intergovernmental Panel on Climate Change. IPCC Special Report: Carbon Dioxide Capture and Storage. Technical report, Intergovernmental Panel on Climate Change (IPCC), 2005.
- [24] Vattenfall, 2014. URL https://corporate.vattenfall.com/.
- [25] E. Van Selow, P. Cobden, R.W. Van den Brink, J.R. Hufton, and A. Wright. Performance of sorption-enhanced water-gas shift as a precombustion CO<sub>2</sub> capture technology. *Energy Procedia*, 1:689–696, 2008.
- [26] R. Reijers, E. Van Selow, P. Cobden, J. Boon, and R. Van den Brink. Sewgs process cycle optimization. *Energy Procedia* 4, 1155-1161, 2011.
- [27] Steve Rackley. *Carbon Capture and Storage*. Butterworth-Heinemann/Elsevier, 2009.
- [28] Subhash C. Singhal and Kevin Kendall. *High Temperature Solid Oxide Fuel Cells: Fundamentals, Design and Applications*. Elsevier, Oxford and NY and Yushima. 2003.
- [29] Jaroslaw Milewski. *Advanced Methods of Solid Oxide Fuel Cell Modeling*, chapter SOFC Modeling, pages 91–200. Springer London, London, 2011. ISBN 978-0-85729-262-9. doi: 10.1007/978-0-85729-262-9\_5. URL http://dx.doi.org/10.1007/978-0-85729-262-9\_5.
- [30] Yoshio Matsuzaki and Isamu Yasuda. Electrochemical oxidation of H<sub>2</sub> and CO in a H<sub>2</sub>-H<sub>2</sub>O-CO-CO<sub>2</sub> system at the Interface of a Ni-YSZ Cermet Electrode and YSZ Electrolyte. *Journal of The Electrochemical Society*, 147(5): 1630–1635, 2000. doi: 10.1149/1.1393409. URL http://jes.ecsdl.org/content/147/5/1630.abstract.
- [31] E. Perry Murray, T. Tsai, and S. A. Barnett. A direct-methane fuel cell with a ceria-based anode. *Nature*, 400(6745):649–651, August 1999. ISSN 0028-0836. URL http://dx.doi.org/10.1038/23220.
- [32] Nico Woudstra. *Sustainable Enegy Systems: Limitations and challenges based on exergy analysis.* PhD thesis, Delft University of Technology, 2012.
- [33] Bloom Energy. ES-5700 Energy Server Datasheet, 2015. URL http://www.bloomenergy.com/fuel-cell/es-5700-data-sheet/.

- [34] SOLIDPower. EnGen-2500 Datasheet, 2014. URL http://www.solidpower.com/wp-content/uploads/2014/03/Data\_Sheet\_Engen2500\_eng.pdf.
- [35] D. Mogensen, J.-D. Grunwaldt, P.V. Hendriksen, K. Dam-Johansen, and J.U. Nielsen. Internal steam reforming in solid oxide fuel cells: Status and opportunities of kinetic studies and their impact on modelling. *Journal of Power Sources*, 196(1):25 38, 2011. ISSN 0378-7753. doi: http://dx.doi.org/10.1016/j.jpowsour.2010.06.091. URL http://www.sciencedirect.com/science/article/pii/S0378775310010785.
- [36] Jianguo Xu and Gilbert F Froment. Methane steam reforming, methanation and water-gas shift: I. intrinsic kinetics. *AIChE Journal*, 35(1):88–96, 1989.
- [37] G. Brus, Y. Komatsu, S. Kimijima, and J. S. Szmyd. An analysis of biogas reforming process on Ni/YSZ and Ni/SDC catalysts. *International Journal of Applied Thermodynamics*, 15(1):43–51, 3 2012. ISSN 1301-9724. doi: 10.5541/jjot.315.
- [38] Viswanathan Arcotumapathy, Feraih Sh Alenazey, Raja L. Al-Otaibi, Dai-Viet N. Vo, Faisal M. Alotaibi, and Adesoji A. Adesina. Mechanistic investigation of methane steam reforming over ce-promoted Ni/SBA-15 catalyst. *Applied Petrochemical Research*, 5(4):393–404, 2015. ISSN 2190-5533. doi: 10.1007/s13203-015-0121-2. URL http://dx.doi.org/10.1007/s13203-015-0121-2.
- [39] Kaihu Hou and Ronald Hughes. The kinetics of methane steam reforming over a ni/ $\alpha$  al2o catalyst. *Chemical Engineering Journal*, 82:311 328, 2001. ISSN 1385-8947. doi: http://dx.doi.org/10.1016/S1385-8947(00) 00367-3. URL http://www.sciencedirect.com/science/article/pii/S1385894700003673.
- [40] A.K. Avetisov, J.R. Rostrup-Nielsen, V.L. Kuchaev, J.-H. Bak Hansen, A.G. Zyskin, and E.N. Shapatina. Steady-state kinetics and mechanism of methane reforming with steam and carbon dioxide over ni catalyst. *Journal of Molecular Catalysis A: Chemical*, 315(2):155 162, 2010. ISSN 1381-1169. doi: http://dx.doi.org/10.1016/j.molcata.2009.06.013. URL http://www.sciencedirect.com/science/article/pii/S1381116909002866. In memory of M.I. Temkin.
- [41] Wei Wang, Chao Su, Yuzhou Wu, Ran Ran, and Zongping Shao. Progress in solid oxide fuel cells with nickel-based anodes operating on methane and related fuels. *Chem. Rev.*, 113(10):8104–8151, October 2013. ISSN 0009-2665. doi: 10.1021/cr300491e. URL http://dx.doi.org/10.1021/cr300491e.
- [42] Kouta Asai, Yoshiyuki Nagayasu, Koji Takane, Shinji Iwamoto, Eriko Yagasaki, Ken ichi Ishii, and Masashi Inoue. Mechanisms of methane decomposition over ni catalysts at high temperatures. *Journal of the Japan Petroleum Institute*, 51(1):42–49, 2008. doi: 10.1627/jpi.51.42.

- [43] M.V.C. Sastri, B. Viswanathan, and S. Srinivasa Murthy. *Metal Hydrides*. Narosa Publishing House New Delhi, 1998.
- [44] Daniele Fiaschi and Riccardo Carta. CO<sub>2</sub> abatement by co-firing of natural gas and biomass-derived gas in a gas turbine. *Energy*, 32(4):549 567, 2007. ISSN 0360-5442. {ECOS} 05. 18th International Conference on Efficiency, Cost, Optimization, Simulation, and Environmental Impact of Energy Systems {ECOS} 05.
- [45] Heidi C. Butterman and Marco J. Castaldi. CO<sub>2</sub> as a carbon neutral fuel source via enhanced biomass gasification. *Environmental Science & Technology*, 43(23):9030–9037, 2009. PMID: 19943684.
- [46] John A. Mathews. Carbon-negative biofuels. *Energy Policy*, 36(3):940 945, 2008. ISSN 0301-4215.
- [47] Vattenfall. Vattenfall's energy portfolio and the European energy system. Technical report, VATTENFALL, 2011. URL http://corporate.vattenfall.com/globalassets/corporate/about\_vattenfall/generation/six\_sources\_of\_energy\_one\_energy\_system.pdf.
- [48] J. Th. G. M. Eurlings. Process performance of the SCGP at Buggenum IGCC. In *Gasification Technologies Conference*, 1999.
- [49] Hans Pastoors. Materials behavior in the Nuon Power IGCC Plant in Buggenum. *Materials at High Temperatures*, 20(1):61–65, 2003.
- [50] Wa Willeboer. Coal gasification for electricity generation. In 19th World Gas Conference: Milan 20/23 June 1994, International Gas Union, 1994.
- [51] Marco Kanaar and Carlo Wolters. Update of Nuon Power Buggenum plant performance and fuel flexibility. In *Proceedings of the 2nd International Conference on Clean Coal Technologies for our future, Sardinia, Italy*, pages 1–20, 2005.
- [52] E.J.O. Promes, T. Woudstra, L. Schoenmakers, V. Oldenbroek, A. Thallam Thattai, and P.V. Aravind. Thermodynamic evaluation and experimental validation of 253 mw integrated coal gasification combined cycle power plant in buggenum, netherlands. Article accepted for publication, Applied Energy.
- [53] Zhongqing Ma, Yimeng Zhang, Qisheng Zhang, Yongbiao Qu, Jianbin Zhou, and Hengfei Qin. Design and experimental investigation of a 190 kWe biomass fixed bed gasification and polygeneration pilot plant using a double air stage downdraft approach. *Energy*, 46(1):140 147, 2012. ISSN 0360-5442. Energy and Exergy Modelling of Advance Energy Systems.
- [54] Ana-Maria Cormos, Cristian Dinca, and Calin-Cristian Cormos. Multi-fuel multi-product operation of IGCC power plants with carbon capture and storage (CCS). *Applied Thermal Engineering*, 74(0):20 27, 2015. ISSN 1359-4311. 6th International Conference on Clean Coal Technologies {CCT2013}.

- [55] Alexander Buttler, Christian Kunze, and Hartmut Spliethoff. Igcc-epi: Decentralized concept of a highly load-flexible IGCC power plant for excess power integration. *Applied Energy*, 104(0):869 879, 2013. ISSN 0306-2619.
- [56] Xiangping Zhang, Truls Gundersen, Simon Roussanaly, Amy L. Brunsvold, and Suojiang Zhang. Carbon chain analysis on a coal IGCC CCS system with flexible multi-products. *Fuel Processing Technology*, 108(0):146 153, 2013. ISSN 0378-3820. Special Issue of {APCRE11}.
- [57] Li Zhou, Shanying Hu, Yourun Li, and Qihong Zhou. Study on co-feed and co-production system based on coal and natural gas for producing DME and electricity. *Chemical Engineering Journal*, 136(1):31 40, 2008. ISSN 1385-8947.
- [58] J.C. Meerman, A. Ramirez, W.C. Turkenburg, and A.P.C. Faaij. Performance of simulated flexible integrated gasification polygeneration facilities. Part A: A technical-energetic assessment. *Renewable and Sustainable Energy Reviews*, 15(6):2563 2587, 2011. ISSN 1364-0321.
- [59] Carlo Wolters. Operating experiences at the Willem Alexander Centrale. In *Presentation at Gasification Technology Council Conference*, 2003.
- [60] B. Coda, M.K. Cieplik, J.M. Jacobs, and J.H.A. Kiel. Impact of biomass cofiring on ash formation and ash behaviour in IGCC plants. Technical report, Energy research center of the Netherlands (ECN), 2004.
- [61] Raziyeh Khodayari. Vattenfall strategy and experiences on co-firing of biomass and coal. In *Presentation at IEA Clean Coal Conference*. Vattenfall Research and Development, 2012.
- [62] M.J.C. van der Stelt, H. Gerhauser, J.H.A. Kiel, and K.J. Ptasinski. Biomass upgrading by torrefaction for the production of biofuels: A review. *Biomass and Bioenergy*, 35(9):3748 3762, 2011. ISSN 0961-9534.
- [63] Jaya Shankar Tumuluru, J. Richard Hess, Richard D. Boardman, Christopher T. Wright, and Tyler L. Westover. Formulation, pretreatment, and densification options to improve biomass specifications for co-firing high percentages with coal. *Industrial Biotechnology*, 8(3):113–132, June 2012. ISSN 1550-9087.
- [64] Bjorn Forsberg. Black Pellets: A Fuel for Power Choosing Pellet Fuel to Cut Costs and Improve Operations. Presentation: Nordic Baltic Bioenergy Riga, April 2015.
- [65] Jayanta Deb Mondol, David McIlveen-Wright, Sina Rezvani, Ye Huang, and Neil Hewitt. Techno-economic evaluation of advanced IGCC lignite coal fuelled power plants with CO<sub>2</sub> capture. *Fuel*, 88(12):2495 2506, 2009. ISSN 0016-2361.

- [66] Christian Kunze and Hartmut Spliethoff. Modelling of an IGCC plant with carbon capture for 2020. *Fuel Processing Technology*, 91(8):934 941, 2010. ISSN 0378-3820.
- [67] F. Emun, M. Gadalla, T. Majozi, and D. Boer. Integrated gasification combined cycle (IGCC) process simulation and optimization. *Computers & Chemical Engineering*, 34(3):331 338, 2010. ISSN 0098-1354.
- [68] Emanuele Martelli, Thomas Kreutz, and Stefano Consonni. Comparison of coal IGCC with and without CO<sub>2</sub> capture and storage: Shell gasification with standard vs. partial water quench. *Energy Procedia*, 1(1):607 614, 2009. ISSN 1876-6102.
- [69] Werner Renzenbrink, Johannes Ewers, Dietmar Keller, Karl Josef Wolf, and Wolfgang Apel. RWE's 450 MW IGCC/CCS project Status and outlook. *Energy Procedia*, 1(1):615 622, 2009. ISSN 1876-6102.
- [70] Ligang Zheng and Edward Furinsky. Comparison of Shell, Texaco, BGL and KRW gasifiers as part of IGCC plant computer simulations. *Energy Conversion and Management*, 46(11-12):1767 1779, 2005. ISSN 0196-8904.
- [71] Jong Jun Lee, Young Sik Kim, Kyu Sang Cha, Tong Seop Kim, Jeong L. Sohn, and Yong Jin Joo. Influence of system integration options on the performance of an integrated gasification combined cycle power plant. *Applied Energy*, 86 (9):1788 1796, 2009. ISSN 0306-2619.
- [72] Calin-Cristian Cormos, Anamaria Padurean, and Paul Serban Agachi. Technical evaluations of carbon capture options for power generation from coal and biomass based on integrated gasification combined cycle scheme. *Energy Procedia*, 4(0):1861 1868, 2011. ISSN 1876-6102.
- [73] Calin-Cristian Cormos. Hydrogen and power co-generation based on coal and biomass/solid wastes co-gasification with carbon capture and storage. *International Journal of Hydrogen Energy*, 37(7):5637 5648, 2012. ISSN 0360-3199.
- [74] Victoria Maxim, Calin-Cristian Cormos, and Paul Serban Agachi. Design of integrated gasification combined cycle plant with carbon capture and storage based on co-gasification of coal and biomass. In M.C. Georgiadis E.N. Pistikopoulos and A.C. Kokossis, editors, 21st European Symposium on Computer Aided Process Engineering, volume 29 of Computer Aided Chemical Engineering, pages 1904 1908. Elsevier, 2011.
- [75] Antonio Valero and Sergio Usón. Oxy-co-gasification of coal and biomass in an integrated gasification combined cycle (IGCC) power plant. *Energy*, 31 (10-11):1643 1655, 2006. ISSN 0360-5442. {ECOS} 2003.
- [76] A.V. Bridgwater. The technical and economic feasibility of biomass gasification for power generation. *Fuel*, 74(5):631 653, 1995. ISSN 0016-2361.

- [77] David Brown, Martin Gassner, Tetsuo Fuchino, and François Maréchal. Thermo-economic analysis for the optimal conceptual design of biomass gasification energy conversion systems. *Applied Thermal Engineering*, 29(11-12): 2137 2152, 2009. ISSN 1359-4311.
- [78] Veronika Dornburg and André P.C. Faaij. Efficiency and economy of wood-fired biomass energy systems in relation to scale regarding heat and power generation using combustion and gasification technologies. *Biomass and Bioenergy*, 21(2):91 108, 2001. ISSN 0961-9534.
- [79] David Klein, Nico Bauer, Benjamin Bodirsky, Jan Philipp Dietrich, and Alexander Popp. Bio-IGCC with CCS as a long-term mitigation option in a coupled energy-system and land-use model. *Energy Procedia*, 4(0):2933 2940, 2011. ISSN 1876-6102.
- [80] P. Klimantos, N. Koukouzas, A. Katsiadakis, and E. Kakaras. Air-blown biomass gasification combined cycles (BGCC): System analysis and economic assessment. *Energy*, 34(5):708 714, 2009. ISSN 0360-5442.
- [81] Monica Rodrigues, Andre P.C. Faaij, and Arnaldo Walter. Techno-economic analysis of co-fired biomass integrated gasification/combined cycle systems with inclusion of economies of scale. *Energy*, 28(12):1229 1258, 2003. ISSN 0360-5442.
- [82] Nikolaos G. Tsakomakas, Petros A. Pilavachi, and Apostolos L. Polyzakis. An economic comparison assessment of lignite and biomass IGCC power plants. *Applied Thermal Engineering*, 38(0):26 30, 2012. ISSN 1359-4311.
- [83] J. Fermoso, B. Arias, M.G. Plaza, C. Pevida, F. Rubiera, J.J. Pis, F. Garcia-Pe na, and P. Casero. High-pressure co-gasification of coal with biomass and petroleum coke. *Fuel Processing Technology*, 90(7-8):926 932, 2009. ISSN 0378-3820.
- [84] Chuangzhi Wu, Xiuli Yin, Longlong Ma, Zhaoqiu Zhou, and Hanping Chen. Design and operation of a 5.5 MWe biomass integrated gasification combined cycle demonstration plant. *Energy & Fuels*, 22(6):4259–4264, 2008.
- [85] Krister Staahl and Magnus Neergaard. IGCC power plant for biomass utilisation, Värnamo, Sweden. *Biomass and Bioenergy*, 15(3):205 211, 1998. ISSN 0961-9534.
- [86] Daniele Sofia, Pilar Coca Llano, Aristide Giuliano, Mariola Iborra Hernández, Francisco Garcia Pe na, and Diego Barletta. Co-gasification of coal-petcoke and biomass in the Puertollano IGCC power plant. *Chemical Engineering Research and Design*, 92(8):1428 1440, 2014. ISSN 0263-8762.
- [87] Jos Nederend. Una-k-22 "totaal rapport kolenanalyse v3.3.xls" uit handboek laboratorium amsterdam. Technical report, NUON Power Generation BV, 2012.

- [88] Teunis van der Stelt, Nico Woudstra, Piero Colonna, and et al. *Cycle-Tempo: A program for thermodynamic modeling and optimization of energy conversion systems*. Delft university of Technology, The Netherlands, . URL www.asimptote.com.
- [89] Piero Colonna and Teunis van der Stelt. *FluidProp: A program for the estimation of thermophysical properties of fluids*. Delft university of technology, The Netherlands.
- [90] W Traupel. Thermische turbomaschinen: thermodynamischstromungstechnische berechnung. Springer, Berlin, 4th edition, 2001.
- [91] Jouke Arjen Miedema. CYCLE; A GENERAL COMPUTER CODE FOR THERMO-DYNAMIC CYCLE COMPUTATIONS STUDIES OF COGENERATION IN DISTRICT HEATING SYSTEMS. PhD thesis, Delft University of Technology, 1981.
- [92] Teunis van der Stelt, Nico Woudstra, and Piero Colonna. *Cycle-Tempo: Technical Notes*, . URL www.asimptote.com.
- [93] VDI Gesellschaft. VDI Heat Atlas. Springer, second edition edition, 2010.
- [94] Jinsong Zhou, Qing Chen, Hui Zhao, Xiaowei Cao, Qinfeng Mei, Zhongyang Luo, and Kefa Cen. Biomass-oxygen gasification in a high-temperature entrained-flow gasifier. Biotechnology Advances, 27(5):606 611, 2009. ISSN 0734-9750. doi: http://dx.doi.org/10.1016/j.biotechadv. 2009.04.011. URL http://www.sciencedirect.com/science/article/pii/S0734975009000664. Bioenergy Research & Development in ChinalCBT 2008.
- [95] Mark J. Prins, Krzysztof J. Ptasinski, and Frans J.J.G. Janssen. From coal to biomass gasification: Comparison of thermodynamic efficiency. *Energy*, 32 (7):1248 1259, 2007. ISSN 0360-5442.
- [96] Christian Kunze and Hartmut Spliethoff. Assessment of oxy-fuel, pre- and post-combustion-based carbon capture for future IGCC plants. *Applied Energy*, 94:109 116, 2012. ISSN 0306-2619. doi: http://dx.doi.org/10.1016/j.apenergy.2012.01.013. URL http://www.sciencedirect.com/science/article/pii/S0306261912000190.
- [97] Mohamed Kanniche, Rene Gros-Bonnivard, Philippe Jaud, Jose Valle-Marcos, Jean-Marc Amann, and Chakib Bouallou. Pre-combustion, post-combustion and oxy-combustion in thermal power plant for CO2 capture. *Applied Thermal Engineering*, 30(1):53 62, 2010. ISSN 1359-4311. doi: http://dx.doi.org/10.1016/j.applthermaleng.2009.05.005. URL http://www.sciencedirect.com/science/article/pii/S1359431109001471. Selected Papers from the 11th Conference on Process Integration, Modelling and Optimisation for Energy Saving and Pollution Reduction.

- [98] N. Woudstra, T. P. van der Stelt, and K. Hemmes. The thermodynamic evaluation and optimization of fuel cell systems. *Journal of Fuel Cell Science and Technology*, 3(2):155–164, January 2006. ISSN 2381-6872. doi: 10.1115/1.2174064. URL http://dx.doi.org/10.1115/1.2174064.
- [99] Hartmut Spliethoff. Power Generation from Solid Fuels, chapter Coal-Fuelled Combined Cycle Power Plants, pages 469–628. Springer Berlin Heidelberg, Berlin, Heidelberg, 2010. ISBN 978-3-642-02856-4. doi: 10.1007/978-3-642-02856-4\_7. URL http://dx.doi.org/10.1007/978-3-642-02856-4\_7.
- [100] Sung Ku Park, Tong Seop Kim, Jeong L. Sohn, and Young Duk Lee. An integrated power generation system combining solid oxide fuel cell and oxyfuel combustion for high performance and CO2 capture. Applied Energy, 88 (4):1187 1196, 2011. ISSN 0306-2619. doi: http://dx.doi.org/10.1016/j.apenergy.2010.10.037. URL http://www.sciencedirect.com/science/article/pii/S0306261910004393.
- [101] Sung Ku Park, Ji-Ho Ahn, and Tong Seop Kim. Performance evaluation of integrated gasification solid oxide fuel cell/gas turbine systems including carbon dioxide capture. *Applied Energy*, 88(9):2976 2987, 2011. ISSN 0306-2619. doi: http://dx.doi.org/10.1016/j.apenergy.2011.03.031. URL http://www.sciencedirect.com/science/article/pii/S0306261911002017.
- [102] R. J. Braun, S. Kameswaran, J. Yamanis, and E. Sun. Highly Efficient IGFC Hybrid Power Systems Employing Bottoming Organic Rankine Cycles With Optional Carbon Capture. *Journal of Engineering for Gas Turbines and Power*, 134(2):021801–021801, December 2011. ISSN 0742-4795. doi: 10.1115/1.4004374. URL http://dx.doi.org/10.1115/1.4004374.
- [103] Mu Li, James D. Powers, and Jacob Brouwer. A finite volume sofc model for coal-based integrated gasification fuel cell systems analysis. *Journal of Fuel Cell Science and Technology*, 7(4):041017–041017, April 2010. ISSN 2381-6872. doi: 10.1115/1.4000687. URL http://dx.doi.org/10.1115/1.4000687.
- [104] Mu Li, Jacob Brouwer, Ashok D. Rao, and G. Scott Samuelsen. Application of a detailed dimensional solid oxide fuel cell model in integrated gasification fuel cell system design and analysis. *Journal of Power Sources*, 196 (14):5903 – 5912, 2011. ISSN 0378-7753. doi: http://dx.doi.org/10.1016/ j.jpowsour.2011.02.080. URL http://www.sciencedirect.com/science/ article/pii/S0378775311005076.
- [105] Vincenzo Spallina, Matteo C. Romano, Stefano Campanari, and Giovanni Lozza. A SOFC-Based Integrated Gasification Fuel Cell Cycle With CO2 Capture. *Journal of Engineering for Gas Turbines and Power*, 133(7):071706–071706, March 2011. ISSN 0742-4795. doi: 10.1115/1.4002176. URL http://dx.doi.org/10.1115/1.4002176.

- [106] Thomas A. Adams and Paul I. Barton. High-efficiency power production from coal with carbon capture. *AIChE Journal*, 56(12):3120–3136, 2010. ISSN 1547-5905. doi: 10.1002/aic.12230. URL http://dx.doi.org/10.1002/aic.12230.
- [107] A. Verma, A.D. Rao, and G.S. Samuelsen. Sensitivity analysis of a vision 21 coal based zero emission power plant. *Journal of Power Sources*, 158 (1):417 427, 2006. ISSN 0378-7753. doi: http://dx.doi.org/10.1016/j.jpowsour.2005.09.015. URL http://www.sciencedirect.com/science/article/pii/S0378775305013273.
- [108] Eric Grol. Technical assessment of an integrated gasification fuel cell combined cycle with carbon capture. Energy Procedia, 1(1):4307 4313, 2009. ISSN 1876-6102. doi: http://dx.doi.org/10.1016/j.egypro.2009. 02.243. URL http://www.sciencedirect.com/science/article/pii/S1876610209008868. Greenhouse Gas Control Technologies 9Proceedings of the 9th International Conference on Greenhouse Gas Control Technologies (GHGT-9), 16-20 November 2008, Washington DC, {USA}.
- [109] National Energy Technology laboratory (NETL). Integrated gasification fuel cell performance and cost assessment. Technical report, U.S. Department of Energy (DoE), 2009.
- [110] National Energy Technology laboratory (NETL). The benefits of sofc for coal based power generation. Technical report, U.S. Department of Energy (DoE), 2007.
- [111] National Energy Technology laboratory (NETL). Analysis of integrated gasification fuel cell plant configurations. Technical report, U.S. Department of Energy (DoE), 2011.
- [112] J.P. Trembly, R.S. Gemmen, and D.J. Bayless. The effect of IGFC warm gas cleanup system conditions on the gas-solid partitioning and form of trace species in coal syngas and their interactions with SOFC anodes. *Journal of Power Sources*, 163(2):986 996, 2007. ISSN 0378-7753. doi: http://dx.doi.org/10.1016/j.jpowsour.2006.10.020. URL http://www.sciencedirect.com/science/article/pii/S0378775306020490. Selected Papers presented at the {FUEL} {PROCESSING} {FOR} {HYDROGEN} {PRODUCTION} {SYMPOSIUM} at the 230th American Chemical Society-National Meeting Washington, DC, USA, 28 August 1 September 2005.
- [113] Hossein Ghezel-Ayagh, Richard Way, Peng Huang, Jim Walzak, Stephen Jolly, Dilip Patel, Mike Lukas, Carl Willman, Keith Davis, David Stauffer, Vladimir Vaysman, Brian Borglum, Eric Tang, Michael Pastula, and Randy Petri. Integrated coal gasification and solid oxide fuel cell systems for centralized power generation. ECS Transactions, 26(1):305–313, 2010. doi: 10.1149/1. 3429002. URL http://ecst.ecsdl.org/content/26/1/305.abstract.

- [114] Mu LI, Ashok D. Rao, Jacob Brouwer, and G. Scott Samuelsen. Design of highly efficient coal-based integrated gasification fuel cell power plants. Journal of Power Sources, 195(17):5707 - 5718, 2010. ISSN 0378-7753. doi: http://dx.doi.org/10.1016/j.jpowsour.2010.03.045. URL http://www.sciencedirect.com/science/article/pii/S0378775310004544.
- [115] Souman Rudra, Jinwook Lee, L. Rosendahl, and H. T. Kim. A performance analysis of integrated solid oxide fuel cell and heat recovery steam generator for IGFC system. *Frontiers of Energy and Power Engineering in China*, 4(3): 402–413, 2010. ISSN 1673-7504. doi: 10.1007/s11708-010-0122-x. URL http://dx.doi.org/10.1007/s11708-010-0122-x.
- [116] Nicholas S. Siefert and Shawn Litster. Exergy and economic analyses of advanced IGCC-CCS and IGFC-CCS power plants. Applied Energy, 107: 315 - 328, 2013. ISSN 0306-2619. doi: http://dx.doi.org/10.1016/ j.apenergy.2013.02.006. URL http://www.sciencedirect.com/science/ article/pii/S0306261913001141.
- [117] Haiming Jin, Eric D. Larson, and Fuat E. Celik. Performance and cost analysis of future, commercially mature gasification-based electric power generation from switchgrass. *Biofuels, Bioproducts and Biorefining*, 3(2): 142–173, 2009. ISSN 1932-1031. doi: 10.1002/bbb.138. URL http://dx.doi.org/10.1002/bbb.138.
- [118] Woranee Paengjuntuek, Jirasak Boonmak, and Jitti Mungkalasiri. Energy efficiency analysis in an integrated biomass gasification fuel cell system. *Energy Procedia*, 79:430 435, 2015. ISSN 1876-6102. doi: http://dx.doi.org/10.1016/j.egypro.2015.11.514. URL http://www.sciencedirect.com/science/article/pii/S1876610215022468. 2015 International Conference on Alternative Energy in Developing Countries and Emerging Economies.
- [119] Pavan Kumar Naraharisetti, S. Lakshminarayanan, and I.A. Karimi. Design of biomass and natural gas based IGFC using multi-objective optimization. *Energy*, 73:635 652, 2014. ISSN 0360-5442. doi: http://dx.doi.org/10.1016/j.energy.2014.06.061. URL http://www.sciencedirect.com/science/article/pii/S0360544214007609.
- [120] Jhuma Sadhukhan, Yingru Zhao, Nilay Shah, and Nigel P Brandon. Performance analysis of integrated biomass gasification fuel cell (BGFC) and biomass gasification combined cycle (BGCC) systems. *Chemical Engineering Science*, 65(6):1942 1954, 2010. ISSN 0009-2509. doi: http://dx.doi.org/10.1016/j.ces.2009.11.022. URL http://www.sciencedirect.com/science/article/pii/S0009250909008239.
- [121] Korea-ccs 2. URL http://www.globalccsinstitute.com/projects/korea-ccs-2.
- [122] Mark C. Bohm, Howard J. Herzog, John E. Parsons, and Ram C. Sekar. Capture-ready coal plants-Options, technologies and economics

- . International Journal of Greenhouse Gas Control, 1(1):113 120, 2007. ISSN 1750-5836. doi: http://dx.doi.org/10.1016/S1750-5836(07) 00033-3. URL http://www.sciencedirect.com/science/article/pii/S1750583607000333. 8th International Conference on Greenhouse Gas Control TechnologiesGHGT-8.
- [123] Turgut M. Gür. Comprehensive review of methane conversion in solid oxide fuel cells: Prospects for efficient electricity generation from natural gas. *Progress in Energy and Combustion Science*, 54:1 64, 2016. ISSN 0360-1285. doi: http://dx.doi.org/10.1016/j.pecs.2015.10.004. URL http://www.sciencedirect.com/science/article/pii/S0360128515300496.
- [124] Mohammad A. Khaleel and J.Robert Selman. Chapter 11 cell, stack and system modelling. In Subhash C Singhal and Kevin Kendal, editors, *High Temperature and Solid Oxide Fuel Cells*, pages 291 331. Elsevier Science, Amsterdam, 2003. ISBN 978-1-85617-387-2. doi: http://dx.doi.org/10.1016/B978-185617387-2/50028-3. URL http://www.sciencedirect.com/science/article/pii/B9781856173872500283.
- [125] E.J.O. Promes, T. Woudstra, L. Schoenmakers, V. Oldenbroek, A. Thallam Thattai, and P.V. Aravind. Thermodynamic evaluation and experimental validation of 253 MW Integrated Coal Gasification Combined Cycle power plant in Buggenum, Netherlands. *Applied Energy*, 155:181 194, 2015. ISSN 0306-2619. doi: http://dx.doi.org/10.1016/j.apenergy.2015.05.006. URL http://www.sciencedirect.com/science/article/pii/S0306261915005917.
- [126] HIH Saravanamuttoo, GFC Rogers, H Cohen, and PV Straznicky. *Gas Turbine Theory*. Pearson Education Limited (Prentice Hall), 6th edition, 2009.
- [127] R. C. Spencer, K. C. Cotton, and C. N. Cannon. A Method for Predicting the Performance of Steam Turbine-Generators....: 16,500 kw and Larger. *Journal of Engineering for Power*, 85(4):249–298, October 1963. ISSN 0742-4795. doi: 10.1115/1.3677341. URL http://dx.doi.org/10.1115/1.3677341.
- [128] Frank Hanneman and Bu Koestlin. Hydrogen and syngas combustion: precondition for IGCC and ZEIGCC. Siemens AG Power Generation, 2005.
- [129] Ando Yoshimasa, Oozawa Hiroyuki, Mihara Masahiro, and Irie Hiroki. Demonstration of sofc-micro gas turbine (MGT) hybrid systems for commercialization. Technical report, Mitsubishi Heavy Industries, 2015. URL https://www.mhi.co.jp/technology/review/pdf/e524/e524047.pdf.
- [130] Riedel Marc, Nitsche Robert, Henke Moritz, Heddrich Marc P., and Friedrich K. Andreas. Pressurized operation of a 10 layer solid oxide electrolysis stack. In *In proceedings, 12th European Fuel Cell Forum, 5.-8 Jul. 2016, Lucern*, 2016. URL http://elib.dlr.de/105558/.
- [131] J. Kuhn and O. Kesler. Method for in situ carbon deposition measurement for solid oxide fuel cells. *Journal of Power Sources*, 246:430 –

- 437, 2014. ISSN 0378-7753. doi: http://dx.doi.org/10.1016/j.jpowsour. 2013.07.106. URL http://www.sciencedirect.com/science/article/pii/S0378775313013153.
- [132] J. Kuhn and O. Kesler. Carbon deposition thresholds on nickel-based solid oxide fuel cell anodes ii. steam:carbon ratio and current density. *Journal of Power Sources*, 277:455 463, 2015. ISSN 0378-7753. doi: http://dx.doi.org/10.1016/j.jpowsour.2014.07.084. URL http://www.sciencedirect.com/science/article/pii/S0378775314011288.
- [133] Tao Chen, Wei Guo Wang, He Miao, Tingshuai Li, and Cheng Xu. Evaluation of carbon deposition behavior on the nickel/yttrium-stabilized zirconia anode-supported fuel cell fueled with simulated syngas. *Journal of Power Sources*, 196(5):2461 2468, 2011. ISSN 0378-7753. doi: http://dx.doi.org/10.1016/j.jpowsour.2010.11.095. URL http://www.sciencedirect.com/science/article/pii/S0378775310020860.
- [134] C. W. Bale, P. Chartrand, S. A. Degterov, G. Eriksson, K. Hack, R. Ben Mahfoud, J. Melancon, A. D. Pelton, and S. Petersen. Factsage 6.4. URL http://www.factsage.com/.
- [135] Asimptote. Cycle-tempo 5 technical notes. Technical report, ASIMPTOTE, 2014.
- [136] Hans Dieter Baehr. Verbrennungsprozesse, pages 321–359. Springer Berlin Heidelberg, Berlin, Heidelberg, 1966. ISBN 978-3-642-53398-3. doi: 10.1007/978-3-642-53398-3\_8. URL http://dx.doi.org/10.1007/978-3-642-53398-3\_8.
- [137] A. Thallam Thattai, V. Oldenbroek, L. Schoenmakers, T. Woudstra, and P.V. Aravind. Experimental model validation and thermodynamic assessment on high percentage (up to 70gasification combined cycle power plant in Buggenum, The Netherlands. *Applied Energy*, 168:381 393, 2016. ISSN 0306-2619. doi: http://dx.doi.org/10.1016/j.apenergy.2016. 01.131. URL http://www.sciencedirect.com/science/article/pii/S0306261916301192.
- [138] Calin-Cristian Cormos, Ana-Maria Cormos, and Serban Agachi. Power generation from coal and biomass based on integrated gasification combined cycle concept with pre- and post-combustion carbon capture methods. *Asia-Pacific Journal of Chemical Engineering*, 4(6):870–877, 2009. ISSN 1932-2143. doi: 10.1002/apj.354. URL http://dx.doi.org/10.1002/apj.354.
- [139] Calin-Cristian Cormos. Integrated assessment of IGCC power generation technology with carbon capture and storage (CCS). *Energy*, 42(1):434 445, 2012. ISSN 0360-5442. doi: http://dx.doi.org/10.1016/j.energy. 2012.03.025. URL http://www.sciencedirect.com/science/article/pii/S0360544212002162. 8th World Energy System Conference, {WESC} 2010.

- [140] Bert Metz, Ogunlade Davidson, Heleen de Coninck, Manuela Loos, and Leo Meyer. Carbon dioxide capture and storage. Technical report, Intergovernmental Panel on Climate Change (IPCC), 2005.
- [141] EIA. Country analysis of the netherlands. Technical report, Energy Information Administration (EIA), 2015.
- [142] J. Davison. Operating flexibility of power plants with CCS. Technical report, International Energy Agency Greenhouse Gases (IEAGHG), 2012.
- [143] Lars Olof Nord. *Pre-combustion CO*<sub>2</sub> *capture: Analysis of integrated reforming combined cycle*. PhD thesis, Norwegian University of Science and Technology, 2010.
- [144] Machteld van den Broek, Ric Hoefnagels, Edward Rubin, Wim Turkenburg, and André Faaij. Effects of technological learning on future cost and performance of power plants with CO<sub>2</sub> capture. Progress in Energy and Combustion Science, 35(6):457 480, 2009. ISSN 0360-1285. doi: http://dx.doi.org/10.1016/j.pecs.2009.05.002. URL http://www.sciencedirect.com/science/article/pii/S0360128509000215.
- [145] Edward S. Rubin and Haibo Zhai. The cost of carbon capture and storage for natural gas combined cycle power plants. *Environmental Science & Technology*, 46(6):3076–3084, 2012. doi: 10.1021/es204514f. URL http://dx.doi.org/10.1021/es204514f. PMID: 22332665.
- [146] TenneT Holding B.V., http://www.tennet.eu/nl/home.html, August 2014. URL http://www.tennet.eu/nl/home.htmlAccessedon12thAugust2014.
- [147] S.R. Vosen and J.O. Keller. Hybrid energy storage systems for standalone electric power systems: optimization of system performance and cost through control strategies1. *International Journal of Hydrogen Energy*, 24 (12):1139 1156, 1999. ISSN 0360-3199. doi: http://dx.doi.org/10.1016/S0360-3199(98)00175-X. URL http://www.sciencedirect.com/science/article/pii/S036031999800175X.
- [148] R.J. Westerwaal and W.G. Haije. Evaluation solid-state hydrogen storage systems. Technical report, ECN Hydrogen and Clean Fossil Fuels, April 2008.
- [149] Dr. M. Hirscher, editor. *Handbook of Hydrogen Storage: New Materials for Future Energy Storage.* Wiley-VCH, 2010.
- [150] K.C. Hoffman, J.J. Reilly, F.J. Salzano, C.H. Waide, R.H. Wiswall, and W.E. Winsche. Metal hydride storage for mobile and stationary applications. *International Journal of Hydrogen Energy*, 1(2):133 151, 1976. ISSN 0360-3199. doi: http://dx.doi.org/10.1016/0360-3199(76)90067-7. URL http://www.sciencedirect.com/science/article/pii/0360319976900677.

- [151] D. Mori and K. Hirose. Recent challenges of hydrogen storage technologies for fuel cell vehicles. *International Journal of Hydrogen Energy*, 34(10): 4569 4574, 2009. ISSN 0360-3199. doi: http://dx.doi.org/10.1016/j.ijhydene.2008.07.115. URL http://www.sciencedirect.com/science/article/pii/S0360319908009439.
- [152] Louis Schlapbach and Andreas Zuttel. Hydrogen-storage materials for mobile applications. *Nature*, 414(6861):353–358, November 2001. ISSN 0028-0836. URL http://dx.doi.org/10.1038/35104634.
- [153] D. Chabane, F. Harel, A. Djerdir, D. Candusso, O. ElKedim, and N. Fenineche. A new method for the characterization of hydrides hydrogen tanks dedicated to automotive applications. *International Journal of Hydrogen Energy*, In Press, Corrected Proof Note to users:-, 2016. ISSN 0360-3199. doi: http://dx.doi.org/10.1016/j.ijhydene.2015.12.048. URL http://www.sciencedirect.com/science/article/pii/S0360319915304146.
- [154] Xiangyu Meng, Fusheng Yang, Zewei Bao, Jianqiang Deng, Nyallang N. Serge, and Zaoxiao Zhang. Theoretical study of a novel solar trigeneration system based on metal hydrides. *Applied Energy*, 87(6):2050 2061, 2010. ISSN 0306-2619. doi: http://dx.doi.org/10.1016/j.apenergy. 2009.11.023. URL http://www.sciencedirect.com/science/article/pii/S0306261909005108.
- [155] Bokkyu Choi, Dhruba Panthi, Masateru Nakoji, Toshiki Kabutomori, Kaduo Tsutsumi, and Atsushi Tsutsumi. Novel hydrogen production and power generation system using metal hydride. *International Journal of Hydrogen Energy*, 40(18):6197 6206, 2015. ISSN 0360-3199. doi: http://dx.doi.org/10.1016/j.ijhydene.2015.03.029. URL http://www.sciencedirect.com/science/article/pii/S0360319915005972.
- [156] Pierre Hollmuller, Jean-Marc Joubert, Bernard Lachal, and Klaus Yvon. Evaluation of a 5 kW $_p$  photovoltaic hydrogen production and storage installation for a residential home in Switzerland. International Journal of Hydrogen Energy, 25(2):97 109, 2000. ISSN 0360-3199. doi: http://dx.doi.org/10.1016/S0360-3199(99)00015-4. URL http://www.sciencedirect.com/science/article/pii/S0360319999000154.
- [157] Mykhaylo V. Lototskyy, Moegamat Wafeeq Davids, Ivan Tolj, Yevgeniy V. Klochko, Bhogilla Satya Sekhar, Stanford Chidziva, Fahmida Smith, Dana Swanepoel, and Bruno G. Pollet. Metal hydride systems for hydrogen storage and supply for stationary and automotive low temperature PEM fuel cell power modules. *International Journal of Hydrogen Energy*, 40(35): 11491 11497, 2015. ISSN 0360-3199. doi: http://dx.doi.org/10.1016/j.ijhydene.2015.01.095. URL http://www.sciencedirect.com/science/article/pii/S0360319915001639.

- [158] M. Lototskyy, I. Tolj, M.W. Davids, P. Bujlo, F. Smith, and B.G. Pollet. "distributed hybrid" mh-cgh2 system for hydrogen storage and its supply to LT PEMFC power modules. *Journal of Alloys and Compounds*, 645, Supplement 1:S329 S333, 2015. ISSN 0925-8388. doi: http://dx.doi.org/10.1016/j.jallcom.2014.12.147. URL http://www.sciencedirect.com/science/article/pii/S0925838814030758. Supplement Issue: Proceedings from the 14th International Symposium on Metal-Hydrogen Systems: Fundamentals and Applications, 2014 (MH2014).
- [159] A.M. Chaparro, J. Soler, M.J. Escudero, E.M.L. de Ceballos, U. Wittstadt, and L. Daza. Data results and operational experience with a solar hydrogen system. *Journal of Power Sources*, 144(1):165 169, 2005. ISSN 0378-7753. doi: http://dx.doi.org/10.1016/j.jpowsour.2004.12.044. URL http://www.sciencedirect.com/science/article/pii/S0378775305000169.
- [160] Simone Pedrazzi, Gabriele Zini, and Paolo Tartarini. Modelling and simulation of a wind-hydrogen CHP system with metal hydride storage. *Renewable Energy*, 46:14 22, 2012. ISSN 0960-1481. doi: http://dx.doi.org/10.1016/j.renene.2012.03.004. URL http://www.sciencedirect.com/science/article/pii/S0960148112001905.
- [161] Hb-ss-16500-l hydrogen storage tank. URL http://www.hbank.com.tw/fc/ 16500-L.html.
- [162] Solid-h container (HYDROGEN COMPONENTS, INC.). URL http://www.hydrogencomponents.com/hydride.html.
- [163] MH10M (MH10000) METAL HYBRIDE TANK, Pragma Industries. URL http://www.pragma-industries.com/products/hydrogen-storage/mh10m-metal-hydride-tank/.
- [165] Abott and et al. Production of hydrocarbons by steam reforming and fischertropsch reaction., 2008.
- [166] Dowtherm A Heat Transfer Fluid. The Dow Chemical Company, March 1997. URL http://www.dow.com/heattrans/products/synthetic/dowtherm.htm.
- [167] O. Bolland, N. Booth, F. Franco, E. Macchi, G. Manzolini, R. Naqvi, and M.A. Zara. Common framework definition document. Technical report, European Benchmarking Task Force (CAESAR, CESAR and DECARBit projects), 2009.
- [168] M. Gazzani and et al. CO<sub>2</sub> capture in natural gas combined cycle with SEWGS. Part A: Thermodynamic performances. *International Journal of Greenhouse Gas Control*, Volume 105:Pages 206–219, March 2013.

- [169] A. Chaise, P. de Rango, Ph. Marty, and D. Fruchart. Experimental and numerical study of a magnesium hydride tank. *Int. J. of Hydrogen Energy*, 35: 6311–6322, 2010.
- [170] A. Thallam Thattai, B.J. Wittebrood, Theo Woudstra, J.J.C. Geerlings, and Pa Ve Aravind. Thermodynamic System Studies for a Natural Gas Combined Cycle (NGCC) Plant with CO<sub>2</sub> Capture and Hydrogen Storage with Metal Hydrides. *Energy Procedia*, 63:1996 – 2007, 2014. ISSN 1876-6102. doi: http://dx.doi.org/10.1016/j.egypro.2014.11.214. URL http://www. sciencedirect.com/science/article/pii/S1876610214020293. 12th International Conference on Greenhouse Gas Control Technologies, GHGT-12.
- [171] Tae-Hwan Kim, Jung-Sik Choi, Ko-Yeon Choo, Jae-Suk Sung, and Heondo Jeong. Study on the effect of hydrogen purification with metal hydride. In 16th World Hydrogen Energy Conference 2006 (WHEC 2006), 2006.
- [172] Jurriaan Boon, P.D. Cobden, H.A.J. van Dijk, C. Hoogland, E.R. van Selow, and M. van Sint Annaland. Isotherm model for high-temperature, high-pressure adsorption of and on k-promoted hydrotalcite. *Chemical Engineering Journal*, 248:406 414, 2014. ISSN 1385-8947. doi: http://dx.doi.org/10.1016/j.cej.2014.03.056. URL http://www.sciencedirect.com/science/article/pii/S1385894714003349.
- [173] Jurriaan Boon, P.D. Cobden, H.A.J. van Dijk, and M. van Sint Annaland. High-temperature pressure swing adsorption cycle design for sorption-enhanced water gas shift. *Chemical Engineering Science*, 122:219 231, 2015. ISSN 0009-2509. doi: http://dx.doi.org/10.1016/j.ces. 2014.09.034. URL http://www.sciencedirect.com/science/article/pii/S0009250914005387.
- [174] M.K. Cohce, I. Dincer, and M.A. Rosen. Energy and exergy analyses of a biomass-based hydrogen production system. *Bioresource Technology*, 102: 8466–8474, 2011.
- [175] Idehai O. Ohijeagbon, M. Adekojo Waheed, and Someon O. Jekayinfa. Methodology for the physical and chemical exergetic analysis of steam boilers. *Energy*, 53:153–164, 2013.
- [176] R.H. Kehlhofer, J. Warner, H. Nielsen, and R. Bachman. *Combined-Cycle Gas & Steam Turbine Power Plants*. PennWell, 1999.
- [177] Stefano Campanari. Full Load and Part-Load Performance Prediction for Integrated SOFC and Microturbine Systems. *Journal of Engineering for Gas Turbines and Power*, 122(2):239–246, January 2000. ISSN 0742-4795. doi: 10.1115/1.483201. URL http://dx.doi.org/10.1115/1.483201.
- [178] Ivar S. Ertesvag, Hanne M. Kvamsdal, and O. Bolland. Exergy analysis of a gas-turbine combined cycle power plant with precombustion  $CO_2$  capture. *Energy*, 30:5–39, 2005.

- [179] H. C. Patel, T. Woudstra, and P. V. Aravind. Thermodynamic analysis of solid oxide fuel cell gas turbine systems operating with various biofuels. *Fuel Cells*, 12(6):1115–1128, 2012. ISSN 1615-6854. doi: 10.1002/fuce.201200062. URL http://dx.doi.org/10.1002/fuce.201200062.
- [180] Tae Won Song, Jeong Lak Sohn, Jae Hwan Kim, Tong Seop Kim, Sung Tack Ro, and Kenjiro Suzuki. Performance analysis of a tubular solid oxide fuel cell/micro gas turbine hybrid power system based on a quasi-two dimensional model. *Journal of Power Sources*, 142:30 42, 2005. ISSN 0378-7753. doi: http://dx.doi.org/10.1016/j.jpowsour.2004.10.011. URL http://www.sciencedirect.com/science/article/pii/S0378775304010845.
- [181] E. Achenbach. Three-dimensional and time-dependent simulation of a planar solid oxide fuel cell stack. *Journal of Power Sources*, 49(1-3):333 348, 1994. ISSN 0378-7753. doi: http://dx.doi.org/10.1016/0378-7753(93) 01833-4. URL http://www.sciencedirect.com/science/article/pii/0378775393018334. Proceedings of the Third Grove Fuel Cell Symposium The Science, Engineering and Practice of Fuel Cells.
- [182] S. Campanari and P. Iora. Definition and sensitivity analysis of a finite volume SOFC model for a tubular cell geometry. *Journal of Power Sources*, 132 (1-2):113 126, 2004. ISSN 0378-7753. doi: http://dx.doi.org/10.1016/j.jpowsour.2004.01.043. URL http://www.sciencedirect.com/science/article/pii/S0378775304001454.
- [183] Lars Olof Nord, Rahul Anantharaman, and Olav Bolland. Design and off-design analyses of a pre-combustion CO2 capture process in a natural gas combined cycle power plant. *International Journal of Greenhouse Gas Control*, 3(4):385 392, 2009. ISSN 1750-5836. doi: http://dx.doi.org/10.1016/j.ijggc.2009.02.001. URL http://www.sciencedirect.com/science/article/pii/S1750583609000164.
- [184] Giampaolo Manzolini, Ennio Macchi, Marco Binotti, and Matteo Gazzani. Integration of SEWGS for carbon capture in natural gas combined cycle. Part A: Thermodynamic performances . *International Journal of Greenhouse Gas Control*, 5(2):200 213, 2011. ISSN 1750-5836. doi: http://dx.doi.org/10. 1016/j.ijggc.2010.08.006. URL http://www.sciencedirect.com/science/article/pii/S1750583610001349.
- [185] Ryan O'Hayre, Suk-Won Cha, Whitney Colella, and Fritz B. Prinz. Chapter 1: Introduction, pages 1–24. John Wiley & Sons, Inc, 2016. ISBN 9781119191766. doi: 10.1002/9781119191766.ch1. URL http://dx.doi.org/10.1002/9781119191766.ch1.
- [186] Vinod M. Janardhanan, Vincent Heuveline, and Olaf Deutschmann. Performance analysis of a SOFC under direct internal reforming conditions. *Journal of Power Sources*, 172(1):296 – 307, 2007. ISSN 0378-7753. doi: http://dx.doi.org/10.1016/j.jpowsour.2007.07.008. URL http://www.

- sciencedirect.com/science/article/pii/S0378775307014759. {ACS} San Francisco 2006Fuel and Cell Symposium. American Chemical Society National Meeting. San Francisco, {CA} Sept 10-14 2006.
- [187] Cosimo Guerra, Andrea Lanzini, Pierluigi Leone, Massimo Santarelli, and Davide Beretta. Experimental study of dry reforming of biogas in a tubular anode-supported solid oxide fuel cell. *International Journal of Hydrogen Energy*, 38(25):10559 10566, 2013. ISSN 0360-3199. doi: http://dx.doi.org/10.1016/j.ijhydene.2013.06.074. URL http://www.sciencedirect.com/science/article/pii/S0360319913015449.
- [188] Cosimo Guerra, Andrea Lanzini, Pierluigi Leone, Massimo Santarelli, and Nigel P. Brandon. Optimization of dry reforming of methane over Ni/YSZ anodes for solid oxide fuel cells. *Journal of Power Sources*, 245:154 163, 2014. ISSN 0378-7753. doi: http://dx.doi.org/10.1016/j.jpowsour. 2013.06.088. URL http://www.sciencedirect.com/science/article/pii/S0378775313010951.
- [189] Jens R. Rostrup-Nielsen, Jens Sehested, and Jens K. Norskov. Hydrogen and synthesis gas by steam- and CO2 reforming. volume 47 of *Advances in Catalysis*, pages 65 139. Academic Press, 2002. doi: http://dx.doi.org/10.1016/S0360-0564(02)47006-X. URL http://www.sciencedirect.com/science/article/pii/S036005640247006X.
- [190] L. Fan, L. van Biert, A. Thallam Thattai, A.H.M. Verkooijen, and P.V. Aravind. Study of methane steam reforming kinetics in operating solid oxide fuel cells: Influence of current density. *International Journal of Hydrogen Energy*, 40 (15):5150 5159, 2015. ISSN 0360-3199. doi: http://dx.doi.org/10.1016/j.ijhydene.2015.02.096. URL http://www.sciencedirect.com/science/article/pii/S0360319915004760.
- [191] P. Aguiar, C.S. Adjiman, and N.P. Brandon. Anode-supported intermediate temperature direct internal reforming solid oxide fuel cell. i: model-based steady-state performance. *Journal of Power Sources*, 138(1-2):120 136, 2004. ISSN 0378-7753. doi: http://dx.doi.org/10.1016/j.jpowsour. 2004.06.040. URL http://www.sciencedirect.com/science/article/pii/S0378775304006950.
- [192] D. Mogensen, J.-D. Grunwaldt, P.V. Hendriksen, K. Dam-Johansen, and J.U. Nielsen. Internal steam reforming in solid oxide fuel cells: Status and opportunities of kinetic studies and their impact on modelling. *Journal of Power Sources*, 196(1):25 38, 2011. ISSN 0378-7753. doi: http://dx.doi.org/10.1016/j.jpowsour.2010.06.091. URL http://www.sciencedirect.com/science/article/pii/S0378775310010785.
- [193] H.C. Patel, A.N. Tabish, F. Comelli, and P.V. Aravind. Oxidation of h2, CO and syngas mixtures on ceria and nickel pattern anodes. *Applied Energy*, 154:912 920, 2015. ISSN 0306-2619. doi: http://dx.doi.org/10.1016/

- j.apenergy.2015.05.049. URL http://www.sciencedirect.com/science/article/pii/S0306261915006662.
- [194] Martin Andersson, Hedvig Paradis, Jinliang Yuan, and Bengt Sunden. Review of catalyst materials and catalytic steam reforming reactions in sofc anodes. *International Journal of Energy Research*, 35(15):1340–1350, 2011. ISSN 1099-114X. doi: 10.1002/er.1875. URL http://dx.doi.org/10.1002/er.1875.
- [195] Nobuyoshi Nakagawa, Hitoei Sagara, and Kunio Kato. Catalytic activity of Ni-YSZ-CeO<sub>2</sub> anode for the steam reforming of methane in a direct internalreforming solid oxide fuel cell. *Journal of Power Sources*, 92(1-2):88 - 94, 2001. ISSN 0378-7753. doi: http://dx.doi.org/10.1016/S0378-7753(00) 00508-5. URL http://www.sciencedirect.com/science/article/pii/ S0378775300005085.
- [196] E. Achenbach and E. Riensche. Methane/steam reforming kinetics for solid oxide fuel cells. *Journal of Power Sources*, 52(2):283 288, 1994. ISSN 0378-7753. doi: http://dx.doi.org/10.1016/0378-7753(94)02146-5. URL http://www.sciencedirect.com/science/article/pii/0378775394021465.
- [197] Ja Parsons and Sa Randall. Experimental determination of kinetic rate data for sofc anodes. In *SOFC-micromodelling IEA-SOFC Task Report*, pages 43–46, 1992.
- [198] Anthony L Lee, RF Zabransky, and WJ Huber. Internal reforming development for solid oxide fuel cells. *Industrial & engineering chemistry research*, 29 (5):766–773, 1990.
- [199] S. Souentie, M. Athanasiou, D. K. Niakolas, A. Katsaounis, S. G. Neophytides, and C. G. Vayenas. Mathematical modeling of ni/gdc and auni/gdc sofc anodes performance under internal methane steam reforming conditions. *Journal of Catalysis*, 306:116–128, 2013. ISSN 00219517. doi: 10.1016/j.jcat.2013.06.015.
- [200] A.L Dicks, K.D Pointon, and A Siddle. Intrinsic reaction kinetics of methane steam reforming on a nickel/zirconia anode. *Journal of Power Sources*, 86 (1-2):523 - 530, 2000. ISSN 0378-7753. doi: http://dx.doi.org/10.1016/ S0378-7753(99)00447-4. URL http://www.sciencedirect.com/science/ article/pii/S0378775399004474.
- [201] V. D. Belyaev, T. I. Politova, O. A. Mar'ina, and V. A. Sobyanin. Internal steam reforming of methane over ni-based electrode in solid oxide fuel cells. Applied Catalysis A: General, 133(1):47-57, 1995. ISSN 0926860X. doi: 10.1016/0926-860X(95)00184-0. URL http://ac.els-cdn.com/0926860X95001840/1-s2.0-0926860X95001840-main.pdf? \_tid=bcbf116a-89e8-11e4-9f0d-00000aacb361&acdnat=1419259522\_ 52e45688f1a8f792d69b4dd5145e1cb4#page=1&zoom=auto,-186,453.

- [202] Simeon Bebelis, Andonis Zeritis, Constantina Tiropani, and Stylianos G. Neophytides. Intrinsic kinetics of the internal steam reforming of ch4 over a ni-ysz-cermet catalyst-electrode. *Ind. Eng. Chem. Res.*, 39(12):4920–4927, December 2000. ISSN 0888-5885. doi: 10.1021/ie000350u. URL http://dx.doi.org/10.1021/ie000350u.
- [203] Khaliq Ahmed and Karl Foger. Kinetics of internal steam reforming of methane on Ni/YSZ-based anodes for solid oxide fuel cells. Catalysis Today, 63(2-4):479 - 487, 2000. ISSN 0920-5861. doi: http://dx.doi.org/ 10.1016/S0920-5861(00)00494-6. URL http://www.sciencedirect.com/ science/article/pii/S0920586100004946.
- [204] H. Timmermann, D. Fouquet, A. Weber, E. Ivers-Tiffée, U. Hennings, and R. Reimert. Internal reforming of methane at ni/ysz and ni/cgo sofc cermet anodes. *Fuel Cells*, 6(3-4):307–313, 2006. ISSN 1615-6846. doi: 10.1002/fuce.200600002.
- [205] Olga A. Marina, Carsten Bagger, Soren Primdahl, and Mogens Mogensen. A solid oxide fuel cell with a gadolinia-doped ceria anode: preparation and performance. *Solid State Ionics*, 123(1-4):199 208, 1999. ISSN 0167-2738. doi: http://dx.doi.org/10.1016/S0167-2738(99)00111-3. URL http://www.sciencedirect.com/science/article/pii/S0167273899001113.
- [206] J. Hanna, W. Y. Lee, Yixiang Shi, and A. F. Ghoniem. Fundamentals of electroand thermochemistry in the anode of solid-oxide fuel cells with hydrocarbon and syngas fuels. *Progress in Energy and Combustion Science*, (40):74–111, 2014.
- [207] William C. Chueh, Yong Hao, WooChul Jung, and Sossina M. Haile. High electrochemical activity of the oxide phase in model ceria-pt and ceria-ni composite anodes. *Nat Mater*, 11(2):155–161, February 2012. ISSN 1476-1122. URL http://dx.doi.org/10.1038/nmat3184.
- [208] Wei Wang, San Ping Jiang, Alfred Iing Yoong Tok, and Linghong Luo. Gdc-impregnated ni anodes for direct utilization of methane in solid oxide fuel cells. *Journal of Power Sources*, 159(1):68 72, 2006. ISSN 0378-7753. doi: http://dx.doi.org/10.1016/j.jpowsour.2006.04.051. URL http://www.sciencedirect.com/science/article/pii/S0378775306006896. Special issue including selected papers from the 3rd International Conference on Materials for Advanced Technologies (ICMAT 2005, Singapore, Malaysia) and the Summer School on Synthesis of Nanostructured Materials for Polymer Batteries (Augustów, Poland) together with regular papers.
- [209] S. P. Jiang, Sam Zhang, Y. D. Zhen, and A. P. Koh. Performance of GDC-impregnated ni anodes of SOFCs. *Electrochemical and Solid-State Letters*, 7 (9):A282-A285, 2004. doi: 10.1149/1.1783112. URL http://esl.ecsdl.org/content/7/9/A282.abstract.

- [210] Bertha Mosqueda, Jamil Toyir, Akim Kaddouri, and Patrick Gelin. Steam reforming of methane under water deficient conditions over gadolinium-doped ceria. *Applied Catalysis B: Environmental*, 88:361 367, 2009. ISSN 0926-3373. doi: http://dx.doi.org/10.1016/j.apcatb.2008.11.003. URL http://www.sciencedirect.com/science/article/pii/S0926337308004116.
- [211] P. V. Aravind, J. P. Ouweltjes, N. Woudstra, and G. Rietveld. Impact of biomass-derived contaminants on SOFCs with ni/gadolinia-doped ceria anodes. *Electrochemical and Solid-State Letters*, 11(2):B24-B28, 2008. doi: 10.1149/1.2820452. URL http://esl.ecsdl.org/content/11/2/B24.abstract.
- [212] Naotsugu ITOH, Tasuku YAMAMOTO, Takafumi SATO, W. Yu, and Takao OHMORI. Kinetic analysis on low-temperature steam reforming of methane using a ruthenium supported catalyst. *Journal of the Japan Institute of Energy*, 85(4):307–313, 2006. doi: 10.3775/jie.85.307.
- [213] Gilbert F. Froment, Kenneth B. Bischoff, and Juray De Wilde. *Chemical reactor analysis and design 3rd edition*. John Wiley & Sons, 2011.
- [214] S.S.E.H. Elnashaie, A.M. Adris, A.S. Al-Ubaid, and M.A. Soliman. On the non-monotonic behaviour of methane-steam reforming kinetics. *Chemical Engineering Science*, 45(2):491 501, 1990. ISSN 0009-2509. doi: http://dx.doi.org/10.1016/0009-2509(90)87036-R. URL http://www.sciencedirect.com/science/article/pii/000925099087036R.
- [215] I. Chorkendorff and J. W. Niemantsverdriet. *Concepts of modern catalysis and kinetics*, chapter Kinetics, pages 23–78. Wiley-VCH Verlag GmbH & Co. KGaA, 2005. ISBN 9783527602650. doi: 10.1002/3527602658.ch2. URL http://dx.doi.org/10.1002/3527602658.ch2.
- [216] Ka H Yang and Oa A Hougen. Determination of mechanism of catalyzed gaseous reactions. *Chemical Engineering Progress*, 46:146, 1950.
- [217] Jianguo Xu and Gilbert F. Froment. Methane steam reforming, methanation and water-gas shift: I. intrinsic kinetics. *AIChE Journal*, 35(1):88–96, 1989. ISSN 1547-5905. doi: 10.1002/aic.690350109. URL http://dx.doi.org/10.1002/aic.690350109.
- [218] M. Albert Vannice. *Kinetic Data Analysis and Evaluation of Model Parameters for Uniform (Ideal) Surfaces*, pages 106–140. Springer US, Boston, MA, 2005. ISBN 978-0-387-25972-7. doi: 10.1007/978-0-387-25972-7\_6. URL http://dx.doi.org/10.1007/978-0-387-25972-7\_6.
- [219] Ethan S. Hecht, Gaurav K. Gupta, Huayang Zhu, Anthony M. Dean, Robert J. Kee, Luba Maier, and Olaf Deutschmann. Methane reforming kinetics within a ni–ysz sofc anode support. *Applied Catalysis A: General*, 295(1):40–51, 2005. ISSN 0926860X. doi: 10.1016/j.apcata.2005.08.003.

[220] Evgeny Shustorovich and Harrell Sellers. The UBI-QEP method: A practical theoretical approach to understanding chemistry on transition metal surfaces. *Surface Science Reports*, 31(1):1 - 119, 1998. ISSN 0167-5729. doi: http://dx.doi.org/10.1016/S0167-5729(97)00016-2. URL http://www.sciencedirect.com/science/article/pii/S0167572997000162.

## **List of Publications**

#### Journal articles

- **A. Thallam Thattai**, V. Oldenbroek, L. Schoenmakers, T. Woudstra, P. V. Aravind, Experimental model validation and thermodynamic assessment on high percentage (upto 70%) biomass co-gasification at the 253  $MW_e$  integrated gasification combined cycle power plant in Buggenum, The Netherlands, **Applied Energy**, Volume 168, 15 April 2016, Pages 381-393, ISSN 0306-2619.
- **A.** Thallam Thattai, T.Woudstra, B.J.Wittebrood, W.G.Haije, J.J.C.Geerlings, P.V. Aravind *System design and exergetic evaluation of a flexible integrated reforming combined cycle (IRCC) power plant system with carbon dioxide (CO<sub>2</sub>) capture and metal hydride based hydrogen storage, International Journal of Greenhouse Gas Control, Volume 52, September 2016, Pages 96-109, ISSN 1750-5836.*
- **A. Thallam Thattai**, V. Oldenbroek, L. Schoenmakers, T. Woudstra, P. V. Aravind, *Towards retrofitting integrated gasification combined cycle (IGCC) power plants with solid oxide fuel cells (SOFC) and CO<sub>2</sub> capture A thermodynamic case study, Applied Thermal Engineering, Volume 114, 5 March 2017, Pages 170-185, ISSN 1359-4311.*
- **A.** Thallam Thattai, B. J. Wittebrood, T. Woudstra, J. J. C. Geerlings, P. V. Aravind, Thermodynamic system studies for a natural gas combined cycle (NGCC) plant with CO<sub>2</sub> capture and hydrogen storage with metal hydrides, **Energy Procedia**, Volume 63, 2014, Pages 1996-2007, ISSN 1876-6102.
- E. J. O. Promes, T. Woudstra, L. Schoenmakers, V. Oldenbroek, **A. Thallam Thattai**, P. V. Aravind, *Thermodynamic evaluation and experimental validation of 253 MW Integrated Coal Gasification Combined Cycle power plant in Buggenum, Netherlands*, **Applied Energy**, Volume 155, 1 October 2015, Pages 181-194, ISSN 0306-2619.
- L. Fan, L. van Biert, **A. Thallam Thattai**, A. H. M. Verkooijen, P. V. Aravind, *Study of Methane Steam Reforming kinetics in operating Solid Oxide Fuel Cells: Influence of current density*, **International Journal of Hydrogen Energy**, Volume 40, Issue 15, 27 April 2015, Pages 5150-5159, ISSN 0360-3199.

#### Submitted journal article

**A.** Thallam Thattai, L. van Biert, P. V. Aravind, On direct internal methane steam reforming kinetics in operating solid oxide fuel cells with nickel-ceria anodes, submitted to Journal of Power Sources

### **Conference participations**

- **A.** Thallam Thattai, T. Woudstra, P. V. Aravind, *Thermodynamic system study of a natural gas combined cycle (NGCC) plant with direct internal reforming (DIR)-solid oxide fuel cell (SOFC) for flexible hydrogen and power production*, Oral presentation at the 11<sup>th</sup> European SOFC and SOE Forum 2014, Lucerne, Switzerland
- **A. Thallam Thattai**, B. J. Wittebrood, T. Woudstra, J. J. C. Geerlings, P. V. Aravind, *Thermodynamic system studies for a natural gas combined cycle (NGCC) plant with CO\_2 capture and hydrogen storage with metal hydrides*, Oral presentation at the 12th International conference on Greenhouse Gas Control Technologies (GHGT-12), Austin TX, USA.
- **A. Thallam Thattai**, V. D. W. M. Oldenbroek, T. Woudstra, L. Schoenmakers, P. V. Aravind, *System design and model of a 70% biomass co-fired integrated gasification fuel cell (IGFC) plant*, Poster presentation at Fuel Cells 2014 Science & Technology, Amsterdam, The Netherlands
- **A. Thallam Thattai**, J. W. Dijkstra, W. Haije, B. J. Boersma, J. J. C. Geerling, P. V. Aravind, *Thermodynamic system studies on NGCC power plants with pre-combustion CO\_2 capture using SEWGS technology*, Oral presentation at the  $12^{th}$  International conference on Sustainable Energy Technologies (SET-2013), Hong Kong

# **Acknowledgements**

The completion of this work would have been impossible without the support, inputs and encouragement from several colleagues, students, friends, family and medical professionals. I am extremely thankful and grateful to all these people for assisting and supporting me in this long and enjoyable journey.

Firstly, I extend my deepest thanks and gratitude to my co-promoter *Dr. P. V. Aravind* without whom I could never have produced this dissertation. Thanks a lot *Aravind*, particularly for your trust, invaluable support (both on the professional and personal front during the accident period) and crucial inputs during the entire period of this work. Your positive outlook and scientific discussions have always been very helpful for me to move forward and conclude this work. Many thanks to you also to ensure and provide me with financial support throughout this research period.

I would like to express deep thanks to my first promoter *Prof. dr. ir. Bendiks Jan Boersma*. You have been a great inspiration as a mentor *Bendiks Jan* right since I arrived in Delft 8 years ago. Thank you for giving me the opportunity to work on this project and for believing in me. Words cannot express my gratefulness for your huge support to me and my family during and after the difficult times related to my health. Hartelijk bedankt!.

A big token of thanks to my second promoter *Prof. dr. ir. J. J. C. (Hans) Geerlings*. I greatly appreciate your warm encouragement, guidance and helpful discussions in completing this work. Thanks a lot for jointly giving me this opportunity and for being a pillar of support when I needed it. Many thanks to the funding body *SHELL Global Solutions B.V* and the *CATO consortium* to support me financially throughout this journey, including the long medical leave.

I express deep gratitude to *Ir. Theo Woudstra* in providing me extensive technical and personal support during this research period. With a "Midas touch" when it comes to thermodynamic system modeling, it has been a pleasure to work with you *Theo* and particularly to learn so much from you. Thanks a lot for being there always when I needed support, for patiently troubleshooting Cycle-Tempo problems with me and also during challenging times related to my health. Special thanks to *Loek Schoenmakers* and *Dr. Wim Haije* to provide me with extensive support all throughout this work. I am very happy and proud of our collaboration *Loek* and I am very thankful for all your crucial and critical inputs. *Wim*, I really appreciate your enthusiastic outlook in general and your valuable inputs during the course of

this work (particularly to give me the final push in the end!). Furthermore I would like to extend my thanks to *Mr. Jan Wilco Dijkstra* (ECN) in helping me getting started with ASPEN modeling and for providing me with very helpful discussions on system modeling approaches.

I am very fortunate to have had the opportunity to collaborate with extraordinary MSc students, to whom I am very thankful for their help and assistance. Thanks a lot Vincent for assisting me with all your inputs and numerous discussions (3 articles together! Not bad I would say). Many thanks also for your support during and after the accident period. It has been an immense pleasure to work with you Lindert. Technical discussions with you are always very interesting and motivating. Thanks a lot for supporting me extensively in concluding my experimental research. A big token of thanks to Bob Wittebrood for his assistance in developing ASPEN Plus models. It was an enjoyable experience for me to learn modeling tricks and develop approaches together. Carrying out fuel cell experiments and measurements couldn't have been more fun, all thanks to David and Alessandro (Beltrani). David, your wellorganized working style inspired me a lot and it was really a pleasure to work with you. A big thumbs up to the 'Pazzo Italiano' Alessandro (Beltrani) to bring in some renewed energy at a time when research was stagnant. You have been a big help in the lab both for troubleshooting and organization. Thanks a lot both of you for your patience and willingness to spend long hours in the lab.

Experimental research would never have been possible without the help and support from the P&E workshop team. Thanks a lot *Michel, Martijn, Duncan, Gerard, Bas* and *Jaap* for your help in the fuel cell laboratory test stations. An extended token of thanks to management assistants *Eveline van der Veer* (P&E) and *Heleen van Rooien* (MECS) for helping me with all administrative aspects and paperwork in the past 6 years. Additionally, I am very grateful to the TU Delft company doctor *Drs. N.W. Stolp* to help me reintegrate into work after the long medical leave. Many thanks also to the *Erasmus MC doctors and medical team* for their massive efforts and help to fix me after the road accident.

I am very thankful to all my lovely colleagues in the fuel cell group and P&E who provided me with such a lively and comfortable working atmosphere. Thanks a lot *Liyuan* and *Ming* in helping me initiate my experimental research activities. Hartelijk dank *Eva* voor al uw hulp! A special token of thanks to *Tabish* and *Ali* for your support, for tolerating me next to you in office and for all the interesting discussions. Grazie *Ale* and *Giulia* for assisting me in the lab and for making the office so much fun to work in! A big hats off to the Portuguese guy *Bruno* for all his help and support (particularly with Cycle Tempo). Many thanks also to *Ana* (particularly for the daily chocolate dosage!), *Yasser*, *Mayra* and *Jelle*. It has been a pleasure to share the office with you guys! A loud cheers to my old officemates and P&E colleagues *Hassan*, *Gerasimos*, *Giorgos* (*Krintiras*), *Manuela*, *Nafiseh*, *Piotr*, *Kostas*, *Wijjitra*, *Sawat*, *Onursal* and *Christian*! I would really like to thank you guys for your help and support in bringing me back to work after the accident.

Completing this work would never have been possible were it not for the support and friendship of *Hrishikesh (Tiggy)* and *Chokalingam (Choka)*. Thanks a lot *Tiggy* for being such a big support throughout and watching over me (literally in the

office!), pushing me to really think with your absolutely "unsarcastic" comments and help improve my general attitude towards multiple things (including cricket!). I forever owe you a plate of sakkarai pongal! Romba nandri *Choka*, for standing by my side always and your unconditional support during the best and the worst times. Despite all this, guys, I will never forget that witness letter though!

Surviving this research period would be impossible without my lovely flatmates and friends in AvS. Words cannot express my gratitude to you Rohit, for all your help and support you gave me and my family during challenging times after the accident. Thanks a lot also for the many discussions and culinary adventures we had together and for making me in general a more disciplined person. A big hug to my ex-flatmates Sachin, Reshu and Chickoo (Saish) for all your support and making me feel so much at home. Reshu, a big thanks also for designing the cover page! Many thanks to Rahul and Manish for all the extraordinary "discussions" and fun moments together both in Europe and India. I extend a very thankful "hand" finally to you Subbu. Thanks a lot for all your help and the amazing travel memories. A big token of thanks to you, Yash, for all your support and fond memories in the past decade (unbelievable!) and for reviving my interest to some extent in classical music. A big hug and cheers to the darling duo: kuda (Sid) and kachra (Srijith). Many thanks to you guys to always ensure a lively and fun atmosphere around. My utmost gratitude and thanks go to the Ramaerstraat boys Rajat, Purvil, Lalit, Sumit, Trinath and Krishna bhai. Thanks a lot Rajat for being there always to support as a friend, babaji and doctor. Many thanks to you and Purvil particularly for your help to me and my family after the accident. An extended token of thanks also to Bhaskar, Ramavatar, Ashima, Akshay, Damini and Raj for giving me so many cherishable memories.

My family has been one of the biggest support for me to complete this dissertation work. Thanks a lot *Vidhya didi (maternal aunt)* for all your help and support, particularly during the accident period. I cannot imagine how it would all be managed without you being around. A big hug to my lovely adorable cousins *Tejas* and *Manas* for their love. Many thanks *Srikant mama (maternal uncle)*, for all your help and support.

My academic life in school began with one of the greatest teachers: my *Thatha* (*maternal grandfather*). Someone who tutored me and made me realize the value of scientific education, this dissertation is a true dedication to him. The work would never have been possible without his encouragement and unconditional support. Thank you so much *Thatha* for supporting me throughout my research period and for believing in me. Many many thanks *Patti (maternal grandmother)* for providing me with so much love, care and affection (and home food!) always. I couldn't have survived in Delft without all your encouragement, cooking training and tips.

Any language is insufficient to express my gratitude and thankfulness to my parents. *Appa (father)*, you inspired me to become a Mechanical Engineer with that beautiful steam engine you built during my school days; your wisdom, technical prowess and encouragement inspired me enter academic research. Thanks a lot for all your unconditional support and love. To the woman who made me the person I am today, I can only say: I love you *Amma (mother)*. Without you and your

advice, unconditional support, love and care, nothing of this would have started and nothing of this could have ever been possible. Thank you so much for everything!

Aditya Thallam Thattai Delft, the Netherlands June 2017

### About the author



Aditya Thallam Thattai was born on 11<sup>th</sup> September, 1986 in Nagpur, India. He graduated with a Bachelor of Engineering (B.E) degree in Mechanical Engineering from Sardar Patel College of Engineering, University of Mumbai in 2008. Subsequently, he started his studies for a MSc. degree in Mechanical Engineering with a specialization in Solid and Fluid Mechanics (SFM) at TU Delft, the Netherlands and graduated in 2010. During his MSc. studies, he completed a research internship at Micro Turbine Technology B.V (MTT), Eindhoven working on flameless combustion reactor design concepts. He then worked at Nuclear Research and Consultancy Group (NRG), Petten for 10 months to complete his final MSc. thesis on numerical combustion model-

ing and validation studies. Following this, he commenced his doctoral research in February 2011 at TU Delft at the Process and Energy department, Faculty of 3mE. His doctoral research project has been supported by SHELL Global Solutions B.V and Energy Research Center of the Netherlands (ECN) and was within the framework of the CATO2B project, the Dutch national project on carbon capture and storage (CCS). Within this project, he has carried out research activities on developing system concepts and thermodynamic analysis on solid oxide fuel cell (SOFC) integrated power plants and experimental methane steam reforming kinetics in operating SOFCs.